# PHYSICOCHEMICAL AND STRUCTURAL STUDIES OF FERROCENE SCHIFF BASE DERIVATIVES AND SOME ASSOCIATED ADDUCTS



A Thesis Presented in Partial Fulfilment of The Requirements For

The Degree of Master of Science at Massey University

**MASSEY UNIVERSITY**

**NEW ZEALAND**

**ANDREW DAVID LOWE**

**1995**

# DEDICATION

To my parents for keeping me looking towards the future.

And to the words that greeted me, just about every morning

*" have you got any crystals yet ? "*

# ABSTRACT

The results reported in this thesis are an investigation into the synthesis, characterisation, and coordination ability of some new Schiff base ferrocenyl derivatives.

Chapter One gives a brief overview of the practical applications that ferrocene based compounds have been put to, since ferrocenes first synthesis in 1951.

Chapter Two outlines the preparation and characterisation of six new Schiff base ferrocenyl derivatives, along with a new synthesis and full characterisation of a ferrocenyl thiosemicarbazide derivative which was first synthesised in 1968. The X-ray structure of bis-N-(*o*-hydroxybenzylidene) ferrocenylimine, (L11), was established, showing relatively strong intramolecular hydrogen bonding between the Schiff base nitrogen and the hydrogen of the hydroxy group on the phenol.

In Chapter three reduction attempts of the ferrocene derivatives in Chapter 2 are reported. The synthesis and characterisation of a borane adduct of the N-(*o*-hydrazonylpyridine) ferrocenimine ligand, (L2.$BH_3$), is studied. Its single crystal X-ray structure is determined and the adduct is compared to the parent L2 ligand.

Chapter Four contains the preparation and characterisation of the complex $[Zn(L1)Cl]_2$, which is based on the N-(*o*-hydroxybenzylidene) ferrocenylimine ligand, (L1). Five new metal complexes are reported, $[Co(L2)Cl_2]$, $[Ni(L2)Br_2]$, $[Cu(L2)Cl_2]$, $[Co(L2)Br_2]$ and $[Zn(L2)Cl_2]$ based on the L2 ligand, and these are characterised by mass and infra-red spectroscopies.

In Chapter Five the ligands are studied by cyclic voltammetry and Mossbauer spectroscopies, with further cyclic voltammetry studies undertaken on the complexes. The electrochemical oxidation trends observed in the cyclic voltammetry studies on the Schiff base derivatives are in parallel with the Mossbauer studies, which have the results rationalised in terms of electron population movements within the $^{57}$ Fe d-orbitals and the p-orbitals of the cyclopentadienyl rings.

# ACKNOWLEDGEMENTS

I would like to thank the following people who gave me great assistance when undertaking my studies at Massey University.

The biggest thanks go to my supervisors for their supervision and enthusiasm during the frustrating and sometimes trying times that occurred during the research of this project: Associate Professor Eric Ainscough and Professor Andrew Brodie.

Much of this work would not have been possible without the gratefully acknowledged contributions from the following people:

Associate Professor Eric Ainscough and Professor Andrew Brodie for their supervision.
Associate Professor Joyce Waters who introduced me to the world of X-ray crystallography, solved the crystal structures reported, and proof read this thesis.
Dr Raewyn Town for help in the cyclic voltammetry studies.
Associate Professor Ken W. Jolley and Mr John Hastie for obtaining NMR spectral data.
Dr Dennis M$^{c}$ Gavin for collection of all the Mossbauer data.
Mrs M. Dick of Otago University for elemental analysis data.
Dr John Allen of Agricultural Research for Mass Spectral Data.

I would finally like to thank the members of the Department of Chemistry and Bio-Chemistry for their assistance and help.

# CONTENTS

# ABBREVIATIONS

| | |
|---|---|
| $CDCl_3$ | Deuterated chloroform |
| Cp | Cyclopentadiene |
| DBU | 1,8-Diazabicyclo[5.4.0]undec-7-ene |
| dmf | Dimethylformamide |
| dmso | Dimethylsulphoxide |
| DNA | Deoxyribose Nucleic Acid |
| IR | Infra-red |
| NLO | Non-linear optical |
| NMR | Nuclear magnetic resonance |
| ppm | Parts per million |
| SCE | Saturated calomel electrode |
| Sod | Superoxide dismutase |
| Tc | Curie temperature |
| TCNE | Tetracyanoethylene |
| TCNQ | Tetracyanoquinodimethane |
| thf | Tetrahydrofuran |
| TMS | Tetramethylsilane |
| Tn | Neel temperature |
| $\omega$ | Frequency |
| red/ox | Reduction/oxidation |

# LIST OF TABLES

# CHAPTER 1

# GENERAL INTRODUCTION

## 1.0 THE IMPORTANCE OF FERROCENE

The discovery of ferrocene in 1951 opened up a new spectacular branch of chemistry: that of organometallic chemistry [1]. This, at the time, unusual molecule, ferrocene, was the first recognized "cyclo-ene" $\pi$-bonded complex. It was Wilkinson and Fischer who first introduced the concept of the sandwich geometry involving bonding of the aromatic $C_5H_5$ ring to the vicinal iron atom. The wide variety of substitution patterns that are available for the ferrocenyl moiety [2] shows that the $C_5H_5$ ring in ferrocene is similar to other aromatic molecules such as benzene. But, unlike other aromatics, ferrocene does not survive certain vigorous reaction conditions, involved in many aromatic substitution and similar reactions, which benzene does. However, it does undergo Friedel-Crafts acylation, sulfonation and metallation by butyllithium. Its remarkable stability can be related to the fact that it obeys the 18 electron rule. Ferrocene and its derivatives have a wide range of applications in science, technology and medicine the following sections will review just two areas.

1.1) Applications to material science

1.2) Applications to medical science

## 1.1 APPLICATIONS TO MATERIAL SCIENCE

Interactions between metal atoms in molecules have aroused much interest particularly when they take place between two or more different metals. Such studies have been performed on molecules containing donor ligands linked to ferrocene [3-6]. This is because the ferrocene moiety has an inherent ability to act as a redox centre, and it has been found that such centres are sensitive in their response toward other host metals if the ligand donors are appropriately linked to the $C_5H_5$ ring. The Schiff base reaction is

one that may be utilised to bring the redox-active ferrocene unit nearby a site that can detect host metal ions but there are others. Suitable complexes must allow communication between the two metals to occur, e.g. via a conjugated pathway. Understanding of these sorts of interactions is of importance in the field of materials science. A range of compounds have been investigated for the following applications:

a) As molecular switches in controlling supermolecular assemblies [7]

b) As non-linear optical materials [14]

c) As molecular sensors [16]

d) As molecular magnetic materials (ferrocenium salts). [20]

### 1.1.1 SUPERMOLECULAR ASSEMBLIES

The interest in connecting ferrocene into a supermolecular assembly, such as a porphyrin ring, is to construct macrocycles containing multiple redox-active centres. These may serve as new types of electron relay catalysts for redox photochemical reactions which, in the near future, may lead to more efficient light harvesting devices. Such molecules are currently under investigation by many groups. One of the more recent examples [7] is a new porphyrin-ferrocene-quinone linked molecule (**Fig 1.1**).

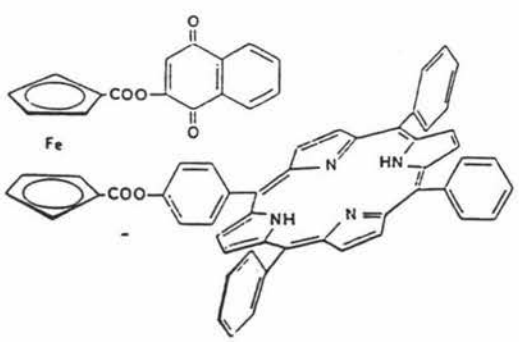


**Fig 1.1**

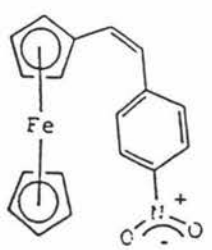


**Fig 1.2**

### 1.1.2 NON-LINEAR OPTICAL (NLO) MATERIALS

One of the second order non-linear optical effects of practical importance is the process of second harmonic generation (SHG). Second harmonic generation is a process by which light of frequency $w$ is converted to frequency $2w$ upon interaction with the non-linear medium. A more important application of this effect is in the laser industry where the limited frequencies available from a laser can be extended thus reducing costs by avoiding the use of multiple lasers.

The development of new materials with large optical non-linearity is an exciting discipline with applications in telecommunications, optical information processing and optical computing [8]. It is now well established that molecular structures that possess both large differences between ground state and excited state dipole moments will have large second-order optical non-linearity. The strategy for some of the organometallic NLO compounds has been to link up an electron-donating metallocene and an electron-withdrawing organic group by a conjugated system.

Molecules with $\pi$ donor-acceptor interactions therefore are promising candidates to fulfil these requirements. While the criteria will ensure large molecular second-order non-linearity it is imperative that the molecular dipole resides in a non-centrosymmetric environment if the molecular non-linear polarisation is to lead to an observable effect in the bulk compound.

Over the past twenty years large efforts have focussed on the synthesis of organic compounds with large SHG efficiencies, whereas the organometallic compounds have received little attention, and up until 1992 there were only a few reports of compounds exhibiting second-order optical non-linearity [9-13]. One of the more famous is (Z) - [1-ferrocenyl-2-(4-nitrophenyl)ethylene] [14] **(Fig 1.2)**. This exhibits a SGH with an efficiency 62 times that of the urea reference standard at 1907nm.

Other NLO materials which also produce significant SGH from 1907nm have been synthesized by linking $[Mo(NO)L(X)]^+$ **(Fig 1.3)** (where X = Cl or I and L = tris(3,5-dimethlylpyrazol-1-yl)hydroborate) to a ferrocene moiety via an aryl or with better effect, diarylazo groups [15]. With this series of NLO materials, only the use of the

ferrocenyl groups to produce active materials has been attributed to the packing arrangement of the crystal lattice to allow phase-matched SHG.

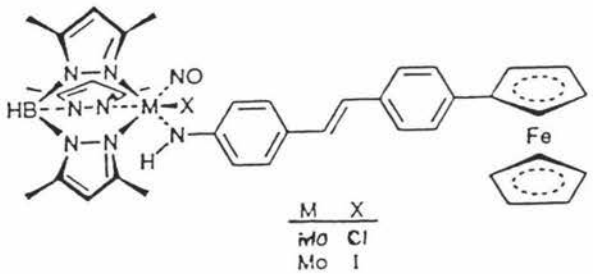


**Fig 1.3**

### 1.1.3 MOLECULAR SENSORS

The area of molecular sensors is one of the fastest growing areas of organometallic chemistry. This is because cyclic voltammetry provides a useful technique to study the presence of an electroactive centre. Ferrocene itself has long been used as a calibrant for this electrochemical technique because of the fully reversible voltammogram that results ($E^1/_2$ = 435mv vs SCE) [$E^1/_2$ conditions are 0.01 mol $dm^{-3}$ in MeCN on a platinum disc].

There have been many reports of studies of heterobimetallic compounds because of their unique chemical character. A large variety of electrochemical responsive units have been synthesised and these can be divided into those containing reducible and those containing oxidizable centres. Both categories have been built into organic and organometallic receptor-host assemblies to provide specific binding sites for cations, anions or neutral organic guest species. A schematic model is shown below.

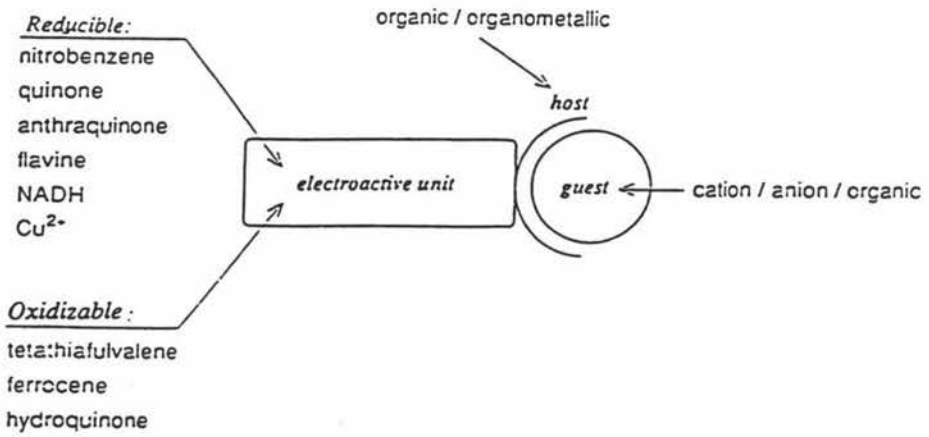

### 1.1.3 (a) Reducible Electroactive Units

Of the reducible electroactive units, the nitrobenzene and quinone-based systems have been used extensively [16]. During reduction, such systems become negatively charged. As a consequence, sensor models possessing reducible electroactive sites often show enhanced cation-binding after reduction. With the presence of a positively charged cation in the host compartment, a system will usually exhibit an anodic shift in the reduction potentials. The magnitude of the anodic shifts is often strongly dependent on the charge/radius ratio of the alkali metal ions. The shifts generally decrease in order $Li^+ > Na^+ > K^+$, reflecting the fact that cation/electroactive unit interaction is strongest for small cations which possess a higher polarising power.

### 1.1.3 (b) Oxidizable Electroactive Units

Oxidizable electroactive units such as ferrocene and tetrathiafulvalene have been used since 1989. Gokel *et al.* [17], linked a ferrocene moiety to a 18-crown $N_2O_4$ macrocycle (**Fig 1.4**) forming a cryptand structure which proved to be an efficient sodium and potassium ion responsive assembly. The cyclic voltammograms of this compound can be seen in diagram 1.1

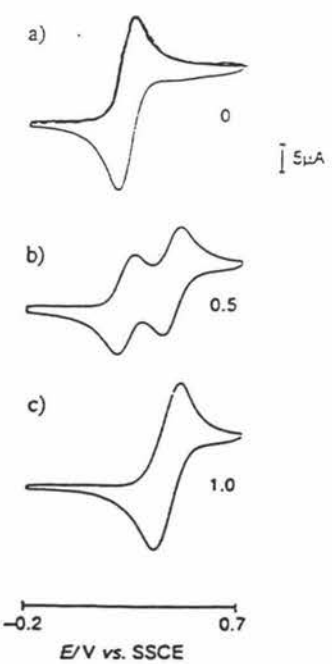


Cyclic voltammograms of Gokel's ferrocene cryptand system, after addition of (a) 0 equivalents, (b) 0.5 equivalents, and (c) 1.0 equivalent of $NaClO_4$.

**Diagram 1.1**

Other examples include several polyoxa- **(Fig 1.5)** and polyoxathiaferrocenophanes [18] . These have been used for redox driven sodium ion transport across a membrane. Ratajczak *et al.* [19] developed a methodology using high dilution techniques that is still used today to synthesise dithio pyridinyl ferrocenyl dimers **(Fig 1.6).**

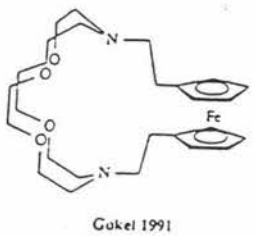


**Fig 1.4**

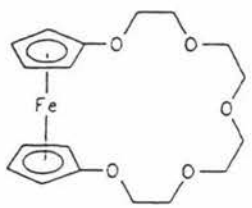


**Fig 1.5**

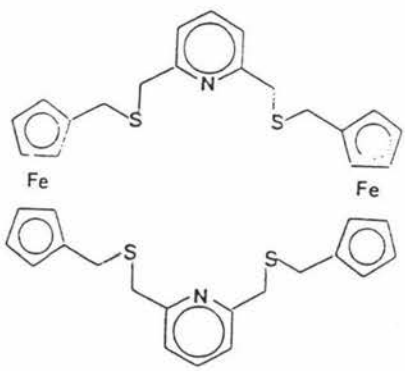


**Fig 1.6**

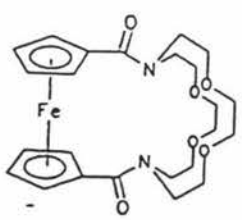

**Fig 1.7**

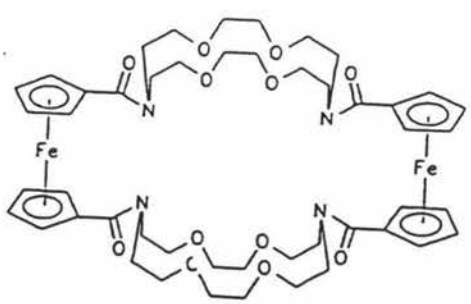

**Fig 1.8**

The ferrocene cryptand [Fc 2,2 ] **(Fig 1.7)** has been prepared by a reaction of 1,1'-bis(chlorocarbonyl)ferrocene with diaza-18-crown-6-ether and was reported to be an ion selective binding agent as is the dimer [Fc(2,2);(2,2)Fc] **(Fig 1.8).**

### 1.1.4 FERRICINIUM SALTS

Highly magnetic materials are essential for frictionless bearings, switches, motors and the recording of sound and pictures on optical disc. Powerful electromagnets are also used to store energy and are used in superconductors.

The following terms are defined before continuation:

| | |
|---|---|
| paramagnetism | possessed by atoms or an ions with one or more unpaired electrons in random orientation; occurs when in a magnetic field. |
| ferromagnetism | the magnetic moments on the separate molecules or ions all align in the same way. |
| antiferromagnetism | paramagnetic molecules or ions that have as many magnetic moments aligned in one direction as in the other direction giving a net magnetism of zreo. |
| Ferrimagnetism | paramagnetic molecules or ions that have as many magnetic moments aligned in one direction as in the other direction, with the resultant moment, being greater than zero. |

For all the spins in a solid to align, either ferromagnetically or antiferromagnetically, the interaction among spins must be stronger than the thermal energies that affect individual electrons by making their spins jostle and disorder each other throwing their spins out of alignment. Thermal energies increase with temperature, whereas the interactions among spins are usually independent of temperature. This

means that above a certain critical temperature, called the Curie temperature (Tc) for ferromagnets and Neel temperature (Tn) for antiferromagnets, the thermal energies overcome the spin interactions and the material becomes paramagnetic. A diagram simulating the electron spins for each of the different forms of magnetism is shown in diagram 1.2

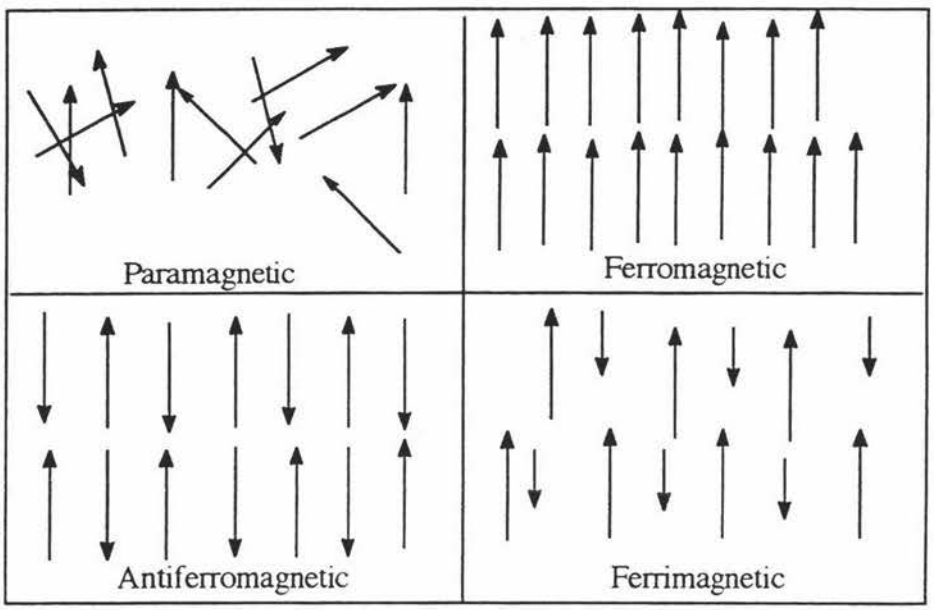


**Diagram 1.2**

In order to design an organomagnet containing a 3-dimensional array of atoms, molecules or ions must contain uncoupled electrons which have the electrons close enough to have co-operative interactions among them. Partial occupation of a band brought about by electron transfer [21] is also required. Miller *et al.* [20] discovered the first organometallic bulk ferromagnet, $[\{Fe^{III}[C_5(CH_3)_5]_2\}^+[TCNE]^-]$ ($FeCp_2^*TCNE$) where TCNE is tetracyanoethylene (**Fig 1.9**). It appears the highly symmetric pentamethylated ferrocene is important in allowing for co-operative magnetic coupling which gives the ferromagnetic behaviour below the Tc value of 4.8 K.

The ferricinium salts with planar radical anions, such as TCNE, contain chains of alternating donors and acceptors and the difference in magnetic properties depends on the presence of the iron atom, which determines the spin on the cation and the nature of the anion. There is also a requirement that the neighbouring chains be displaced by half a unit along the X-Y diagonal plane, so that the distance between donors in one layer and

the acceptors in an adjacent layer is about the same as the distance between donors and acceptors in the same layer. The salt therefore has a true three dimensional structure and bulk magnetism becomes a possibility.

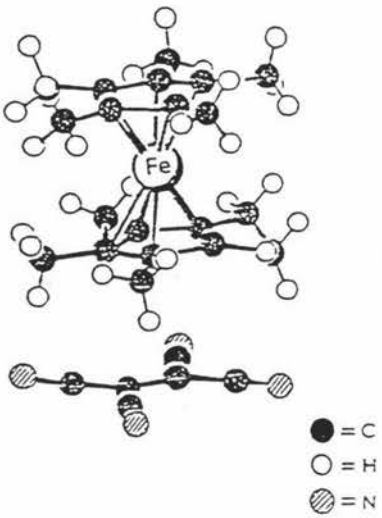


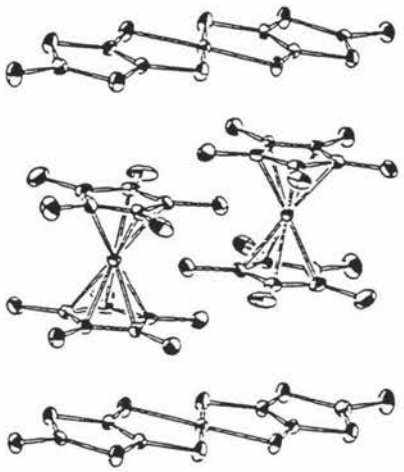

**Fig 1.9** **Fig 1.10**

Since the first organic magnet , $FeCp_2$* TCNE, was synthesised there have been numerous others including those containing the counter ion TCNQ (TCNQ = tetracyano quinodimethane). It was observed that the length of the counter ion influences the structure and hence the intermolecular interactions, and that Tc appears to increase with increasing length of the anion. This has lead to work on synthesising longer counter anions [21]. In an alternative approach, hetero-bimetallic ferromagnetically-ordered molecular assemblies have been studied by Hoffman [22] using a molecular series of charge transfer salts of the type $[Fe(C_5Me_5)_2][Ni(X_2R)_2]$ **(Fig 1.10)** where $X_2R$ represents one of a series of dichalcogolene ligands (2-thioxo-1,3-dithiole-4,5-dithiolate or 1,2-benzenediselenolate). This system was modelled for the stabilization of ferromagnetism by virtual charge transfer between donor and acceptor, with the $X_2R$ unit playing the same role as the planar structure of TCNE. Miller in 1989 investigated the octamethyl ferrocene salts, $[Fe(C_5Me_4H)_2]^+[A]^-$ ([A] = TCNE or TCNQ) to observe

the effect symmetry of the ferrocene moiety had on the Tc value. He concluded that the lack of magnetic ordering may be due to poorer interionic overlap within and between the chains which lead to the substantially weaker magnetic coupling compared with that of the $[Fe(C_5Me_5)]^+[A]^-$ system.

## 1.2 APPLICATIONS IN MEDICAL SCIENCE

### 1.2.1 ANTICANCER DRUGS

Rosenberg's [29] wonder drug discovery of diamminedichloroplatinum(II) (cis-platin) **(Fig 1.11)** in 1969 opened up a new and beneficial area in cancer therapy. However the induced side effects of this drug are severe with kidney toxicity, nausea and vomitting, neurotoxicity and a drop in red blood cell reproduction resulting in anaemia, being a problem. For this reason second, and more recently third generation drugs are being synthesised and tested .

The criteria for a second generation drug are:

a) Highly soluble (for potential oral adminstration)

b) Less kidney toxicity

c) Less nausea and vomiting

d) A better penetration of the blood-brain barrier

e) An improved therapeutic index

f) Different mechanism of action

g) Can act synergistically in combination chemotherapy.

For third generation drugs, the criteria also include higher activity per dose compared with carboplatin **(Fig 1.12)**, the best known second generation drug.

Kopf-Maier [30] divides the transition metal complexes, other than platinum group metals into three groups early, medium or late. Metallocene complexes of the general formulation $M(C_5H_5)_2X_2$ (where M = Ti, V, Nb, Mo) and X = $Cl^-$ for example), fall into the early transition metal category. The medium transition metal compounds are

also metallocinium complexes but are salt like rather than neutral in contrast with the early transition metal complexes. They have the general formulation $M(cp)_2X$ (where M = Fe, Co and $X^- = FeCl_4^-$). The late transition metals form compounds containing for example copper and ligands such as thiosemicarbazide.

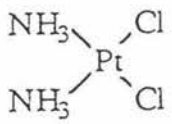


Cisplatin

**Fig 1.11**

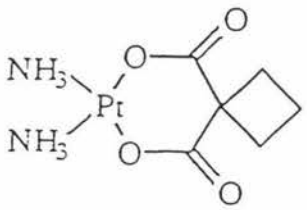


Carboplatin (JM-8)

**Fig 1.12**

The mechanisms by which the anti-tumour complexes function are not well understood, but their interactions with DNA are important and may be generally summarized as:

a) Intercalation
b) Covalent and non-covalent outersphere binding
c) Covalent inner-sphere binding
d) Strand breakage
e) Indirect methods.

The only mechanism that is thought to be important for ferrocene based drugs is the outersphere binding (b). However the other mechanisms will be very briefly reviewed for comparison. Diagram 1.3 summarises the different modes of interaction with the DNA.

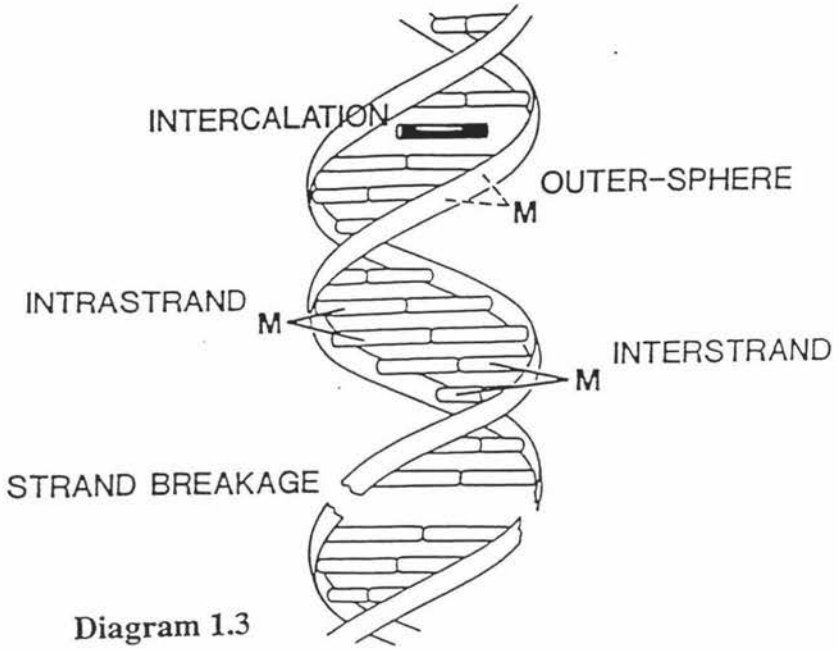


**Diagram 1.3**

Schematic presentation of the modes of interaction of metal complexes with DNA.

### 1.2.1 (a) INTERCALATION

This interaction was originally proposed by Lerman [31] to explain the binding of planar aromatic drugs such as proflavine. Classical intercalation involves the insertion of the planar moloecule between two neighbouring base pairs of DNA to which it is held by van der Waals forces, though electrostatic type interactions may also be present. A non-classical intercalation model has also been proposed, which involves changing the angle of the DNA strand. In this model the presence of an intercalater requires that the helix be extended and locally unwound by the binding reaction. This affects the hydrodynamic properties with an increase in viscosity and results in a stiffening of the double helix, or in simpler terminology it prevents the DNA from dividing, thus stopping replication. Cisplatin provides an example of this mechanism of action. It has been postulated that after the first rate-determining hydrolysis step, the resulting aquachloroplatinum(II) complex co-ordinates preferentially to guanine bases of the DNA [32]. The subsequent reaction with an adjacent nucleotide base leads to damage of the DNA.

On the other hand, it has been suggested that the reaction with other binucleophiles, especially S-containing nucleophiles, proceeds by a direct nucleophilic substitution of the chloride ligand without prior formation of the aquachloroplatinum(II) species [32] as occurs in the reaction below.

$$cis\text{-}[Pt(NH_3)_2Cl_2] \quad \text{------>} \quad cis\text{-}[Pt(NH_3)_2Cl(H_2O)]^+ + Cl^-$$

$$cis\text{-}[Pt(NH_3)_2Cl(H_2O)]^+ \text{ ----->} \quad cis\text{-}[Pt(NH_3)_2(H_2O)_2]^{2+} + Cl^-$$

Since reactions of the above type are important for the activation of the drug on transport to the tumor and for toxic side effects, the labile $Cl^-$ leaving groups were exchanged by less labile leaving groups, such as cyclobutane-1,1-dicarboxylate, in carboplatin. Carboplatin indeed possesses reduced toxicity but also lower antitumour activity due to its low hydrolysis rate [33]. Many groups have tried to reduce the side effects of cisplatin by variations of the neutral ligand.

### 1.2.1 (b) OUTERSPHERE BINDING

The negatively charged backbone of the DNA helix may interact with a variety of positively charged molecules such that, either through columbic interactions or phosphate-oxygen binding, the overall charge is reduced with subsequent effects on the stability of DNA and its conformation.

It has been postulated that ferrocene based drugs function not by the cisplatin method of intercalation but by groove binding to the DNA. It must be noted that only the ferricinium ions have anti-tumour activity whereas the parent ferrocene does not [27]. This suggests that ionic interactions may play an important role in this mechanism. It is postulated that the $\pi$ cloud of the cyclopentadienyl ring interacts with $\pi$ acceptors on the DNA back bone. This stabilizes the ferricinium ions within the groove of the DNA and results in it becoming a blocking group to prevent DNA replication.

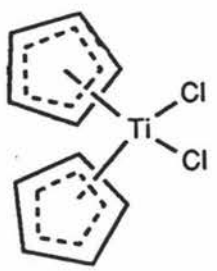


**Fig 1.13**

Another metallocene complex which has been tested against lung and gastrointestinal carcinomas (1990) is a titanocene complex $(C_5H_5)_2TiCl_2$ (**Fig 1.13**). It is believed that the first stage of the mechanism of activation of this drug is similar to that of cisplatin, with fast hydrolysis in an aqueous media giving rise to oxobridged and aqua complexes. These species unlike cisplatin, however, may have high affinity for $PO_4^{3-}$ ions rather than the nitrogen atoms of the nucleotide bases of DNA. It has also been postulated that titanium-amino acid interactions may also take place .

### 1.2.1 (c) COVALENT INNERSPHERE BINDING

A number of metal-aquo ions bind covalently to the bases of DNA such as mercury and causes the DNA structure to be stabilized. The mercury ions bind to the thymine bases substituting for hydrogen bonds and thus forms strong cross links which stabilize the helix [34]. Like the intercalator binding, this effects the hydrodynamic properties of the DNA.

### 1.2.1 (d) STRAND BREAKAGE

Strand breakage involves covalent bond cleavage of the helix backbone and may be either singly stranded or doubly stranded. This again can cause changes in the hydrodynamic properties. Radiation products, especially the hydroxyl radical, are particularly effective in this respect and much of the work on strand breaks centres on this aspect.

### 1.2.1 (e) INDIRECT METHODS

The modes of interaction of these drugs do not function on the tumour cells directly but supress replication of the tumour by deactivating an enzyme that is required for replication.

*i)* Deactivation of the ribonucleoside diphosphate reductase (rdr)

Cupric thiosemicarbazones are used in the deactivation of this key enzyme, which is needed in the synthesis of precursors for DNA replication. It can be deactivated by either complexation of the free ligand by iron at the active site or by coordination of the copper to the free thiols in the enzyme. The subsequent reduction of the coordinated complex results in the release of its thiosemicarbazone [35].

*ii)* Superoxide dismutase (Sod) mimetic activity

Sod is a copper/zinc containing enzyme which catalyses the dismutation of the superoxide radical as follows ;

$$E\text{-}Cu^{2+} + O_2^{\cdot -} \longrightarrow E\text{-}Cu^{+} + O_2 \quad \text{and}$$

$$E\text{-}Cu^{+} + O_2^{\cdot -} + 2\,H^{+} \longrightarrow E\text{-}Cu^{2+} + H_2O_2$$

A deficiency of intracellular Sod in malignant cells can result in an accumulation of superoxide which may attack cellular structure and intiate neoplasia. Other cellular pro-oxidant states (increase concentrations of active oxygen compounds including organic peroxides and oxy-radicals) could also promote the conversion of cells to neoplastic states [36]. It has been shown that Cu (II) salicylates scavenge superoxide and may act as antineoplastic agents.

### 1.2.2 ANTIBIOTIC DRUGS

The formation of stable coordination compounds with heavy metals and aroylhydrazone ligands have shown promise as specific reagents in analytical and extractive chemistry. These types of compounds possess strong biological activity and can inhibit many vital enzymatic reactions that are catalysed by heavy metal ions. It has

been reported that the replacement of aromatic groups by the ferrocenyl moiety in penicillin (**Fig 1.14**) and cephalosporin (**Fig 1.15**) improves their antibiotic activity [37]. In these molecules, ferrocene has two aromatic rings that can undergo substitution. Thus the antibiotic molecules may be modified in three dimensions without changing the profile required for biological activity.

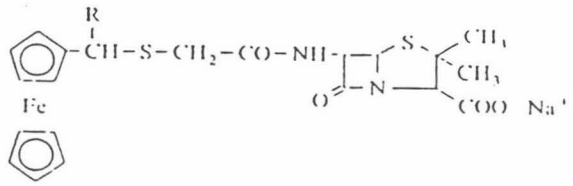


**Fig 1.14**

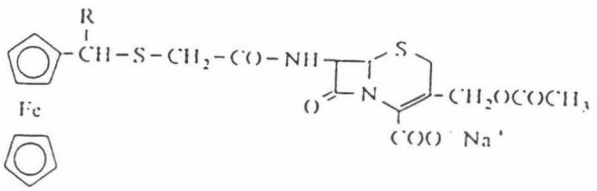


**Fig 1.15**

# CHAPTER 2

# METHODS FOR THE SYNTHESIS OF FERROCENE ORGANO DERIVATIVES AND SOME OF THEIR METALLO COMPLEXES

## 2.1 INTRODUCTION

Many of the substitution products of ferrocene arise from a common precusor formed by lithiation of ferrocene. This reaction is achieved by use of either n-butylithium [39], for di-substituted lithiation, or tert-butylithium [72] for the mono lithiated cyclopentadiene ring. Lithiation is followed by addition of the appropriate electrophile, e.g. dimethyl formaldehyde results in the formation of ferrocene carboxaldehyde. Compounds synthesised by this method are given below and from these other organo derivatives may be prepared.

| | | |
|---|---|---|
| (i) | ferrocene acylchloride | [7] |
| (ii) | ferrocene carboxaldehyde | [39] |
| (iii) | ferrocene amine | [24] |
| (iv) | ferrocene carboxylic acid | [24] |

The following is a general review of ferrocene derivatives. Their wide variety reflects the expanding research within this area with the interest being the potential commercial applications and financial rewards. Because of their diversity, classification schemes have been devised. In one scheme Beer [38] classified macrocycles according to an electrochemical response when an attached macrocycle interacted with differrent chemical species. This is detailed as follows:

(i) electrochemical recognition of cations

(ii) electrochemical recognition of anions

(iii) electrochemical recognition of neutral species.

However, a second classification includes molecules that do not utilize or emphasise the host-guest recognition concept used above.

The types of ferrocenes are:

(i) ferrocene phosphines

(ii) ferrocenylophanes

(iii) ferrocene macrocycles

(iv) bidentate and tridentate ferrocene complex molecules

(v) non-coordinating ferrocene molecules.

### 2.1.1 FERROCENYLPHOSPHINES

Ferrocenylphosphine ligands are widely used in homogeneous catalysis utilising transition metal complexes. A method of synthesising these phosphine ferrocenyl [23] derivatives is given in Scheme 2.1, where the lithium salts then react with the appropriate bases. The preparation of metal complexes of these molecules is as yet unpublished.

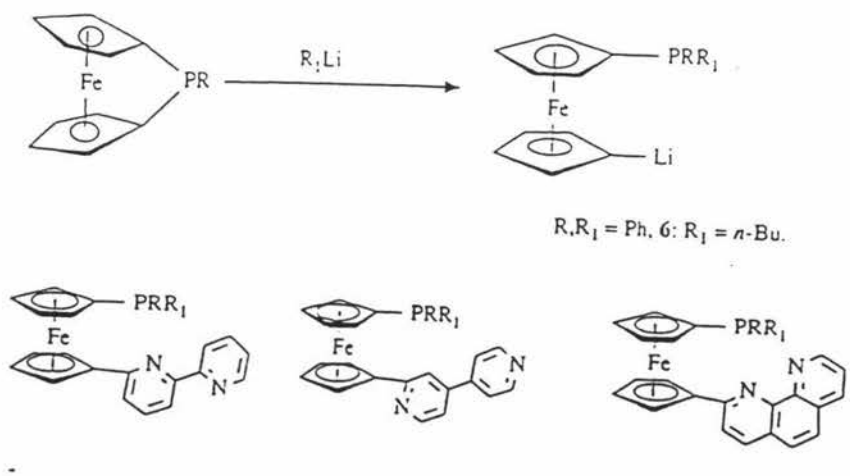


**Scheme 2.1**

Similar methods may be used to prepare the ligands depicted **(Fig 2.1)** where they are shown bound to palladium [43]. It's interesting to note that the many variations of

binding of these phosphino ferrocene derivatives may be important in biology where stereo isomerisation is very important to activity.

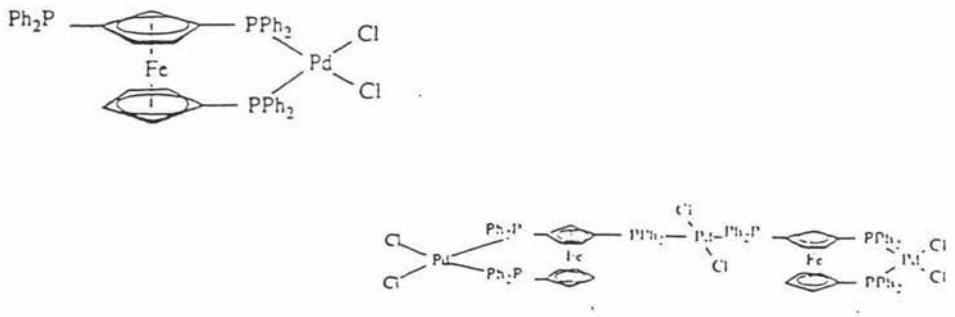

**Fig 2.1**

Cullen and Butler [41] have used polymetallation of ferrocene as a route to poly-substituted ferrocenes such as tris- and tetrakisdiphenylphosphino derivatives. This synthesis was extended [42] to further poly-substituted ferrocenes such as 1,1-bis(diphenylphosphino)-3,3-bis(trimetlylsilyl) ferrocene (Scheme 2.2).

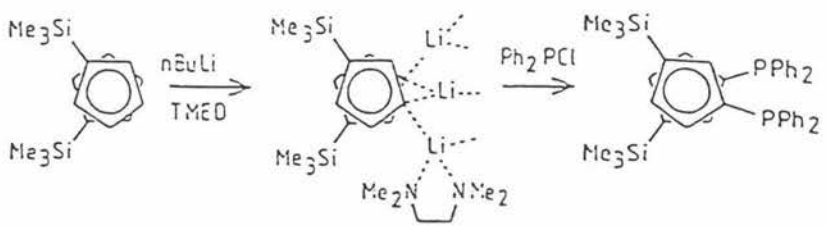

**Scheme 2.2**

Other ferrocenylphosphines and their complexes are shown below:

$LM(CO)_5$

M = Mo, W

L = $FcPh_2P$ , $Fc_2PhP$ (Fc = C5H5-Fe-C5H4)

The study of a metallocene linked to cyclo(thia)phosphazenes **(Fig 2.2)** has been undertaken but no metal complexes have been reported [26].

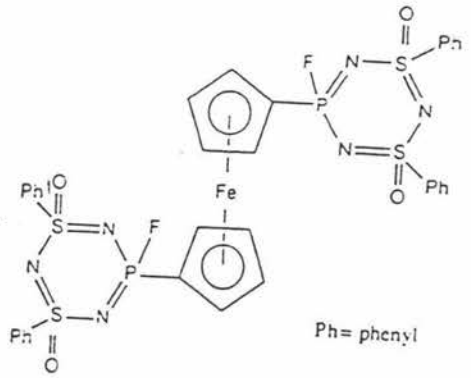


**Fig 2.2**

The ferrocenylphosphonium molecules **(Fig 2.3)** have also been studied [45].

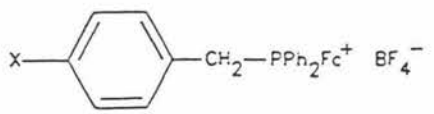

1 a, X = H; b, X = OMe; c, X = F, d, X = CN

**Fig 2.3**

Phosphorus-containing bis-ferrocene macrocycles have been synthesized [46] by Schiff base reactions via Scheme 2.3

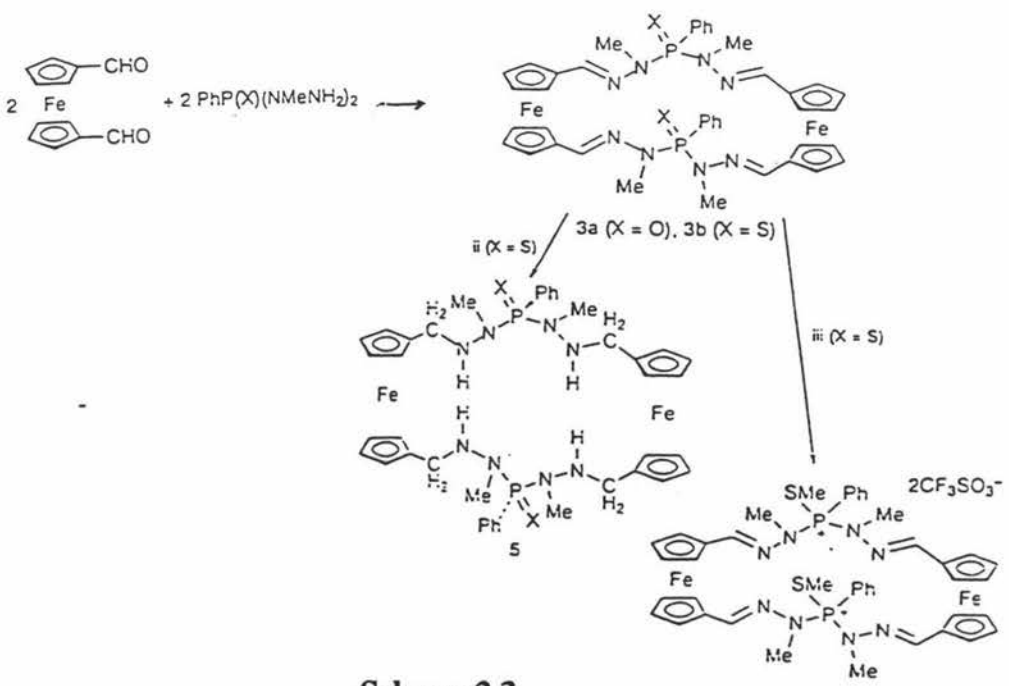


**Scheme 2.3**

## 2.1.2 FERROCENOPHANES

The preparation of the simplest ferrocenophanes [47] shown in Scheme 2.4 is initated with the synthesis of the dilithium salt, tricyclo[9.3.0.0]tetradeca-4,7,11,14-tetraene.

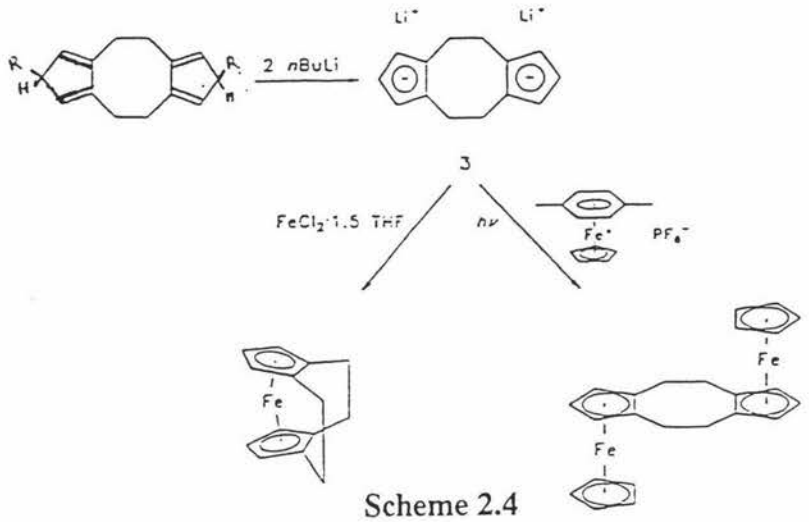


Scheme 2.4

An analogue of a ferrocenophane is zirconocenophane dichloride prepared as in Scheme 2.5.

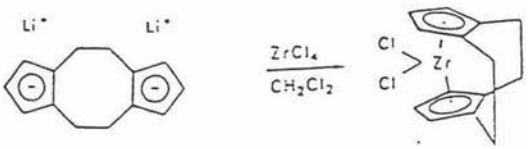


**Scheme 2.5**

A more complicated ferrocenophane is illustrated [48] in Scheme 2.6. The synthesis of this ferrocenylpyridine uses three sequential reactions: a condensation, then a modified aldo condensation followed by a Michael addition

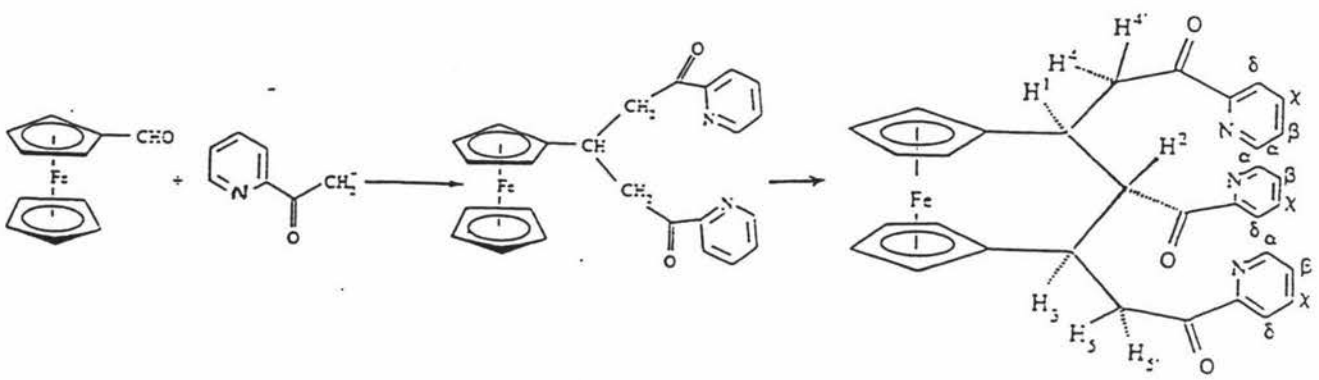


**Scheme 2.6**

Sato [50] synthesised polythia[n]ferrocenophane complexes as in Scheme 2.6a.

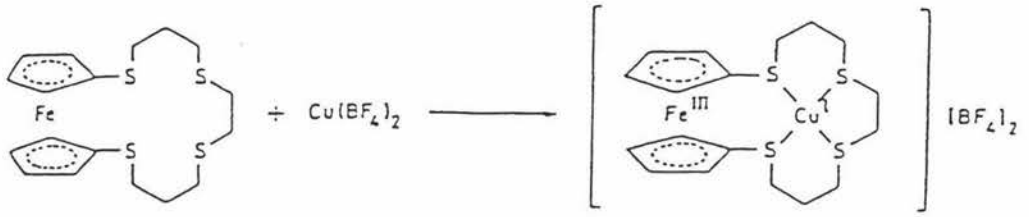


**Scheme 2.6a**

### 2.1.3 FERROCENE MACROCYCLES

Interest in this very large area of ferrocene chemistry arises because of the ability of the ferrocene derived molecules to act as a sensitive redox-active unit. Examples are depicted in **Fig 2.4** [49]. Pentaoxa-[13]-ferrocenophane was the first ferrocene to display an anodic shift in the $Fe^{2+}/Fe^{3+}$ redox potential on uptake of $K^+$ ions.

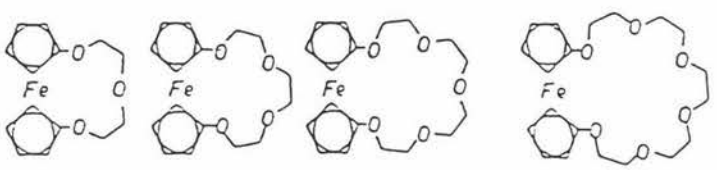


**Fig 2.4**

Scheme 2.7 shows the synthesis of a bis-crown ether derivative.

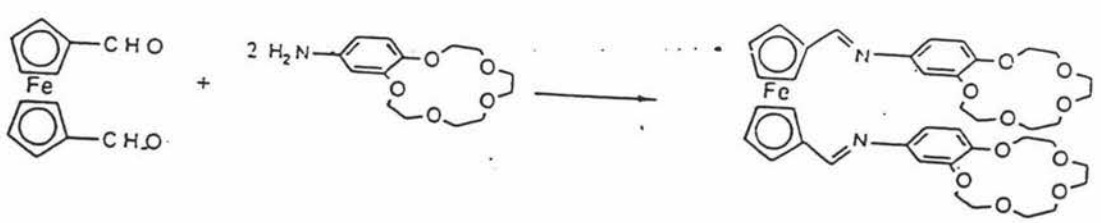


**Scheme 2.7**

Another synthetic method involves the use of the Wittig reaction to produce an

array of products, as in Scheme 2.8, two of which involve crown ethers.

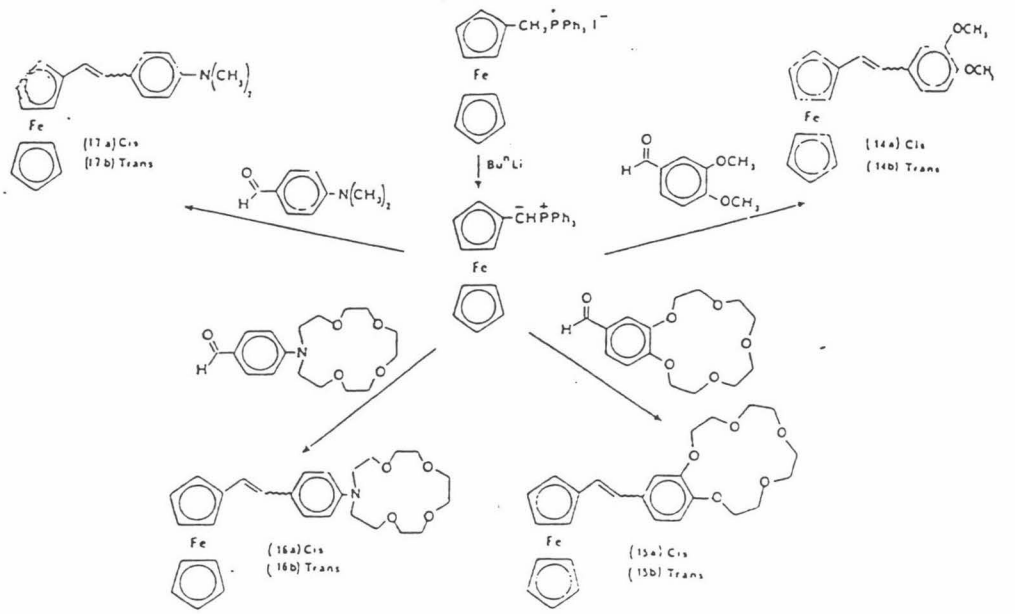

**Scheme 2.8**

The Schiff base condensation reaction has also been utilized to form two compounds in **Fig 2.5**. The reduced product, forms a more stable complex than the unsaturated Schiff base product, and this observation will be referred to again in Chapter 4.

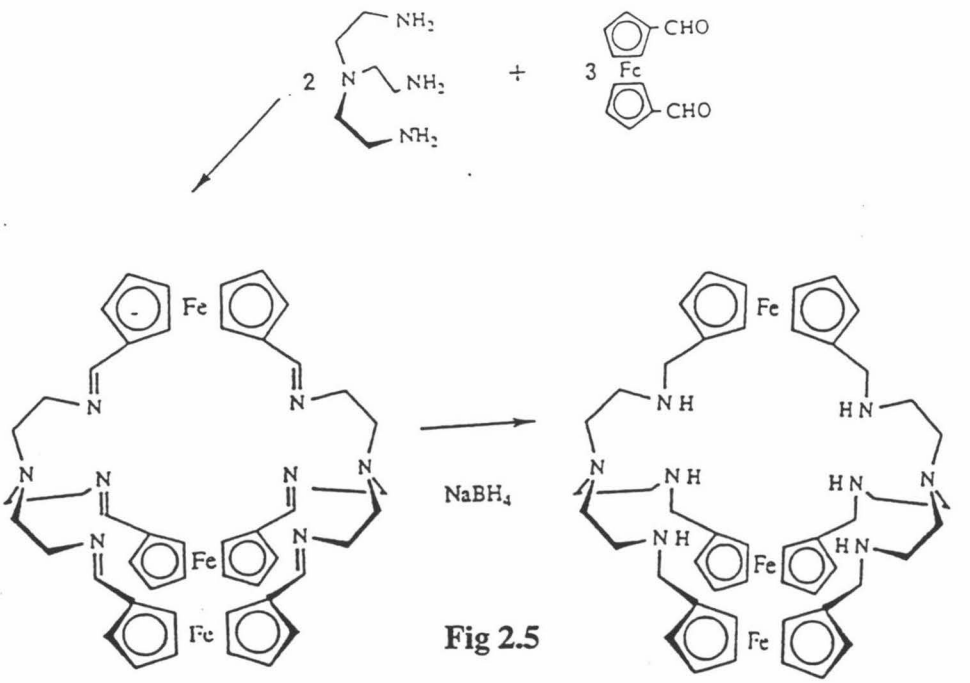

**Fig 2.5**

One of the larger and more elegant macrocyclic ligands to be synthesised [51,52] is the product shown in Scheme 2.9

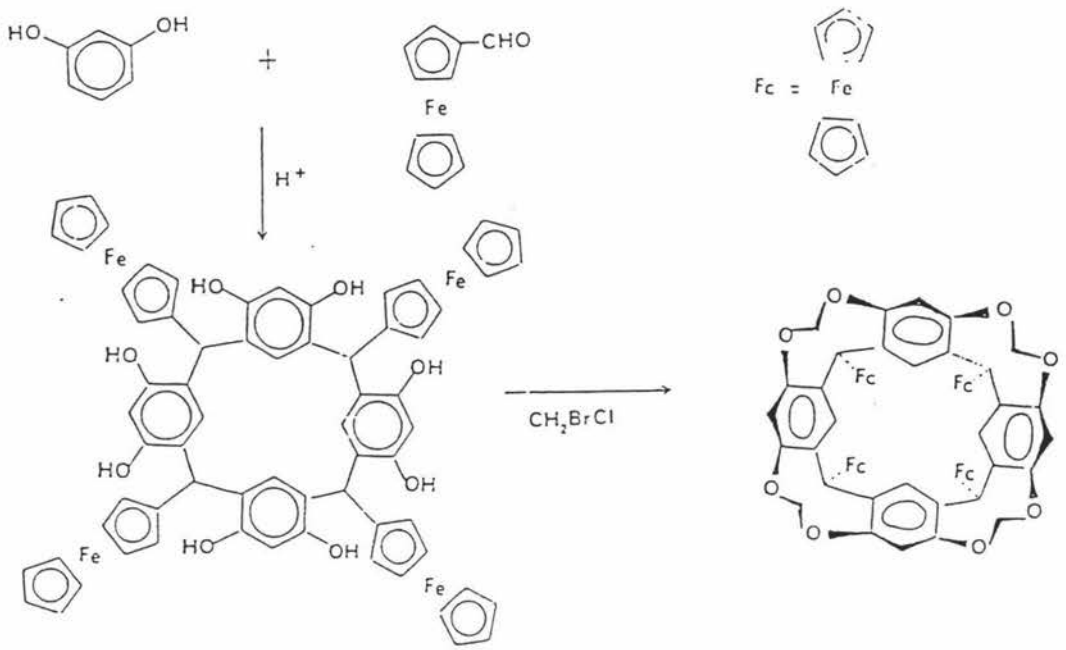


Scheme 2.9

## 2.1.4 BIDENTATE AND TRIDENTATE FERROCENYL LIGANDS AND THEIR COMPLEXES

This class comprises ferrocenes with 'sidearms' that can potentially complex transition metal ions to nitrogen, oxygen or sulphur donor atoms. An example is ferrocenyl thiosemicarbazide [53] which was first synthesised via a Schiff base condensation reaction in 1968 [54]. It forms a 2:1 complex with copper(II) and the postulated structure is given in **Fig 2.6.**

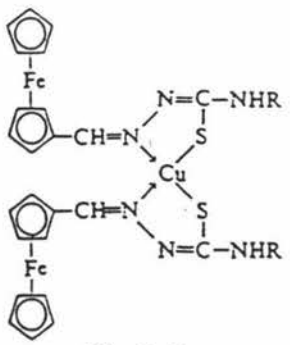


**Fig 2.6**

This work was extended to include further transition metals [53] and the postulated structures of the complexes are given in **Fig 2.7.**

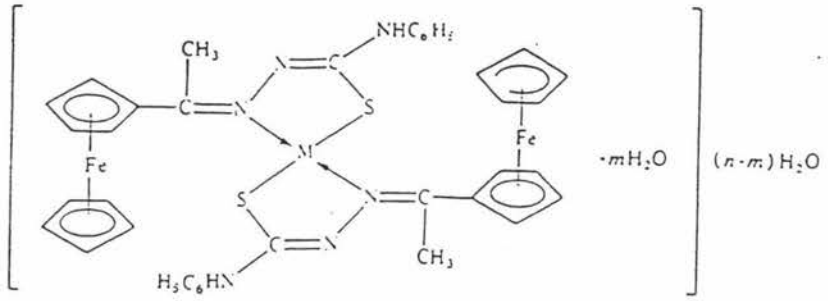

$n=0\sim3,\ m<n$

Suggested structure for the complexes (M = Zn, Ni, Co, Cd, Cu).

**Fig 2.7**

Wiles and Suprunchuk [54] investigated substituted thiosemicarbazones of ferrocene and varied the R, R1, R2 groups to study what effect this had on the UV and IR spectra. These can be represented by the structural formula

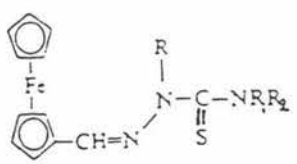

R = $CH_3$ or H

R1 = H or $CH_3$,

R2 = $CH_3(CH_2)_6$, $C_2H_5$, $CH_3$

Ferrocenyl thenoylhydrazone (**Fig 2.8**) has also been prepared by a Schiff base condensation reaction and studied with a variety of metals [55].

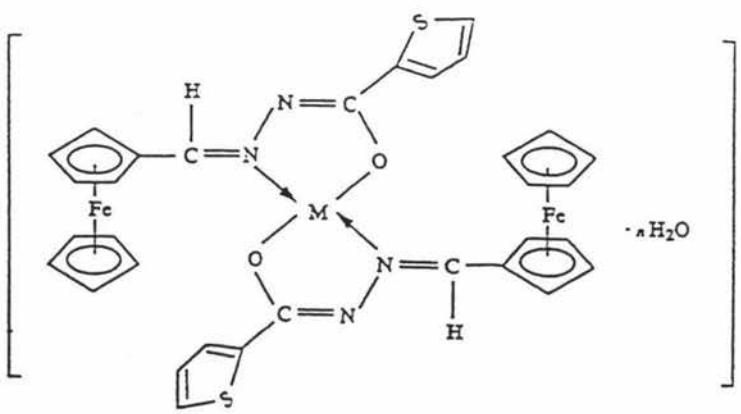

Suggested structure for the complexes: M = Cu, Ni and Hg; $n = 0$; M = Co; $n = 2$.

**Fig 2.8**

In 1990 a series of bis-pyridylhydrazones of 1,1'-diacetylferrocenes (**Fig 2.9**) were characterised [56]

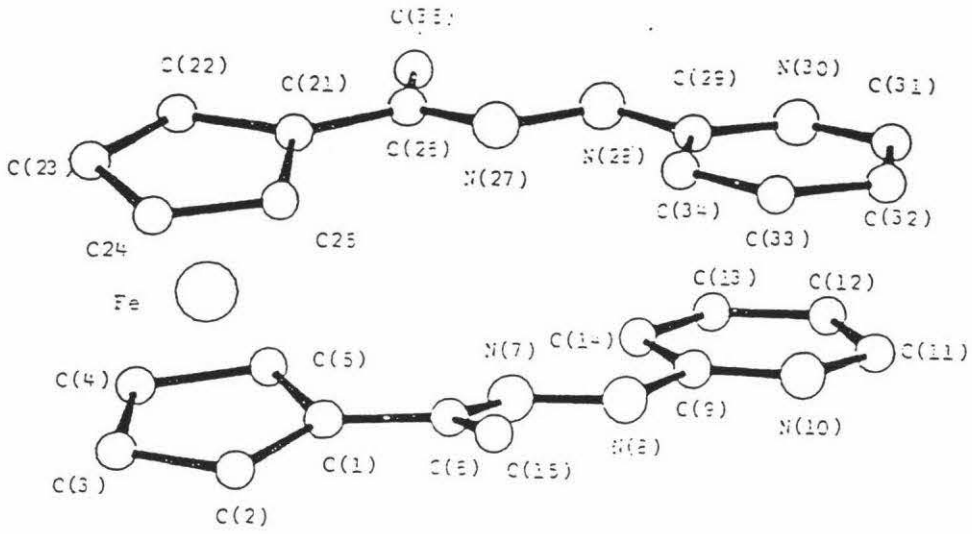


**Fig 2.9**

Although no attempt to complex these to metals was reported, there is an indication that complexation could occur. Acetylferrocenylnapthoylhdrazones have been prepared [57] and their complexes with lead(II) studied (**Fig 2.10**).

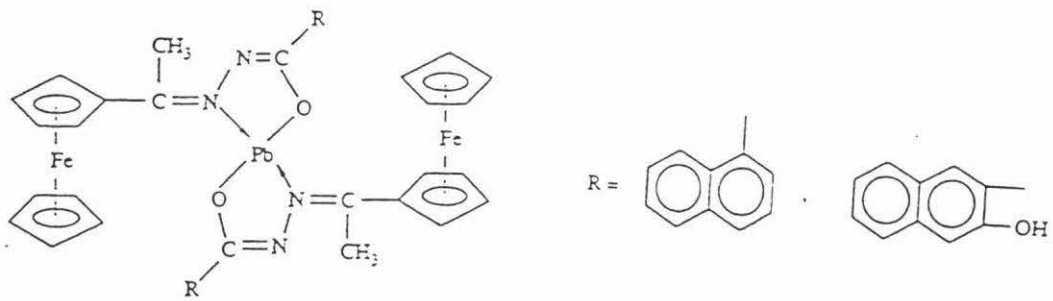


**Fig 2.10**

Facile orthometallation of the cyclopentadienyl ring by palladium (II) occurs when $((CH_3)_2SO)_2PdCl_2$ [27, 58] reacts with the appropriate Schiff base (**Fig 2.11**)

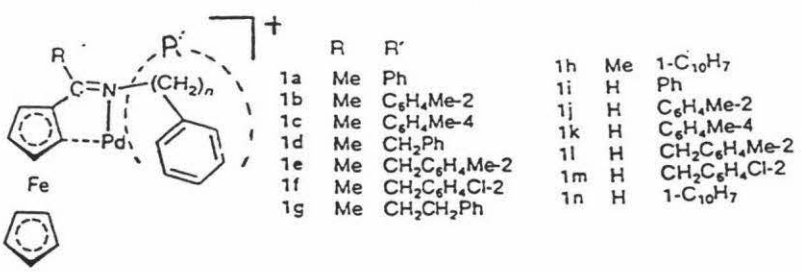


| | R | R′ | | | |
|---|---|---|---|---|---|
| 1a | Me | Ph | 1h | Me | 1-$C_{10}H_7$ |
| 1b | Me | $C_6H_4Me$-2 | 1i | H | Ph |
| 1c | Me | $C_6H_4Me$-4 | 1j | H | $C_6H_4Me$-2 |
| 1d | Me | $CH_2Ph$ | 1k | H | $C_6H_4Me$-4 |
| 1e | Me | $CH_2C_6H_4Me$-2 | 1l | H | $CH_2C_6H_4Me$-2 |
| 1f | Me | $CH_2C_6H_4Cl$-2 | 1m | H | $CH_2C_6H_4Cl$-2 |
| 1g | Me | $CH_2CH_2Ph$ | 1n | H | 1-$C_{10}H_7$ |

**Fig 2.11**

Similar ortho metallations have been observed with ferrocenyl bipyridines [59] **(Fig 2.12).**

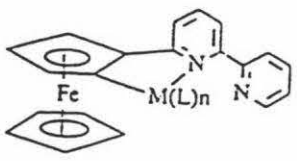


**Fig 2.12**

Terpyridyl substitution on the ferrocenyl ring (Scheme 2.10) has been reported by Constable [60]. Preliminary studies have shown that the terpyridyl ligands complex to Ru.

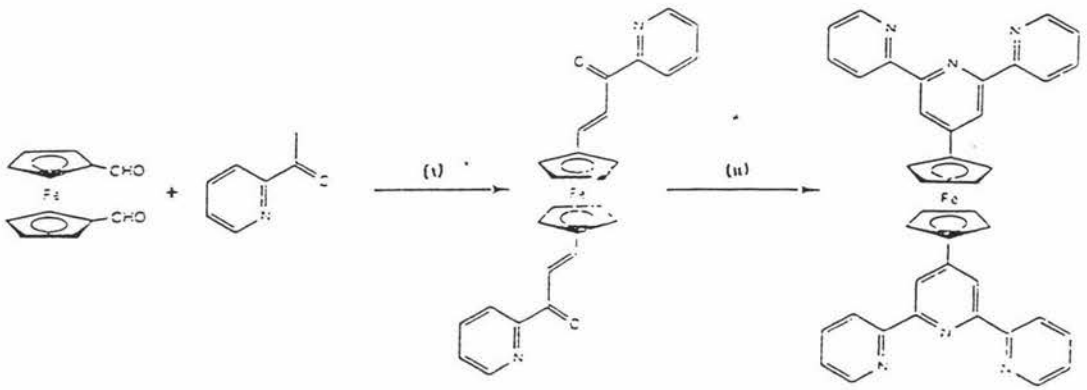

(i) EtOH, NaOH (aqueous, 2 M), 30 min. (ii) EtOH, N-[1-oxo-2-(2-pyridyl)ethyl]pyridinium iodide, $[NH_4][OAc]$, 2 h, 80 °C.

**Scheme 2.10**

A Schiff base product N-(o-hydroxybenzylidene)ferrocenamide (HL) was reported [24] which formed complexes with transition metals in a 2:1 conformation $[ML_2]$. These complexes were characterised by cyclic voltammetry and x-ray crystallography. The $CuL_2$ complex X-ray structure is shown below.

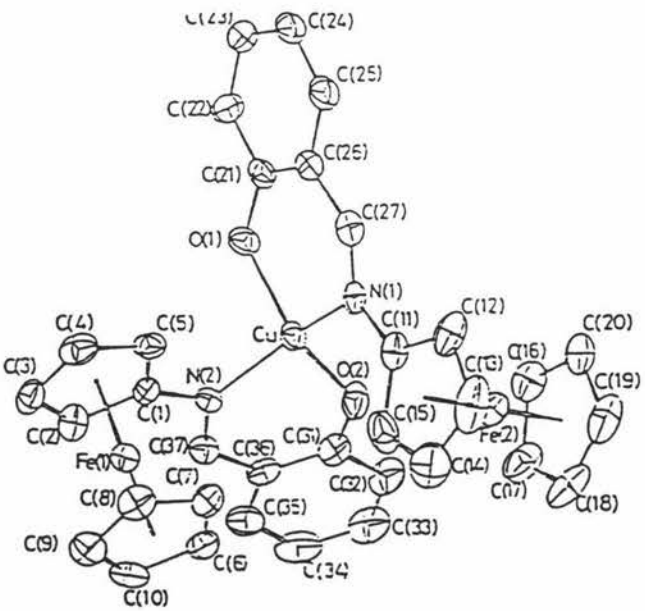


. An ORTEP drawing of $[CuL_2]$

## 2.1.5 NON COORDINATING FERROCENYL MOLECULES

Not all substituted ferrocene compounds are specifically designed for complexation, but they can still be classified as redox active because of the ferrocene

moiety present. Interest has been aroused by the possibility of using these molecules in catalysis. For example Plenio [61] prepared the two compounds shown in **Fig 2.13**, to study the factors governing the mechanism of the electron-transfer process in catalysis.

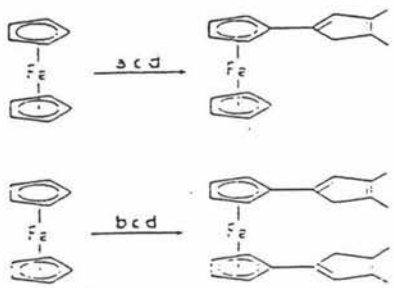


(a) *t*-BuLi; (b) 2 *n*-BuLi/tmeda; (c) 3,4-dimethyl-cyclopentenone; (d) aqueous $NH_4Cl$, *p*-TosOH.

Fig 2.13

Multielectron catalysis has also been studied by Astruc [62] where the synthesis of an interesting polynuclear iron-containing species (**Fig 2.14**) displays a single six-electron cyclo-voltammetric wave, one electron arising from each ferrocene unit.

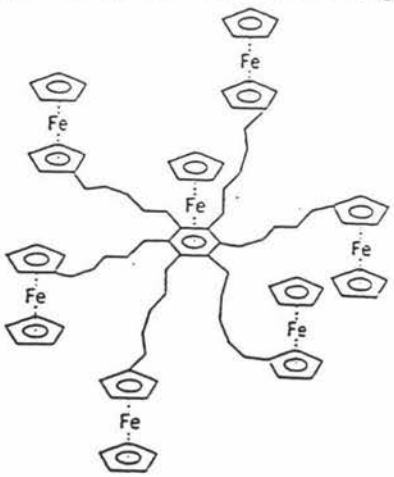


**Fig 2.14**

The area of magnetism has attracted a lot of attention, especially in those organic based molecules that exhibit bulk ferromagnetic behaviour. For example the decamethylferrocene product [64], **(Fig 2.15),** is synthesised by the partial oxidation of the decamethyl ferrocene with TCNE. Its analogue the decaethyl ferrocene product [62], **(Fig 2.16),** has also been formed by partial oxidation of its iron core but by a different

oxidising reactant, TCNQ. This area has been discussed in greater detail in Chapter 1.

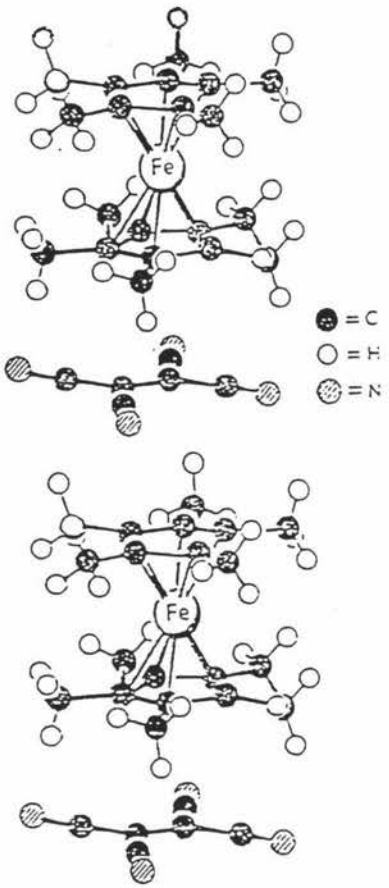


Fig 2.15

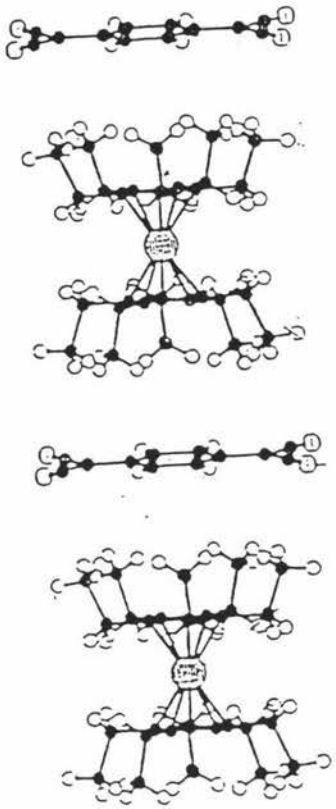

Fig 2.16

## 2.2 THE PRESENT STUDY

The major aim of this work was to synthesise new bidentate and tetradentate Schiff base ligands based on ferrocene monocarboxaldehyde and 1.1'-ferrocene dicarboxaldehyde. At the commencement of this study there were only a few reported derivatives of this type, with most studies having concentrated on Schiff bases that contained a single imine-N. However the Schiff base reaction provides a convenient method of giving a derivative that contains at least two donor atoms and hence some variety in the ligand type.

The second aim was to carry out a preliminary study on the coordinating behaviour of the ligands prepared with a selection of metal ions so that structures could be determined, and the influence of the metal ion on the electronic properties of the ferrocene iron atom deduced. If two metal centres are brought into close proximity, electronic communication may pass between them via direct interaction or, as in this study, by conjugated pathways. It is believed that conjugation is necessary but not imperative for this communication. Attempts to reduce the imine bonds in the Schiff base ligands were made in an attempt to alter the degree of conjugation in the ligands and hence their electronic properties. This should be sensed by the iron atoms for both the free and complexed ligands. This approach is designed to probe the ability of the various ligands to host ions and to determine whether the altered electronic properties will be sensed by the iron atoms. The ready accessibility of the ferrocene monocarboxaldehyde aided the synthesis of new mono Schiff base ligands whereas the improved preparation of 1,1'- ferrocene dicarboxaldehyde [76] allowed a more convenient synthesis of bis-Schiff base ligands. Thus a study of both the mono- and bis-ligands was carried out in parallel. The lack of bis-Schiff base reactions reported in the literature has provided new possibilities for the host-guest class of molecules.

The present work was intended as a preliminary investigation into the general study regarding multicentre metal molecules involving various aspects of both organometallic and coordination chemistry. The synthesis, characterisation and reactivity of the Schiff base ligands will be presented first, followed by a study of their complexing characteristics.

# EXPERIMENTAL

## 2.2.1 PREPARATION OF FERROCENYL MONO-SCHIFF BASES

These were prepared by the Schiff base condensation of ferrocene carboxaldehyde with the appropriate amine in a 1:1 molar ratio, according to Scheme 2.11. The reactions were best carried out using non-polar solvents such as benzene or toluene under an inert atmosphere. The reaction mixtures were refluxed in a Dean- Stark apparatus where the water produced was continually removed from the reaction. The recovered yields were of the order of 60%. Details are given in Experimental Section 2.3.

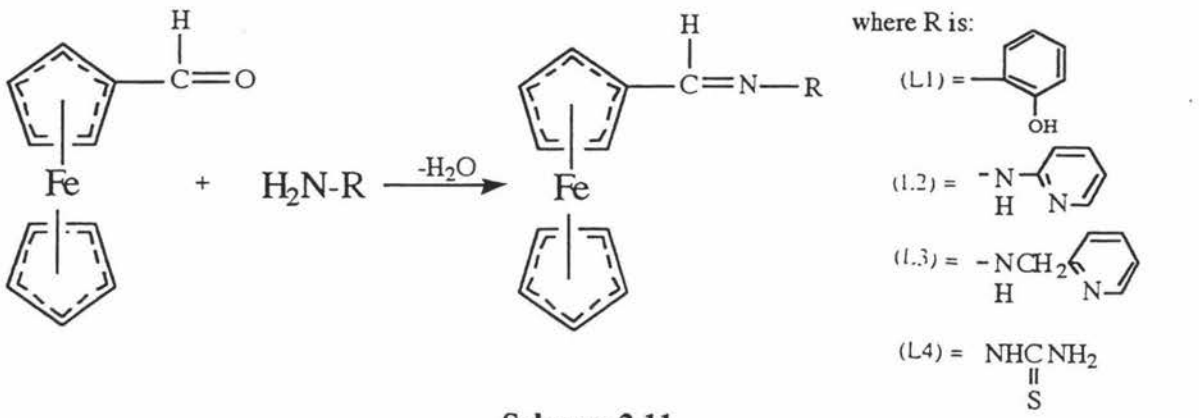


**Scheme 2.11**

## 2.2.2 PREPARATION OF FERROCENYL BIS-SCHIFF BASES

These were prepared by the Schiff base condensation of 1,1'-ferrocene dicarboxaldehyde with the appropriate amine, in a 1:2 molar ratio, according to Scheme 2.12 [40]. The reaction conditions were similar to the mono Schiff base reactions above, but required longer refluxing time to ensure complete reaction of both aldehyde groups had occured. The yields were approximately 20% lower than the mono-Schiff base reactions. Details are given in the Experimental Section 2.3.

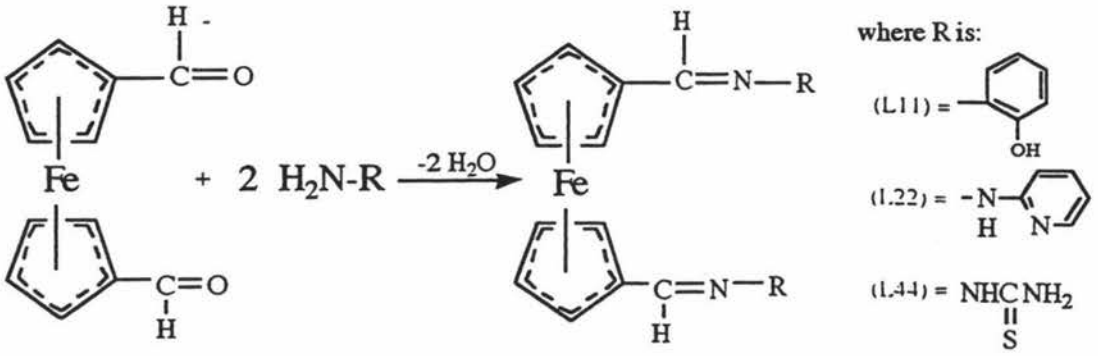


**Scheme 2.12**

## 2.3 SYNTHESIS OF THE SCHIFF BASE DERIVATIVES

### 2.3.1 N-(*0* -HYDROXYBENZYLIDENE) FERROCENYLIMINE ( L1 )

To a solution of ferrocene carboxaldehyde (1.50g , 7.00 mmol) dissolved in 150 ml dry benzene was added 2-aminophenol (0.76g , 6.96 mmol) dissolved in 30 ml benzene. The mixture was under reflux in an argon atmosphere for four hours using a Dean Stark apparatus, after which time the solvent was removed using a rotary evaporator. The resulting oil was dissolved in a minimum amount of chloroform and chromatographed on a silica gel column (70-400*u*m mesh) using a 10% methanol, 90% dichoromethane solvent mixture as the eluent. The first band to come off the column was unreacted ferrocene carboxaldehyde. The second band was collected and taken to dryness, using a rotary evaporator, to form a dark red oil. The product was precipitated from this using a hexane /methanol mixture .

Yield: 66% (1.44g), M.P. 97-99°C.

Found: C, 66.92; H, 4.95; N, 4.60

Calculated for ($C_{17}H_{15}NOFe$):

C, 66.90; H, 4.95; N, 4.60

**NMR ($CDCl_3$) $^1H$ Δ (ppm):**

4.23 (s, 5H, $C_5\underline{H}_5$); 4.52 (t, J = 1.8 Hz, 2H , $C_5\underline{H}_4$); 4.81 (t, J = 1.8 Hz, 2H, $C_5\underline{H}_4$); 8.59 (s, 1H, C<u>H</u>=N); 7.23 (dd, J = 8.1 Hz, 1H, $C_6\underline{H}_4$); 6.98 (dd, J = 8.1 Hz, 1H, $C_6\underline{H}_4$); 7.16 (td, J = 7.7 Hz, 1H, $C_6\underline{H}_4$); 6.88 (td , J = 7.7 Hz, $C_6\underline{H}_4$); 8.58 (s,1H, O<u>H</u>).

**$^{13}C\{^1H\}$Δ (ppm):**

69.31 ($\underline{C}_5H_5$) , 68.90 ($\underline{C}_5H_4$) , 71.56 ($\underline{C}_5H_4$) , 80.11 ($\underline{C}_5H_4$), 158.78 (<u>C</u>=N), 136.58 ($\underline{C}_6H_4$) , 156.44 ($\underline{C}_6H_4$), 115.62 ($\underline{C}_6H_4$) , 119.96 ($\underline{C}_6H_4$) , 127.59 ($\underline{C}_6H_4$) , 114.72 ($\underline{C}_6H_4$).

**IR ($cm^{-1}$)** (nujol mull, NaCl disk)

1611 s, 1586 s, 1285 m, 1163 m, 1100 m, 1034 m, 998 m , 955 m, 955 m , 818 s, 745 s

### 2.3.2 N-(*O* -HYDRAZONYLPYRIDINE) FERROCENYLIMINE ( L2 )

To ferrocene carboxaldehyde (1.50g , 7.00 mmol) dissolved in 150 ml dry benzene, was added 2-hydrazinopyridine (0.76g , 6.96 mmol), dissolved in 30 ml benzene. The mixture was stirred under reflux in an argon atmosphere for six hours using a Dean Stark apparatus. The volume was reduced using a rotary evaporator until a brown crystalline solid formed. This solid was dissolved in a minimum amount of chloroform and chromatographed on a silica gel column (70-400*u*m mesh) using a 10% methanol, 90% dichoromethane solvent mixture as eluent. The second band was collected and taken to dryness using a rotary evaporator (the first band was unreacted starting material).

Yield : 50%, (1.06g) , M.P. 164-166°C.

Found: C, 62.64; H, 4.72; N, 13.84

Calculated for ($C_{16}H_{15}N_3Fe$):

C, 62.97; H, 4.95; N, 13.76

**NMR ($CDCl_3$) $^1H$ Δ (ppm):**

4.19(s, 1H, $C_5\underline{H}_5$); 4.34 (t, J = 1.5 Hz, 1H, $C_5\underline{H}_4$); 4.59 (t, J = 1.7 Hz, 1H , $C_5\underline{H}_4$); 6.74 (t, J = 5.5 Hz, 1H, $C_5\underline{H}_4N$); 7.26 (d, J = 4.2 Hz, 1H , $C_5\underline{H}_4N$) ; 7.58 (t , J = 5.6 Hz, 1 H, $C_5\underline{H}_4N$); 8.11 (d, J = 4.0 Hz, 1H, $C_5\underline{H}_4N$); 8.45 (s, 1H, N$\underline{H}$); 7.60 (s, 1H, C$\underline{H}$=N).

**$^{13}C\{^1H\}$ Δ (ppm):**

69.02($\underline{C}_5H_5$) , 66.95 ($\underline{C}_5H_4$) , 69.54 ($\underline{C}_5H_4$), 80.25 ($\underline{C}_5H_4$) , 139.2 0($\underline{C}$=N) , 156.70 ($\underline{C}_5H_4N$) , 147.35 ($\underline{C}_5H_4N$), 115.07 ($\underline{C}_5H_4N$), 138.02 ($\underline{C}_5H_4N$), 107.32 ($\underline{C}_5H_4N$).

**I.R ($cm^{-1}$) (nujol mull, NaCl disk):**

3118br m , 1593 s , 1537 m , 1299 m , 1203 w , 1126 m , 1084 m , 998 m , 809 w , 771 w.

### 2.3.4 N-(*O* -METHYLPYRIDINE) FERROCENYLIMINE ( L3 )

2-aminomethylpyridine (0.51g, 4.60 mmol) was added to a 150 ml round-bottomed flask with ferrocene carboxaldehyde (1.00g, 4.60 mmol) added to it. The flask was then left for an hour. 100 ml dry benzene was then added and the solution was refluxed for two hours using the Dean Stark apparatus (which had 3A molecular seives added to it).

The solution was cooled and solvent removed using a rotary evaporator to give a brown oil. To the oil, 5 ml hexane was added and the mixture stirred in an ice bath vigorously for 1-2 minutes. The solvent was removed using a rotary evaporator until brown crystals appeared. (The flask was warmed gently during this work-up). Some irreproducibility was observed with this preparation.

Yield : 68% (0.48g), M.P. 75°C

Found: C, 66.81; H, 5.27; N, 9.50

Calculated for ($C_{17}H_{16}N_2Fe$)

C, 67.00; H, 5.30; N, 9.20

**NMR($CDCl_3$) $^1H$ Δ (ppm):**

4.18 (s, 5H, $C_5\underline{H}_5$); 4.38 (t, J = 1.8 Hz , 2H , $C_5\underline{H}_4$); 4.70 (t, J = 1.8 Hz , 2H , $C_5\underline{H}_4$); 4.79 (s, 2H, $C\underline{H}_2$); 7.37 (d, J = 7.7 Hz, 1H, $C_5\underline{H}_4$); 7.66 (t, J = 7.3 Hz, 1H, $C_5\underline{H}_4N$); 8.56 (d, J = 4.0 Hz, 1H , $C_5\underline{H}_4N$); 7.17 (t, J = 4.0Hz, 1H, $C_5\underline{H}_4N$); 8.43 (s, 1H, $C\underline{H}$=N).

**$^{13}C\{^1H\}$ Δ (ppm):**

68.90 ($\underline{C}_5H_5$) , 68.42 ($\underline{C}_5H_4$) , 70.35 ($\underline{C}_5H_5$) , 70.35 ($\underline{C}_5H_4$) , 163.21 ($\underline{C}$=N) , 60.75 ($\underline{C}H_2$) , 159.18 ($\underline{C}_5H_4N$) , 121.95 ($\underline{C}_5H_4N$) , 136.38 ($\underline{C}_5H_4N$) , 121.69 ($\underline{C}_5H_4N$) , 149.05 ($\underline{C}_5H_4N$).

**IR** (nujol mull , NaCl disk):

1635 s , 1581 m , 1293 m , 1243 m , 1098 m , 997 m , 843 m , 813 m , 781 m , 750 m.

### 2.3.3 1,3-DIAMINO-2-HYDROXYPROPANE FERROCENYL DERIVATIVE (L5)

To a solution of ferrocenecarboxaldehyde (0.86, 4.00 mmol) dissolved in 50 ml dry benzene was added 1,3-diamino-2-hydroxypropane (0.18g, 2.00 mmol) in a 150 ml round-bottomed flask. The solution was stirred under reflux for 1 hour in a nitrogen atmosphere, using a Dean Stark apparatus. The cooled solution was reduced in volume using a rotary evaporator until a yellow precipitate started to form. After standing the precipitate was filtered and washed with hexane then dried on a vacuum line.

| | |
|---|---|
| Yield: | 58% (0.24g), M.P. 55-58 °C |
| Found: | C, 61.34; H, 6.46; N, 9.11 |
| Calculated for ($C_{14}H_{18}N_2Fe$+ 0.25 $C_6H_6$) | |
| | C, 60.90; H, 6.40; N, 9.10 |

The $^1H$, $^{13}C$ results are very difficult to interpret because according to Baldwin's rules#, internal cyclisation can occur resulting in a mixture of isomers (see chapter 2 section 2.6). According to the proton NMR all of the possible isomers appear to be present. As a result a detailed assignment was not attempted.

**NMR($CDCl_3$) $^1H$ Δ (ppm):**

8.21, 8.17, 7.36, 4.65, 4.38, 4.33, 4.30, 4.26, 4.25, 4.19,4.17, 3.62, 3.15, 1.97

**$^{13}C\{^1H\}$ Δ (ppm):**

163.3, 90.70, 70.55, 69.08, 68.59, 68.19,. 67.81, 66.40, 66.20, 65.30, 62.34, 52.49, 50.71 , 45.58.

**IR ($cm^{-1}$)** (nujol mull, NaCl disk):

3282w br, 3156w br, 1671 m br, 1347 w, 1145 s, 1101 s, 1053 s, 1028 s, 998 w, 830 w, 796 w.

# The cycloaddition product of L5, pre-determined by Baldwin's rules, are is given Section 2.6.

### 2.3.5 N-THIOSEMICARBAZIDE FERROCENYLIMINE (L4)

This is an alternative preparation to that reported in the literature [54].

To ferrocene monocarboxaldehyde (1.50g, 7.00 mmol), dissolved in dry benzene, thiosemicarbazide (0.64 g, 7.00 mmol) was added. The solution was refluxed for 2.5 hours in an argon atmosphere, cooled and the volume reduced, using a rotary evapourator, until a red precipitate started to form. The solution was filtered and the red/brown precipitate which formed on standing was recrystallized from ethanol.

Yield: 60% (1.20 g), M.P. 190°C

Found: C, 50.40; H, 4.74; N, 14.84

Calculated for ($C_{12}H_{13}N_3SFe$)

C, 50.17; H, 4.53; N,14.63

**NMR($CDCl_3$) $^1H$ Δ (ppm):**

9.93 (s, 1H , N<u>H</u> ); 7.83 (s, 1H, C<u>H</u>=N); 7.21 (s, 1H , N<u>H</u>$_2$); 6.37 (s, 1H , N<u>H</u>$_2$), 4.58 (t, J = 1.8 Hz , 2H , $C_5$<u>H</u>$_4$); 4.43 (t, J = 1.8 Hz , $C_5$<u>H</u>$_4$); 4.21 (s, 5H, $C_5$<u>H</u>$_5$).

**$^{13}C\{^1H\}$ Δ (ppm):**

177.18 (<u>C</u>=S) , 145.38 (<u>C</u>=N) , 145.26 (<u>C</u>=N) , 76.53 ($\underline{C}_5H_4$) , 71.56 ($\underline{C}_5H_4$) , 70.61($\underline{C}_5H_4$) , 69.70 ($\underline{C}_5H_5$) , 69.08 ($\underline{C}_5H_5$) , 68.15 ($\underline{C}_5H_4$) , 67.68 ($\underline{C}_5H_4$).

**IR ($cm^{-1}$)** (nujol mull, NaCl disk):

3407 s, 3238 s , 3146 s br, 1600 s , 1530 s , 1373 s , 1330 m , 1291m , 1246 m , 1166 w , 1163 m , 1048 w , 993 m , 772m.

### 2.3.6 BIS - N-(*0* -HYDROXYBENZYLIDENE) FERROCENYLIMINE (L11)

To 1,1'-ferrocene dicarboxaldehyde (0.30g , 1.20 mmol) in 150 ml dry benzene was added 2-aminophenol (0.27g , 2.4 mmol) dissolved in 30 ml benzene. The mixture was stirred under reflux in an argon atmosphere for five hours using a Dean Stark apparatus. The solvent was removed using a rotary evaporator until an oil appeared. The oil was dissolved in a minimum amount of chloroform and chromatographed on a silica gel column (70-400*um* mesh) using a 10% methanol, 90% dichoromethane solvent mixture as eluent. The second band was collected and the volume reduced using a rotary evaporator until a red crystalline precipitate formed. (The first band was unreacted starting material.)

Yield: 55% (0.28 g), M.P. 176-177°C

Found: C, 66.75; H, 4.71; N, 6.41

Calculated for ($C_{24}H_{20}N_2O_2Fe$)

C, 67.94; H, 4.75; N, 6.59

**NMR($CDCl_3$) $^1H$ Δ (ppm):**

4.78 (t, J = 1.8 Hz, 2H, $C_5\underline{H}_4$); 4.56 (t , J = 1.8 Hz, 2H, $C_5\underline{H}_4$); 8.44 (s , 1H , C<u>H</u>=N); 6.98 (d, J = 6.6 Hz, 1H, $C_6\underline{H}_4$); 6.81 (t, J = 6.6Hz, 1H, $C_6\underline{H}_4$); 7.13 (t, J = 6.6 Hz, 1H, $C_6\underline{H}_4$); 6.93 (d, J = 6.6 Hz, 1H, $C_6\underline{H}_4$); (The OH group proton is in flux and not detected).

**$^{13}C$ {$^1H$} Δ (ppm):**

71.23 ($\underline{C}_5H_4$) , 72.39 ($\underline{C}_5H_4$) , 80.91( $\underline{C}_5H_4$) , 159.39 (<u>C</u>=N) , 137.19 ($\underline{C}_6H_4$) , 151.15 ($\underline{C}_6H_4$) , 116.53 ($\underline{C}_6H_4$) , 120.10 ($\underline{C}_6H_4$) , 127.91 ($\underline{C}_6H_4$) , 115.36 ($\underline{C}_6H_4$).

**IR ($cm^{-1}$)** (nujol mull , NaCl disk) :

1618 s , 1577 w , 1460 s , 1280 s , 1250 s , 1219 m , 1165 s , 1095 m , 968 w , 932 w , 874 m , 827 s , 757 s.

### 2.3.7 BIS -N-(*O* -HYDRAZONYLPYRIDINE) FERROCENYLIMINE (L 22)

To a solution of 1,1'-ferrocene dicarboxaldehyde (0.134g, 0.55mmol) dissolved in 60 ml of benzene was added 2-hyradrazinopyridine (0.121g, 1.1mmol) in 40ml dry benzene. The mixture was refluxed in an argon atmosphere for two hours using the Dean Stark apparatus. On cooling to room temperature excess solvent was removed using a rotary evaporator to give an oil. Chloroform was added in excess and the oil triturated for three-four minutes after which time a red precipitate formed. The solution was then filtered.

Yield: 0.08 g (37%), M.P. > 300°C

Found: C, 61.56; H, 4.64; N,19.53

Calculated for ($C_{22}H_{20}N_6Fe$)

C, 62.28; H, 4.75; N, 19.80

**NMR $^1H$ ( $d_6$-dmso) Δ (ppm):**

4.36 (t, J =1.6 Hz, 2H , $C_5\underline{H}_4$); 4.59 (t, J = 1.8 Hz, 2H, $C_5\underline{H}_4$); 6.66 (t, J = 3.5 Hz, 1H, $C_5\underline{H}_4N$); 7.04 (d, J = 4.2 Hz, 1H, $C_5\underline{H}_4N$); 7.51 (t, J = 3.5 Hz, 1H $C_5\underline{H}_4N$); 8.04 (d, J = 3.7 Hz, 1H , $C_5\underline{H}_4N$); 7.75 (s , 1H , C<u>H</u>=N) , no appearance of NH at 298 K .

**NMR{$^1H$}$^{13}C$ Δ (ppm):**

74.22 ($\underline{C}_5H_4$), 71.38($\underline{C}_5H_4$), 85.96 ($\underline{C}_5H_4$), 142.32 (<u>C</u>=N), 160.99 ($\underline{C}_5H_4N$), 110.03 ($\underline{C}_5H_4N$), 141.54 ($\underline{C}_5H_4N$), 118.15 ($\underline{C}_5H_4N$), 151.53 ($\underline{C}_5H_4N$)

**IR ($cm^{-1}$)** (nujol mull, NaCl disk):

3185 w br , 1598 s , 1538 s , 1329 m , 1375 m , 1303 m , 1239 m , 1205 m , 1128 s , 1084 m , 1024 w , 991 w , 940 w , 899 w , 818 m , 763 s.

### 2.3.8 BIS -N- (THIOSEMICARBAZIDE) FERROCENYLIMINE (L44)

To 1,1'-ferrocene dicarboxaldehyde (2mmol,0.426g) in 80 ml of toluene was added thiosemicarbazide (0.18g, 4.00 mmol). The solution was then refluxed for 6 hours in an argon atmosphere. On cooling the solution the solvent was removed using a rotary evaporator until a red precipitate started to form. The red product was filtered and recrystallized from 30 ml ethanol.

Yield: 56% (0.16g); M.P. > 300°C

Found: C, 43.80; H, 4.03 ; N, 20.42

Calculated for ($C_{14}H_{16}N_6S_2Fe$)

C , 43.30 ; H, 4.10 ; N , 21.64.

**NMR$^1$H ($CDCl_3$)Δ (ppm):**

8.06 (t, J = 1.9 Hz, 1H, N$\underline{H}_2$); 7.81 (s, 1H, C$\underline{H}$=N); 7.64 (t, J =1.1 Hz, 1H, N$\underline{H}_2$); 4.71 (d, J = 1.0 Hz, 2H, $C_5\underline{H}_4$); 4.39 (d, J = 1.1 Hz, 2H, $C_5\underline{H}_4$).

**NMR$^{13}$C{1H}Δ (ppm):**

67.98, ($\underline{C}_5H_4$); 70.75, ($\underline{C}_5H_4$); 79.49, ($\underline{C}_5H_4$); 42.09, ($\underline{C}$=N); 176.42, ($\underline{C}$=S).

**IR ($cm^{-1}$)** (nujol mull, NaCl disk)

3489 w br, 3271 m br , 3140 m br , 2044 s br , 1647 w , 1581 s , 1536 s , 1326 m , 1272 m , 1249 w , 1097 w , 1023 w , 935 w , 835 w , 822 w , 760 w.

# RESULTS AND DISCUSSION

## 2.4 SINGLE CRYSTAL X-RAY DISCUSSION OF THE LIGAND L11

The structure of L11 is depicted in diagrams 2.1 and 2.2 which also gives the numbering system used. Hydrogen atoms are numbered according to the atoms to which they are attached. Selected bond lengths and angles are listed in Table 2.2.

The molecule consists of discrete monomeric units with two substituted phenol residues in a chiral arrangement facing each other. Both of the phenol residues are bonded to the ferrocene moiety via the carbon atom of a Schiff base moiety. The geometry of the organometallic residue is very similar to that observed in other bis substituted ferrocene structures [56,75]. The two cyclopentadienyl rings are approximately parallel to each other (dihedral angle 0.85(0.77)°) as expected, in comparison with the 1.0-1.66°[56,75] reported for other substituted ferrocene systems. The ferrocene framework is approximately eclipsed with a small twist angle of approximately 1.0° which is in accord with other previous 1,1'-disubstituted ferocene studies [82, 83]. However the substituents on C(31) and C(11) are not eclipsed since one has been shifted by one carbon atom from the superimposed position (diagram 2.2).

The planes through the two organic "tethers", consisting of atoms C(36), N(21), C(37) in one and C(16), N(11), C(17) in the other, lie at angles 15(1)° and 13(1)° respectively from those of their associated cyclopentadienyl rings. Each of the phenol rings, C(37-42) and C(17-22) lies at an angle of 71.9(0.3)° and 70.5(0.4)° respectively to that of their associated cyclopentadiene rings C(31-35) and C(11-15). This approximately orthogonal geometry of the two phenol rings relative to their cyclopentadienyl rings works against conjugation between the two aromatic moieties. The bond lengths and angles of the cyclopentadienyl rings (C-$C_{ave}$ 1.41Å; C-C-$C_{ave}$ 108.0°) lie within reported C-$C_{ave}$ bond lengths (1.42-1.48Å) and C-C-$C_{ave}$ bond angles of 108.0(8)° [75]. The Fe-C distances range between 2.01(1)-2.08(1)Å and compare well with reported data of 2.07Å [56] and 2.05(1) [75] for other di substituted ferrocenes.

The planes of the two phenol rings C(37-42) and C(17-22) are at an angle of 81.4(0.3)° to one other and are in an 'anchored' geometry through O-H·····N intramolecular hydrogen bonding. This occurrs between the O(11) hydrogen atom on the C(17-22) phenol ring and the N(21) nitrogen atom in the "tether" between the C(31-35) cyclopentadiene and the C(37-42) phenol rings. This N····O bond distance is 2.85(0.01)Å and the corresponding H···N length is 2.06(0.01)Å. Another intramolecular hydrogen bond also occurs between the O(21) hydrogen H(21) atom of the C(37-42) phenol ring and the N(11) nitrogen atom of the organic "tether" between the C(17-22) phenol and the C(11-15) cyclopentadiene rings. This N····O distance is 2.80(0.01)Å and the corresponding O-H····N bond distance is 2.04(0.01)Å (diagram 2.2)

The bond lengths between the Schiff base atoms C(16) and N(11) and C(36) and N(21) appear to differ from one another (1.24(1)Å; 1.31(1)Å respectively). However in view of the range of values observed for the distances within the aromatic moieties it seems unlikely that these differences indicate a significant difference in bond type. The average of the two values is in accord with the data presented in Table 2.1

**Table 2.1 A Comparison of X-ray data C=N Bond lengths**

| compound | C=N (Å) | ref |
|---|---|---|
| L21 | 1.28 | this work |
| HL@ | 1.278(11) | [24] |
| L1! | 1.269(5) | [27] |
| 1,1-bispyridylhydrazone | 1.289 | [56] |
| 5OHFPTSC* | 1.270 | [77] |
| ATSC# | 1.286 | [77] |

@ N-(o-hydroxybenzylidene)ferrocenamine
! 1-benzyl ferroceneimide
* 5-hydroxy-2-formylpyridine thiosemicarbazone
# acetone thiosemicarbazide

Similar arguments apply to the bond lengths C(31)-C(36), C(11)-C(16) (1.40(1)Å; 1.50(1)Å) and those of lengths N(11)-C(17) (1.46(9)Å) and N(21)-C(37) (1.40(1)Å). As a result it can be concluded that little electron delocalisation between the phenol and the cyclopentadienyl moieties occurs. The average $C\text{-}C_{phenyl}$ bond lengths are 1.372Å for the C(37-42) ring and 1.355Å for the C(17-22) ring, both being in accord with those in other six carbon aromatic systems (1.395(3)Å)[86].

**Table 2.1**

**Selected bond lengths [Å] and angles [°] forL11**

| | |
|---|---|
| O(11)-C(18) | 1.290(11) |
| O(21)-C(38) | 1.433(12) |
| N(11)-C(16) | 1.235(11) |
| N(11)-C(17) | 1.459(9) |
| N(21)-C(36) | 1.311(10) |
| N(21)-C(37) | 1.396(10) |
| C(11)-C(16) | 1.506(12) |
| C(31)-C(36) | 1.402(13) |
| | |
| C(16)-N(11)-C(17) | 116.1(8) |
| C(36)-N(21)-C(37) | 118.4(7) |
| C(15)-C(11)-C(12) | 108.1(9) |
| C(15)-C(11)-C(16) | 127.8(10) |
| N(11)-C(16)-C(11) | 122.4(9) |
| C(22)-C(17)-N(11) | 120.0(8) |
| C(18)-C(17)-N(11) | 117.4(7) |
| O(11)-C(18)-C(17) | 124.6(7) |
| O(11)-C(18)-C(19) | 119.4(8) |
| N(21)-C(36)-C(31) | 124.6(9) |
| C(38)-C(37)-N(21) | 118.2(8) |
| N(21)-C(37)-C(42) | 125.5(8) |
| C(39)-C(38)-O(21) | 115.8(9) |
| C(37)-C(38)-O(21) | 120.6(8) |

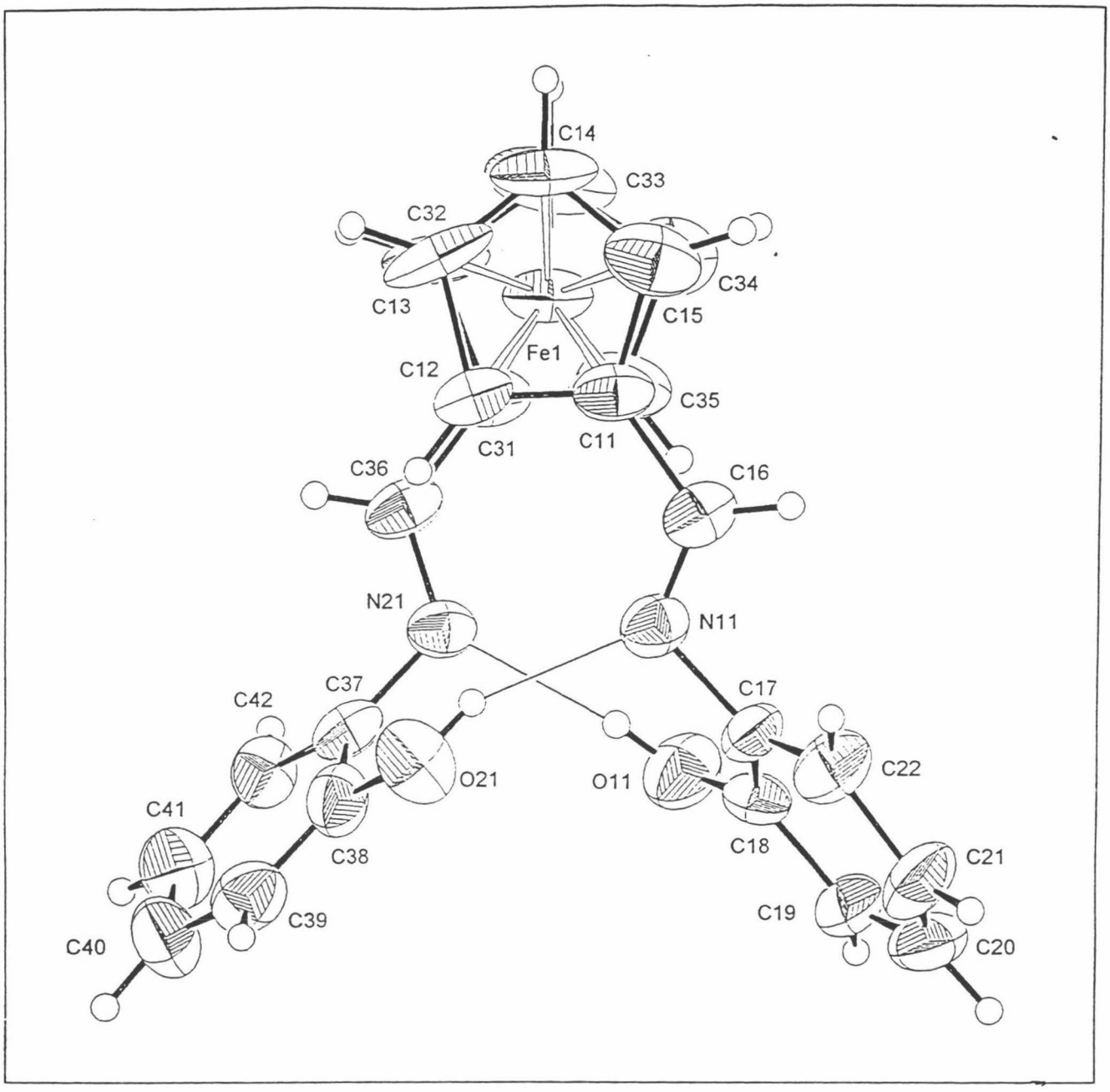


**Diagram 2.1.** ZORTEP diagram of L11 showing the intramolecular bonding. Thermal ellipsoids are shown where non-hydrogen atoms are drawn at the 50% probability levels. Those for hyrogen are drawn at arbitary levels for reasons of clarity.

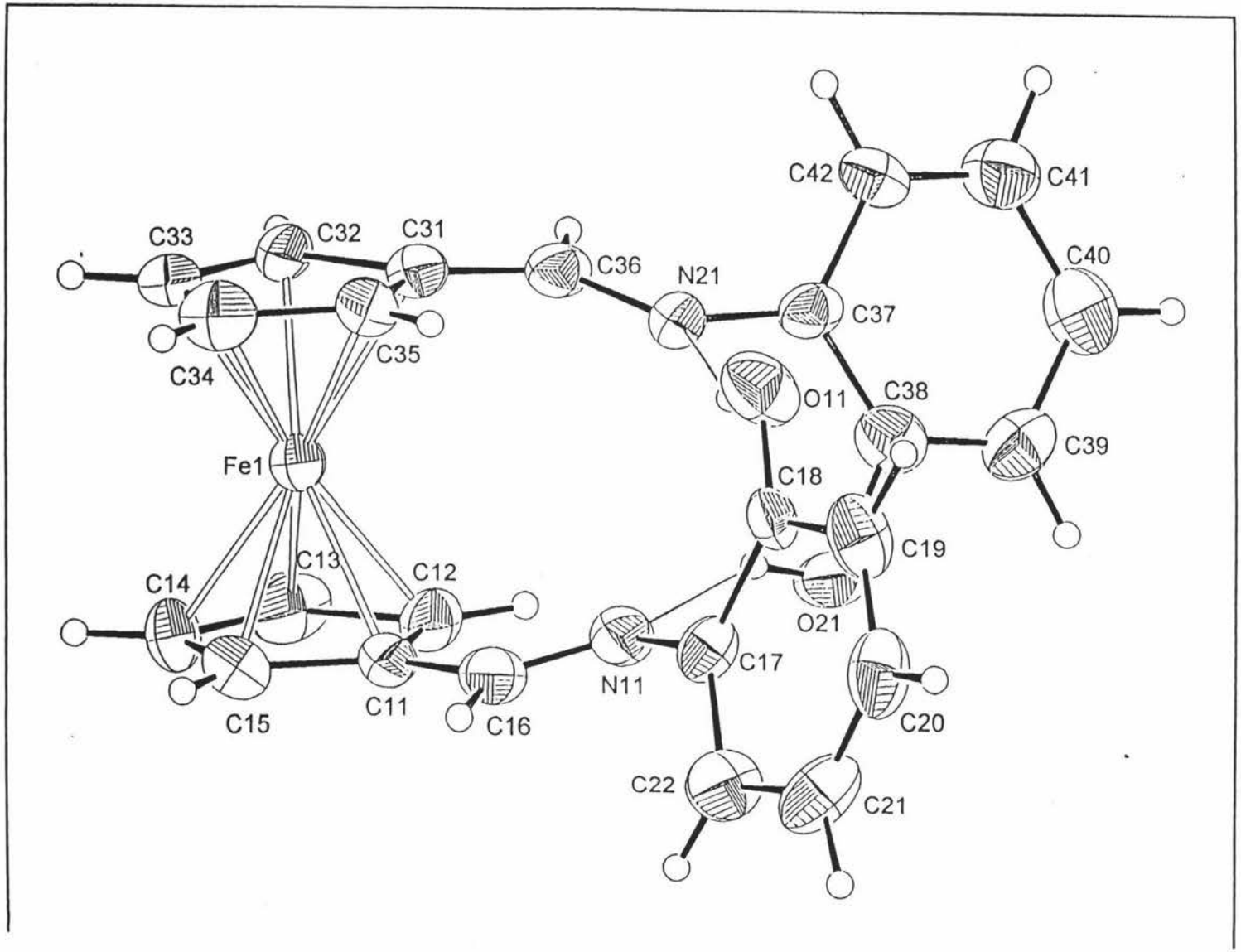


**Diagram 2.2.** ZORTEP diagram of L11 where thermal ellipsoids are shown for non-hydrogen atoms are drawn at the 50% probability levels. Those for hydrogen are drawn at arbitary levels for reasons of clarity.

### 2.5.1 (a) DISSCUSSION OF THE $^1H$ SPECTRUM OF L1

The detailed spectral results are given in the Experimental Section 2.3.1. These assignments are discussed below.

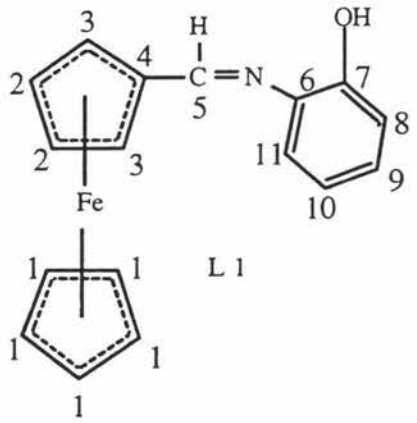


The structure depicted above gives the proton numbering scheme for L1.

The H(1) cyclopentadienyl ring protons (integral 5) resonated at 4.23 ppm. The H(2) protons, at 4.52 ppm integrated as 2 protons as did the H(3) protons, at 4.80 ppm. This pattern for the ferrocene moiety has been observed before and the relative chemical shifts appear to be within reported literature values [39,54,55].

The imine proton H(5) at 8.59 ppm which integrates as one, has moved to a lower frequency to 1.4 ppm from the aldehyde proton in the ferrocene carboxaldehyde parent.

The aromatic proton chemical shifts were assigned with the aid of a $^1H$ x $^{13}C$ (HETCOR) spectrum, shown in **Fig 2.17**. An expansion of the spectrum of the aromatic protons, which relates to the following discussion is given in **Fig 2.18**. The four protons on the phenol ring give a distinctive splitting pattern (triplet, doublet, triplet, doublet) with each showing further coupling. The triplet of doublets at 6.88 ppm ($^2J$ = 7.7 Hz), integrates as one proton and was assigned as H(9). Secondary splitting ($^3J$ = 1 Hz) was associated with cross coupling with H(11). The doublet of doublets at 6.98 ppm ($^2J$ = 8.1 Hz) was assigned to H(11) and this integrated as a single proton, with secondary splitting $^3J$ = 1 Hz. A triplet of doublets at 7.16 ppm ($^2J$ = 7.7 Hz) was assigned to H(10) and this integrated as a single proton, as did the doublet of doublets at 7.23 ppm ($^2J$ = 8.1 Hz) assigned to H(8).

### 2.5.1 (b) DISCUSSION OF THE $^{13}C$ SPECTRUM OF L1

The cyclopentadienyl carbons have been assigned in accord with those found by Roberts *et al.* [56]. The cyclopentadienyl carbons β C(3) at 68.90 ppm are found at a higher frequency relative to the α C(2) carbons at 71.56 ppm, indicating electron withdrawal by the substituted organic moiety. The C(1) carbons of the unsubsituted ring are all equivalent and appear between the peaks of C(3) and C(2) at 69.31ppm. The C(4) carbon is located at 80.11ppm. This is at a higher frequency from the C(3) carbons even though apparent electron withdrawal would be experienced. However, the C(4) may also experience deshielding from the electromagnetic field that is generated by the imine bond. The resultant effect is that the C(4) carbon is moved to a higher frequency from that of the C(3) carbon. These observations are consistent with all the other carbon $^{13}C$ mono-substituted ligand spectra. The imine carbon C(5) appears at 158.78ppm. The phenol ring has been assigned by the cross correlation of the $^{1}H$ x $^{1}H$ (COSY) spectrum (**Fig 2.27**) of L 11 and the $^{1}H$ x $^{13}C$ (HETCOR) spectrum of L1 (**Fig 2.17**). The two quaternary carbons C(6) and C(7) appear at chemical shift positions 136.58ppm and 151.44ppm. As expected the carbons 8, 9, 10 and 11 are all doublets in the coupled spectrum and appear at chemical shift positions, 115.61, 119.96, 127.60 and 114.72ppm respectively.

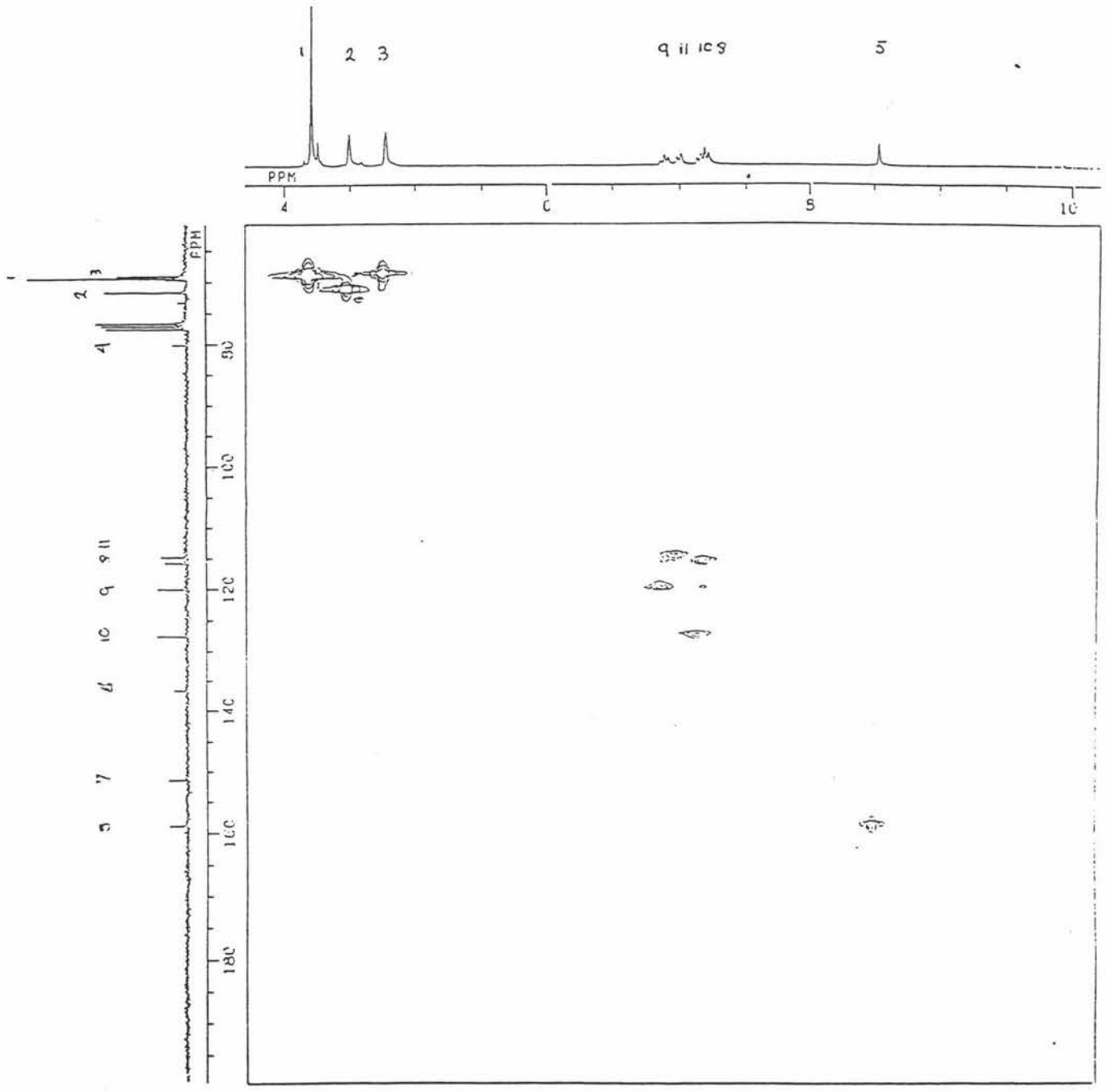


**Fig 2.17**

$^{1}H$ x $^{13}C$ (HETCOR) spectrum of L1 in $CDCl_3$.

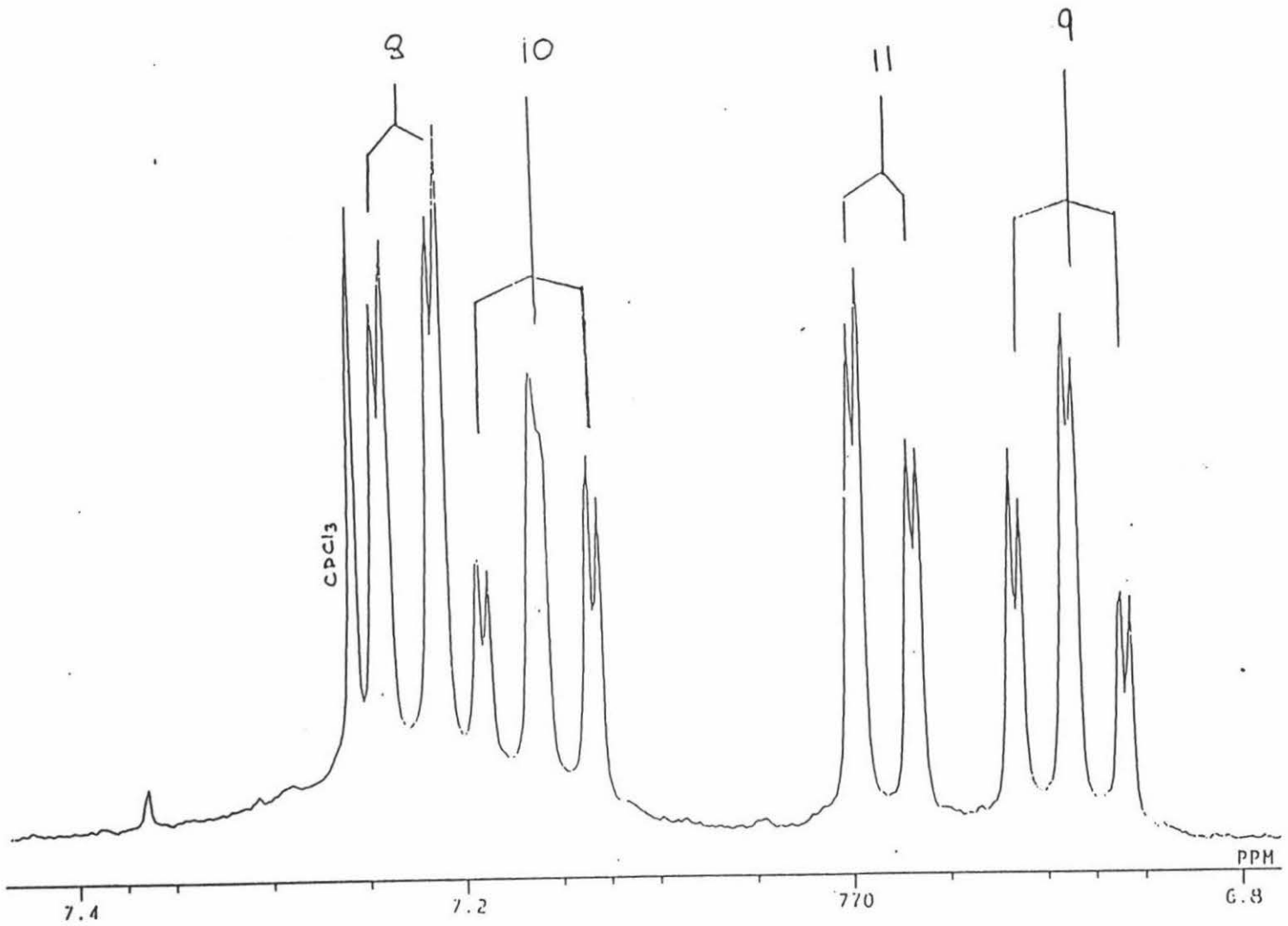


**Fig 2.18**

$^1$H NMR expansion of the aromatic region (6.8-7.4 ppm) of the spectrum of L1.

### 2.5.1 (a) DISCUSSION OF THE $^1H$ SPECTRUM OF L2

The detailed spectral results are given in the Experimental Section 2.3.2. These assignments are discussed below.

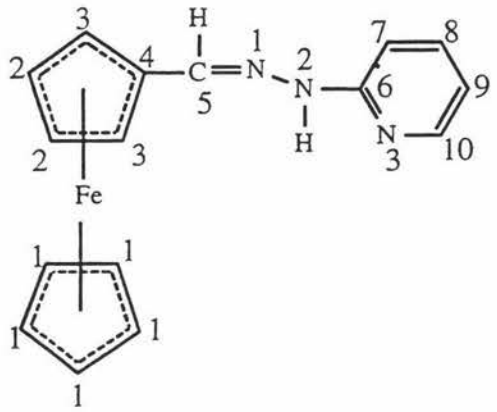


The proton numbering scheme is depicted in the structure above.

The splitting patterns for the ferrocene moiety are as reported for L1 with chemical shift values of 4.19, 4.34, 4.59 ppm for protons 1, 2 and 3 respectively.

The imine proton H(5)(7.60 ppm) has moved up field from the ferrocene carboxaldehyde standard by (2.36 ppm). This could be attributed to the general weak delocalisation as has been reported by Houlton et al. [56] in the "tether" atom C(5), N(1), N(2) which provides more shielding relative to the proton on the aldehyde. The N(2) proton appears as a broad singlet at 8.45 ppm and integrates as a single proton. The protons on the pyridine ring have been assigned with the aid of the $^1H$ x $^{13}C$ (HETCOR) spectrum **(Fig 2.19)** and the $^1H$ x $^1H$ (COSY) spectrum of L3 **(Fig 2.20)**. The expanded aromatic region is shown in **Fig 2.21.** The splitting pattern observed for the $^2J$ coupling of the aromatic protons is a triplet, doublet, triplet, doublet in a 1:1:1:1 integrated ratio. The triplet 6.74 ppm ($^2J$ = 5.5 Hz) is due to H(8) with a doublet at 7.26 ppm for H(7). In very close proximity to each other is a triplet and a singlet. The triplet at 7.58 ppm is due to H(9) and the singlet to the imine proton. The doublet at 8.11 ppm is assigned to H(10). Secondary coupling is not well resolved.

### 2.5.2 (b) DISCUSSION OF THE $^{13}C$ SPECTRUM OF L2

The chemical shift assignments of the cyclopentadienyl carbons are in accord with those found by Roberts *et al.* [56]. The cyclopentadienyl carbons C(1) are located at 69.02ppm. The C(2) carbons are located at 69.54 ppm whereas those for C(3) are found at 66.95 ppm. The quaternary carbon C(4) is located at 80.25 ppm, the imine carbon (5) is at 139.20 ppm. Pyridine carbon chemical shifts have been assigned with the aid of the assigned spectra of 2-aminopyridine [89], $^{13}C$ Tables by Kemp [90] and cross correlated with the $^{1}H$ x $^{13}C$ (HETCOR) spectrum (**Fig 2.19**) of L2. Carbons C(7), C(8), C(9) and C(10) of the pyridine ring all appear as doublets in the coupled spectrum and are located at chemical shifts position 107.32, 138.02, 115.07 and 147.35 ppm. The quaternary C(6) carbon is located at 156.96 ppm respectively.

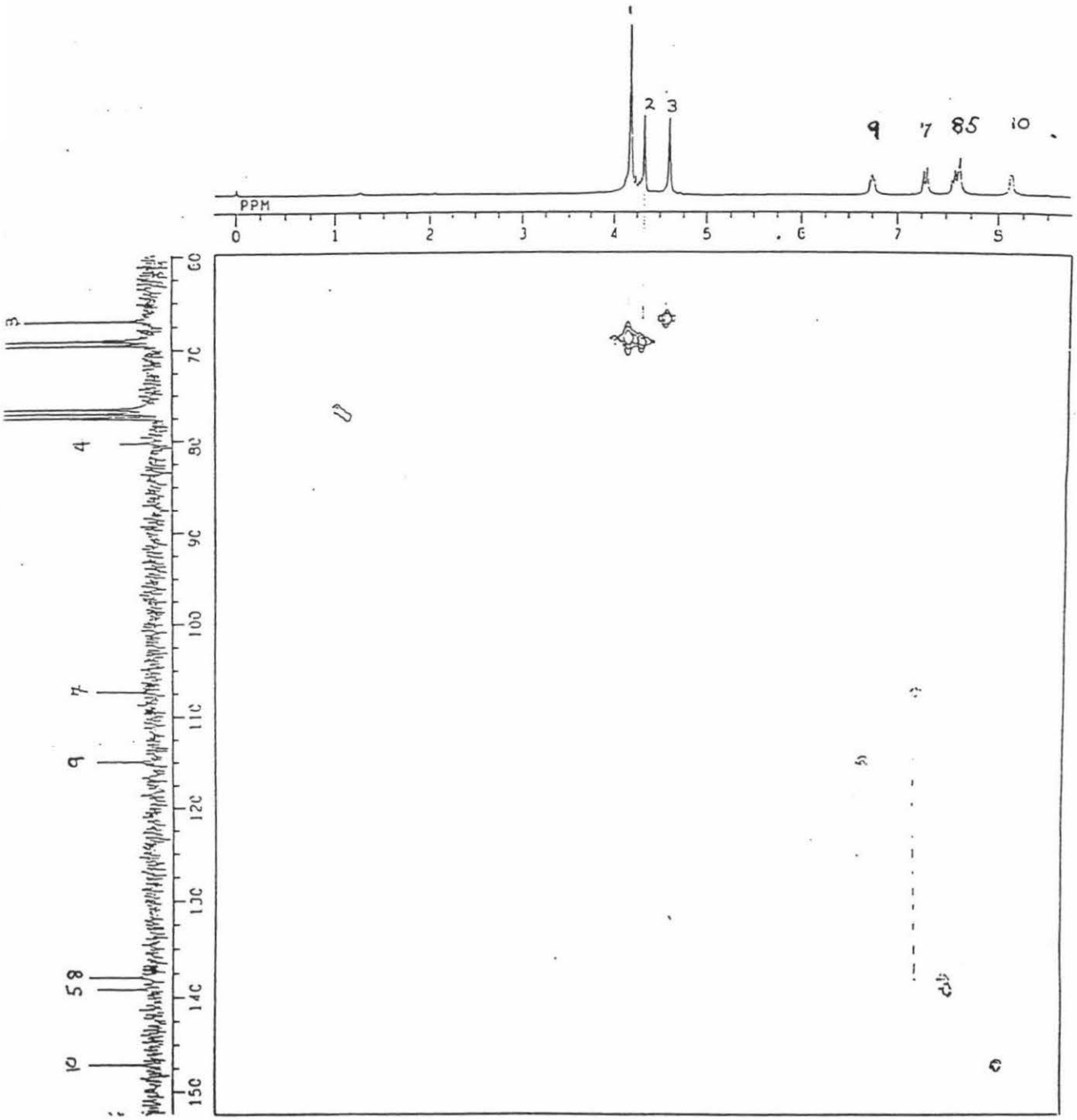


**Fig 2.19**

$^{1}H$ x $^{13}C$ (HETCOR) spectrum of L2 in $CDCl_3$.

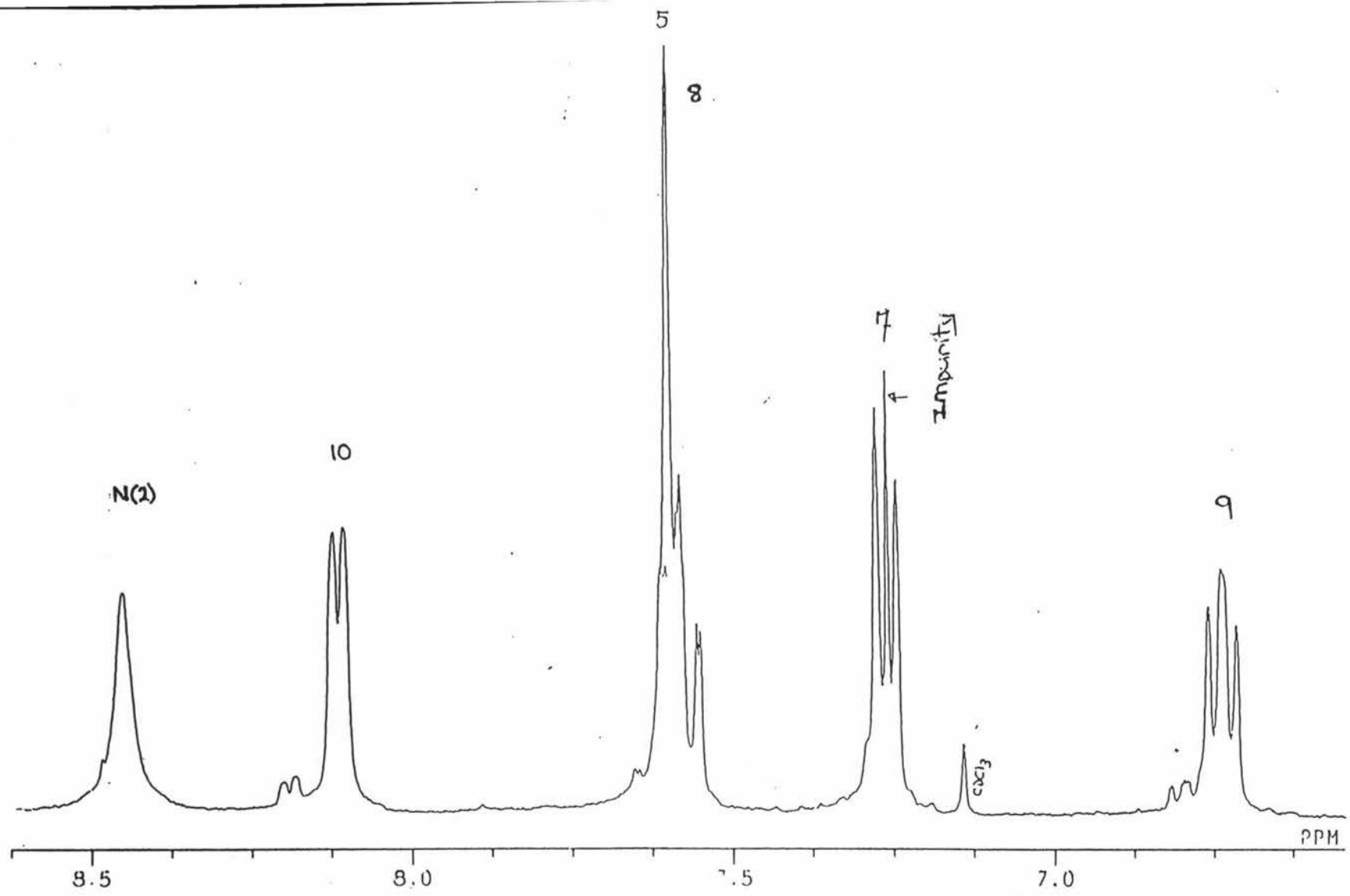


**Fig 2.21**

Expansion of L2 $^1$H NMR spectrum of the region 6.5-8.5 ppm in $CDCl_3$.

## 2.5.3 (a) DISCUSSION OF THE $^1H$ SPECTRUM OF L3

The detailed spectral results are given in the Experimental Section 2.3.4. These assignments are discussed below.

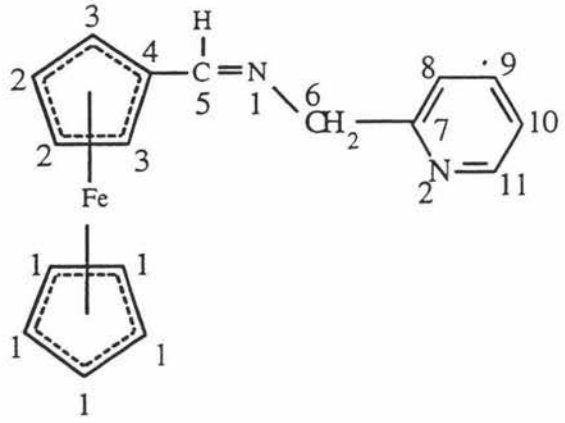


The proton numbering scheme for L3 is as depicted above. The ferrocene moiety has a splitting pattern as reported in L1 with chemical shifts positions at (4.18, 4.38, 4.70 ppm) for protons 1 , 2 and 3 respectively. The imine proton H(5) at 8.43 ppm is a singlet which integrates as 1 proton and is found at a lower frequency (1.53 ppm) than that of the ferrocene carboxaldehyde parent. The aromatic pyridine protons have been assigned by the use of $^1H$ x $^1H$ (COSY) (**Fig 2.20**) and $^1H$ x $^{13}C$ (HETCOR) (**Fig 2.22**) spectrum. The $^2J$ coupling constant splitting patterns observed are consistent with the pyridine ring of L2. The triplet, doublet, triplet, doublet protons integrate as a 1:1:1:1 proton ratio. The first triplet is associated with H(10) (7.17 ppm: $^2J$ = 4.0 Hz) and can clearly be seen to be coupled to both H(11) and H(9) in **Fig 2.20**. The doublet at 7.37 ppm H(8) has $^2J$ = 7.7 Hz and is only coupled to H(9). The H(9) proton is a triplet at 7.66 ppm with $^2J$ = 7.3 Hz and is also coupled to both protons of H(8) and H(10). Proton H(11) is a doublet at 8.56 ppm ($^2J$ = 4.0 Hz) and it is coupled to H(10).

### 2.5.3 (b) DISCUSSION OF THE $^{13}C$ NMR SPECTRUM OF L3

The ferrocenyl moiety was assigned in accord with data reported by Roberts *et al.* [56] with C(1) carbons at 68.91 ppm, C(2) carbons at 70.35 ppm and the chemical shift positions of C(3) at 68.42 ppm. The quaternary carbon C(4) is located at 80.05 ppm. The C(5) imine carbon is located at chemical shift position of 163.22 ppm and is reported as a doublet in the coupled spectrum. The methyl carbon C(6) appears at 66.75 ppm and coupled spectrum is a triplet but the resolution is impaired because of the ferrocenyl carbons. The pyridine ring carbons were assigned with aid from the assigned spectrum of α-picoline ($C_6H_7N$) [89] and the $^1H$ x $^{13}C$ (HETCOR) spectrum (**Fig 2.22**) of L3. The pyridine carbons with the exception of the quaternary carbon, C(7), at 159.19 ppm, all appear as doublets in the coupled spectrum. Carbon C(8) is located at 121.95 ppm, C(9) at 136.37 ppm and carbons C(10) and C(11) at 121.69 ppm and 149.05 ppm respectively.

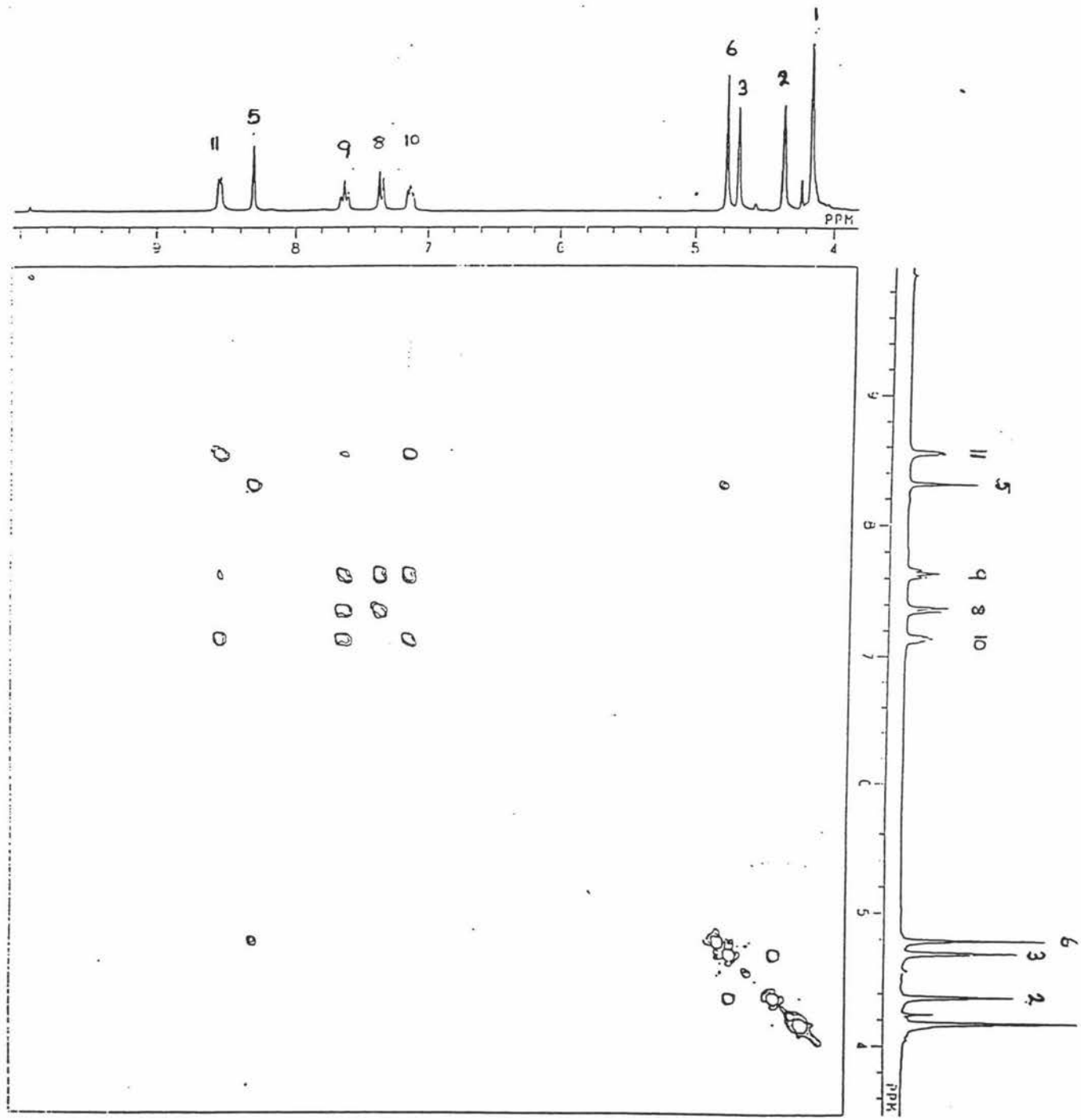


**Fig 2.20**

$^{1}H$ x $^{1}H$ (COSY) spectrum of L3 in $CDCl_3$.

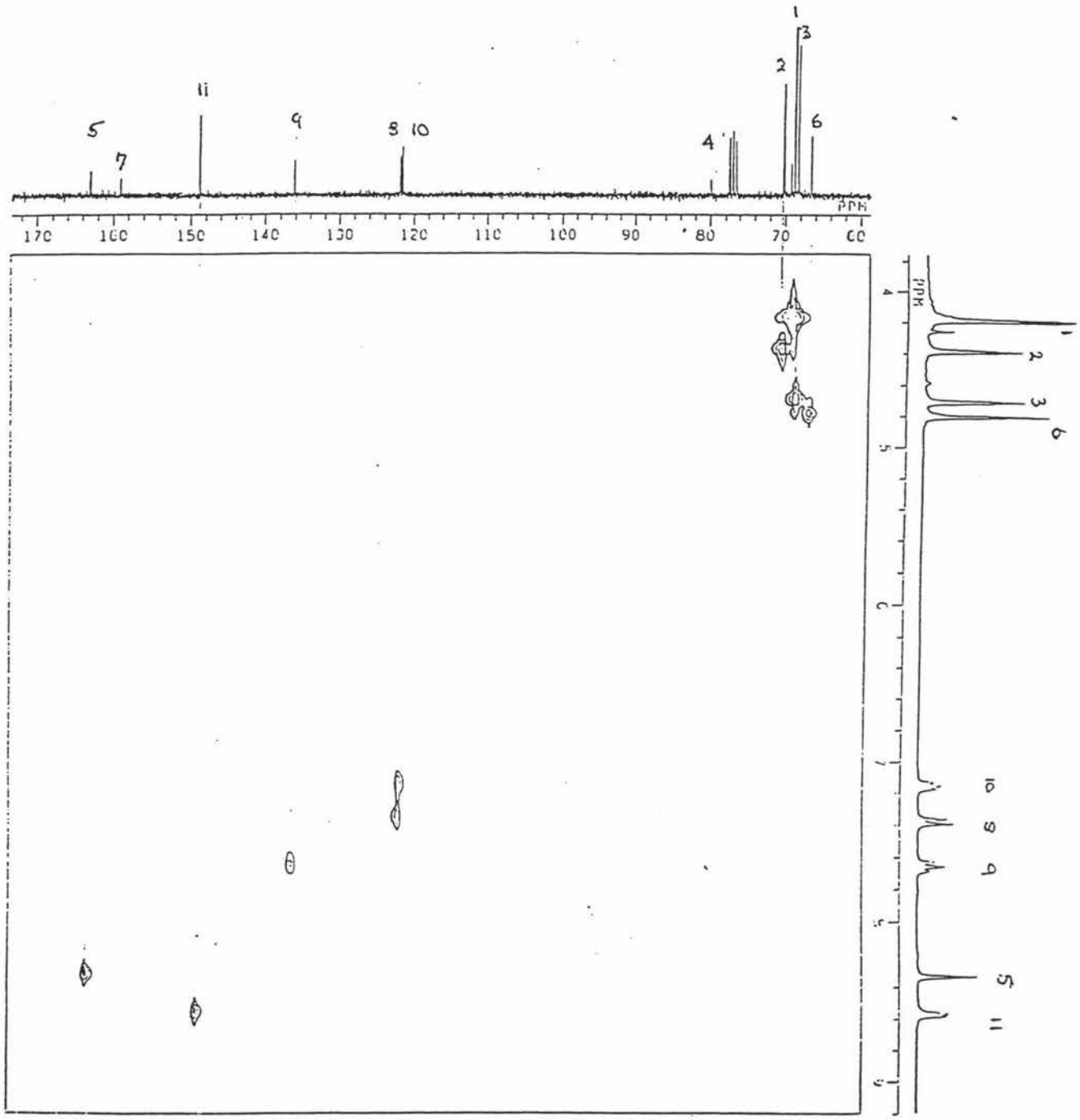


**Fig 2.22**

$^{1}H$ x $^{13}C$ (HETCOR) spectrum of L3 in $CDCl_3$.

### 2.5.4 (a) DISCUSSION OF THE $^1$H SPECTRUM OF L4

The detailed spectral results are given in the Experimental Section 2.3.5. These assignments are discussed below.

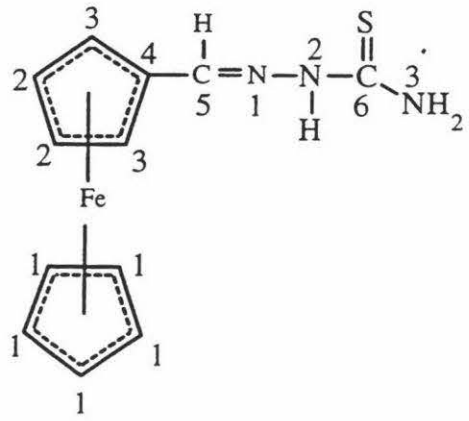


The numbering scheme is as depicted above and $^1$H NMR spectrum is displayed in **Fig 2.23.** The proton NMR of the ferrocene moiety is the same as observed for for the other ligands, chemical shifts being H(1, 4.21 ppm), H(2, 4.38 ppm), and H(3, 4.59 ppm). The imine proton H(5, 7.83 ppm) is found at a lower frequency, with marked shift of 2.1 ppm compared with the ferrocene carboxaldehyde parent and integrates as a single proton. The two protons on N(3) integrate as two separately spaced broad singlets at 8.06 ppm and 7.64 ppm in a 1:1 ratio. This indicates that these protons are not in equivalent environments which is consistent with the findings from other results [65]. This inequivalence may be attributed to partial double bond character arising from electron delocalisation in the thiosemicarbazide system and/or hydrogen bonding which causes hindered rotation of the C(6) -N(3) bond. The N(2) proton integrates as 1 proton at chemical shift position (9.92 ppm).

## 2.5.4 (b) DISCUSSION OF THE $^{13}C$ SPECTRUM OF L4

The cyclopentadienyl carbons of the ferrocene moiety have been assigned in accord with those found by Roberts *et al.* [56]. The carbons of C(1), C(2) and C(3) unexpectedly appear as doublets in the decoupled spectrum, and are located at chemical shift positions centred at 69.34 ppm, 70.85 ppm and 67.85 ppm. The C(4) quaternary carbon resonates at 76.52 ppm and tentatively assigned as a singlet, but this region of the spectrum is obscured by overlapping $CDCl_3$ solvent peaks. The doubling up of carbon peaks is consistent with isomers of the ligand, as found in the spectra of L5 and isomers of thiosemicarbazide based ligands [65]. **Fig 2.24** shows the two possible cis and trans isomers possible. The spectrum of L4, is shown in **Fig 2.23.**

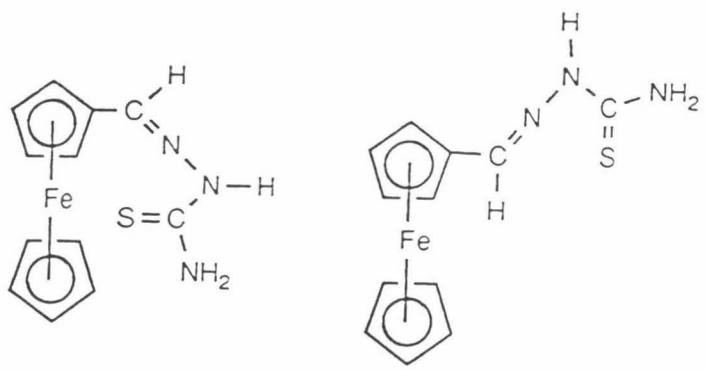


**Fig 2.24**

The C(6) carbon appears as a singlet at 177.18 ppm and this is consistent with cis-trans isomerisation where the carbon is in identical environments.

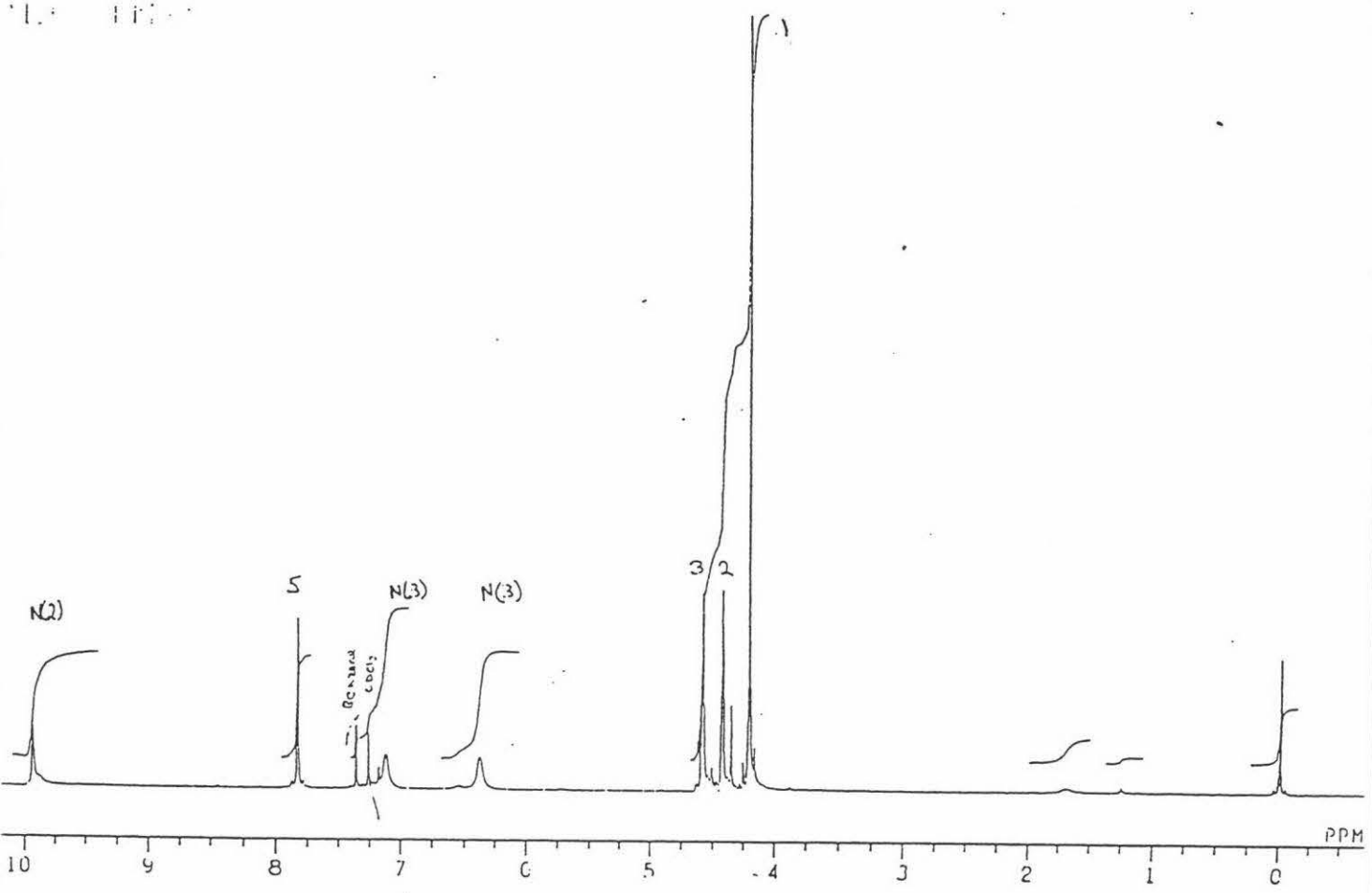


**Fig 2.23**

NMR spectra of L4 in $CDCl_3$.

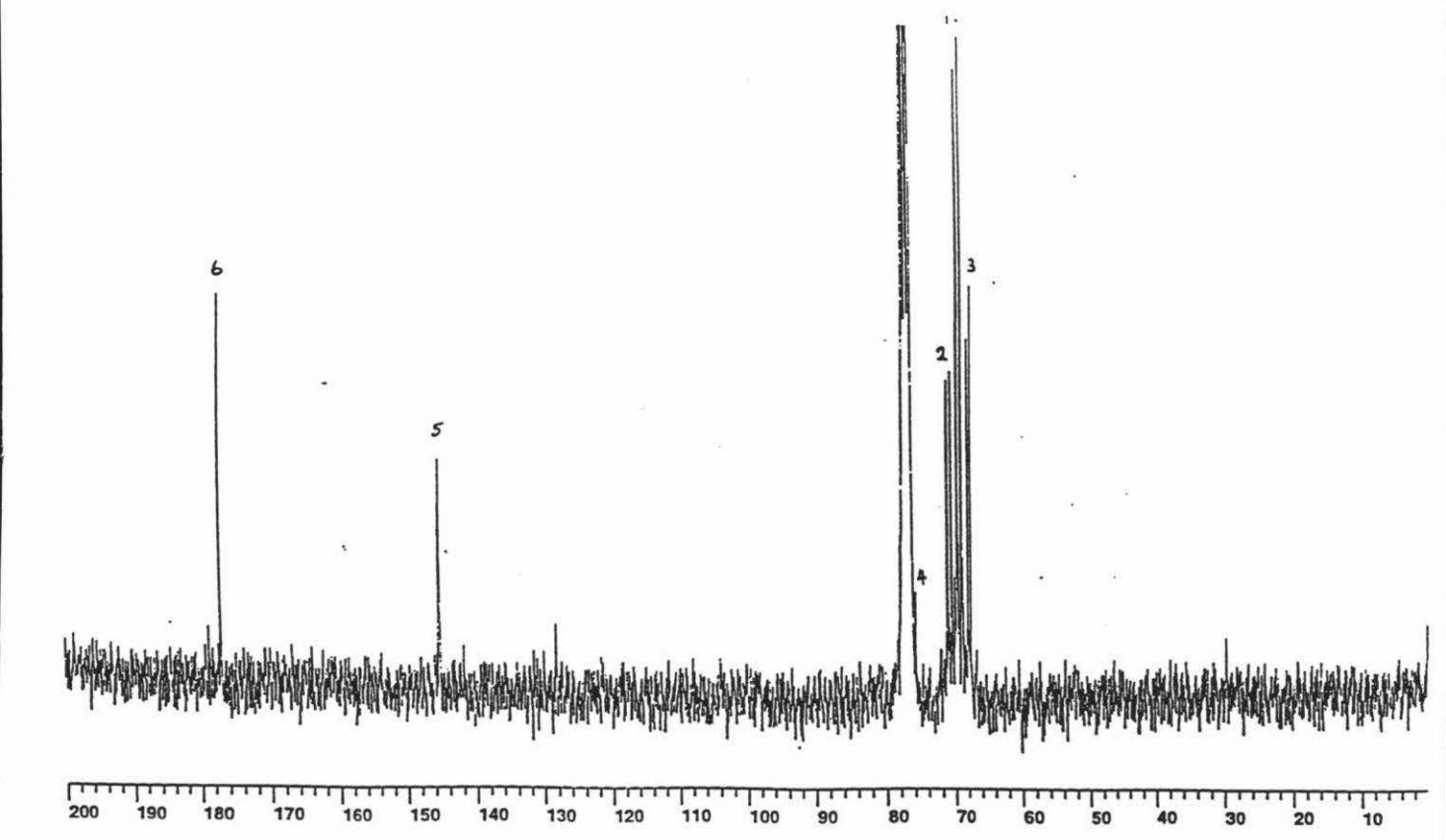

## 2.5.5 (a) DISCUSSION OF THE $^1H$ SPECTRUM OF L 11

The detailed spectral results are given in the Experimental Section 2.3.6. These assignments are discussed below.

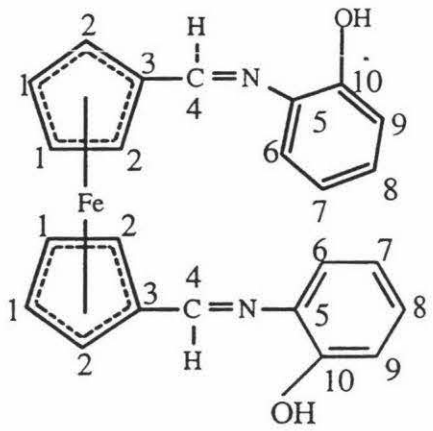


The numbering scheme is depicted above and the assignment of the protons was established with the aid of both HETCOR ($^1H$ x $^{13}C$) **(Fig 2.25)** and $^1H$ x $^1H$ (COSY) spectrum **(Fig 2.26).**

The bis-substituted ferrocene moiety displays two weakly split singlets each integrating as 4 protons. The first singlet, H(1), appears at 4.56 ppm, the second H(2) at 4.78ppm. Each cyclopentadiene ring appears to be equivalent and this has been observed also by others [71]. The imine proton H(4) (8.44 ppm) integrates as two protons and appears as a singlet . The splitting pattern observed for the phenol ring appears to be different from that of the mono-substituted ligand. The $^2J$ couplings which give rise to a triplet , doublet, triplet , doublet pattern in L1 are replaced by a triplet , doublet , doublet , triplet $^2J$ pattern in the L11 derivative as can be seen in the expansion **(Fig 2.27)**, although the integration observed is still in a 1:1:1:1 ratio. The first triplet of doublets at 6.81 ppm is associated with H(8) with $^2J$ = 6.6 Hz and secondary coupling $^3J$ = 1 Hz . The doublet of doublets centred at 6.93 ppm is H(6) with $^2J$ = 6.6 and $^3J$ = 1 Hz. The next doublet of doublets (H(9)) at 6.98 ppm has moved to a lower frequency relative to the mono-substituted L1 ligand, and appears between the triplet of doublets of H(7), (7.13 ppm) and the doublet of doublets for H(6). The doublet of doublets for H(9) centred at 6.98 ppm has

moved because of hydrogen bond interactions between the hydroxy groups on the phenol rings and the opposite imine N atoms as observed in the single crystal X-ray structure (**Diagram 2.2**).

### 2.5.5 (b) DISCUSSION OF THE $^{13}C$ SPECTRUM OF L11

Cyclopentadienyl carbon assignments have been based on those given by Roberts *et al.* [56]. The carbon C(1) resonance is located at 72.39 ppm and the carbon C(2) at chemical shift position 71.23 ppm. The quaternary carbon C(3) resonance is located at 80.91 ppm, that for the imine carbon C(4) at chemical shift position 159.39 ppm. The hydrogen bonding observed in the solid state which anchors the phenol rings at almost orthogonal positions to each other, appears to affect the ligand minimally in the solvent, resulting in equivalent environments for both of the phenol rings as evident by the lack of mulitiple peaks in the pyridine carbons in the decoupled spectra. The phenol ring carbons have been assigned with the aid of Kemp [90] and the HETCOR spectrum of L11 (**Fig 2.25**). The two quaternary carbons C(5) and C(6) are difficult to distinguish their resonances are found at 151.15 ppm and 137.19 ppm. The carbons C(6), C(7), C(8) and C(9) are located at 115.36, 127.91, 120.10 and 116.53 ppm respectively.

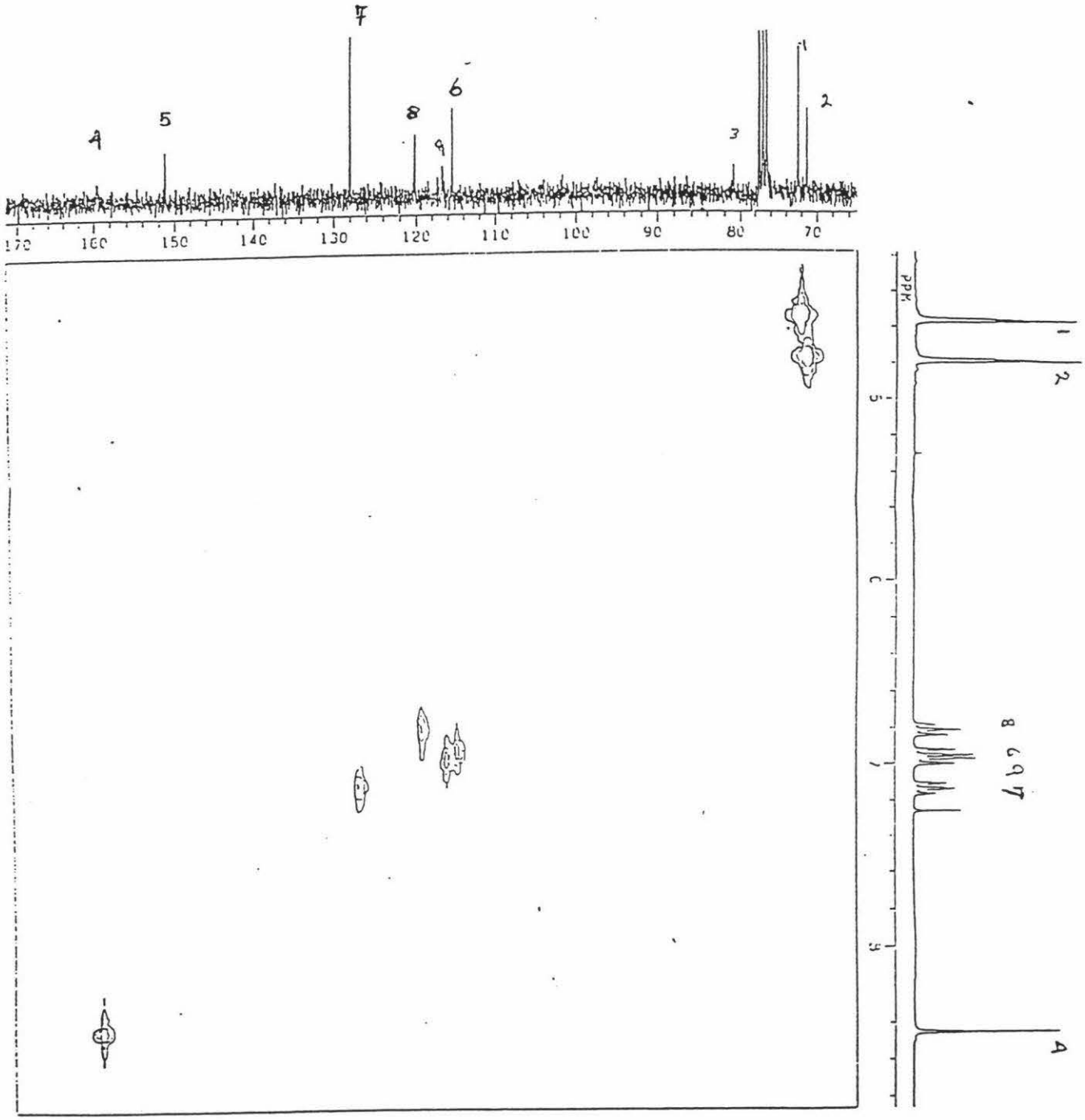


**Fig 2.25**

$^{1}H$ x $^{13}C$ (HETCOR) spectrum of L11 in $CDCl_3$.

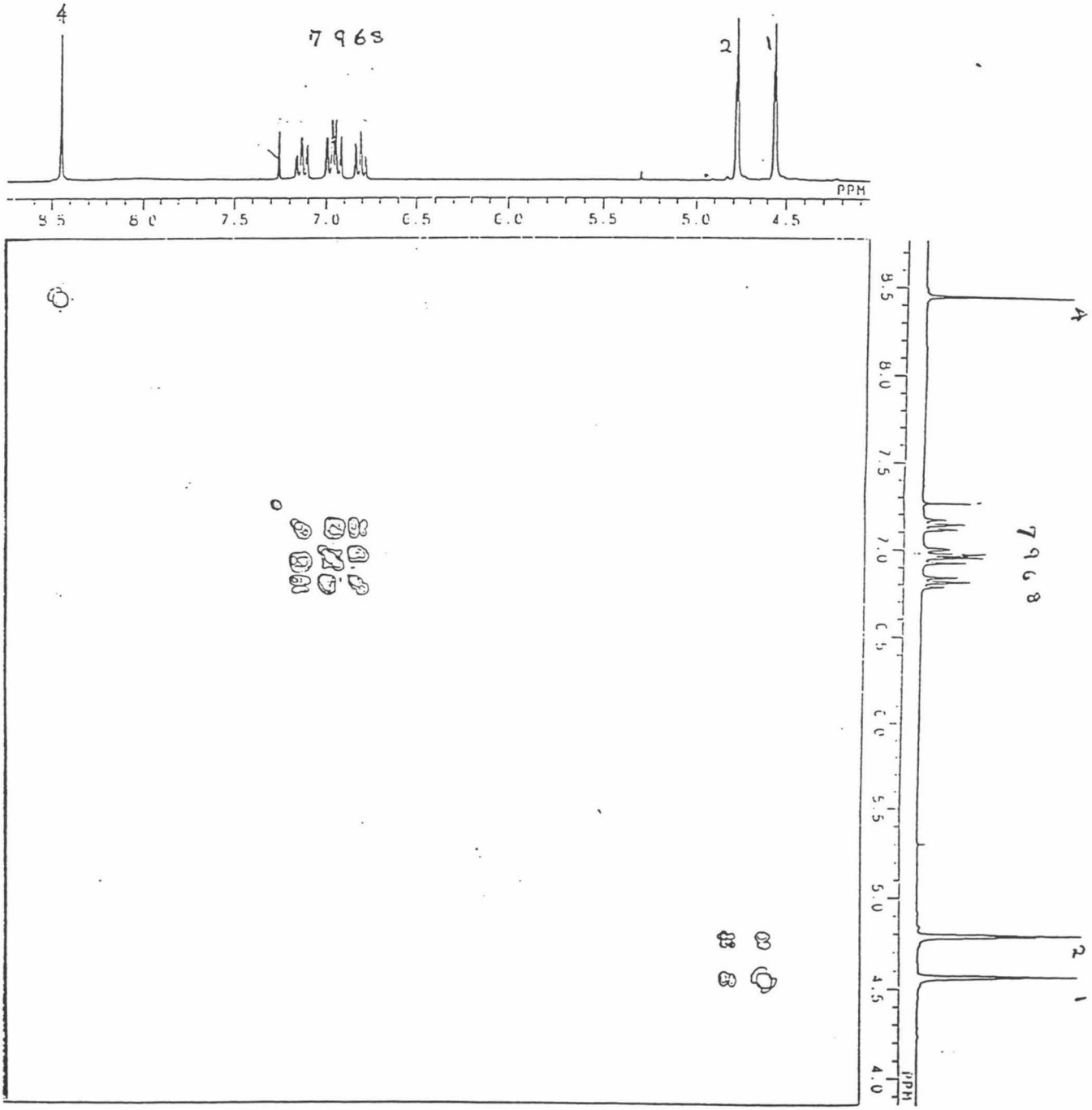


**Fig 2.26**

$^{1}H$ x $^{1}H$ (COSY) spectrum of L11 in $CDCL_3$.

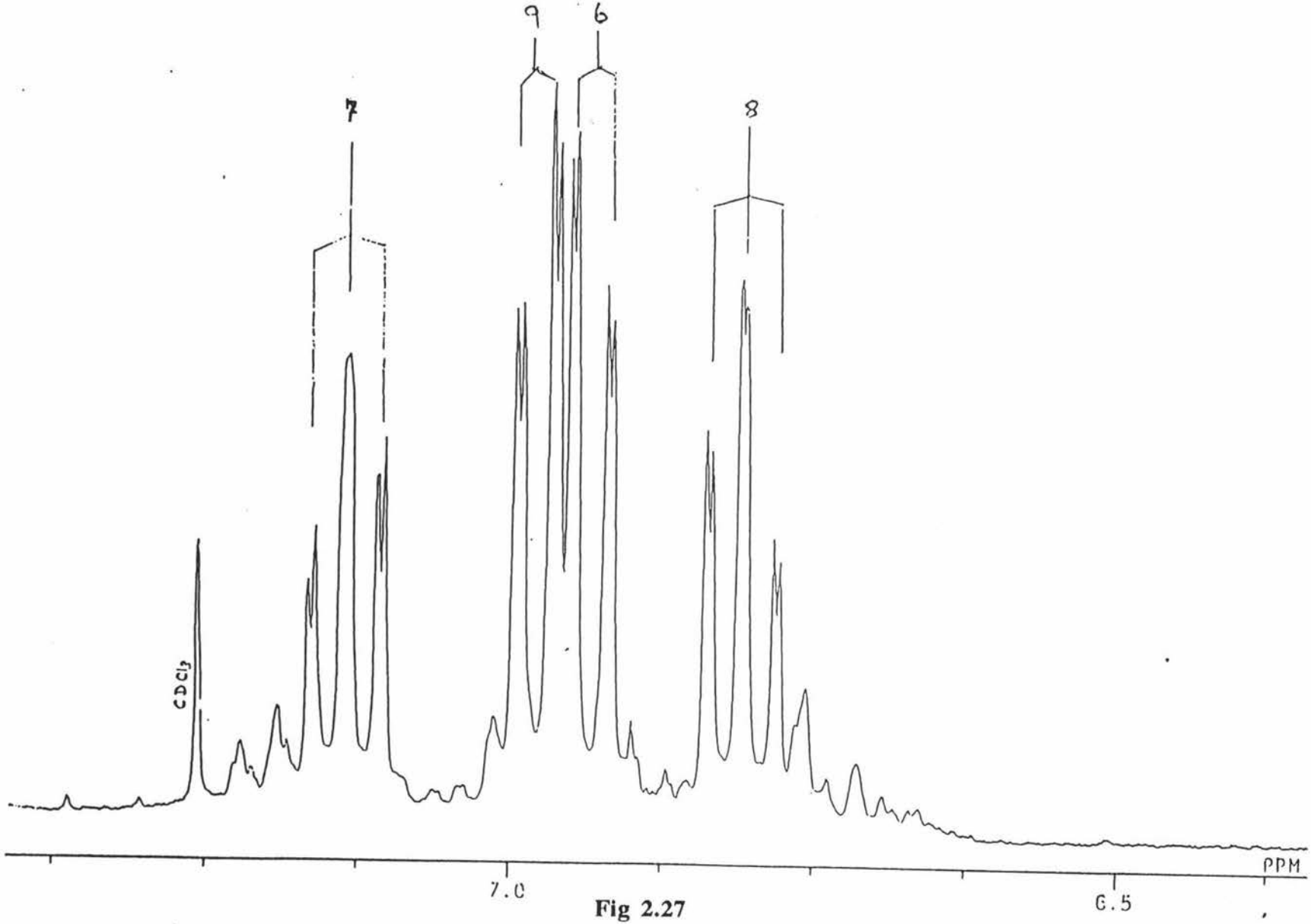


**Fig 2.27**

Expansion of the aromatic region (6.5-7.6 ppm) of the L11 $^{1}H$ NMR spectrum.

## 2.5.6 (a) DISCUSSION OF THE $^{1}H$ SPECTRUM OF L 22

The detailed spectral results are given in the Experimental Section 2.3.7. These assignments are discussed below.

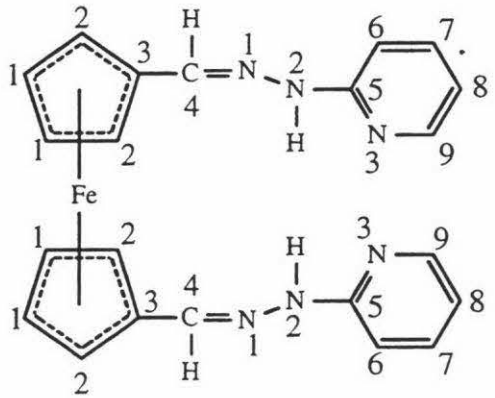

The numbering scheme is depicted as above. The protons were assigned by cross correlation with the mono substituted 2-hydrazinopyridine ligand L2, using $^{1}H$ x $^{13}C$ (HETCOR) **(Fig 2.19)** and $^{1}H$ x $^{1}H$ (COSY) **(Fig 2.20)** spectra.

The ferrocene moiety once again shows two singlets at 4.36 ppm H(1), and 4.59 ppm, H(2), integrating in a 4:4 ratio. The imine protons H(4) at 7.75 ppm are equivalent and integrate as two protons **(Fig 2.28).** The N(2) proton could not be located. The pyridine ring protons appear in the usual triplet, doublet, triplet, doublet pattern. The triplet associated with H(8), centred at 6.66 ppm with $^{2}J = 3.5$ Hz, integrates as 2 protons as does the doublet for H(6) at 7.04 ppm with $^{2}J = 4.2$ Hz. The H(7) triplet integrates as 2 protons and appears at 7.51ppm with $^{2}J = 3.5$ Hz. The last doublet (H(9)) is centred at 8.04 ppm with $^{2}J = 3.7$ Hz.

## 2.5.6 (b) DISCUSSION OF THE $^{13}C$ SPECTRUM OF L22

Cyclopentadienyl carbons have been assigned according to Roberts *et al.* [56]. The carbon C(1) resonance is located at 74.22 ppm, the C(2) chemical shift is at 71.38, the quarternary carbon C(3) at 89.60 ppm and the imine carbon C(4) appears at 142.32 ppm. The pyridine ring carbon assignments have been based on the correlation of the mono-substituted 2-hydrazino derivative L2 using the $^{1}H$ x $^{1}H$ (COSY) **(Fig 2.20)** spectrum and

the $^{13}C$ decoupled spectrum of L22 (**Fig 2.29**). The quaternary carbons C(5) is located at 160.99 and the carbons of C(6), C(7) are observed at positions 110.03 and 141.54 ppm respectively. The resonances of carbons C(8) and C(9) are located at 118.15 and 151.53 ppm respectively. A comparison of the bis- versus mono-2-hydrazinopyridine derivatives chemical shift position comparison cannot be undertaken as the NMR experiments were conducted in different solvents.

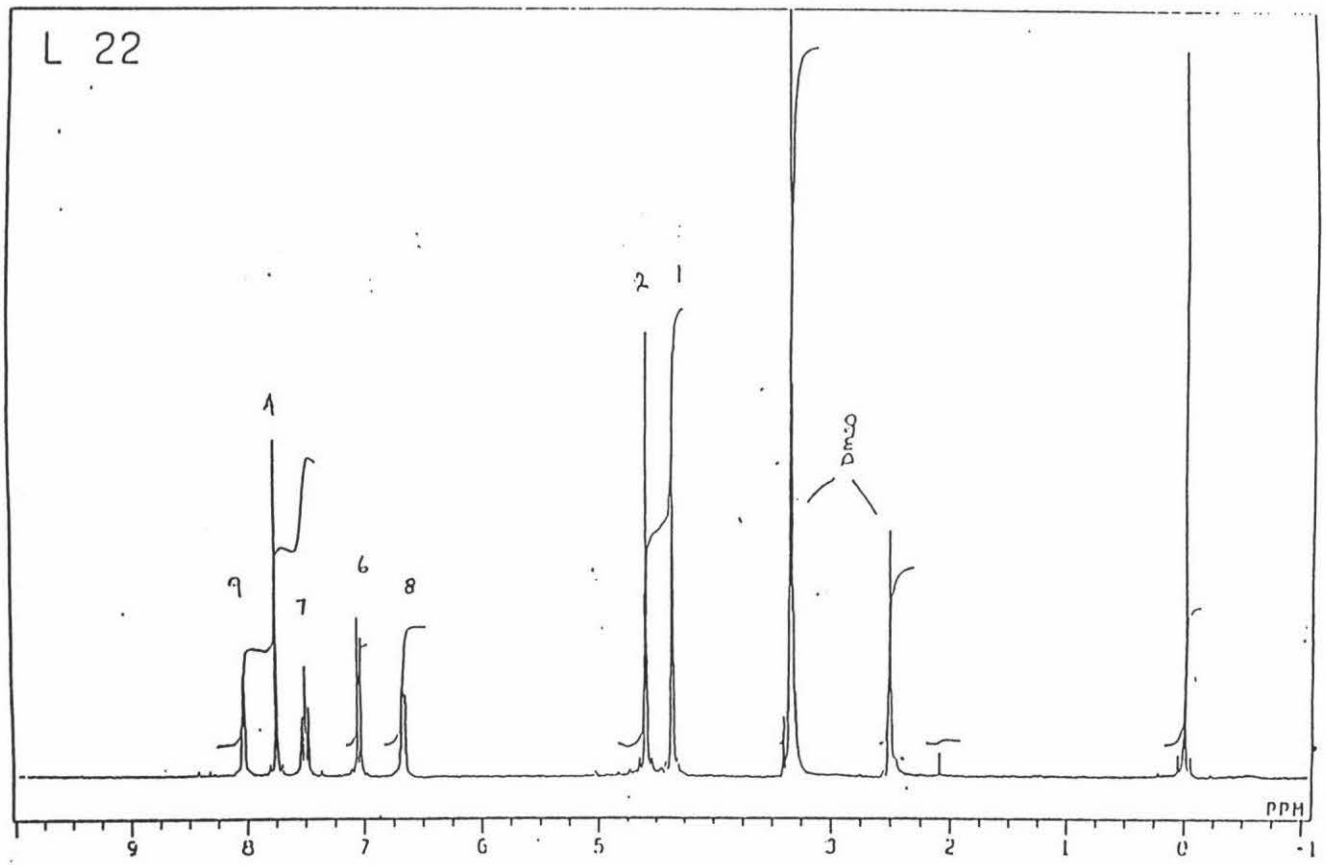


**Fig 2.28**

$^1$H NMR spectrum of L22 in $d_6$-dmso.

## 2.5.7 (a) DISCUSSION OF THE $^{1}H$ SPECTRUM OF L 44

The detailed spectral results are given in the Experimental Section 2.3.8. These assignments are discussed below.

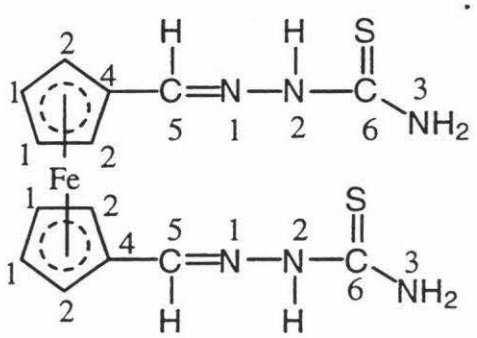

The numbering scheme is depicted as above. The ferrocene moiety shows two weakly split singlets at 4.39 ppm for H(1) and at 4.70 ppm for H(2). This is a similar pattern to that observed for L11 and L22, with each peak integrating as four protons. The imine protons at 7.81 ppm H(5) integrate as two. The N(2) proton was not detected. The N(3) protons integrate as four protons but appear as two broad singlets at 8.07 and 7.65 ppm in a 2 : 2 ratio. This inequivalence may be attributed to partial double bond character from electron delocalisation in the thiosemicarbazide system and/or hydrogen bonding, which causes hindered rotation of the C(6) -N(3) bond as observed with the L 4 ligand.

## 2.5.7 (b) DISCUSSION OF THE $^{13}C$ SPECTRUM OF L44

Cyclopentadienyl carbons have been assigned according to the reported results by Roberts *et al.* [56]. The cyclopentadienyl C(1) resonances appear at 70.75 ppm with the resonance of the C(2) carbons at 67.99 ppm. The quaternary carbon C(4) resonance is located at 70.49 ppm and is a single sharp peak. This is in contrast to the L4 derivative (mono-thiosemicarbazide derivative), which has a doublet occurring at approximately this position. This suggests that the cis/trans isomeric geometries are not occurring in the bis thiosemicarbazide derivative. This is feasible when a model is considered, the steric

constraints imposed by the addition of another 'arm', makes the formation of both isomers very difficult. The resonance of the C(5) carbon atom is observed at 142.09 ppm with the C=S carbon resonance appears at a chemical shift position of 176.42 ppm. The $^{13}C$ NMR spectrum of L44 can be seen in Fig 2.29.

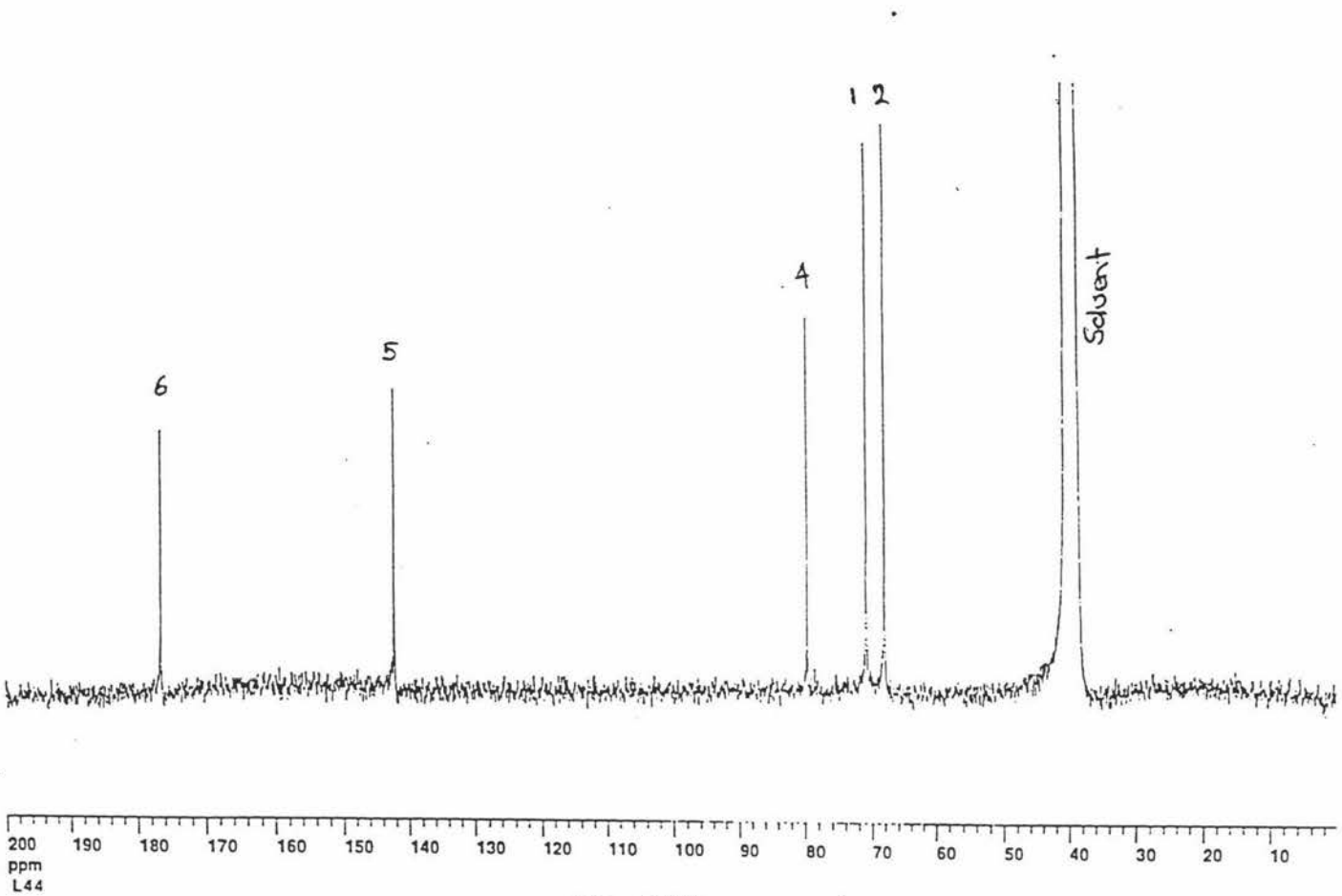


**Fig 2.29**

$^{13}C$ NMR spectrum of L44 in $CDCl_3$.

## 2.5.8 SUMMARY OF $^1$H NMR SPECTRA

**Table 2.3**
**$^1$H NMR SPECTRA FOR THE FERROCENE DERIVATIVES (ppm)`**

| DERIVATIVES | $C_5H_5$ | $C_5H_4$ | $C_5H_4$ | C(H)= N |
|---|---|---|---|---|
| **L1** | 4.23 | 4.52 | 4.81 | 8.59 |
| **L2** | 4.19 | 4.34 | 4.81 | 7.60 |
| **L3** | 4.18 | 4.38 | 4.70 | 8.43 |
| **L4** | 4.21 | 4.43 | 4.58 | 7.83 |
| **L 11** | | 4.56 | 4.78 | 8.44 |
| **L 22*** | | 4.36 | 4.59 | 8.02 |
| **L 44** | | 4.39 | 4.71 | 7.81 |

* This spectrum was measured in $d_6$-DMSO as solvent, all others were measured in $CDCl_3$

The $^1$H NMR spectra for the mono- and bis-substituted ferrocene derivatives are shown in Table 2.3. There appear to be no significant chemical shift differences between any of the ligands as far as the two cyclopentadienyl rings are concerned. The observed chemical shifts of the imine protons vary significantly and this appears to be related to the degree of multiple bond character in the C=N bond. The aminophenol derivative, L1, has an isomer, HL [24] and a similar derivative, based on acetyl ferrocene carboxaldehyde [27]. The structures of both latter species have been determined and the double bond character is confined to the imine bond. The methylpyridinyl ferrocene derivative, L3, does not have N-N connecting atoms in the 'tether', and is also expected to have no mulitiple bond character in the 'tether' except between the imine bond. Hence a greater deshielding effect is exerted on the imine protons in L1, L11 and L3 than that of the aminohydrazinopyridine based derivatives (L2, L22) and thiosemicarbazide (L4, L44) ligands (Diagram 2.3) where delocalisation within the 'tethering' atoms exists.

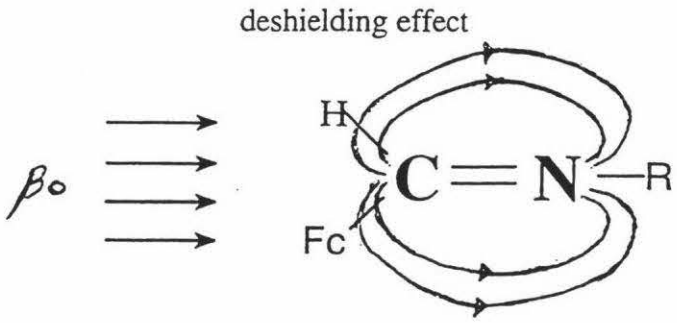


**Diagram 2.3**

For the bis-substituted ferrocene derivatives, L21, L22 and L28 the imine proton chemical shifts are very similar to these observed for their mono-substituted analogues. For L1 and L21 the aromatic proton chemical shifts are also similar when the mono- and bis-substituted ferrocene derivatives are compared. These pattern changes have already been discussed (Section 2.5.5).

## 2.6 INFRA-RED SPECTRAL DATA COMPARISON OF FERROCENE DERIVATIVES

**Table 2.4**

Selected Infra-Red Spectral Data of the Ferrocene Derivatives ($cm^{-1}$)

| LIGAND | IMINE BOND | ν( O-H) | ν( N-H) |
|---|---|---|---|
| L1 | 1611 | 3000* | |
| L2 | 1593 | | 3185 |
| L3 | 1635 | | |
| L4 | 1600-1635* | | 3354,3246,3161 |
| L5 | no reported bond | 3200* | 3282* |
| L11 | 1618 | 3000* | |
| L22 | 1598 | | 1385 |
| L44 | 1614 | | 3356,3250,3164 |

* Could not be assigned with certainty because of other bands in this region

Table 2.4 lists the ν(C=N) stretching frequencies for the Schiff base ferrocene compounds which range from 1593-1635 $cm^{-1}$. These frequencies vary according to the degree of electron delocalisation between the atoms that are involved in the 'tether' and the varying degree of electron withdrawing capability of the organic substituents. The frequency is largest for L3 (1635$cm^{-1}$) consistent with the localisation of electron density within the imine bond [27], whereas that for L2 (1593$cm^{-1}$) suggests greater electron delocalisation occurs [56]. The stretching frequency for L11 at 1618$cm^{-1}$ implies some multiple bond character throughout the 'tether' and the structural data supports this view.

For L11 a broad ν(O-H) stretching frequency is observed at 3000 $cm^{-1}$ which is considerably shifted from the 3500-3100$cm^{-1}$ range where it is often found. This lowering of the wavenumber is consistent with hydrogen bonding, as is observed for the X-ray structure determination of this molecule where the OH group is hydrogen bonded to the

imine nitrogen of the second 'arm'.

The NH vibrational stretches of the hydrazinopyridine based ligands, L2 and L22, are both observed at 3185 $cm^{-1}$.

The 1,3-diamino-2-hydroxy derivative L5 has a ν(N-H) absorption at 3282$cm^{-1}$ which is partly obscured by the ν(O-H) band. This is an extremely complex spectrum with an indication of several isomers present. No ν(C=N) stretching frequency is observed and this is consistent with Baldwin's rules [90] of cyclisation in adducts resulting from the tautomerism of the imine bond. A possible product of this cyclisation is depicted in **Fig 2.30.**

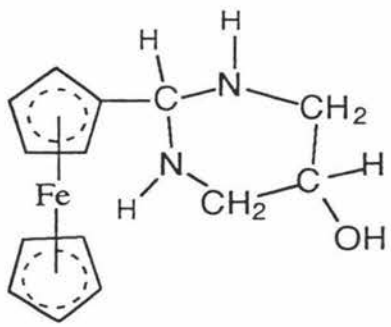


**Fig 2.30**

The thiosemicarbazide derivatives, L4 and L44, both show broad ν(CH) stretching vibrations at 3354, 3246, 3161. However the imine ν(C=N) vibrations are difficult to assign due to the presence of overlapping bands.

The C-H out of plane bending vibration observed for ferrocene itself at 815$cm^{-1}$ has been observed for the ligands in the range of 830-807$cm^{-1}$ but these are very weak and detection is difficult.

## 2.7 MASS SPECTROSCOPIC ANALYSIS OF THE FERROCENE DERIVATIVES

**Table 2.5 Liquid SIMS Mass Data of Parent Molecular Ions of the Schiff base Derivatives**
**Fe = $Fe^{56}$**
**m/z**

| Ferocene Mono Dervatives | | Calculated | Observed Ion | Found (relative intensity) |
|---|---|---|---|---|
| amino phenol | (L1) | 305 | $M^+$ | 305 (100%) |
| 2-hydrazinopyridine | (L2) | 305 | $M^+$ | 305 (100%) |
| 1,3-amino-2-hydroxypropane | (L5) | 286 | $M^+$ | 286 (100%) |
| 2-aminomethylpyridine | (L3) | 304 | $MH^+$ | 305 (100%) |
| thiosemicarbazide | (L4) | 287 | $M^+$ | 287 (100%) |
| **Ferrocene Bis Derivatives** | | | | |
| Bis amino phenol | (L11) | 424 | $MH^+$ | 425 (100%) |
| Bis 2-hydrazinopyridine | (L22) | 424 | $MH^+$ | 425 (100%) |
| Bis thiosemicarbazide | (L44) | 388 | $MH^+$ | 389 (90%) |

Table 2.5 lists the parent molecular ions for the Schiff base derivatives [$M^+$] or their protonated ions [$MH^+$]. Supporting the integrity of these species, isotope abundance calculations have been performed and are reported at the end of this discussion.

The aminophenol derivative L1 appears to have a two pathway breakdown pattern. The first is the stronger fragmentation pattern and has the parent ion $M^+$ at 305(100%) losing one of the cyclopentadiene rings. This results in a peak at 240(15%) which is assigned to the [Fe-$C_5H_4$-C=N-phenol] ion. This then loses the imine atoms, the phenol ring, and the cyclopentadiene ring but picks up a proton to produce an ion at 121(18%), which is assigned to [$C_5H_5$-Fe]$^+$. The second pathway involves the gradual disintegration of the phenol ring, resulting in a peak at 214(6%) which is assigned to the [$C_5H_5$-Fe-$C_5H_4$-CH=$NH_2$]$^+$ ion. The ferrocene ion peak at 186 is then observed. The rest of the fragmentation process resembles that of the first path.

The fragmentation pattern for the hydrazinopyridinyl derivative, L2, resembles the second pathway fragmentation process of L1, with the loss of the aromatic pyridine ring. This results in a peak assigned as $[C_5H_5\text{-}Fe\text{-}C_5H_4\text{-}CN]^+$ at 211 (20%). The cyanide function is lost next leaving the ferrocene peak at 186 (10%). This is then followed by the loss of a cyclopentadiene ring to give the $[C_5H_5\text{-}Fe]^+$ ion (mass 121) followed by the $Fe^+$ ion with a peak at 56.

The L3 derivative which is based on aminomethylpridine, resembles very closely the fragmentation process of L2. Fragmentation of the methylpyridine leaves a peak at 214 (20%) which is assigned to the $[C_5H_5\text{-}Fe\text{-}C_5H_4\text{-}CH{=}NH_2]^+$ ion. The next predominant peak at 109 (25%) is consistent with the loss of the substituted cyclopentadiene ring and partial fragmentation of the second ring to give the unusual $[C_4H_4FeH]^+$ ion. $Fe^+$ is also observed at 56.

L5 is the 1,3-diamino-2-hydroxypropane derivative and is an isomeric mixture with no imine bond present. The absence of any aromatic substituted substituents makes for an easier fragmentation process with a parent $M^+$ ion at 286 (100%). The organic substituent is then lost leaving the ferrocene peak at 186 (15%) with the $[FeH]^+$ ion is detected at 57 (25%).

The thiosemicarbazide derivative L4 has a simple fragmentation pattern. The parent ion 287 (100%) fragments to form an ion at 212 (12%) which is assigned to $[C_5H_5\text{-}Fe\text{-}C_5H_4\text{-}CHN]^+$ and this then fragments until $[FeH]^+$ is detected at 57.

The bis-substituted ferrocene breakdown pathways of L11 (425,100%) and L22 (425,100%) resemble their mono substituted analogues very closely, once one of the organic arms has been lost. Each leaves a peak which is consistent with the parent ion of its mono derivative. However the bis substituted thiosemicarbazide L44 appears to follow a different fragmentation process from that of the mono version. A parent peak $MH^+$ is located at 389 (90%) and instead of a mono peak at 287 a large peak at 252 has been assigned to $[C_5H_5\text{-}Fe\text{-}C_5H_4CH{=}N{=}N\text{-}CN]^+$. The $[FeH]^+$ was located at 57 (50%).

## 2.8 SUMMARY

Schiff base condensation reactions have resulted in the formation of the ferrocene imine derivatives in about 65% yield. Seven new potential bi- and/or tetra-dentate chelating ligand systems have been characterised, however, the method has not been successful for six other reactions. These include the reaction of the amines such as 2-(diphenylphosphino)benzeneamine, ethylenediamine and 2-aminoethylpyridine with the mono ferrocene carboxaldehyde, and of 2-aminomethylpyridine, 1,3-diamino-2-hydroxypropane and ethylenediamine with the 1,1'-ferrocene dicarboxaldehyde.

According to the $^{1}$HNMR and IR spectroscopic evidence, 2-(diphenylphosphino)benzeneamine failed to react with the appropriate aldehyde. Excluding ethylenediamine, the remaining amines produced species containing $\nu$(C=N) stretching frequencies. However the imine bonds were very susceptible to hydrolysis and the compounds were unable to be characterised. The ethylenediamine species produces an insoluble polymeric product with the 1,1'-ferrocene dicarboxaldehyde, which was characterised by both mass and IR spectroscopy.

The seven Schiff base derivatives were all characterised by the usual spectroscopic techniques. With the exception of the 2-hydrazinopyridine derivatives, L2 and L22, they were all susceptible to hydrolysis in solution, but, excluding L3 (aminomethylpyridine base mono ligand) were all air stable.

The $^{1}$H, $^{13}$C NMR and I.R spectra of the bis-ferrocene 1,1'-ferrocene dicarboxaldehyde derivatives, L11, L22 and L44, are all similar to the spectra of their corresponding mono-ferrocene carboxaldehyde analogues.

# CHAPTER 3

## REDUCTION OF THE SCHIFF BASE DERIVATIVES

### 3.1 INTRODUCTION AND AIMS

The ability of the ferrocene moiety to sense the uptake of a host metal ion at the guest site is said to be dependent on the degree of conjugation between the two sites although some studies suggest that this is not always crucial. One difficulty encountered by others during the complexation of a guest into the host site of ferrocene Schiff base ligand systems is the hydrolysis of the imine bond resulting in the formation of ferrocene carboxaldehyde [24] and iron oxo species [68].

The imine derivatives give rise to some degree of conjugation between the ferrocene moiety and the donor atoms, but this remains absent in non-conjugated ligands. The latter ligands could be studied for comparison if the Schiff base ligands could be reduced without decomposition. It is envisaged that a comparision of the two forms of the ligand, once complexed, would aid in the elucidation of the mechanism of communication between the metal centres within the complex. The reduced ligands would be able to form stable complexes without the hydrolysis problems associated with the Schiff base ligands.

The main aim in this chapter was to prepare ferrocene Schiff base derivatives in which the imine bond had been reduced. There are many reducing agents that can be employed and those that have been tried have been used in the reduction of other multiple bond systems. For example, success has been achieved with reactions using reductants such as $NaBH_4$ or $LiAlH_4$ in tetrahydrofuran under reflux in an argon atmosphere, or, hydrogenation of the imine with the use of activated palladised carbon in an hydrogen atmosphere. The more commonly used methods involve the use of the $BH_4^-$ ion. This reacts by nucleophilic attack on the electrophilic centre whereas the related $B_2H_6$ attacks electron rich positions. $NaBH_4$ will reduce RCOOR but not $RCO_2R$ whereas $B_2H_6$ will reduce both substrates.

# EXPERIMENTAL

## 3.2 PRELIMINARY INVESTIGATION INTO THE REDUCTION OF THE FERROCENE COMPOUNDS

The ferrocene Schiff base compounds, L1 and L2, were used in a preliminary investigation to determine any difficulties that might be encountered during the process of imine bond reduction. These compounds were chosen because of their ready availability and, if a synthetic process were established, preparation of the reduced compounds could be executed on a gram scale. Once a successful reduction protocol was established then attempts to reduce the less readily available compounds derived from 1,1'-ferrocene dicarboxaldehyde would be attempted.

L1, which has the organic phenol residue associated with it, was trialled first. The initial method involved reaction of L1 dissolved in dichloromethane containing palladised carbon under a hydrogen atmosphere for 22 hrs. The solution was then filtered and the solvent reduced to dryness using a rotary evaporator. The $^1$H NMR spectrum revealed that the L1 compound was unchanged.

The second attempt used $NaBH_4$ in methanol as the reductant and this was stirred with the Schiff base compound for 30 minutes. Again, after work up, the $^1$H NMR spectrum showed that no reduction had taken place but it did reveal that the ligand had started to undergo decomposition to produce ferrocene carboxaldehyde as one product. This is in accord with the ready hydrolysis of L1 already noted.

Reduction of ligand L2 was attempted using four different methods. The first method was to react $LiAlH_4$ in thf with L2 in an inert atmosphere under reflux for 30 min. The $^1$H NMR spectrum showed no reaction had taken place.

The second method was to react L2 dissolved in a thf-methanol mixture, with $NaBH_4$ under reflux for 10 minutes. After work-up the $^1$H NMR spectrum showed a weak absorption at 2.2 ppm, consistent with a product containing a $CH_2$ group, but the presence of complex absorptions in the 1.0-3.7 ppm range suggested decomposition of the Schiff base compound had also occured. As a variation of the above method, excess $NaBH_4$ was

added in methanol and this was followed by refluxing for 1 hr. However, after work up, the $^1$H NMR spectrum indicated a total break down of the Schiff base.

The third method involved use of palladised carbon in dichloromethane in a hydrogen atmosphere. After 12 hours a sample was extracted and the $^1$H NMR spectrum revealed the presence of unreacted ligand L2. The reaction was left a further 24 hr after which time the solution was filtered and taken to dryness using a rotary evaporator. The orange red powder was chromatographed on silica gel with a 10% ethanol, 90% dichloromethane solution as eluent, this produced three bands. These were all subjected to investigation by their $^1$H NMR spectra. The first band showed that some reduction (>10%) had occurred but the sample required further purification. The second band showed that the pyridine ring had undergone cleavage to expose an aliphatic carbon nitrogen chain which was still connected to the ferrocene moiety. The third band did not contain the ferrocene moiety but only $CH_3$ and $CH_2$ groups which have possibly resulted from further decomposition of the cleaved pyridine ring. The complicated nature of this reaction meant it was not a practical method to achieve a reduced product and it was abandoned.

The fourth method also failed to produce the reduced product but it did give a new adduct of $BH_3$. It involved the use once again, $NaBH_4$ (in an extreme excess), dissolved in thf and deionised water (5:1 v/v). The solution was heated and stirred vigorously. A full description of the $BH_3$ complex produced in this reaction is discussed in the following section.

### 3.2.2 PREPARATION OF L2.$BH_3$

To a 100 ml solution of the ferrocene derivative, L2 (0.47g , 1.50 mmol), in thf was added 40 ml of deionised water. The solution was stirred and heated strongly (50-60 C°) and $NaBH_4$ (1.50g, 39.00 mmol) was added slowly. (CAUTION: upon addition hydrogen is evolved.) The solution was stirred for approximately 50 minutes, with stopping every 10 minutes to ensure hydrogen was still being evolved. (Addition of more $NaBH_4$ may be necessary.) After 50 min the organic orange/yellow phase was decanted from the aqueous phase and washed 3 times with a 50:50 water/diethylether solution to remove excess $NaBH_4$. It was then taken to dryness using a rotary evaporator, dissolved in $CHCl_3$ and filtered twice. The yellow crystalline product was then chromatographed using (silica gel, 70-500 mesh) a 10% ethanol / 90% dichloromethane solution as eluent and the first band was collected as the product.

Yield: 85% (0.43g), M.P.155 $^0$C

Found: C, 60.13 : H, 5.46 : N, 13.24

Calculated for ($C_{16}H_{18}N_3BFe$):

C, 60.24: H, 5.68 : N, 13.17

**NMR($CDCl_3$)$^1$HΔ (ppm):**

4.22( s, 5H, $C_5\underline{H}_5$) , 4.41(t , J = 1.8 Hz, 2H, $C_5\underline{H}_4$) , 4.63 (t , J = 2.0Hz, 2H, $C_5\underline{H}_4$) , 6.71 (t , J = 6.8 Hz, 1H, $C_5\underline{H}_4N$) , 7.52 (d , J = 8.8 Hz , 1H , $C_5\underline{H}_4N$) , 7.68 (t , J = 6.9 Hz, 1H, $C_5\underline{H}_4N$), 8.15 (d, J = 8.8, 1H, $C_5\underline{H}_4N$), 7.88 (s, 1H, C$\underline{H}$=N) , 9.32 (s, 1H, N$\underline{H}$)

**$^{13}$C {$^1$H}Δ (ppm):**

67.59 ($\underline{C}_5H_4$), 69.24 ($\underline{C}_5H_5$), 70.30 ($\underline{C}_5H_4$), 78.56 ($\underline{C}_5H_4$), 109.90 ($\underline{C}_5H_4N$), 113.3 ($\underline{C}_5H_4N$), 139.64 ($\underline{C}_5H_4N$), 145.56 ($\underline{C}_5H_4N$), 145.60 ( $\underline{C}$=N), 152.71 ($\underline{C}_5H_4N$)

**IR** (nujol mull, NaCl disk)

3263 s, 2287m, 2247m, 1623s , 1578s , 1320s , 1157 w, 1087w , 938w , 814w , 759m

# RESULTS AND DISCUSSION

## 3.3.1 FORMATION OF THE L2.$BH_3$ COMPLEX

The conditions involved in this attempted reduction of L2 are extreme and the expected product was expected to be a mixture of cleaved ferrocene and a break-down product of the organic residue, but surprisingly this was not the case.

The colour of the organic solution changed from a brown/red to a lighter yellow colour after 15 min duration in the reaction. It was suspected that the reduced derivative had been formed but the $^1$H NMR spectrum proved that this was not so, since no $CH_2$ protons were observed. However there was a change in the pyridine region of the spectrum. This combined with the well defined melting point of 155° C, which was different from the parent L2 compound, indicated that the product was different from the the starting material. Mass spectroscopy supplied the first indication that a light atom such as boron was present, but the co-ordination mode was uncertain as was the identity of the boron species. Under the conditions employed, a $B(OH)_x$ species might be expected to form as a dimeric or polymeric hydroxo bridged species with L2. It was not until the single crystal X-ray structure was solved that the borane species was identified and an explanation for the increase in wavenumber of the $\nu$(C=N) stretching vibration could be provided.

In one preparation, when the reaction was not heated after addition of $NaBH_4$, no reaction occurred. This means that heating is very important for the formation of the $BH_3$ adduct.

The synthesis of this adduct was not able to be achieved by a $BH_3$ transfer reaction, using a commercially available $BH_3$:thf solution which was injected into a nitrogen filled, two-necked round bottomed flask containing the L2 ligand dissolved in thf and stirred at room temperature for three hours. An $^1$H NMR indicated the presence of a new compound, but the compound needed futher purification. There also appeared to be a large amount of cleaved L2 ligand and it is suggested that this reaction could be further investigated, with the synthesis done in a liquid nitrogen/ acetone mixture to minimise the breakdown of the starting materials.

### 3.3.2 A PROPOSED MECHANISM FOR THE L2.$BH_3$ REACTION

The mechanism by which the L2.$BH_3$ complex forms is difficult to assess. It is tentatively suggested that in the organic phase, under the conditions of the experiment, a transient diborane ($B_2H_6$) or a $BH_3$ species forms. The, $B_2H_6$, species would undergo symmetric cleavage in the presence of the ferrocene moiety, this would produce a cleaved electron deficient, $BH_3$ species. This species can then associate with excess $H_2$ gas (derived from the excess $NaBH_4$) for sufficient time to allow the L2 ligand to react with it (Scheme 3.1).

$$BH^-_4 + {}^{\delta+}H\text{-}OH \xrightarrow{\text{(aqueous phase)}} BH_3 + H_2 + OH^-$$

$$BH_3 + H_2 + OH^- \xrightarrow{\text{(organic phase)}} \text{`}BH_3\cdots H_2\text{'}$$

$$\text{`}BH_3\cdots H_2\text{'} + L2 \rightarrow L2.BH_3 + H_2$$

Scheme 3.1

There are reports of $B_2H_6$ being formed according to the reaction Scheme 3.2 [96].

$$2NaBH_4 + H_2SO_4 \rightarrow Na_2SO_4 + B_2H_6 + 2H_2$$

Scheme 3.2

However this reaction occurs under acidic conditions which would cause the L2 ligand to decompose. No other suggested mechanisms have been proposed and it is believed that the compound produced is the first solid state $BH_3$ adduct to be characterised by the X-ray diffraction technique.

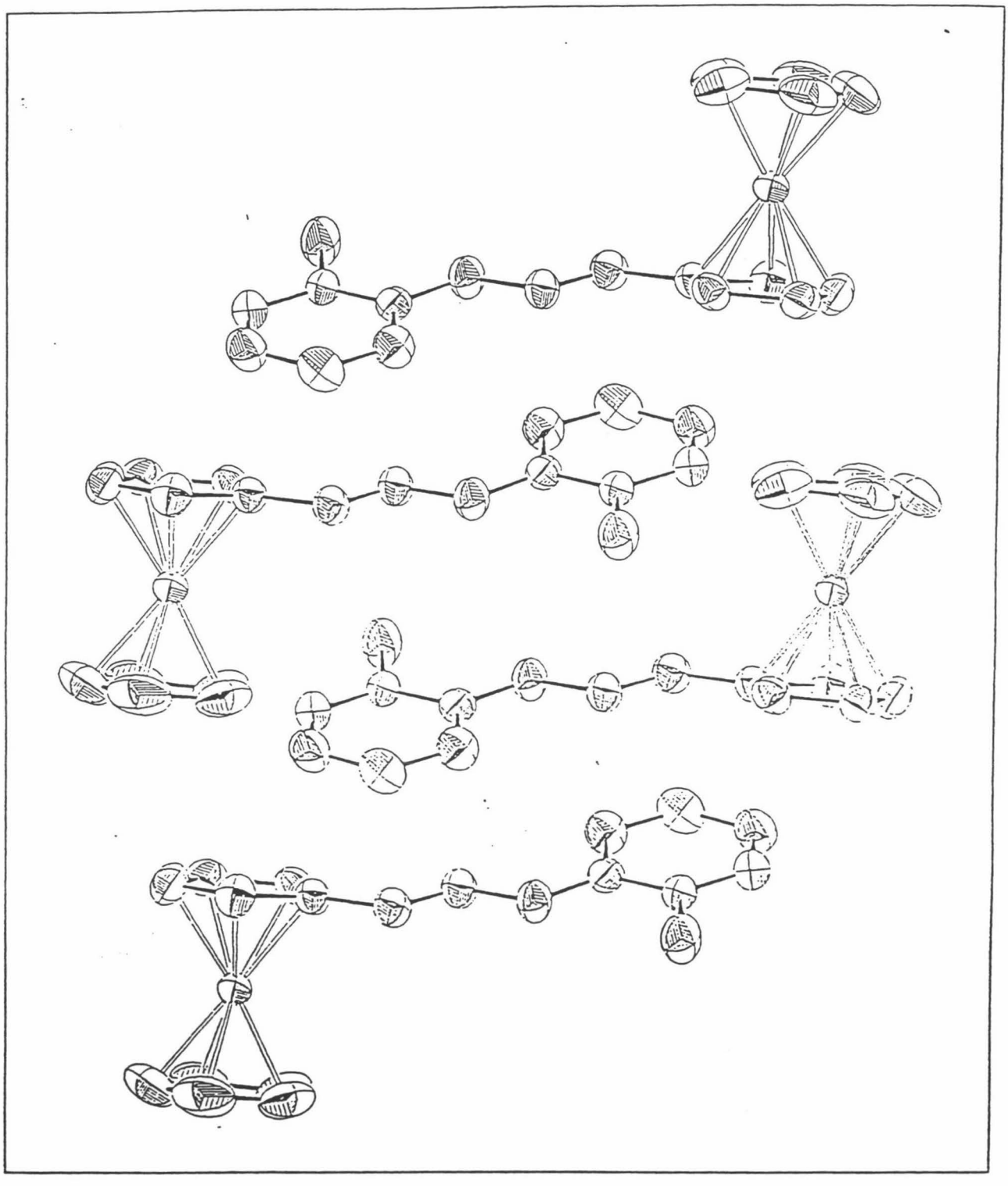

**Fig 3.0** Packing arrangement of the L2.$BH_3$ molecule

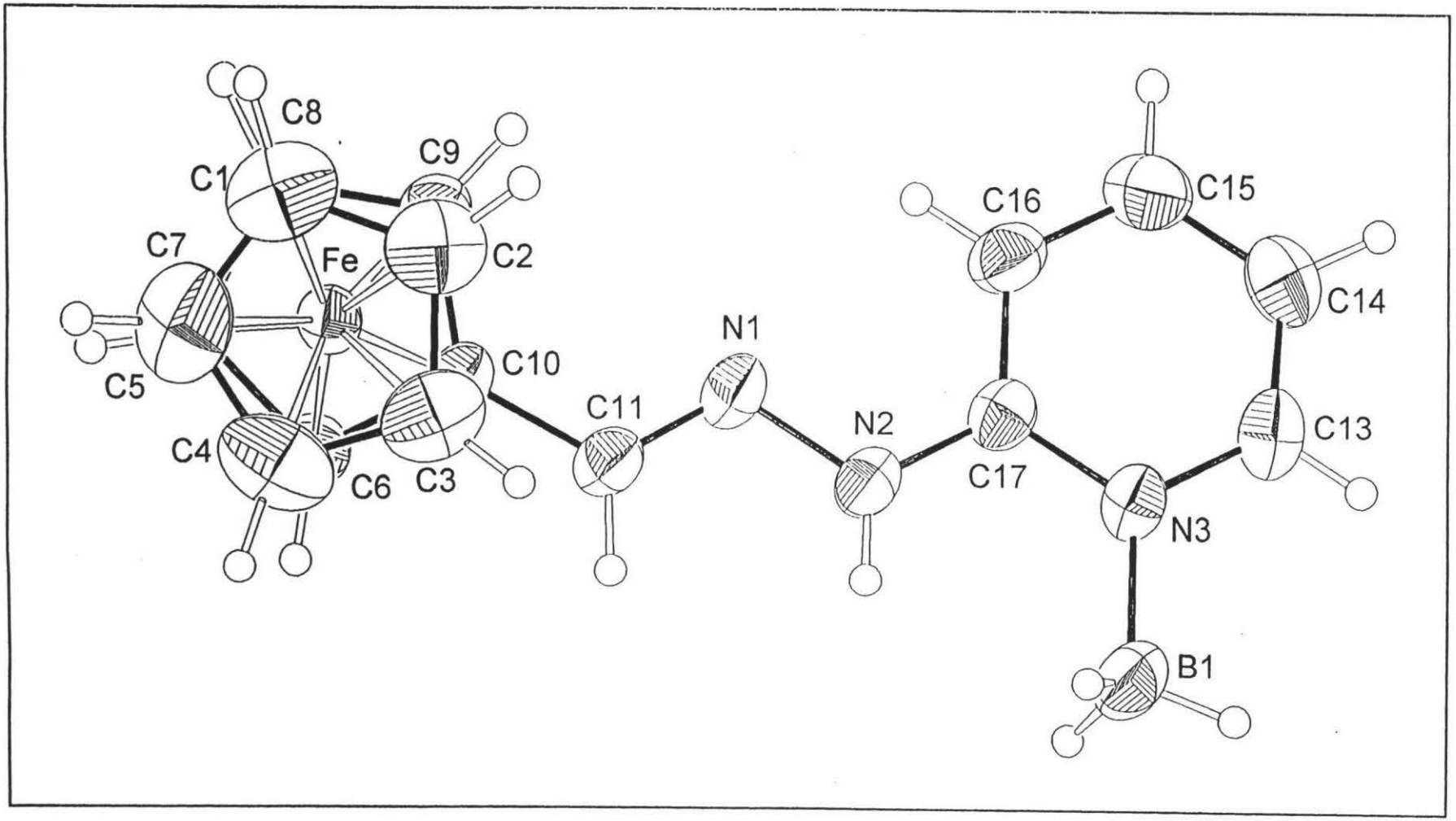


**Fig 3.1**

ZORTEP diagram of L2.$BH_3$ where thermal ellipsoids are shown for non-hydrogen atoms are drawn at the 50% probability levels. Those for hydrogen are drawn at arbitary levels for reasons of clarity.

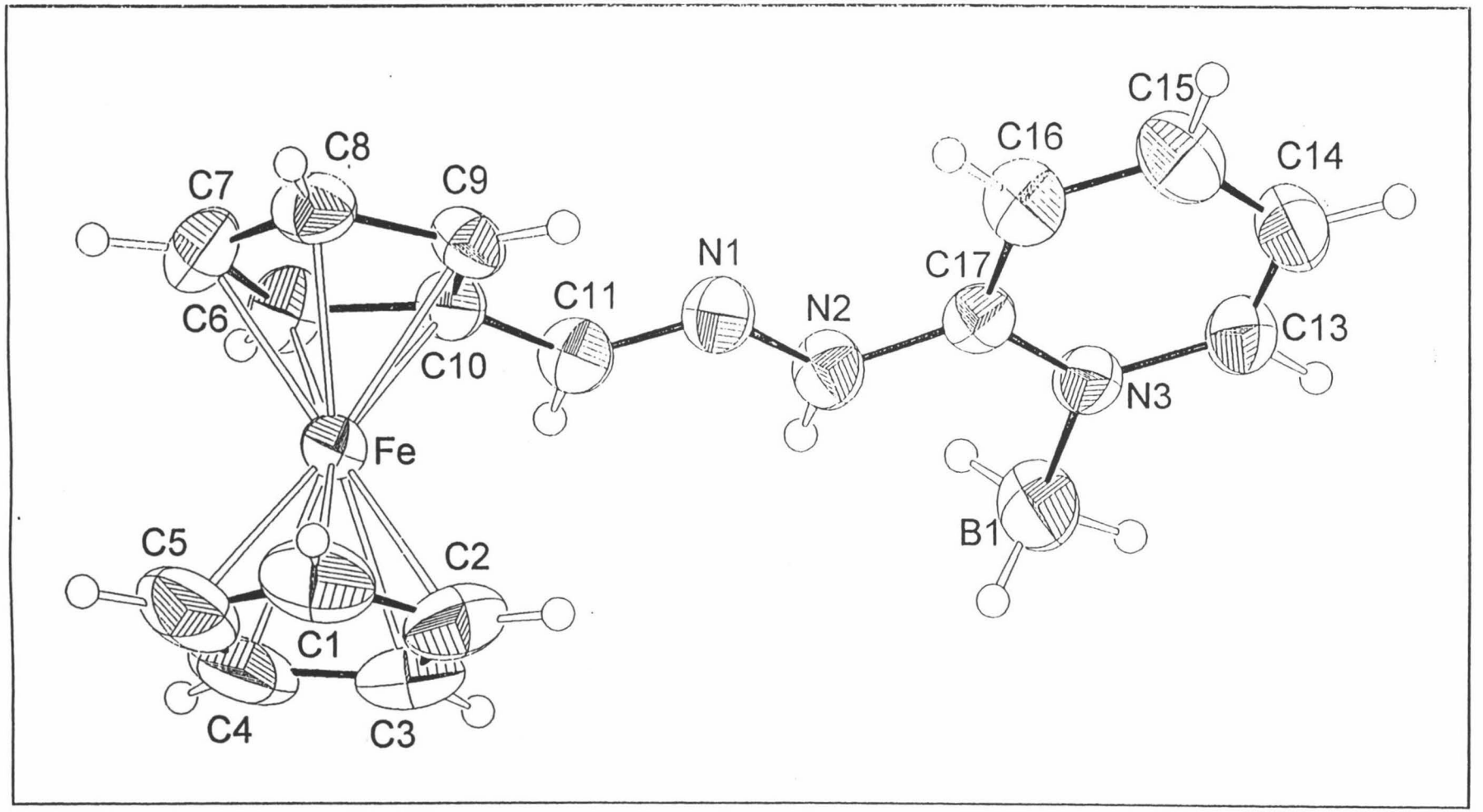


**Fig 3.2**

ZORTEP diagram of L2.$BH_3$ where thermal ellipsoids are shown for non-hydrogen atoms are drawn at the 50% probability levels. Those for hydrogen are drawn at arbitary levels for reasons of clarity.

Table 3.1 Selected bond lengths [Å] and angles [°] for **L2.BH$_3$**

| | |
|---|---|
| N(1)-C(11) | 1.264(2) |
| N(1)-N(2) | 1.387(2) |
| N(2)-C(17) | 1.350(2) |
| C(10)-C(11) | 1.459(2) |
| N(3)-C(17) | 1.352(2) |
| N(3)-C(13) | 1.355(3) |
| N(3)-B(1) | 1.596(3) |
| C(13)-C(14) | 1.360(3) |
| C(14)-C(15) | 1.382(3) |
| C(15)-C(16) | 1.365(3) |
| C(16)-C(17) | 1.401(3) |
| | |
| C(11)-N(1)-N(2) | 116.2(2) |
| C(17)-N(2)-N(1) | 117.8(2) |
| N(1)-C(11)-C(10) | 120.7(2) |
| C(17)-N(3)-C(13) | 118.3(2) |
| C(17)-N(3)-B(1) | 121.8(2) |
| C(13)-N(3)-B(1) | 120.0(2) |
| N(3)-C(13)-C(14) | 123.2(2) |
| C(13)-C(14)-C(15) | 118.5(2) |
| C(16)-C(15)-C(14) | 119.7(2) |
| C(15)-C(16)-C(17) | 119.5(2) |
| N(2)-C(17)-N(3) | 117.4(2) |
| N(2)-C(17)-C(16) | 122.0(2) |
| N(3)-C(17)-C(16) | 120.6(2) |

## 3.4 SINGLE-CRYSTAL X-RAY STRUCTURE OF L2.$BH_3$

The structure of L2.$BH_3$ is depicted in **Fig 3.1** which gives the numbering system used. Hydrogen atoms are numbered according to the atoms to which they are attached. Selected bond distances and angles are listed in Table 3.1. The molecule consists of discrete monomeric units with the potentially monodentate Schiff base bonded to a carbon substituent on the ferrocene system. The geometry of the organometallic residue is very similar to that observed in other mono-substituted ferrocene structures [27,77]. The two cyclopentadienyl rings are approximately parallel to each other (dihedral angle $0.87(0.16)^0$) as expected in comparison with the $1.0\text{-}1.66^0$ [27,68] reported for other substituted ferrocene systems. The twist angle of 8° between the two cyclopentadienyl rings shows that the ferrocene framework is nearly eclipised, which is normal [75].

The plane through the organic "tether", consisting of atoms C(11), N(1), N(2), lies at an angle of $16.7(0.3)^0$ to that of the plane of the C(6)-C(10) ring. The pyridine ring is twisted a further $7.0(3)^0$ from the C(11)-N(2) plane. As a result the two aromatic rings (i.e. pyridine and cyclopentadienyl) lie at an angle of $22.8(1)^0$ to one another .

The bond lengths and angles within the two cyclopentadiene rings (C-$C_{ave}$ 1.410(4)Å; C-C-$C_{ave}$ $107.8(3)^0$) lie within reported C-$C_{ave}$ bond lengths (1.40-1.46(1)Å) and C-C-$C_{ave}$ bond angles (108.08(8)°) [77]. The Fe-C distances range between 2.024(2)-2.044(2)Å and compare well with reported data of 2.031- 2.052(4) Å[68] and 2.026 - 2.135 [81] for other mono-substituted ferrocenes.

Since there is only a small angular twist (22.8(1)°) between the planes of the pyridine and cyclopentadiene ring electron delocalisation between these two moieties is possible but appears to be minimal. The C=N bond length is 1.264(2) Å, and is at the shorter end of the C=N bond length range reported in the literature (1.25(3)-1.289 Å, Table 3.2) indicating that strong multiple bond character is present.

The bond distance C(10)-C(11) is 1.459(2) Å and this compares well with bond lengths in similar compounds which range from 1.460(8)-1.469(5) Å and shows the expected shortening of a C-C bond *exo* to an aromatic ring system.

The N(1)-N(2) bond length of 1.387(2) Å compares well with the values (1.374-1.398 Å) reported for 1,1'-bispyridylhydrazone by A. Houlton *et al.* [56] who compared N-N and N-C bond lengths with those found by Palenik *et al.* [77] in 5-hydroxy-2-formylpyridine thiosemicarbazone and concluded that a small measure of delocalisation is present in the system. This delocalisation, which results in the shortening of the N(1)-N(2) bond length from 1.404(8)Å, has been attributed to the interaction of this bond with the ferrocene moiety attached to the $sp^2$ carbon of the C=N bond. This suggests that there is some interaction with the cyclopentadiene ring and that the system can be regarded as a weakly delocalised system.

The bond length for N(2)-C(17) which lies *exo* to the pyridine ring at 1.350(2)Å compares well with other similar bonds as shown in Table 3.2. The N(2)-C(17) bond of L2.$BH_3$ is one of the shorter bond distances in the table and is in accord with the presence of electron delocalisation.

**Table 3.2 Related Bond Lengths of Similar Compounds to L2.$BH_3$ (Å)**

| Compound | C= N | N - N | N - C | reference |
|---|---|---|---|---|
| 1,1-bispyridylhydrazone | 1.289 | 1.384 | 1.377 | [56] |
| 5OHFPTSC* | 1.270 | 1.379 | 1.366 | [77] |
| ATSC# | 1.286 | 1.398 | 1.342 | [77] |
| L2.$BH_3$ | 1.264(2) | 1.387(2) | 1.350(2) | This work |

* 5-hydroxy-2-formylpyridine thiosemicarbazone

\# acetone thiosemicarbazone

Of particular interest is the $BH_3$ substituted pyridine ring. The bond length N(3)-$C_{ave}$ is 1.353(3) Å and appears to be slightly longer than that found in other pyridyl systems which are also substituted at the ortho positions and where values averaging 1.335(7)Å [60] are reported. However these bond lengths do compare well with pyridine rings that complex through the lone pair of the nitrogen atom in the pyridine system

(1.33Å) as for example in [$BCl_3(NC_5H_5)$] and in the p-cymene pyrazine complex [76].

As expected the B atom deviates little from the plane of the pyridine ring (0.036(4)°) and the B(1)-N(3) bond length of 1.596(3) Å is comparable with other observed B-N bond lengths ( see Table 3.3 ).

**Table 3.3 Some Comparable Bond Distance Data for B-N Adducts (Å)**

| Compound | ( B - N ) | Reference |
|---|---|---|
| $L2.BH_3$ | 1.596(3) | this work |
| $BCl_3(C_5H_5N)$ | 1.592(3) | [78] |
| $BCl_3(NMe_3)$ | 1.575(10) | [79] |
| $BCl_3(NCMe)$ | 1.562(8) | [80] |
| $C_{35}H_{32}NBFe_3$ | 1.623(5) | [74] |
| $BCl_3NH_3$ | 1.579(4) | [73] |

The C-C bonds lengths within the pyridine ring range from 1.360-1.401(3)Å (ave = 1.377(3)Å) and are in accord with other pyridine system in the range 1.375(8)-1.361(7) [60,70,92,93,94], as are the C-N bond distances in the pyridine ring. The crystal packing arrangement of the $L2.BH_3$ compound can be seen in **Fig 3.0**.

## 3.5 MASS SPECTRUM OF $L2.BH_3$ $^{11}B$, $^{56}Fe$ (m/z)

The positive ion mass spectrum of $L2.BH_3$ was recorded using the liquid SIMS technique in a $NBA/CHCl_3$ matrix. Peaks are given with respect to $^{56}Fe$ and $^{11}B$. Two very intense peaks occur, one at 317(70%) which is assigned to $[M-2H]^+$ and a second is the parent ligand peak, $[M-BH_3]$ at 305(100%). The fragmentation processes that occur once the $BH_3$ group is lost follows closely that of the parent ligand, with the loss of the pyridine

ring and part of the 'tether' forming a peak assigned as $[C_5H_5\text{-}Fe\text{-}C_5H_4\text{-}CN]^+$ at 211(40%). A peak at 199 (42%) then appears which has the carbon in the cyanide function removed. This is the species $[C_5H_5\text{-}Fe\text{-}C_5H_4{=}N]^+$, which then loses the N atom to leave the ferrocene$^+$ peak at 185(10%). This is followed by the loss of a cyclopentadiene ring to give $[C_5H_5\text{-}Fe]^+$ ion (mass 121) and then the $[Fe]^+$ ion with a peak at 56. The calculated spectrum, given in **Fig 3.3** along with that observed, shows that the latter is consistent with the presence of Boron (two isotopes, $^{11}B$ = 80.09% and $^{10}B$ = 19.91%).

**Fig 3.3** Calculated isotope abundance calculations for $L2.BH_3$

ISO Isotope Cluster Abundance Calculations 10-APR-95

Formula: (NOM,ACC,SPE) Mode: (NOM,ACC,SPE) NOM

| Element | #Atoms | #Isotopes | Element | #Atoms | #Isotopes | Element | #Atoms | #Isotopes |
|---|---|---|---|---|---|---|---|---|
| C | 16 | 2 | | | | | | |
| H | 16 | 1 | | | | | | |
| N | 3 | 1 | | | | | | |
| B | 1 | 2 | | | | | | |
| FE | 1 | 2 | | | | | | |

Spectrum: (SPE)

| Mass | %Int | Mass | %Int | Mass | %Int | Mass | %Int | Mass | %Int |
|---|---|---|---|---|---|---|---|---|---|
| 314 | 1.5025 | 317 | 100.0000 | 320 | 0.0764 | | | | |
| 315 | 6.3177 | 318 | 17.5404 | 321 | 0.0027 | | | | |
| 316 | 24.6697 | 319 | 1.4650 | | | | | | |

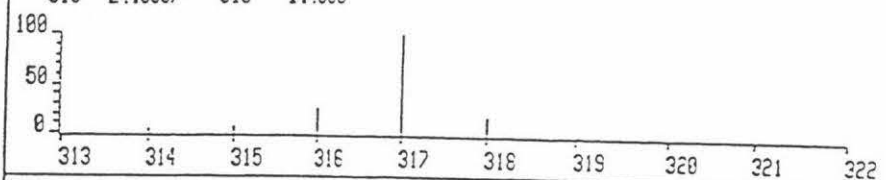


?=help RETURN=next ESC=previous 'C=compute 'X=exit 'H=hardcopy 'L('LX)=List(exit)

Obesrved spectrum for $L2.BH_3$

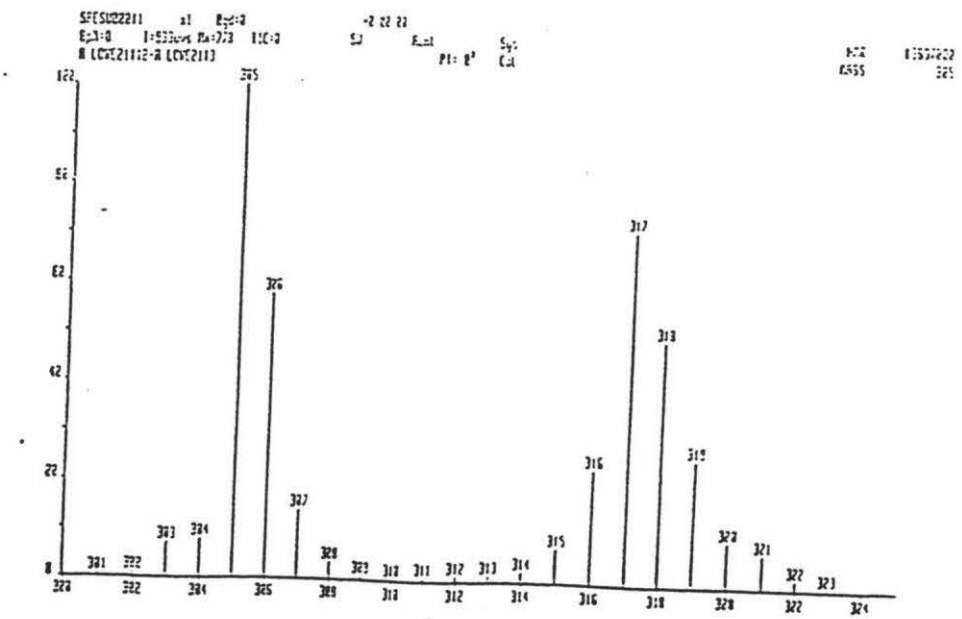

## 3.6 IR SPECTRAL COMPARISON OF L2 AND L2.$BH_3$

**Table 3.4 IR Spectra of L2 and L2.$BH_3$($cm^{-1}$)**

| Assignment | L2 | L2.$BH_3$ |
|---|---|---|
| ν (N-H) stretch | 3181, 3141 | 3263 |
| ν (N-H) bending | 1537 | 1578 |
| ν (C=N) stretch | 1594 | 1623 |
| ν ($C_5H_5$) bending | 809 | 814 |
| ν (B–H) stretch | - | 2287, 2247 |

IR data are given in Table 3.4. In the borane adduct of the 2-hydrazinopyridine ferrocene derivative (L2.$BH_3$) the bond at 3263$cm^{-1}$ is assigned as a ν(N-H) stretching frequency, possibly with an accompanying bending frequency at 1578 $cm^{-1}$. The ν(C=N) vibrational stretch has moved from 1594 to 1623$cm^{-1}$ on co-ordination of borane which suggests the imine-N is not bound to the boron. The cyclopentadiene ν(C-H) out-of-plane bending vibration observed at 814 $cm^{-1}$ changes little from that of the parent Schiff base (at 809 $cm^{-1}$). The ν(B-H) stretching vibrations occur in the region 2247-2287 $cm^{-1}$ and are consistent with terminal BH interactions with the boron bound to the pyridine ring. This was confirmed by X-ray analysis.

## 3.7 $^1$H NMR SPECTRAL COMPARISON

**Table 3.5 Comparison of L2 and L2. $BH_3$ Spectra (ppm)**

| Atom | L2.$BH_3$ | L2 |
|---|---|---|
| C(1)-C(5) | 4.23 | 4.19 |
| C(7), C(8) | 4.42 | 4.34 |
| C(9), C(6) | 4.64 | 4.59 |
| C(11) | 7.89 | 7.60 |
| C(16) | 7.53 | 7.26 |
| C(15) | 6.71 | 6.74 |
| C(14) | 7.69 | 7.58 |
| C(13) | 8.15 | 8.11 |
| N(2) | 9.34 | 8.45 |
| B-H | | 2.8-1.9* |

*There is some uncertainty with this assignment

Table 3.5 above shows a comparison of the chemical shift positions of the protons of L2 and L2.$BH_3$. The proton numbering scheme is depicted in the structure below. The hydrogen atoms are numbered according to the carbon atoms to which they are attached.

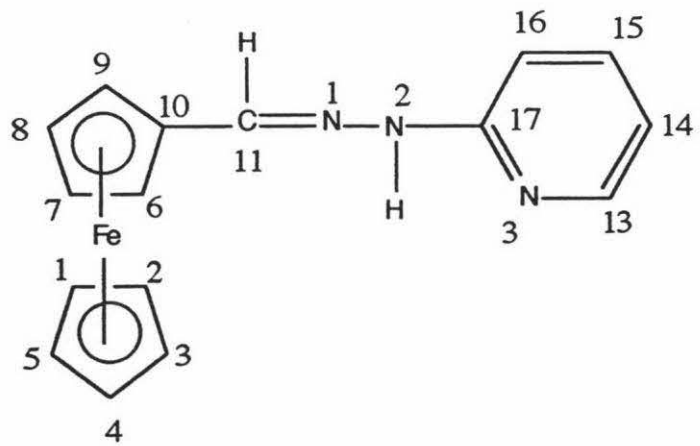

For L2.$BH_3$ the cyclopentadiene ring protons on C(1)-C(5) give rise to the resonance at 4.23 ppm with integral 5. Each of cyclopentadienyl ring protons C(6-9) and C(7-8) integrate as 2 and the resonances appear as a pair of slightly split singlets at 4.64ppm and 4.42ppm. The imine proton has moved to higher frequency by 0.29 ppm relative to the L2 parent compound. The N(2) proton integrates as one and gives rise to a broad singlet at 9.43ppm a frequency 0.89 ppm higher than L2.

The aromatic pyridine region gives rise to the same splitting pattern as its parent precursor which is a triplet , doublet , triplet , doublet combination in a 1:1:1:1 integrated ratio. The triplet at 6.71ppm ($^2J$ = 6.8 Hz) is assigned to the proton on C(15): a doublet at 7.52 ($^2J$ = 8.8 Hz) is assigned to the proton on C(16). The overlap of splitting patterns noted in the ligand L2 for the protons on C(14) and the imine proton does now not occur for L2.$BH_3$. These peaks are separated by 0.2 ppm and appear at 7.68 ppm ($^2J$ = 6.9 Hz) and 7.89 ppm, both of which integrate as single protons. The doublet that appeared at 8.11 ppm and was assigned to the proton on C(13), has moved down field and appears at 8.15 ppm ($^2J$ = 8.8 Hz) but still integrates as a single proton. The B-H proton resonances are very weakly detected at 2.8-1.9 ppm and appear as extremely broad peaks. This is consistent with protons being fluxional on the NMR time scale and being attached to a quadrupole nucleus.

The effect of complexing $BH_3$ with L2 through the pyridine nitrogen is similar to that of complexing of a transition metal with most of the proton chemical shifts moving to a higher frequency. However for H(13) the larger transition metal ions result in a shift to lower frequency.

## 3.8 $^{13}$C-NMR SPECTRAL COMPARISON

**Table 3.6 Comparison of L2 and L2.$BH_3$ $^{13}$C Data (ppm)**

| CARBON | L2 | L2.$BH_3$ |
|---|---|---|
| C(1)-(5) | 69.02 | 70.30 |
| C(7),C(8) | 69.54 | 69.24 |
| C(6),C(9) | 66.95 | 67.59 |
| C(10) | 80.25 | 78.56 |
| C(11) | 139.20 | 145.56 |
| C(17) | 156.97 | 152.71 |
| C(16) | 107.32 | 109.90 |
| C(15) | 138.02 | 139.64 |
| C(14) | 115.07 | 113.30 |
| C(13) | 147.35 | 145.60 |

The numbering scheme used is shown in Section 3.7, while the, $^{13}$C data for the L2 parent compound and L2.$BH_3$ are shown in Table 3.6. The cyclopentadienyl carbons have been assigned in accord with those found by Roberts *et al.* [56]. The cyclopentadienyl carbon resonances for β C(7) and C(8) at 69.24 ppm are deshielded relative to those assigned to the α C(6) and C(9) carbons at 67.59ppm indicating electron withdrawal by the hydrazone. This is enhanced for the L2.$BH_3$ adduct compared with that of the parent ligand. The β position in the ferrocene shows similar effects to the *para* position in benzene, the chemical shifts of which appear to be largely controlled by charge density.

The $^{13}$C chemical shifts for C(16) and C(16) of L2.$BH_3$ move to higher frequencies while C(13) and C(14) move to a lower frequencies relative to L2.

## 3.9 SUMMARY

Reduction of the Schiff base derivatives has proved extremely difficult, with decomposition or no reduction occurring in most instances. This suggests reduction probably occurrs at a slower rate than decomposition and this is confirmed by $^{1}H$ NMR spectra of the reaction mixtures. The palladised-carbon method gave the most positive indication that some reduction of the imine bond of the 2-hydrazinopyridine ligand had occurred but this method was not a practical synthetic one.

The novel synthesis of L2.$BH_3$ involves a pathway whereby $BH_3$ is extracted from a solution containing $NaBH_4$ in a large excess. The $^{1}H$ and $^{13}C$ NMR spectra for L2.$BH_3$ closely resembles those for the parent L2 ligand, as does the mass spectroscopic data. The X-ray structural analysis indicates that a minimal amount of delocalisation is present through the 'tethering' atoms that connect the ferrocene moiety to the pyridine residue. The new borane adduct, L2.$BH_3$, is an extremely stable molecule with the B-N bond length comparable with B-N bond distances in other similar adducts. $BH_3$ may be regarded as a stronger Lewis acid than $BF_3$ [70]. For $BH_3CO$ and $BH_3PF_3$, it has been suggested that there is a small amount of $\pi$ back bonding in which B-H bonding electrons are partly shared with $\pi$ acceptor orbitals of CO or $PF_3$ [70]. There may also be a small amount of similar $\pi$ back-bonding present in L2.$BH_3$, between the B-H bonded electrons and the $\pi$ acceptor orbitals of the pyridine ring. This would contribute to the stability of the co-ordinated $BH_3$ group.

Reactions involving $NaBH_4$ have been conducted on the 2-hydrazinopyridine precusor compounds and the bis-hydrazino derivative L22 with evidence that the latter compound undergoes a similar reaction to that of the L2 ligand. The $BH_3$ transfer reaction using thf:$BH_3$ was not successful in producing the L2.$BH_3$ adduct. A postulated mechanism by which the $BH_3$ species is formed in the reaction solution has been proposed.

# CHAPTER 4

## METALLO-DERIVATIVES OF SCHIFF BASE SUBSTITUTED FERROCENES

### 4.0 INTRODUCTION

Two factors motivated a study of the metallo-derivatives of ferrocene Schiff base ligands. The first was the ability of the iron atom within the ferrocene moiety to detect the presence of a host metal ion via electronic effects. The second factor is that such complexes can display mulitiple electron-transfer processes. This is because of their potential to act as electron transfer catalysts [86,87,88]. In either case it is important to establish the mode of coordination of the ligands to the metal ions. Very few studies of this type are presently available.

Formylferrocene thiosemicarbazones synthesised by Suprunchuck *et al.* [54] have been reported to complex with copper(II) in a 2.1 ratio as in **Fig 4.1.** Characterisation of the ligand and its complexes were very incomplete with IR spectroscopy being used as the main tool of identification. Difficulty in obtaining pure complexes was also commented on.

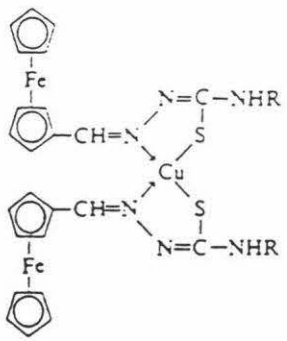


**Fig 4.1**

Twenty-four years after the Suprunchuck's study, a parallel study with Schiff based derived ligands from acetylferrocene and thiosemicarbazides (HAFTSC) was published by Xiaoxian *et al.* [53]. Complexes of the type $M(AFTSC)_2$ (M = Cu(II),

Co(II), Zn(II), Ni(II) and Cd(II)) were reported and co-ordination of the ligands discussed in the following manner. The NH bond adjacent to the C=S bond will tautomerise into the thioenol form which then loses a proton and results in a deprotonated complex involving a metal-sulfur bond as seen in **Fig 4.1**. The complexes were characterised in the usual way except that no X-ray crystal structures were reported.

Aza-thiosemicarbazones and thenoylhydrazones also undergo condensation reactions with formylferrocene to give Schiff base ligands that complex with Cu(II), Ni(II), Co(II) and Hg(II) in a 2:1 ratio. A representative postulated structure is shown in **Fig 4.2**. The structure is based on evidence from the cyclic voltammetry data, microanalysis, NMR and UV spectroscopy and molar conductivities.

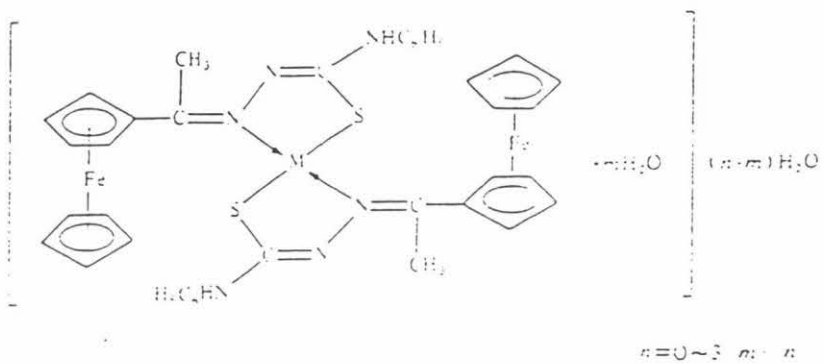

Suggested structure for the complexes (M = Zn, Ni, Co, Cd, Cu).

**Fig 4.2**

Hongyun *et al.* [57] also studied hydrazone systems and have isolated Pb(II) complexes, and these have added to the promising results from other arylhydrazones in the field of analytical and extractive chemistry. The co-ordinating mode of the ligand is similar to that in the complexes of Yongxiang *et al.* [55] with binding of the azomethine nitrogen and enolic oxygen atoms. (See **Fig 4.3**). Attempts to grow crystals failed.

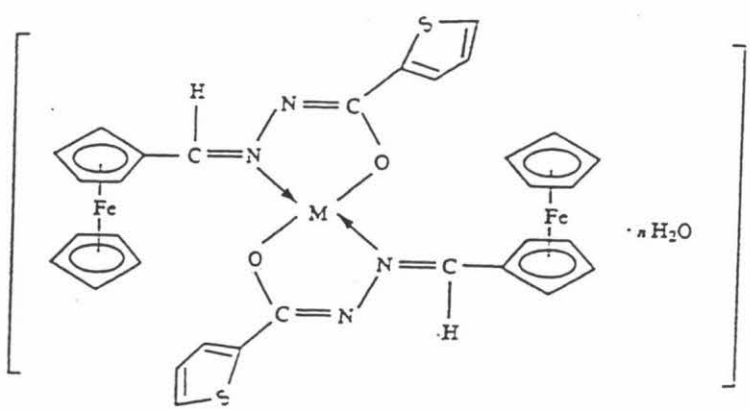

Suggested structure for the complexes: M = Cu, Ni and Hg: $n = 0$; M = Co: $n = 2$.

**Fig 4.3**

Bracci *et al.* [24] reported on the Schiff base ligand, N-(-o-hydroxybenzyl)-ferroceneamine (HL) **(Fig 4.4).** This ligand was complexed with a range of first row transition metals Cu(II), Ni(II), Co(II) and Zn(II) to form a rare series of non-orthometallated complexes of the type $M(L)_2$, where the imine bond is still intact. The characterisation of these compounds was reported in the usual manner, but it was noted that the purity and the reproducibility of the complexes varied at times.

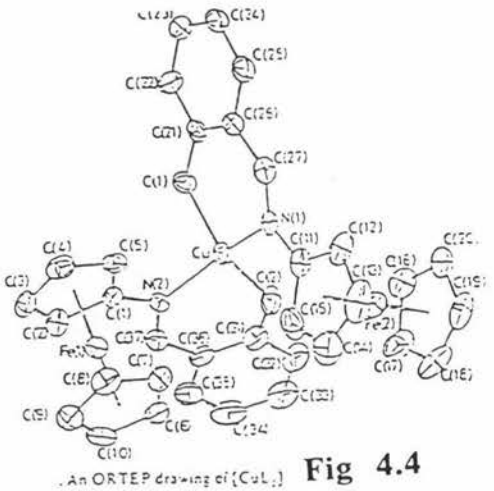

An ORTEP drawing of $[CuL_2]$ **Fig 4.4**

Esteven *et al.* [85] has focussed on dinuclear rhodium(II) complexes which incorporate the ferrocene moiety as in **Fig 4.5.** These were characterised by conventional methods, with the cyclic voltammetry results revealing that the $Fe^{2+} \rightarrow Fe^{3+}$ oxidation potential was greater than that of ferrocene. This suggests electron withdrawal occurs from the ferrocene moiety .

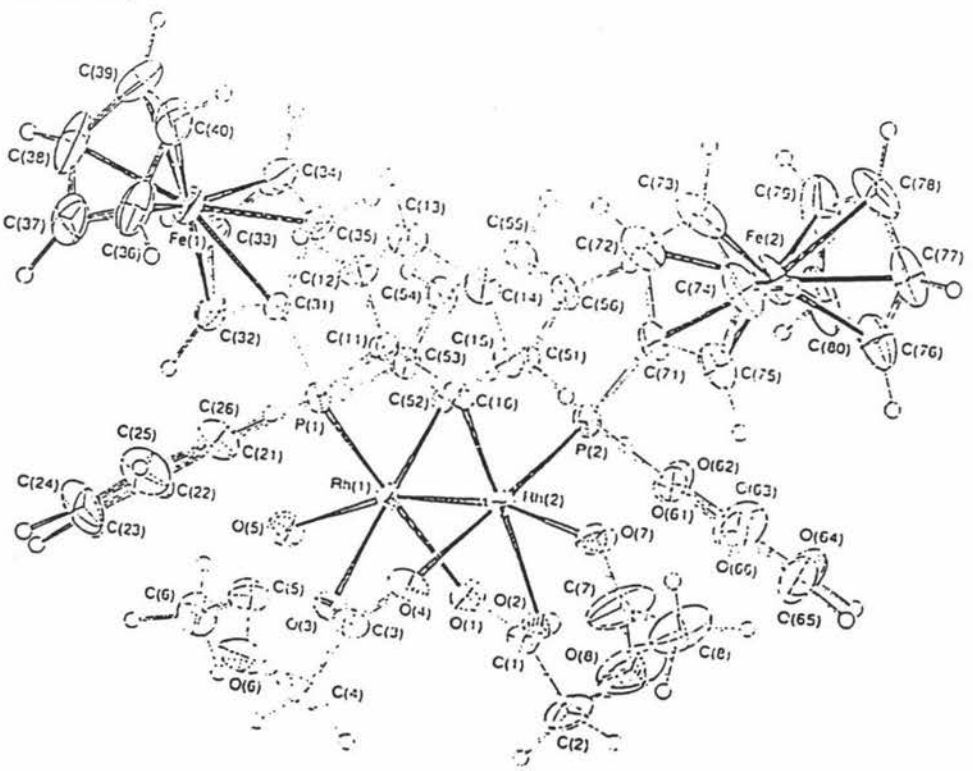

Sato *et al.* [50] has synthesised ferrocenothiacrown ethers which have been complexed with Ag(I), Cu(I) and Pd(II) for potential use in catalytic reactions. An example of this type of complex is shown in **Fig 4.6**.

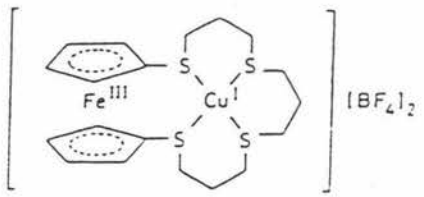


**Fig 4.6**

Bosque *et al.* [27] have reported the properties of ferrocenylamines and their cyclopalladated derivatives. These were found to be stable with the apparent stability arising because of the orthometallation that occurs between the cyclopentadienyl ring of the ferrocene and the Pd atom. Studies with other transition metals were not reported by these authors.

## 4.1 THE PRESENT STUDY

The objectives of this chapter are to study the coordinating characteristics of the range of ferrocene derivatives synthesised in Chapter 2 where the chelating atoms were varied and the 'tethers' had different lengths and atoms, to determine whether the host/guest interactions are sensed by the ferrocene ion. The interactions that occur with first row transition metals are studied with the view to obtaining stoichiometries and determining the structures of any complexe formed. The usefulness of such ligands in sensing devices is commented on.

# EXPERIMENTAL

## 4.2. PREPARATION OF COMPLEXES

### 4.2.1 COMPLEXES OF L1

**$[Zn(L1)Cl]_2$ xDBU. yDBUHCl. zthf.w $H_2O$**

To a warm solution of L1 (0.3g, 0.98 mmol) and 0.2g of DBU in 5 ml of thf was added dropwise to a solution of $ZnCl_2$ (0.134g, 0.98 mmol) in dry thf (15ml). The stirred solution turned red and the volume was reduced to 5-6 ml by warming, whereupon an oil precipitated. The mixture was placed in an ice bath and after 3-5 minutes red crystals formed. The complex was washed repeatedly with water (to remove DBUHCl) and dried on a vacuum line.

Yield: 0.58g (75%) M.P. 200-207°C

Found: C, 50.90 ; H, 5.72 ; N, 6.60

Calculated for ($C_{34}H_{28}N_2Fe_2Zn_2O_2Cl_2$ + 0.3 DBU+ 1.6 DBUHCl + 1 thf + 3.3 $H_2O$):

C, 50.80; H, 5.60 ; N, 6.58

**$^1$H NMR ($CDCl_3$)Δ:**

4.34 (s, 5H, $C_5H_5$), 4.67 (s, 2H, $C_5H_4$), 5.23 (s, 2H, $C_5H_4$), 6.60 (t, J = 7 Hz, 1H,

$C_6H_4$), 6.73(d, J = 7 Hz, 1H, $C_6H_4$), 7.07( t, J = 7 Hz, 1H, $C_6H_4$), 7.37 (d, J = 7 Hz, 1H, $C_6H_4$), 8.71 (s, 1H, C=N), 11.17 (s, 1H, OH)

There is also thf present (triplet 3.70 ppm, singlet 1.25 ppm) and both protonated and deprotonated DBU with multiplets at: (3.48-3.43 ppm), (2.84-2.81ppm), (2.06-2.04 ppm), (1.89-1.67ppm).

**IR** (nujol mull NaCl disk):

3383 br w, 3192 brw, 1641s, 1593 m, 1577m, 1264m, 1152w, 1104w, 830s, 767s

### 4.2.2 COMPLEXES OF L2

#### 4.2.2 (a) $Cu(L2)Cl_2$

To a warm solution of L2 (0.153g, 0.5 mmol) and 0.2g of triethylorthoformate in 5 ml of thf was added dropwise a solution of $CuCl_2$ (0.085g, 0.5 mmol) in dry ethanol (15ml). The stirred solution turned black and the volume was reduced to 5-6 ml by warming, whereupon black microfine crystals precipitated. The mixture was placed into an ice bath and left for an hour. The solution was then filtered and washed with ice cold ethanol.

Yield: 0.103g (17%) M.P. >220°C

Found: C, 44.10; H, 3.93; N, 9.43; Cl, 15.77

Calculated for ($C_{16}H_{15}N_3Cl_2CuFe$):

C, 43.8; H, 3.5; N, 9.5; Cl, 15.95

**I.R** (nujol mull, NaCl disk)

3189 brw, 1610s, 1561s, 1492w, 1246m, 1055m, 1007m, 825w, 917w, 763m, 722w

### 4.2.2 (b) $Co(L2)Cl_2$

To a warm solution of L2 (0.2g, 0.65 mmol) in 5 ml of thf was added dropwise a solution of $CoCl_2$ (0.156g, 0.65 mmol) in dry thf (15ml). The stirred solution turned red and the volume was reduced to 5-6 ml by warming. The mixture was then placed into an ice bath, whereupon a red precipitate formed. The solution was then filtered and the precipitate was washed with cold ethanol and dried on a vacuum line.

Yield: 0.16 g (48%), M.P > 200°C

Found: C, 43.74; H , 3.20; N, 9.14

Calculated for ($C_{16}H_{15}N_3Cl_2Co$):

C, 44.1; H, 3.4; N, 9.6

**IR** (nujol mull, NaCl disk)

3251brm, 1621s, 1594w, 1536s, 1423w, 1326w, 1261m, 1154w, 1095m, 1001w, 945w, 845w, 814w, 768m

### 4.2.2 (c) $Ni(L2)Br_2$

To a warm solution of L2 (0.2g, 0.65 mmol) in 5 ml of thf was added dropwise a solution of $NiBr_2$ (0.143g, 0.65 mmol) in dry thf (15ml). The stirred solution turned red/brown and the volume was reduced to 5-6 ml by warming. The mixture was placed into an ice bath, whereupon an oil formed. The complex was precipitated by the addition of cold pentane to the oil, which formed as a light brown/red powder. This was washed with cold ethanol/pentane twice then air dried.

Yield: 0.199g (58%) M.P >200°C

Found: C, 36.47; H, 4.51; N, 7.56

Calculated for ($C_{16}H_{15}N_3FeNiBr_2$):

C, 36.69; H, 2.89; N, 8.82

**IR** (nujol mull, NaCl disk)

3330br w, 3177 br w, 1617s, 1571w, 1534m, 1480w, 1320w, 1282w,1 254w, 1203w, 1152w, 1254w, 1203w, 1152w, 1124w, 1082m, 1000w, 953w, 898w, 821w, 767m

### 4.2.2 (d) $Co(L2)Br_2$

To a warm solution of L2 (0.18g, 0.59 mmol) in 5 ml of thf was added dropwise a solution of $CoBr_2$ (0.127g, 0.59 mmol) in dry thf (15ml). The stirred solution turned black and the volume was reduced to 5-6 ml by warming. The mixture was placed into an ice bath, whereupon an oil formed. The complex was precipitated by the addition of a mixture of cold pentane/ ethanol to form a black precipitate which was dried on the vacuum line.

Yield: 0.08g (25%) , M.P. >200°C

Found: C, 39.81 ; H, 3.49; N, 8.50

Calculated for ($C_{16}H_{15}N_3FeCoBr_2$):

C, 37.25; H, 2.88 ;N, 8.02

**IR** (nujol mull, NaCl disk)

3180 b w, 1611s, 1564w, 1317w,1 273w, 1244w, 1205w, 1151m, 1069w, 1042w, 1017w, 915w, 823m, 756m

### 4.2.2 (e) $Zn(L2)Cl_2$

To a warm solution of L2 (0.25g, 0.8 mmol) in 5 ml of thf was added dropwise a solution of $ZnCl_2$ (0.127g, 0.59 mmol) in dry thf (15ml). The stirred solution turned red and the volume was reduced to 5-6 ml by warming. The mixture was placed into an ice bath, whereupon an oil formed. The complex was precipitated by the addition of a mixture

of cold pentane/ ethanol to form a red precipitate which was dried on the vacuum line.

Yield: 0.25g (69%) , MP >200°C

Found: C, 43.77; H, 3.42 ; N, 9.55

Calculated for ($C_{16}H_{15}N_3FeZnCl_2$):

C, 43.53; H, 3.42 ; N, 9.50

**IR** (nujol mull, NaCl disk):

3263bm, 1622s, 1571w, 1539s, 1327w, 1236w, 1262w, 1205w, 1154w, 1124w, 1100m, 1000w, 947w, 935w, 895w, 813w, 769m

## 4.3 IR SPECTRA OF THE COMPLEXES OF L1 AND L2

### $[Zn(L1)Cl]_2$.xDBU.yDBUHCl.zthf.w$H_2O$

A summary of the IR vibrational frequencies for the complex of L1 is shown in Table 4.1. The complex $[Zn(L1)Cl]_2$.xDBU.yDBUH.zthf displays a weak broad stretch from DBU at 3192 $cm^{-1}$ assignable to a $\upsilon$(N-H) stretch of a protonated amine, hence supporting the presence of DBUHCl. The $\nu$(O-H) stretches for water appear as broad peaks at 3383 and 3242 $cm^{-1}$. The $\upsilon$(C=N) stretching vibration at 1642 $cm^{-1}$ has increased by about 30 $cm^{-1}$ from the parent ferrocene Schiff base ligand. This observation was initially unexpected as co-ordination of a metal to the Schiff base imine nitrogen atom was expected and is usually accompanied by a drop in wavenumber. This finding suggested that the Schiff base imine nitrogen is in fact not bound to the metal but the deprotonated oxygen atom on the phenol ring is. The cyclopentadienyl ring out-of-plane deformation bending vibrations can be seen at 831 and 806 $cm^{-1}$ in comparison with 817 $cm^{-1}$ for the free ligand, although the resolution if these absorbtions is not very good because of other nearby vibrations.

**Table 4.1 A Summary of Vibrational Frequencies of The L1 Complex ($cm^{-1}$)**

| Vibrational mode | L1 | $[Zn(L1)Cl]_2$ |
|---|---|---|
| C=N stretching vibration | 1611 | 1642 |
| C-C-C deformation bending | 818 | 831, 806 |

**The Complexes of L2 $[M(L2)X_2]$** (M = Cu, Co, Ni, Zn; X = Cl, Br)

The υ(N-H) stretching vibration from the hydrazino chain of the ligand appears as a typically broad peak and is observed in all spectra although the exact position varies from 3192-3059 $cm^{-1}$. The υ(C=N) stretch of the imine bond of the parent ligand is at 1593 $cm^{-1}$ but all of the complexes show an increase in wavenumber in the range 1610-1621 $cm^{-1}$. This result, which resembles that of the L1 complex, suggests that the imine nitrogen atoms do not bind to the metals. As well the υ(N-H) bending vibrations are found in the range 1534-1571 $cm^{-1}$ in the complexes compared with 1537$cm^{-1}$ in L2. The aromatic pyridine ring has an out-of-plane C-C-C bending vibration at 998 $cm^{-1}$ for L2 and this vibration is clearly observed in all of the complexes. The cyclopentadienyl ring C-C-C bending deformation vibrations are observed in the range 813-827$cm^{-1}$ but their weak nature combined with overlapping nearby bands makes detection difficult in the complexes. A summary of the common IR vibrations is shown in Table 4.2.

**Table 4.2 Common IR Vibrational Frequencies ($cm^{-1}$)**

| vibration | N-H | C=N | N-H bending | $C\text{-}C_{pyridine}$ bending | $C_5H_5$ bending |
|---|---|---|---|---|---|
| L2 | 3118 | 1593 | 1537 | 998 | 810 |
| $Cu(L2)Cl_2$ | 3116 | 1610 | 1561 | 1007 | 827 |
| $Co(L2)Cl_2$ | 3251 | 1621 | 1536 | 1001 | 814 |
| $Co(L2)Br_2$ | 3059 | 1611 | 1566 | 1017 | 823 |
| $Ni(L2)Br_2$ | 3177 | 1616 | 1571, 1537 | 1000 | 821 |
| $Zn(L2)Cl_2$ | 3247 | 1621 | 1539 | 1000 | 813 |

## 4.4 LIQUID SIMS MASS SPECTROSCOPY OF THE COMPLEXES

### 4.4.1 Mass Spectrum of $[Zn(L1)Cl]_2.xDBU.yDBUHCl.zthf.wH_2O$

The apparent non-stoichiometric amounts of DBU, DBUHCl and thf complicates the mass spectrum of the titled compound but interpretation is still possible. A number of ions were detected and these match well with their respective isotope abundance calculations.

**Table 4.3Mass Spectral Summary for**

**$[Zn(L1)Cl]_2.xDBU.yDBUHCl.zthf.wH_20$**

**Fe = $^{56}$Fe**
**Zn = $^{64}$Zn**
**m/z**

| Observed Ions | Calculated | Found (relative Intensity) |
|---|---|---|
| $\{[Zn(L1)Cl]_2(DBU)(DBUH)\}^+$ | 1151 | 1151 (5%) |
| $\{[Zn(L1)Cl]_2thf\}^+$ | 882 | 882 (15%) |
| $[Zn(L1)Cl]_2^+$ | 809 | 809 (8%) |
| $[Zn(L1)Cl_2(DBU)]^+$ | 593 | 593 (35%) |
| $[Zn(L1)Cl]^+$ | 404 | 404 (16%) |
| $L1^+$ | 305 | 305 (100%) |

* $DBUH^+$ is the protonated form of DBU

The most intense peak at 305 is assigned as $[L1]^+$ (100%) ligand and any lower mass ions that appear simulate the free ligand (L1) fragmentation pattern. (See Chapter 2.) A number of other peaks have been identified and these are ions which not only contain the Zn atom and L1 ligand, but also incorporate either thf solvent and/or the DBU. The highest mass peak located at 1151 (6%) has been assigned to the $[C_{52}H_{61}O_3N_6Cl_3Fe_2Zn_2]^+$ ion which is the dinuclear complex containing DBU and protonated DBU. A peak at 882(10%) has been assigned to the $[Zn(L1)Cl]_2^+$ complex + thf, $[C_{38}H_{36}O_3N_2Cl_2Fe_2Zn_2]^+$. The loss of thf from the 882 ion results in the formation of the complex $[Zn(L1)Cl]_2^+$ ion, $(C_{34}H_{27}O_2Cl_2Fe_2Zn)^+$, with a peak at 809 (7%). The species at 593 (35%) is assigned to

the $[Zn(L1)Cl_2(DBU)]^+$ ion, $(C_{26}N_3OH_{30}FeZnCl_2)^+$. DBU and $Cl^-$ are then both lost to form an ion located at 404 (15%) and assigned to $[C_{17}H_{14}NOFeZnCl]^+$. This is then followed by formation of the ligand ion at 305 (100%) by the loss of $Zn^{2+}$ and $Cl^-$ ions. A summary is given in Table 4.3, with the isotope abundance calculations appearing in Appendix III.

## 4.4.2 COMPLEXES OF L2

A summary of all the more abundant ions is given in Table 4.4.

### 4.4.2(a) $[Cu(L2)Cl_2]$

The highest molecular weight species occurs at 708(20%) and perhaps surprisingly has been assigned to the $Cu(L2)_2Cl^+$ ion ($C_{32}H_{28}N_4Fe_2CuCl^+$). This loses a Cl species to give a fragment at 673(15%) with the empirical formula of $[C_{32}H_{28}N_4Fe_2Cu^+]$ the $Cu(L2)_2^+$ ion. The fragment at 405(15%) is assigned to the $Cu(L2)Cl^+$ ion ($C_{16}H_{14}N_2$ $FeCuCl^+$) . This then loses the Cl species to leave the ion $Cu(L2)^+$, ($C_{16}H_{14}N_2FeCu^+$) at 368(40%). The loss of the copper ion leaves the parent protonated ligand, $L2H^+$, ($C_{16}H_{15}N_2Fe^+$), located at 306 (35%). The fragmentation of $L2H^+$ follows closely that of the free ligand that has already been discussed for L2 in Chapter 2.

### 4.4.2(b) $[Co(L2)Cl_2]$

This complex underwent a similar fragmentation process to that of $[Cu(L2)Cl_2]$, with an ion at 708 (45%) assigned to the $Co(L2)_2Cl^+$ species,$[C_{32}H_{28}N_4Fe_2CoCl^+]$, showing the ease with which this ion is formed and suggesting a 2:1 ligand to $CoCl_2$ species should be able to be synthesised. Loss of a Cl species and $H_2$ produces the $Co(L2)_2^+$ ion,$[C_{32}H_{28}N_4Fe_2Co^+]$, at 669 (50%). The $Co(L2)Cl^+$ ion, $[C_{16}H_{14}N_2FeCoCl^+]$, is located at 400 (30%). An ion resulting from the loss of Cl ion is found at 363 (40%) and is assigned to the $Co(L2)H^+$ ion $[C_{16}H_{14}N_2FeCoH^+]$. Cobalt is then cleaved to leave the parent deprotonated ligand ($L2^+$, ($C_{16}H_{14}N_2Fe^+$) at 304 (24%). The fragmentation of the remaining deprotonated L2 ligand mimics that of the free ligand discussed in Chapter 2.

### 4.4.2(c) $[Ni(L2)Br_2]$

This complex also follows a very similar fragmentation process to that of $[M(L2)Cl_2]$ (M = Cu, Co) and gives confidence that this is typical for such species. The highest molecular weight species occurs at 749 (50%) and is assigned to the $Ni(L2)_2Br^+$ ion, $[C_{32}H_{28}N_4Fe_2NiBr^+]$. A Br species is then lost to give the $Ni(L2)_2^+$ ion,$[C_{32}H_{28}N_4Fe_2Ni^+]$, at 667 (55%). The peak at 442 (30%) is assigned to the $Ni(L2)Br^+$ ion, $[C_{16}H_{14}N_2FeNiBr^+]$. Another Br species is then lost forming the $Ni(L2)^+$ ion, $[C_{16}H_{14}N_2FeNi^+]$, at 363 (60%). Loss of the $Ni^{2+}$ ion results in the formation of the protonated $L2H^+$ ion, $[C_{16}H_{14}N_2FeH^+]$. Fragmentation of the $L2H^+$ pattern also follows that of the free ligand discussed in Chapter 2.

**Table 4.4 Common Ions Present in the Mass Spectra of the Complexes**

**Cu = $^{63}$Cu , Ni = $^{58}$Ni , Co = $^{59}$Co , Fe = $^{56}$Fe**

| | m/z | | | | |
|---|---|---|---|---|---|
| | $M(L2)_2X$ | $M(L2)_2$ | $M(L2)X$ | $M(L2)$ | L2 |
| $Cu(L2)Cl_2$ | 708 | 673 | 405 | 368 | 305 (L2) |
| $Ni(L2)Br_2$ | 749 | 667 | 442 | 363 | 306 (L2H) |
| $Co(L2)Cl_2$ | 708 | 669 | 400 | 363 | 304 (L2-H) |

Isotope abundance calculations for the ions appearing in Table 4.4 are in the Appendix III.

## 4.5 LIGANDS AND THEIR ASSOCIATED COMPLEXES

Below is a review of attempts at preparing transition metal coordination complexes of the ligand series reported in chapter 2. Details of complexes that were characterised can be found in Section 4.3.

### 4.5.1 COMPLEXES OF L1

The L1 ferrocene derivative was designed as a bidentate ligand, but spectroscopic data and analytical results provide evidence that it functions as a mono-dentate ligand. In the complex $[Zn(L1)Cl]_2.zthf.xDBU.yDBUHCl.wH_2O$ loss of the phenolic ν(O-H) stretching frequency in the infrared spectrum and the formulation of the complex from analytical and mass spectral data suggest co-ordination of the deprotonated oxygen atom. Furthermore the increase in the ν(C=N) stretching frequency on bonding to $Zn^{2+}$ suggests that the imine nitrogen is not bound. Models do suggest that strain is introduced when L1 is in the bidentate co-ordination mode. The absence of imine nitrogen bonding leaves a vacant metal co-ordination site which may be filled by thf, water, solvent, or DBU (the latter, in non-stoichiometric amounts). DBUHCl appears to be trapped in the lattice as well. The complex seems to act as a 'sink' for other species in the reaction mixture and this may help to explain the difficulty in obtaining 'good' elemental analyses. The formulation of this compound as a dimer is justified by mass spectral data and postulated a structure is given in **Fig 4.7.**

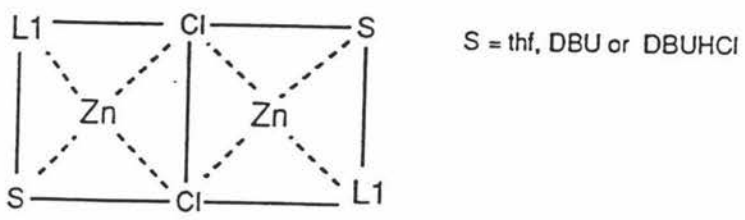


**Fig 4.7** Postulated structure for $[Zn(L1)Cl]_2zthf.xDBU.yDBUHCl.wH_2O$

If the above reaction is performed in the presence of sodium ethoxide acting as a base in ethanol (instead of DBU), a black impure precipitate was obtained. The infra-red spectrum indicated the presence of a ν(C=O) stretching frequency at 1585 $cm^{-1}$ which is consistent with 'free' ferrocene carboxaldehyde. The nature of the base seems to be an imporatnt factor in the success of these reactions.

Attempts to bind transition metals species such as $MX_2$ (M= Ni, Co, Cu) to L1 in ethanol or thf (1:2 ratio) in the pesence of $NaOCH_3$ have been unsuccessful. Elemental analyses revealed low carbon and high nitrogen values. Hydrolysis of the imine bond may have occurred and as previously discussed a different base may be required in further studies.

### 4.5.2 COMPLEXES OF L2

Complexes of the type $M(L2)X_2$ (M= Cu, Co, Ni) and (X= Cl, Br) have been isolated when the reactants are in a 1:1 ratio (Section 4.3). Infra-red evidence for all of the complexes is consistent with non-coordination of the imine nitrogen and hence only the pyridine nitrogen is likely to be bound as has already been observed for $L2.BH_3$. The three coordinate mononuclear form is therefore incorrect and a dinuclear form is suggested. The discrepancy between the theoretical and obtained analytical elemental results in some cases may be explained by the addition of non-stoichiometeric amounts of solvent trapped in the lattice. Mass spectral data have detected the presence of the mononuclear species, $M(L2)X^+$, ion and all show the presence of $[M(L2)_2X]^+$. Attempts to synthesise this latter species seems warranted in the future. A possible structure for the $[M(L2)X_2]$ species is given in **Fig 4.8**

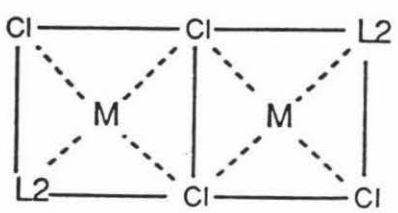


Fig 4.8

### 4.5.3 COMPLEXES OF L44

It was postulated that this ligand would complex to Cu(II) and show promise as a anti-tumor compound. The complex has two structural features that many deactive a tumor. The first feature involves the ferrocene moiety, which would be oxidised either before infusion into the patient or in the oxygen rich media of the cell, causing the formation of the ferricinium ion. This would then interact with the DNA by binding in the minor grove and prevent replication. The second method involves the thiosemicarbazide moiety, which would transport the copper into the cell and upon its release, would allow a reaction of the Cu with the enzyme superoxide dismutase (sod) as per reaction in Chapter 1 (section 1.2). The resultant accumulation of superoxide would then attack the cellular structures of the tumor.

The complex was prepared by the addition of L44 to a solution of hydrated copper acetate in absolute ethanol. This produced a black product, but the analytical figures indicated it was not pure enough for further study. It was felt that more research should be conducted on this system.

### 4.5.4 OTHER ATTEMPTED REACTIONS

Attempts to prepare complexes with L5, L3, L11 and L22 are given in Appendix III. In general these reactions give rise to products that were unidentifiable due to possible hydrolysis of the imine bond or partial oxidation of the ferrocene iron. Models suggest that the potentially bi- or tetra-dentate ligands L11 and L22 do not bind to metal ions without considerable strain which may lead to ready decomposition.

## 4.6 SUMMARY

Even though six complexes were characterised, more than twenty complexation reactions failed to give a identifiable products. The reasons as to why these complexation reactions failed are varied, with evidence that the ligand undergoes hydrolysis, such as in L1, or produces a μ-oxo bridged species as has occurred in bis-hydrazone systems similar to L22. However it appears that none of the complexes produced involve the chelation of the imine nitrogen to a metal. This inability of the nitrogen to chelate may explain some of the difficulties encountered in the fitting of elemental analysis figures and the difficulties in recovering the complex from the reaction solution. For the L1 complex, this explanation means the vacant co-ordination site of the metal, caused by the non-chelation of the imine nitrogen, is occupied by either solvent or by organic base such as DBU, as deduced from the IR and $^1$H NMR spectral evidence.

For L2, mass spectroscopic evidence suggests that the vacant coordination site is not occupied by solvent but that it allows dimerisation to occur. Also the detection of species such as $[M(L2)_2X]^+$ suggests that their synthesis should be attempted.

The reactions with the bis-thiosemicarbazide ferrocenyl ligand (L44) also needs further research, since there is evidence that the complex had formed. However there were also high levels of impurities present which resulted in poor elemental analysis data fitting.

# CHAPTER 5

## PHYSICOCHEMICAL STUDIES OF THE LIGANDS AND THEIR COMPLEXES

## 5.1 INTRODUCTION

### 5.1.1 CYCLIC VOLTAMMETRY (CV)

This is a very useful tool as a qualitative "diagnostic" technique and has been widely used for mechanistic studies of redox systems.

CV uses a repetitive triangular waveform. The potential of the working electrode is swept back and forth between two designated values ("switching potentials"). Many cycles can be performed but typically 3-5 are done until the voltammogramme is stable.

The potential range is chosen according to location of the redox couple of interest. The current is measured at the working electrode, as a function of potential, in a stirred solution. CV can be used to generate a new species during the forward scan, then its properties are studied on the reverse scan.

**IMPORTANT PARAMETERS IN CV**

| | | |
|---|---|---|
| Magnitudes of peak currents | anodic current | ($i_p^a$) |
| | cathodic current | ($i_p^c$) |
| Peak potentials | anodic potential | ($E_p^a$) |
| | cathodic potential | ($E_p^c$) |

In voltammetry, current is normally measured as a function of the applied potential. The relationship between the concentration at the electrode surface and the potential for a reversible process is given by the Nernst equation (Equation 1).

$$E = E^o - {}^{RT}/_{nF} \ln C_{ox} / C_{red} \quad \cdots\cdots\cdots\cdots \quad (1)$$

where E = electrode potential

$E^o$ = standard red / ox potential

$C_{ox}$ = concentration of the oxidant species

$C_{red}$= concentration of the reduced species

A limitation of CV is the accurate measurement of the peak current . This is because the establishment of a correct base line is difficult, especially for complicated systems. The reverse scan is the most problematic since the base line is not the same as the residual current for an identical experiment in a supporting electrolyte alone.

The ferrocene molecule contains iron which can be considered to be in a 2+ oxidation state and is the accepted standard for this electro-chemical technique with $E_p^c$ = 464 mV and $E_p^a$ = 550 mV.

For a system which is electrochemically and chemically reversible (i.e. the product of the electrode process is stable) equation 2 applies.

$$\Delta E_p = E_p^a - E_p^c = (0.059 / n)\ V \quad \text{at } 25\ ^0C \quad \ldots\ldots\ldots \quad (2)$$

where: n = no of electrons involved

$E_p$ is independent of scan rate and has $i_p^a = i_p^c$

A diagram relating to the measurement and interpretation of the data from the cyclic voltammogramme is shown beiow.

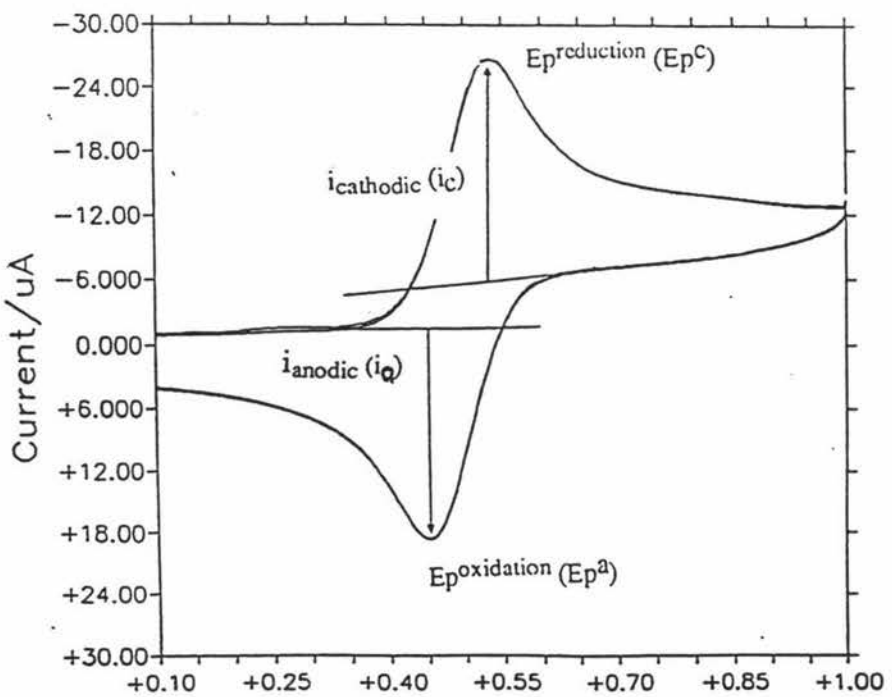

The Half wave potential ($E^{1/2}$) approximates the $E^0$ potential in a reversible system and the formal electrode potential and is given by equation 3

$$E^{1/2} = {}^1/_2 \ (E_p{}^a + E_p{}^c) \quad \ldots\ldots\ldots\ldots\ldots\ldots\ldots\ldots \quad (3)$$

As the scan rate (R) is increased, $i_p{}^a$ and $i_p{}^c$ increase proportionally to $R^2$. For a reversible couple, plots of $i_p{}^a$ and $i_p{}^c$ verses ($R^{1/2}$), should be linear with intercept at the origin.

CV is a useful probe for unstable reduced or oxidised species. They can be regenerated electrochemically by a reverse scan. The longer the delay between the generation of the species and the reverse scan (i.e the slower the scan rate ), the lower will be $i_p$. This allows a method of detection and characterization assessment of impure or mixed ligand or complexed systems .

### 5.1.2 MÖSSBAUER SPECTROSCOPY

Mössbauer results are reported in two parameters, the isomer shift (i.s) and the quadrupole splitting (q.s). Isomer shift reflects the total s electron density at the nucleus on the iron atom and is therefore sensitive to the oxidation state, the nature of the ligands and the coordination number. If there is strong covalent bonding, ($\delta$) (defined below) decreases for Fe(II) and approaches the $\delta$ value for Fe(III). Thus the method gives a sensitive means of confirming the oxidation state of Fe. The variation of electron density on the nucleus of the s shell can be summarised below.

$$(\delta) \text{ is proportional to } \{|\psi_a(0)|^2 - |\psi_e(0)|^2\} \{<R_e^2> - <R_g^2>\}$$

$\delta$ = Doppler velocity given to the source to observe a resonance.

$\psi_a$ = s density at the nucleus for the absorber.

$\psi_e$ = s density at the nucleus for the emitter.

$R_e$ = effective nuclear charge radius for excited state.

$R_g$ = effective nuclear charge radius for ground state.

There is thus some analogy with nmr chemical shifts. The q.s. is a measure of the symmetry of the electronic environment of the iron nuclus. It increases with increase in the electric field gradient at the nucleus, and is equal to half the nuclear quadrupole coupling constant that would be obtained from nuclear quadrupole resonance (NQR) spectroscopy. High symmetry (cubic, octahedral, tetrahedral geometry) gives zero q.s. and a single line spectrum is observed. An electric field gradient may arise either in the valence shell or when the coordination geometry has less than cubic symmetry, causing a disruption of the symmetry within the applied field. The field gradient results in a splitting of the first excited state into two energy levels of Fe. This splitting is the quadrupole splitting.

The i.s. is determined from the centre of the two resulting peaks.

From NQR theory $\quad q.s. = (^1/_2\, e^2\, Qq)$

and the coupling constant is $\quad e^2\, Qq / h$

where: e is the unit of electrostatic charge

Q is the measure of deviation of the nuclear charge distribution

$M_I$ is the nuclear spin angular momentum quantum number

q is the electric field gradient

So

If $M_I = +\text{-}\ ^3/_2$ the sign of the coupling constant is positive

If $M_I = +\text{-}\ ^1/_2$ the sign of the coupling constant is negative

Ferrocene has an intriguing form of relaxational averaging that is involved with the electric field gradient. Ferrocene's electric field gradient at the nucleus is derived from the sandwich structure in which the electron density along the molecular axis is different from that perpendicular to it. Ferrocene has a well resolved quadrupole splitting at 2.37 $mm\text{-}s$, with i.s. at 0.52 $mm\text{-}s$. Further details on the technique of Mossbauer spectrocopy may be obtained from reference [69].

## 5.2 THE PRESENT STUDY

The aim of this chapter is to probe the electronic properties of the iron atom in the various substituted ferrocenes by CV and Mossbauer spectroscopy. The first property to be exploited is the reduction/oxidation process which enables the ferrocene to act as the reference (similar to TMS in $^1$H NMR). It undergoes a reversible oxidation and displays full Nernstian behaviour (i.e. $Ip^a$:$Ip^c$ = 1, $Ep^a$ -$Ep^c$ = 79 mV and the oxidation is a diffusion controlled process, which produces a straight line when the scan rate verses current is plotted). It was anticipated that like ferrocene, the Schiff base derivatives would display similar Nernstian behaviour but at a different Ep potentials because of the substituents on the cyclopentadienyl ring.

Trends in the isomer shifts and the quadrupole splitting of the iron centres from Mössbauer spectroscopy for the same Schiff base derivatives would be similarly rationalised. These results should be complementary to those of CV, and be related to the electron density and field gradient at the iron centre. These in turn will be related to the presence of the imine bond and its various substituted organic substituents. Hence a better understanding of the electronic changes that occur on formation of a Schiff base and its adducts will be obtained.

# RESULTS AND DISCUSSION

## 5.3 ELECTROCHEMICAL ANALYSIS OF THE FERROCENE DERIVATIVES

Cyclic voltammetric (CV) experiments on the ferrocene substituted Schiff base derivatives and the reference species (ferrocene and ferrocene monocarboxaldehyde) were carried out in N,N-dimethylformamide (dmf) at room temperature (20 $^{0}$C) in the presence of tetrabutylammonium perchlorate ($NBu_4ClO_4$) as the ionic buffer. The reference electrode was a saturated Ag/AgCl electrode and the working electrode was a 3 mm glassy carbon electrode with platinum as the auxiliary electrode. The solutions for analysis were prepared by the addition of 5 ml of ligand solution (approximately 2.26 $x10^{-3}$ mol $l^{-1}$ in dmf) to the cell followed by the addition of 5ml of $NBu_4ClO_4$ (approximately 2.26 $x10^{-3}$ mol $l^{-1}$ in dmf) to give a final concentration for both of approximately 1.13 $x10^{-3}$ mol $l^{-1}$. Attention was centred on the first one-electron oxidation and reduction, $Fe^{II} \rightarrow Fe^{III} \rightarrow Fe^{II}$, which changes the ferrocenyl group into the ferricinium cation and back to ferrocene. Data for the oxidation and reduction of the ferrocene substituted Schiff bases are summarized in Table 5.1.

The tabulated data show that ferrocene carboxaldehyde ($Ep^a$ = 932 mV) is more difficult to oxidise than the ferrocene ($Ep^a$ = 550 mV) and it is also harder to oxidise any ferrocene Schiff base derivative containing a C=N bond since $Ep^a$ also becomes more positive when the reaction is conducted under the same conditions. The L1 derivative ($Ep^a$ = 823 mV) is harder to oxidise than the ferrocene ($Ep^a$ = 550 mV) which is to be expected since the imine bond and phenol ring are electron withdrawing, thus decreasing the electron density on the iron nucleus which in turn decreases the ease of oxidation of the iron atom. This observation is consistent with observed Mössbauer results (Section 5.4). The L2 derivative undergoes a similar trend to that of L1 with the oxidation process ($Ep^a$) of the iron occurring at a more positive value than that of ferrocene, but less positive than the L1

derivative itself ($Ep^a$ (L2) = 694 mV cf. $Ep^a$( L1)= 823 mV). The oxidation process appears to be easiest with systems that are either fully saturated, as in L5, or where delocalisation throughout the substituted moiety attached to the ferrocene is present as occurs in L4. The ease of oxidation of the mono-substituted ferrocene ligand can be summarised as L1 < L2 < L4 < L5. (The L3 ferrocene derivative, decomposed before CV or Mossbauer techniques of characterisation could be conducted on them.)

The bis substituted ferrocene derivatives, L11 and L22, both have $Ep^a$ values greater than their mono substituted parent analogues. For the L44 derivative which is based on thiosemicarbazide, the ferrocene oxidation process is not observed. This has also been noted by Duan *et al.* [95], with other Schiff base systems, but there was no explanation as to why the one electron oxidation process does not occur.

It is interesting to note that a comparison of the L2 ligand with that of the borane adduct L2.$BH_3$ (Table 5.2) shows a 24 mV difference with the L2.$BH_3$ complex being easier to oxidise than the parent ligand.

**Table 5.1 Summary of the Peak Potentials ($Ep^{a/c}$) of the Ferrocene derivatives**

| Ferrocene Derivatives | Conc of derivative ($x10^{-3}$ mol $l^{-1}$) | Conc of $NBu_4ClO_4$ ($x10^{-3}$ mol $l^{-1}$) | $Ep^a$ (mV) | $Ep^c$ (mV) | $E^{1/2}$ (mV) | $Ep^a$- $Ep^c$ (mV) |
|---|---|---|---|---|---|---|
| L1 | 1.16 | 1.16 | 823 | 682 | 752 | 141 |
| L2 | 1.16 | 1.16 | 694 | 588 | 641 | 106 |
| L5 | 1.16 | 1.16 | 540 | 460 | 500 | 80 |
| L4 | 1.16 | 1.16 | 634 | 542 | 588 | 92 |
| L11 | 1.16 | 1.16 | 932 | 700 | 816 | 232 |
| L22 | 1.16 | 1.16 | 1013 | 713 | 863 | 300 |
| L44 | 1.16 | 1.16 | there is no ox/red of ferrocene | | | |
| Ferrocene | 1.16 | 1.16 | 550 | 464 | 507 | 86 |

**Table 5.2 Comparison of peak potentials for L2 and L2.$BH_3$**

| | Conc ($x10^{-3}$mol $l^{-1}$) ferrocene derivative | Conc (mol $l^{-1}$) $NBu_4ClO_4$ | $Ep^a$ (mV) | $Ep^c$ (mV) | $Ep^a$-$Ep^c$ (mV) | $E^{1/2}$ (mV) |
|---|---|---|---|---|---|---|
| Ferrocene | 1.16 | 1.16 | 550 | 464 | 86 | 507 |
| L2 | 1.16 | 1.16 | 694 | 588 | 106 | 641 |
| L2.$BH_3$ | 1.16 | 1.16 | 670 | 541 | 129 | 605 |

The relative ease of oxidation of L2.$BH_3$ indicates that electron flow back to the Fe centre *via* π-conjugation between the Schiff base chelated ring through the C(10)-C(17) chain of L2.$BH_3$ is greater than that of the free L2 ligand. X-ray data (Chapter 3) on L2.$BH_3$ suggests a degree of delocalisation and some back π → $N_{py}$ donation, which allows for an easier oxidation of the $Fe^{II}$ → $Fe^{III}$ atom. This is likely to be propagated through the skeletal system of the π-bonds. A similar argument, although one in which oxidation is more difficult, has been proposed by Bracci *et al.* [24] for the N-(*o*-hydroxybenzyliene) ferrocenamine derivative.

Nernstian behaviour of the ferrocene Schiff base derivatives, L1, L2, L11 and L22, is extremely difficult to assess, since the base lines on which the $Ip^a$ and $Ip^c$ currents are measured are difficult to establish. The difference between anodic and cathodic peak potentials ($Ep^a$ - $Ep^c$) for L1, L2, L11 and L22 are higher than expected for a totally reversible process (ferrocene under same conditions is $Ep^a$ - $Ep^c$ = 86 mV). However, because of the fluxional gradients of the base lines in the oxidation and reduction processes, the ratio between the cathodic and anodic intensities cannot be calculated. A representative diagram is shown in **Fig 5.1** for the L1 ferrocene derivative.

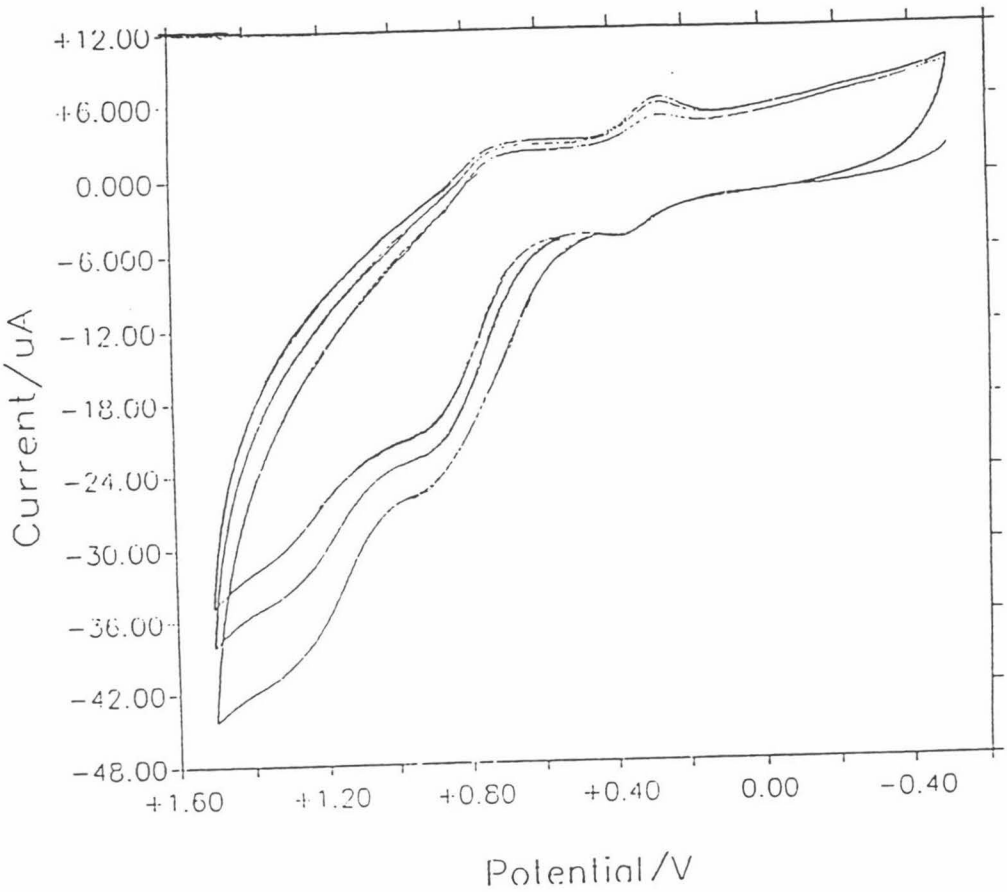


**Fig 5.1**

The number of electrons involved in the oxidation process was not able to be calculated from equations given in the introduction of this chapter, but it would appear that the ratio $Ip^a : Ip^c \neq 1$. From these results, the oxidation / reduction process is not reversible and does not display Nernstian behaviour. This possibly suggests that a chemical reaction is coupled with the electrochemical one. The appearance of a peak at a more negative potential than that of ferrocene, could be attributed to the reduction of the C=N group bound to the ferrocene moiety as has been observed by Duan *et al.* [95].

The $L2.BH_3$ complex appears to be quasilabile but the appearance of a peak at a more positive potential than that of the ferrocene based peak is still evident. The $Ep^a - Ep^c$ is 64.5 mV and the ratio $Ip^a : Ip^c = 2.47$. However the voltammogramme is clear and stable with reduction/oxidation occurring in the region expected for a ferrocene based

electrochemical process. The cyclic voltammogrammes of both the ferrocene and L2.$BH_3$ are shown in **Fig 5.2.**

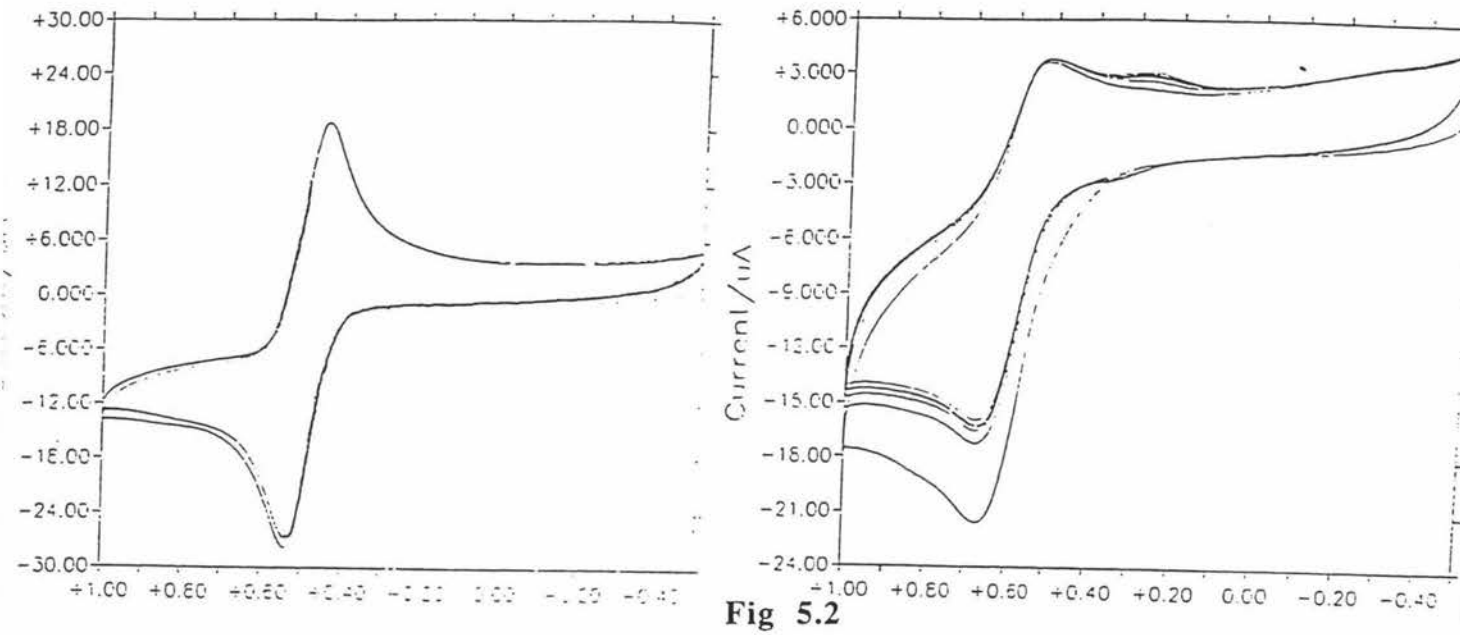


**Fig 5.2**

The only ferrocene derivatives to approximate to Nernstian behaviour are L5 and L4. The former has a ratio of $Ip^a : Ip^c = 1.06$ and $E^c - Ep^a = 80$ mV, however for the latter, $Ep^a - Ep^c = 92$ mV but the ratio $Ip^a : Ip^c \neq 1$. These results suggest that the electrochemical process occurring, as found for L2.$BH_3$, is not fully reversible and may be regarded as quasilabile. Ip data have been summarised in Table 5.3

**Table 5.3 Ip Data For Species Approximating Nernstian Behaviour** (μA)

| Ligand | $Ip^a$ | $Ip^c$ | $Ip^a : Ip^c$ |
|---|---|---|---|
| Ferrocene | 2.25 | 2.43 | 1.03 |
| L1 | 2.17 | 1.72 | 1.24 |
| L2 | 6.20 | 0.98 | 0.6 |
| L5 | 1.02 | 0.96 | 1.06 |
| L4 | 1.69 | 1.17 | 1.44 |
| L2.$BH_3$ | 1.28 | 5.18 | 2.47 |

Finally, the $Ep^a$ values for all the derivatives, except L5, are greater than that for ferrocene. As already discussed in Chapter 2 the presence of an imine bond results in a larger value for $Ep^a$. No such bond is present in L5. Thus the CV of this species is not complicated by the presence of possible chemical reduction products from the C=N bond. This then lends support for the suggestion that some reduction of the imine bond may occur in the CV of the Schiff base derivatives.

### 5.3.1 CYCLIC VOLTAMMETRY OF THE COMPLEXES OF L1 AND L2

The cyclic voltammogrammes produced for the transition metal complexes of L1 and L2 were not simple well defined voltammograms. The sample cyclic-voltammogramme of $[Ni(L2)Br_2]$ shown in **Fig 5.3.** illustrates this.

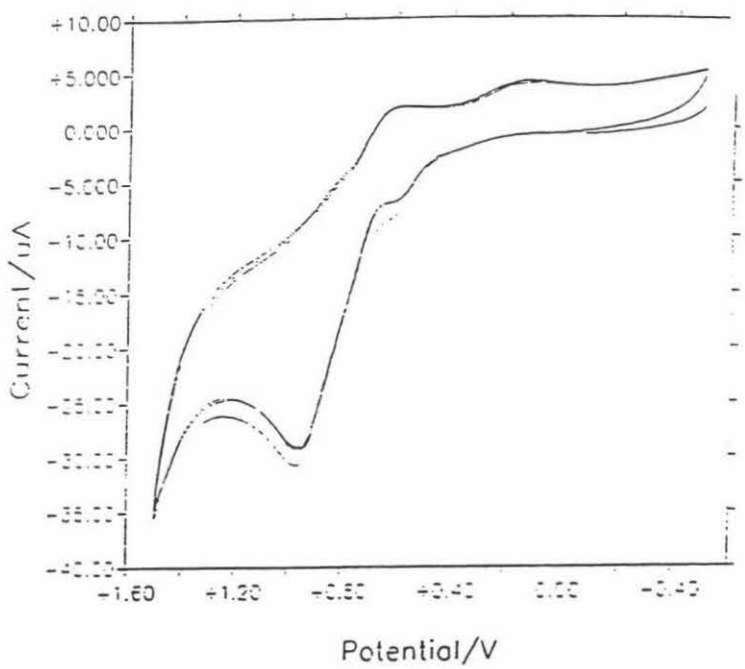


**Fig 5.3**

As a result of the undefined base lines, $Ip^a$ and $Ip^c$ values could not be calculated and only $Ep^a$ and $Ep^c$ values were used since they were more clearly defined. A summary of the data for the complexes is shown in Table 5.4.

**Table 5.4 Summary of the Peak Potentials for the Complexes (mV)**

| Sample | $Ep^a$ | $Ep^c$ | $E^{1/2}$ |
|---|---|---|---|
| $Zn(L2)Cl_2$ | 793 | 560 | 677 |
| $Ni(L2)Br_2$ | 965 | 614 | 789 |
| $Co(L2)Cl_2$ | 814 | 540 | 677 |
| $Cu(L2)Cl_2$ | 728 | 385 | 556 |
| $Co(L2)Br_2$ | 986 | 654 | 820 |
| [Zn(L1)Cl]zthf.xDBU.yDBUHCl. $wH_2O$ | 854 | 564 | 709 |

The Ep values indicate that the complexes do not behave in a Nernstian manner. There is also evidence for the presence of other species from the appearance of extra peaks in the voltammogramme. These peaks appear to be irreversible as do those of the complexes, indicating that chemical side reactions could be occurring simultaneously with the electrochemical reactions. The nature of these species, may arise from a combination of reduction of the imine bond and decomposition of the complex but more research is required to confirm these speculative suggestions. However in all cases the $Ep^a$ values are higher than for the uncomplexed species indicating that the difficulty of oxidation is increased by having a charged species, such as a transition metal, in conjunction with an electron withdrawing substituent on one of the ferrocenyl rings. The same observations have been noted by Bracci *et al.* [23]. They stated with their complex systems (using N-(*o*-hydroxbenzylidene) ferroceneamine) that the electron withdrawing ability of the metal functions through the skeletal sigma-bonding system in the ligand, which increases the difficulty for the oxidation process.

## 5.4 MOSSBAUER SPECTRA ON THE FERROCENYL DERIVATIVES

The Mossbauer spectra were obtained in transmission mode at room temperature (18 °C) using a constant acceleration spectrometer with a 10 mm Ci source of $^{57}Co$ in Rh. Data were transferred to a computer using EG and G ORTEC multichannel scaling hardware and software. The spectra were computer-fitted using a non-linear least-squares program. Metallic iron was used to calibrate the velocity scale and as a reference for the isomer shifts. The Mossbauer data of the ferrocene derivatives has been summarised in Table 5.5.

**Table 5.5 Ferrocene Mossbauer Results ($mms^{-1}$)**

| Sample | Isomer Shift | Quadrupole Splitting |
|---|---|---|
| ferrocene | 0.44 ± 0.003 | 2.39 ± 0.01 |
| ferrocene monocarboxaldehyde | 0.44 ± 0.01 | 2.23 ± 0.02 |
| L1 | 0.429 ± 0.003 | 2.212 ± 0.007 |
| L2 | 0.433 ± 0.008 | 2.27 ± 0.002 |
| L4 | 0.434 ± 0.007 | 2.28 ± 0.01 |
| L11 | 0.436 ± 0.009 | 2.19 ± 0.02 |
| L22 | 0.44 ± 0.02 | 2.11 ± 0.04 |
| L44 | 0.42 ± 0.01 | 2.10 ± 0.02 |
| $L2.BH_3$ | 0.435 ± 0.007 | 2.28 ± 0.01 |

The isomer shift (i.s.) does not vary between samples with the errors of each sample insufficient to infer that one result is significantly different from another. This suggests that the s-electron density at the nucleus for the $^{57}Fe$ atoms is constant. These will not be discussed further.

The interest is in the quadrupole splitting (q.s.), and this can be related to the bonding of the cyclopentadienyl rings to the iron atom, which in turn is governed by the substituents attached to the cyclopentadienyl rings.

Silver *et al.* [96], has attempted to present an overall qualitative understanding of the bonding to give insight into a series of substituted ferrocenes. The following qualitative discussion has been based primarily on papers by Silver *et al.*[27,96,97] and a book by Greenwood and Gibbs [98].

Electron-withdrawing substituents, such as the imine bond, cause a decrease in the q.s. relative to ferrocene [99,100]. Because an imine bond is present in all the ferrocene derivatives in this study, this may be regarded as constant, and is one of the factors contributing to a lowering of q.s. relative to ferrocene. The variation in q.s. between different samples may then be regarded as being caused by the substituted organic moiety attached to the cyclopentadienyl rings.

It has been shown by magnetic Mossbauer measurements that the quadrupole coupling constant for the ferrocene is positive. Because of residual doubts about the sign of field gradients arising from opposing definitions in the literature [98] and from unknown shielding and antishielding effects, it is preferred to keep discussions of quadrupole splitting in terms of the quadrupole coupling constant; this is positive for axial symmetric fields. Sandwich compounds have axially symmetric fields and hence display quadrupole splitting. The isomer shifts (i.s.) are relatively invariant and have been treated as constant. However the i.s. results differ from those reported by Silver *et al.* [96] (0.429 mm/s c.f. 0.52 mm/s) and a correction factor may be required for the results reported in Table 5.5 so that they may be compared with Silver's [96] results. This discrepency is difficult to resolve, but will not affect the following discussion on the q.s. values for the ferrocenyl derivatives as they are independent of the i.s.

The important consequences of the bonding , as far as the $^{57}$Fe Mossbauer spectra are concerned, are the contibutions of the Fe 3d and 4p orbitals to the q.s. and the effects that occur when these contributions are modified by substituents. Band formation in the solid state is also important. Trautwein *et al.* [101] have reported that the Fe 4p orbitals, particularly the $4p_z$, contribute to the q.s. but Silver *et al.* [96] prefer the suggestions of other workers [102,103], which assume that axial orbitals, $3d_z^2$ and $4p_z$ are essentially non-bonding in these systems because their energies are high relative to the ligand orbitals of axial symmetry. It

follows that their populations are constant and that their negative contributions to q.s. are insensitive to ligand substitution. The $4p_x$ and $4p_y$ orbitals of Fe are of $e_1$ symmetry. These are also considered to give a constant (probably zero) contribution to the q.s.. This is in good agreement with energy calculations of Greenwood [98] who showed that the 4s orbitals give no effective field gradient and there is good evidence to show that any contribution from the 4p orbitals will be small in comparison to that from the 3d orbitals. This was because of the greater radial expansion of the 3d orbitals.

The remaining asymmetric orbitals are the two sets of Fe 3d orbitals of symmetry $e_1$ and $e_2$. The $e_2$ electron density gives a positive contribution to q.s. and the $e_1$ a negative contribution of magnitude one half that of the $e_2$ set (per electron). The contribution of these orbitals to q.s. may be written as in equation 5, where $p_2$ and $p_1$ represent the electron populations

$$q.s. \propto (2p_2 - p_1) \quad \cdots\cdots\cdots\cdots \quad (5)$$

of $e_2$ and $e_1$ orbitals respectively. Both these populations are sensitive to ligand substitution on the cyclopentadienyl rings, but q.s. is twice as sensitive to changes of $p_2$ as it is to changes of $p_1$.

Generally then changes in q.s. will be controlled by changes in the populations of the $e_2$ and $e_1$ orbitals, i.e. changes in the back bonding and forward donation of electrons respectively (electron population movements are summarised in **Fig 5.4**). Therefore $\Delta$(q.s.) can be expressed in most cases by equation 6 where $p_{2a}$ and $p_{2b}$ are the electronic populations of the $e_2$ orbitals of the given compounds and of the parent respectively, with similar definitions of $p_{1a}$ and $p_{1b}$.

$$\Delta(q.s.) \propto [2(p_{2a} - p_{2b}) - (p_{1a} - p_{1b})] \quad \cdots\cdots\cdots\cdots \quad (6)$$

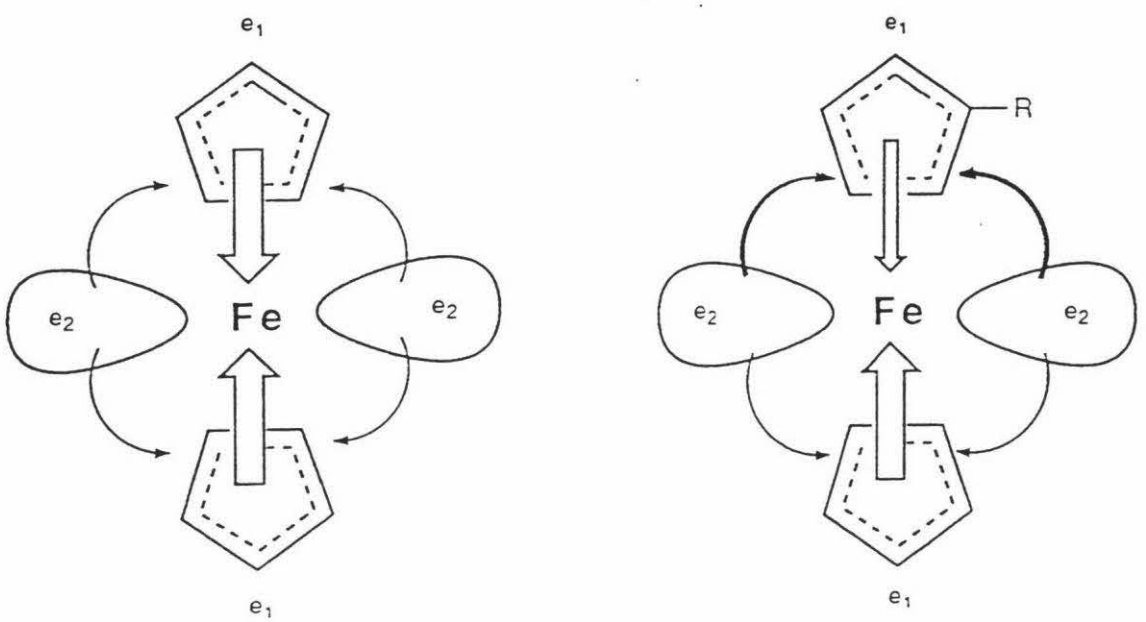


Ferrocene

Substituted ring containing an electron withdrawing group

**Fig 5.4**

Fig 5.4 summarises the following information schematically. Consider a ferrocene which has an electron withdrawing group on one of the $C_5H_5$ rings. The main component in the bonding is the $e_2$ back bonding iron-to-ring donation. When this is large, the $e_1$ ring-to-iron donation is small, and hence a small q.s. is observed, as the $p_2$ component of equation 5 is very 'small' and the $p_1$ component is 'large'. As substituent(s) are varied the $e_1$ donation will alter and this as a consequence will change the demand for back bonding. It bears to keep in mind that the contribution from $p_2$ (iron to ring back donation) is as twice as sensitive to q.s. as $p_1$ (ring to metal donation). The q.s. data in Table 5.5 have now been rationalised in terms of $p_1$ and $p_2$ electron population contributions. Thus the ferrocene derivative with the largest $p_1$ or smallest $p_2$ contribution will have the smallest q.s. relative to ferrocene, which can then be related to the electron withdrawing capabilities of the organic substituents on the cyclopentadienyl rings.

### 5.4.1 MONO-SUBSTITUTED FERROCENYL DERIVATIVES

Ferrocene may be regarded as having $2p_2 - p_1 = 0$, or having no bias in the electron populations in the e orbitals. Thus L4 (thiosemicarbazide derivative) and L2 (hydrazinopyridine derivative) may be regarded as having the least electron withdrawing groups associated with the substituted cyclopentadienyl rings. Which of the derivatives has the least withdrawing groups cannot be differentiated as the absolute values associated with q.s. overlap (2.28(1) c.f. 2.27(2) $mms^{-1}$) cannot be distinguished. This result is consistent with those observed in the CV studies, where the $Ep^c$ values for the $Fe^{II} \rightarrow Fe^{III}$ oxidation process were the smallest. L1, the phenol based derivative, had the smallest q.s. for the mono-substituted species and implies it contained the strongest electron withdrawing substituent.

The q.s. of the borane adduct ($L2.BH_3$) is very similar to the parent derivative, L2, with q.s. of 2.28 (1) c.f. 2.27 (2) mm/s respectively. This result is not unexpected, as the electrons in the hydrogen atoms of the $BH_3$, which may be involved in back-bonding to the $\pi$- acceptor orbitals of the pyridine ring, as well as the pyridine donation are a long way removed from the electronic interactions of the $e_1$ and $e_2$ populations which influence the q.s. The Mossbauer results do parallel those found in the CV studies.

### 5.4.2 BIS-SUBSTITUTED FERROCENYL DERIVATIVES

L44 (bis-thiosemicarbazide derivative) has the smallest q.s. of 2.10(2) mm/s with L22 (bis-hydrazinopyridine derivative) nearby at 2.11(4) mm/s. The changes in q.s. relative to ferrocene indicate that the effect of two hydrazinopyridine substituents, is roughly double that of one (0.28 c.f 0.12 mm/s). However, perhaps surprisingly, for L11 which is the bis phenol derivative, the q.s. (2.19 mm/s) is a little less than that for the mono-phenol derivative L1 (2.212 (7) mm/s). The general decrease associated with the q.s. values for the bis-derivatives, in comparison with their mono-analogues, may be accounted for by the fact that as both rings have a 'high' $p_1$ occupation value and Fe has a 'low' $p_2$ occupation value, the

q.s. values are reduced to some extent. However for the mono-substituted derivatives, the substituted ring has a 'high' $p_1$ occupation, whereas in the other ring (which is unsubstituted) the $p_1$ population is 'lower', (and may be regarded as a better electron donor) giving a total $p_1$ population less than that for the bis-derivative. At the same time the net $p_2$ population will be lessened a little, but to still give a larger q.s. value than that for the bis-derivatives and smaller than that for the free substituted ferrocene. **Fig 5.5** below summarises schematically the effects of the electron population movements which result in the decrease of the quadruple splitting for the bis-derivatives and the mono-derivatives.

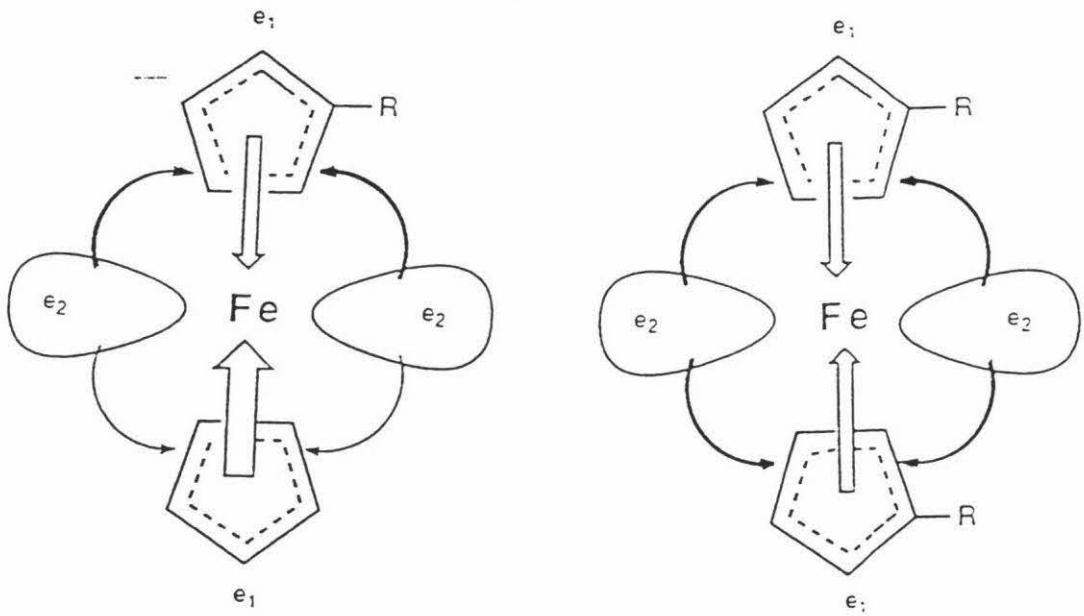


**Fig 5.5**

## 5.5 Summary

The trend to lower q.s values on going from the mono to the bis-derivatives, as well as the trend within each type , is in agreement with the CV studies that show more positive values for $Ep^a$ as q.s. decreases. Hence even though the sample size is small, it would seem that the Mossbauer results do appear to parallel those of the CV studies.

The presence of an imine or carbonyl substituent on the cyclopentadienyl ring has an electron withdrawing effect in that it lowers q.s. and increases $Ep^a$. These values are further

influenced by the nature of the groups attached to the imine (or carbonyl) bond, and if they are electron withdrawing, will 'fine tune' q.s. to lower values and $Ep^a$ to more positive values. Hence the iron senses electronically the presence of such structural features and groups. Below in Diagram 5.1 is shown the Mossbauer spectrum of L1, which is representative of all the Mossbauer spectra obtained.

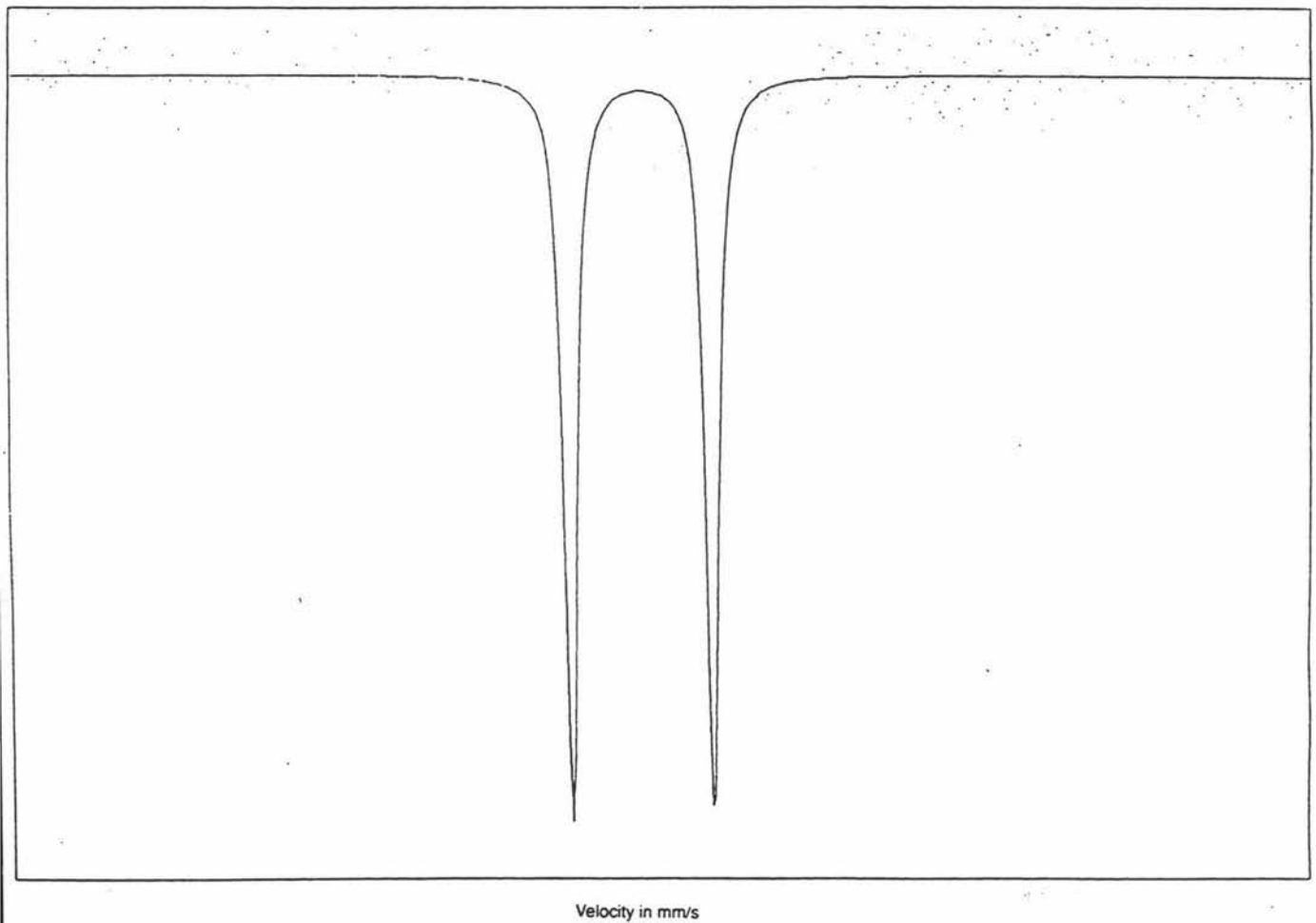


**Diagram 5.1**

## REFERENCES


1 T.W. Kealy, P.L. Pauson, *Nature* , **168** , 1039 - 40, (1951)

2 Ed. J Silver, Blackie Academic and Professional, *P.L. Pauson, in Chemistry of Iron* , Chapman and Hall, Glasgow, **Ch. 4**, 84 - 98, (1993)

3 A. Houlton, P.T. Bishop, R.M.G. Roberts, J. Silver and M. Herberhold, *J. Organomet. Chem.*, 364 - 381, (1989)

4 A. Houlton, R.M.G. Roberts, J Silver and M.G. Drew, *J. Chem. Soc. Dalton Trans.*, 1543, (1990)

5 A. Houlton, S.K. Ibrahim, J.R. Dilworth and J. Silver, *J. Chem. Soc. Dalton Trans.*, 2421, (1990)

6 J. Silver, *J. Chem. Soc. Dalton Trans.*, 3573, (1990)

7 Paul D. Beer, S.S. Kurek, *Journal of Organometallic Chemistry*, **366**, C9 - C12, (1989)

8 D. J. Williams, *Angew. Chem.* Int. Edn. Engl., **23**, 690, (1984)

9 C.C. Frazier, M.A. Harvey, M.D. Cockerham, E.A. Chauchard and Chi H. Lee, *J. Phys. Chem.*, **90**, 5703, (1986)

10 D.F. Eaton, A.G. Anderson, W. Tam, *Chem. Phys. Lett.*, **133**, 244, (1987)

11 L.T. Cheng, W. Tam and D.F. Eaton, *Organometallics*, **9**, 2857, (1990)

12 M.L.H. Green, S.R. Marder, M.E. Thompson, J.A. Bandy, D. Bloor, P.V. Kolinsky and R.J. Jones, *Nature*, **330**, 360, (1987)

13 B.J. Coe, C.J. Jones, J.A. McCleverly, D. Bloor and R.J. Kolinsky, *J. Chem. Soc. Chem. Commun.*, 1485, (1989)

14 Heather E. Bunting, M.L.H. Green, S.R. Marder, M.E. Thompson, C. Bloor, P.V. Kolinsky, R.J. Jones, *Polyhedron*, **Vol. II**, No. 12, 1489 - 1999, (1992)

15 B.J. Coe, T.A. Hamor, C.J. Jones, J.A. McCleverly, D. Bloor, G.H. Cross, T.L. Axon, *J. Chem. Soc. Dalton Trans.*, 673 - 681, (1995)

16 T. Jorgensen, T. Kruse, T. Becher,*Chemical Society Reviews* , 46 - 48, (1994)

17 A. Kaifer, L. Echegoyen, D.A. Custowski, D.M. Croli, G.W. Gokel, *J. Am. Chem. Soc.*, **105**, 7168, (1983)

18 M.C. Grossel, M.R. Goldspink, J. A. Hriljac, S.C. Weston, *Organometallics*, **10**, 851 - 860, (1990)

19 P.D. Beer, J.E. Natron, S.L. Brown, *Journal of Organometallic Chemistry*, **377**, C23 - C26, (1989)

20 J.S. Miller, J. Calabrese, H. Rommelmann, S.R. Chiltipeddi, J.H. Zang, W.M. Reiff, A.J. Epskin, *J. Am. Chem. Soc.*, **109**, 769 - 781, (1987)

21 Allan, E. Underhill, *Chemistry in Britian*, **August**, 708 - 710.

22 W.E. Brederick, J.A. Thompson, M.R. Godfrey, M. Sabat, B.M. Hoftman, *J. Am .Chem. Soc.*, **111**, 7656 - 7657, (1989)

23 I.R. Butler, L.J. Hobson, S.M.E. Macan, D.J. Williams, *Polyhedron,* **Vol. 12**, No. 15, 1901 - 1905, (1993)

24 M. Bracci, E. Encolani, B. Floris, M. Basselti, A. Chiesi-Uilla, C. Guastini, *J. Chem. Soc. Dalton Trans.*, 1357 - 1363, (1990)

25 C. Duran, X. Shen, X. You, *Polyhedron*, **Vol. 13**, No. 3, 385 - 388, (1994)

26 P. Zanello, G. Opromolla, G. Giorgi, J. C. Van de Grampel, H.F.M. School, *Polyhedron*, **Vol. 12**, No. 11, 1329 - 1333, (1993)

27 R. Bosque, M. Font-Bardia, C. Lopez, J. Sales, J. Silver, X Solans, *J. Chem. Soc. Dalton Trans.*, 747 - 752, (1994)

28 G.G.A. Balavoine, G. Doisneau, T. Fillebeen-Khan, *Journal of Organometallic Chemistry*, **412**, 381 - 382, (1991)

29 B. Rosenberg, L. Van de Camp, J.E. Trosko, V.H. Mansour, *Nature*, **222**, 385, (1962)

30 P. Kopf-Maier and H. Kopf, *Chem. Rev.*, 1137-1187, (1987)

31 L.S. Lerman, *J. Mol. Biol.*, **3**, 18, (1961)

32 R. Gust, H. Schonenberger, J. Kritzenberger, Klaus-Jurgen Range, U. Kelment T. Burgemeister, *Inorg. Chem.*, **32**, 5939-5950, (1993)

33 J.E. Schurig, W.C. Rose, J.J. Catino, R.C. Gaver, B.H. Long, H. Madissoo, R. Canetta, *In Carboplatin (JM8), Current Perspectives and Future Directions.* P.A. Brunn, R Canetta, R.F. Ozols, M. Rozenawig, Eds. W.B. Saunders Co. Philadelphia, P.A., 3, (1990)

34 S.J. Berners-Price, P.J. Sadler, *Chem. in Britain*, **June**, 541, (1987)

35 W.E. Levinson, *Antibotics Chemotherapy*, **27**, 288, (1989)

36 P.A. Gerutti, *Science*, **227**, 375, (1985)

37 D. Scutaru, L. Tataru, I. Mazilu, E. Diaconu, T. Lixandru, C. Sionionescu, *Journal of Organometallic Chemistry*, **Vol. 1**, 81 - 85, (1991)

38 P. D. Beer, *Advances in Organic Chemistry*, **Vol. 39**, (1992)

39 U.T. Mueller-Westerholft, Z. Yang, G. Ingram, *Journal of Organometallic Chemistry* , **463**, 163-167, (1993)

40 J. Mc Murray, *Organic Chemistry 2nd Ed*, Brooks/Cole Pub Co. Pacific Grove, California, 675, (1988)

41 I.R. Butler, W.R. Cullen, *Organomeltallics*, **5**, 2537, (1986)

42 R.A. Brown, A. Houlton, R. M.G. Roberts, J. Silver, *Polyhedron*, **Vol. 11**, No. 20, 2611-2619, (1992)

43 I.R. Butler, L.J. Hobson, S.M.E. Macan, D.J. Williams, *Polyhedron*, **Vol. 12**, No. 15, 1901-1905, (1993)

44 J. Kotz, C. Nivert, *Organometallic Ligands*, 387 - 405, (1972)

45 C. Imrie, T. Modro, P.H. Van Rooyens, *Polyhedron*, **Vol. 13**, No. 11, 1677-1682, (1994)

46 B. Belavaux-Nicot, V. Gauri, Douziech, R. Mathieu, *J. Chem. Soc. Chem. Commun.*, 585 - 587, (1995)

47 K. Hafner, C. Mink, H.J. Linder, *Angew. Chem., Int. Ed. Engl.*, **33**, No. 14, 1479 - 1494, (1994)

48 I.R. Butler, S. McDonald, M.B. Hersthouse, K.M. Abdu Malikk, *Polyhedron*, **Vol. 14**, No. 4, 529 - 539, (1995)

49 J.F. Biernat, T. Wilczenski, *Tetrahedron*, **36**, 2521, (1980)

50 M. Sato, K. Katada, S. Nakashima, H. Sano, S. Akabori, *J. Chem. Soc. Dalton Trans.*, 1979, (1990)

51 P.D. Beer, M.G.B. Drew, A. Ibbotson, E.L. Tike, *J. Chem. Soc.Chem. Commun.*, 1498, (1988)

52 P.D. Beer, E.L. Tite, M.G.B. Drew, A. Ibbotson, *J. Chem. Soc. Dalton Trans.*, 2543, (1990).

53 Z. Xiaoxian, L. Yongmin, N. Fajun, M. Yongxiang, *Polyhedron*, **Vol. II**, No. 4, 447 - 451, (1992)

54 D.M. Wiles, T. Suprunchuk, *Canadian Journal of Chemistry*, **Vol. 46**, 1865-1890, (1968)

55 S. Xaocheng, S. Qingbao, W. Xiodi, M. Yongxiang, *Polyhedron*, **Vol. 13**, No. 14, 2101 - 2105, (1994)

56 A. Houlton, J.R. Dilworth, R.M.G. Robertts, J. Silver, *Polyhedron*, **Vol. 9**, No. 22, 2751 - 2757, (1990)

57 Z. Hongyun, L. Feng, C. Peikun, C. Deji, C. Dongli, Z. Hangquan, *Polyhedron*, **Vol. 12**, No. 2, 165-170, (1993)

58 P. Ramani, R. Ranatunge-Bandarage, B.H. Robinson, J. Simpson, *Organometallics*, **Vol. 13**, 500 - 510, (1994)

59 I. Butler, N. Burke, L.J. Hobson, H. Finderegg, *Polyhedron*, **Vol. 11**, No. 19, 2435 - 2439, (1992)

60 E.C. Constable, A.J. Edwards, M. Dolores Marcos, P.R. Rathby, R. Martinez-Manez, M.J.L. Tendero, *Inorganic Chimica Acta* , **224**, 11 - 14, (1994)

61 H. Plenio, *Organometallics*, **Vol. 11**, 1856-1859, (1992)

62 L. Fillaut, J. Lanares, D. Astruc, *Angew. Chem. Int. Ed. Engl.*, **Vol. 33**, 2460 - 2462, (1994)

63 Kai-Ming Chi, J.C. Calabrese, W.M. Reiff, J.S. Miller, *Organometallics*, **Vol. 10**, 688 - 693, (1991)

64 N. Hall, *New Scientist*, February, (1987)

65 J.D. Ranford, *Thesis* , (Massey University), 217, (1988)

66 A.M. Osman, M.A. El Maghraby, K.M. Hassan, *Bull Chem. Soc. Jpn.* , **48**, 1975, (1983)

67 M. Herberhold, M. Ellinges, W. Kremnitz, *Journal of Organometallic Chemistry*, **Vol. 241**, 227, (1983)

68 J. Cano, A. Benito, R. Martinez-Manez, J. Soto, J. Raya, F. Lloret, M. Julve, M. Dolores Marcos, E. Sinn, *Inorganic Chimica. Acta.* , **Vol. 231**, 45 - 56, (1995)

69 J.E. Hugheey, *Inorganic Chemistry*, 3rd Ed. Harper and Row Publishers Inc., N.Y. 10022, (1983)

70 F.A. Cotton, G. Wilkinson, *Advanced Inorganic Chemistry 5th Ed.*, A Wiley-Interscience Publication, John Wiley and Sons, N.Y., (1988)

71 G.G.A. Balavoine, G. Doisneau, T. Fillebeen-Khan, *Journal of Organometallic Chemistry* , **412**, 381 - 382, (1991)

72 D. Guillaneux, H.B. Kagan, *J. Org. Chem.*, **60**, 2502 - 2505, (1995)

73 A.G. Avent, P.B. Hitchcock, M.F. Lappert, D. Sheny Uri, G Mignani, C. Richard, E. Roche, *J. Chem. Soc. Chem. Communications*, 855- 856, (1995)

74 M. Soriano-Garcia, R.A. Toscano, T. Lopez, A. Campero-Celis, *Journal of Crystallographic and Spectroscopic Research*, **Vol. 17**, No. 6, (1987)

75 R.M.G. Roberts, J. Silver, B.M. Yamin, M.G.B. Drew, U. Ebertiadt, *J. Chem. Soc. Dalton Trans.*, 1549 - 1556, (1988).

76 D.A. Tocker, R.O. Gould, T.A. Stephenson, M.A. Bennett, J.P. Ennett, T.W. Matheson, L. Sawyer, U.K. Shan, *J. Chem. Soc. Dalton Trans.*, 1571 - 1581, (1983)

77 G.J. Palenik, D.F. Rendle, W.S. Cater, *Acta. Cryst.*, B30, 2390, (1974)

78 K.H. Topel, K. Hensen, M. Trowel, *Acta. Crystallogr. Sect. B, Struct.Crystallorg.*, **37**, 969, (1981)

79 H. Hess, *Acta. Crystallogr., Sect. B Struct. Crystallogr.*, **25**, 2338, (1969)

80 B. Swanson, D.F. Shriver, J.A. Fbers, *Inorganic Chem.*, **8**, 2182, (1969)

81 J. Silver, R.M.G. Roberts, *Journal of Organometallic Chemistry*, **263**, 235, (1984)

82 G.J. Palenik, *Inorganic Chem.*, **9**, 242, (1979)

83 G. J. Palenik, *Inorganic Chem.*, **8**, 2744, (1969)

84 *Internatrional Tables for X-Ray Crystallography*, **Vol. III**, The Kynoch Press, Birmingham, England, (1962)

85 F. Estevan, P. Lahuerta, J. Latorre, E. Peris, S. Garica-Granda, F. Gomez-Beltran, A. Aguirre, M.A. Salvodo, *J. Chem. Soc. Daltons Trans.*, 1681 - 1688, (1993)

86 R.H. Clayton, M.H. Chisholm, J.C. Huffuman, E.B. Lobkovsky, *J. Am. Chem. Soc.*, **113**, 8709, (1991)

87 B. Corain, B. Longato, G. Favero, D. Ajo, G. Pilloni, U. Russo, F.R. Kreissl, *Inorganic Chim. Acta.*, **157**, 259, (1989)

88 G. Pilloni, B Longato, B Corain, *Journal of Organometallic Chemistry.*, **420**, 57, (1991)

89 L.F. Johnson, W.C. Jankowski, *Carbon-13 NMR Spectra*, Spectra 109,165, Wiley-Interscience Publication, JohnWiley and Sons, New York, London, Sydney, Toronto, (1972)

90 W. Kemp, *Organic Spectroscopy*, Second Edition, MacMillan Education Ltd., Houndsmills, Basingstoke, Hampshire, London, (1987)

91 J. March, *Advance Organic Chemistry, Reaction Mechanisms and Structure*, A.Wiley-Interscience Publication, (1992)

92 B. Bak, L. Hansen-Nygaard, J. Rastrup-Anderson, *J. Mol. Spectroscopy*, **2**, 361-368, (1958)

93 K.Ijima, I. Onishi, S. Shibata, *Chem. Lett.*, 251-254, (1983)

94 K.Topel, K Hensen, M. Tromel, *Acta. Crystallogr.*, **B37**, 971-969, (1981)

95 C.Duan, X. Shen, X. You, *Polyhedron*, **Vol 13**, No 3, 385-388, (1994)

96 J. Silver, A. Houlton, P.T. Bishop, R.M.G. Roberts, *J. Chem. Soc. Dalton Trans.*, 2181-2184, (1990)

97 A. Houlton, P.T. Bishop, R.M.G. Roberts, J. Silver, M. Herberhold, *Journal of Organometallic Chemistry*, **364**, 381-389, (1989)

98 N.N. Greenwood, T.C. Gibbs, *Mossbauer Spectroscopy*, 233-237, Chapman, Hall Ltd. London, (1971)

99 R.M.G. Roberts, J. Silver, *Journal of Organometallic Chemistry*, **263**, 235 and refs therein, (1984)

100 L. Korecz, H. Abou, G. Ortaggi, M. Graziani, U. Belluco, K. Burger, *Inorg. Chim. Acta.*, **9**, 209, (1974)

101 A. Trautwein, R. Reschke, I. Dezi, E. Hams, *J. Phys. (Paris)*, **37**, C6-463, (1976)

102 W. Moffit, *J. Am. Chem. Soc.*, **76**, 3386, (1954)

103 F. Varret, J. P. Mariot, J. R. Hamon, D. Astruc, *Hyperfine Interact.*, **39**, 67, (1988)

104 O. J. Belchenko, P.V. Schastnev, V.S. Bashuroua, *Journal of Organometallic Chemistry*., **187**, 375, (1980)

# APPENDIX I

Table A.I.1. Crystal data and structure refinement for L11.

| | | |
|---|---|---|
| Identification code | alf21 | |
| Molecular formula | $[Fe(cp\text{-}CH{=}N\text{-}C_5H_4OH)_2]$ | |
| Empirical formula | $C_{24}\ H_{20}\ Fe\ N_2\ O_2$ | |
| Formula weight | 424.27 | |
| Temperature | 293(2) K | |
| Wavelength | 0.71073 Å | |
| Crystal system | Monoclinic | |
| Space group | Cc | |
| Unit cell dimensions | a = 16.655(4) Å | alpha = 90 ° |
| | b = 9.236(4) Å | beta = 129.34(2) ° |
| | c = 16.469(6) Å | gamma = 90 ° |
| Volume | 1959.3(12) $Å^3$ | |
| Z | 4 | |
| Density (calculated) | 1.438 $Mg/m^3$ | |
| Absorption coefficient | 0.793 $mm^{-1}$ | |
| F(000) | 880 | |
| Crystal size | 0.95 x 0.32 x 0.31 mm | |
| Theta range for data collection | 2.59 to 28.47 ° | |
| Index ranges | 0<=h<=20, 0<=k<=12, -20<=l<=17 | |
| Reflections collected | 2520 | |
| Independent reflections | 2520 [R(int) = 0.0000] | |
| Refinement method | Full-matrix least-squares on $F^2$ | |
| Data / restraints / parameters | 2520 / 2 / 264 | |
| Goodness-of-fit on $F^2$ | 1.098 | |
| Final R indices [I>2sigma(I)] | R1 = 0.0456, wR2 = 0.1079 | |
| R indices (all data) | R1 = 0.0608, wR2 = 0.1211 | |
| Absolute structure parameter | 0.00(4) | |
| Extinction coefficient | 0.0043(6) | |
| Largest diff. peak and hole | 0.599 and -0.438 $e.A^{-3}$ | |

# APPENDIX I

Table A.I.2. Atomic coordinates ( x $10^4$) and equivalent isotropic displacement parameters ($A^2$ x $10^3$) for L11. U(eq) is defined as one third of the trace of the orthogonalized Uij tensor.

| | x | y | z | U(eq) |
|---|---|---|---|---|
| Fe(1) | 5947(2) | 7686(1) | 7572(2) | 54(1) |
| O(11) | 6167(6) | 2544(8) | 6613(6) | 63(2) |
| O(21) | 5768(5) | 2649(8) | 8545(5) | 61(2) |
| N(11) | 7217(5) | 4114(7) | 8512(6) | 45(2) |
| N(21) | 4710(5) | 4080(7) | 6658(5) | 42(2) |
| C(11) | 7174(7) | 6636(10) | 8849(7) | 48(2) |
| C(12) | 6308(7) | 6593(9) | 8849(6) | 49(2) |
| C(13) | 6114(8) | 8130(9) | 8881(7) | 73(3) |
| C(14) | 6764(10) | 9025(9) | 8876(8) | 74(3) |
| C(15) | 7419(9) | 8074(13) | 8863(8) | 70(3) |
| C(16) | 7637(6) | 5315(9) | 8750(7) | 47(2) |
| C(17) | 7721(6) | 2960(8) | 8376(7) | 42(2) |
| C(18) | 7122(7) | 2245(7) | 7392(7) | 40(2) |
| C(19) | 7625(8) | 1095(9) | 7294(9) | 57(2) |
| C(20) | 8634(9) | 707(9) | 8116(10) | 61(3) |
| C(21) | 9169(8) | 1365(10) | 9031(8) | 64(3) |
| C(22) | 8736(9) | 2595(10) | 9189(9) | 61(2) |
| C(31) | 4741(7) | 6582(10) | 6279(7) | 52(2) |
| C(32) | 4435(8) | 8086(9) | 6293(7) | 63(3) |
| C(33) | 5133(11) | 8933(11) | 6276(7) | 91(4) |
| C(34) | 5851(8) | 8093(11) | 6269(8) | 73(3) |
| C(35) | 5575(8) | 6703(11) | 6265(7) | 61(2) |
| C(36) | 4314(6) | 5388(9) | 6411(6) | 46(2) |
| C(37) | 4192(6) | 2989(9) | 6749(6) | 42(2) |
| C(38) | 4728(7) | 2242(9) | 7669(8) | 52(2) |
| C(39) | 4305(7) | 1192(10) | 7854(8) | 59(2) |
| C(40) | 3283(8) | 754(12) | 7047(10) | 68(3) |
| C(41) | 2721(7) | 1500(11) | 6073(8) | 60(2) |
| C(42) | 3172(6) | 2539(9) | 5952(7) | 46(2) |

# APPENDIX I

Table A.I.3. Bond lengths [Å] and angles [°] for L11

| | | | |
|---|---|---|---|
| Fe(1)-C(15 | 2.012(11) | C(13)-C(14) | 1.37(2) |
| Fe(1)-C(33) | 2.014(10) | C(14)-C(15) | 1.41(2) |
| Fe(1)-C(11) | 2.021(9) | C(17)-C(22) | 1.376(14) |
| Fe(1)-C(13) | 2.032(9) | C(17)-C(18) | 1.418(12) |
| Fe(1)-C(35) | 2.037(10) | C(18)-C(19) | 1.424(10) |
| Fe(1)-C(31) | 2.046(9) | C(19)-C(20) | 1.38(2) |
| Fe(1)-C(32) | 2.048(10) | C(20)-C(21) | 1.32(2) |
| Fe(1)-C(12) | 2.049(9) | C(21)-C(22) | 1.455(12) |
| Fe(1)-C(14) | 2.071(10) | C(31)-C(36) | 1.402(13) |
| Fe(1)-C(34) | 2.083(11) | C(31)-C(35) | 1.407(14) |
| O(11)-C(18) | 1.290(11) | C(31)-C(32) | 1.485(12) |
| O(21)-C(38) | 1.433(12) | C(32)-C(33) | 1.42(2) |
| N(11)-C(16) | 1.235(11) | C(33)-C(34) | 1.43(2) |
| N(11)-C(17) | 1.459(9) | C(34)-C(35) | 1.362(13) |
| N(21)-C(36) | 1.311(10) | C(37)-C(38) | 1.362(14) |
| N(21)-C(37) | 1.396(10) | C(37)-C(42) | 1.398(11) |
| C(11)-C(15) | 1.385(14) | C(38)-C(39) | 1.341(12) |
| C(11)-C(12) | 1.443(13) | C(39)-C(40) | 1.40(2) |
| C(11)-C(16) | 1.506(12) | C(40)-C(41) | 1.42(2) |
| C(12)-C(13) | 1.464(10) | C(41)-C(42) | 1.308(12) |
| | | | |
| C(15)-Fe(1)-C(33) | 124.6(5) | C(13)-Fe(1)-C(12) | 42.0(3) |
| C(15)-Fe(1)-C(11) | 40.2(4) | C(35)-Fe(1)-C(12) | 124.0(2) |
| C(33)-Fe(1)-C(11) | 159.1(5) | C(31)-Fe(1)-C(12) | 106.2(4) |
| C(15)-Fe(1)-C(13) | 65.7(5) | C(32)-Fe(1)-C(12) | 120.9(5) |
| C(33)-Fe(1)-C(13) | 123.8(5) | C(15)-Fe(1)-C(14) | 40.4(5) |
| C(11)-Fe(1)-C(13) | 68.0(4) | C(33)-Fe(1)-C(14) | 108.4(2) |
| C(15)-Fe(1)-C(35) | 123.1(5) | C(11)-Fe(1)-C(14) | 69.0(4) |
| C(33)-Fe(1)-C(35) | 65.5(5) | C(13)-Fe(1)-C(14) | 38.9(5) |
| C(11)-Fe(1)-C(35) | 108.4(4) | C(35)-Fe(1)-C(14) | 157.2(5) |
| C(13)-Fe(1)-C(35) | 162.9(4) | C(31)-Fe(1)-C(14) | 160.6(5) |
| C(15)-Fe(1)-C(31) | 157.4(5) | C(32)-Fe(1)-C(14) | 122.0(4) |
| C(33)-Fe(1)-C(31) | 67.9(4) | C(12)-Fe(1)-C(14) | 70.0(4) |
| C(11)-Fe(1)-C(31) | 121.45(13) | C(15)-Fe(1)-C(34) | 107.6(5) |
| C(13)-Fe(1)-C(31) | 126.1(5) | C(33)-Fe(1)-C(34) | 40.8(5) |
| C(35)-Fe(1)-C(31) | 40.3(4) | C(11)-Fe(1)-C(34) | 121.7(4) |
| C(15)-Fe(1)-C(32) | 159.2(2) | C(13)-Fe(1)-C(34) | 157.8(2) |
| C(33)-Fe(1)-C(32) | 40.8(5) | C(35)-Fe(1)-C(34) | 38.6(4) |
| C(11)-Fe(1)-C(32) | 158.4(4) | C(31)-Fe(1)-C(34) | 68.5(4) |
| C(13)-Fe(1)-C(32) | 107.9(5) | C(32)-Fe(1)-C(34) | 70.5(5) |
| C(35)-Fe(1)-C(32) | 69.0(4) | C(12)-Fe(1)-C(34) | 158.0(4) |
| C(31)-Fe(1)-C(32) | 42.5(3) | C(14)-Fe(1)-C(34) | 122.1(4) |
| C(15)-Fe(1)-C(12) | 68.6(4) | C(16)-N(11)-C(17) | 116.1(8) |
| C(33)-Fe(1)-C(12) | 158.8(5) | C(36)-N(21)-C(37) | 118.4(7) |
| C(11)-Fe(1)-C(12) | 41.5(4) | C(15)-C(11)-C(12) | 108.1(9) |

| | |
|---|---|
| C(15)-C(11)-C(16) | 127.8(10) |
| C(12)-C(11)-C(16) | 123.9(8) |
| C(15)-C(11)-Fe(1) | 69.6(6) |
| C(12)-C(11)-Fe(1) | 70.3(5) |
| C(16)-C(11)-Fe(1) | 121.7(6) |
| C(11)-C(12)-C(13) | 102.5(8) |
| C(11)-C(12)-Fe(1) | 68.2(5) |
| C(13)-C(12)-Fe(1) | 68.3(5) |
| C(14)-C(13)-C(12) | 113.1(9) |
| C(14)-C(13)-Fe(1) | 72.1(6) |
| C(12)-C(13)-Fe(1) | 69.6(5) |
| C(13)-C(14)-C(15) | 104.3(8) |
| C(13)-C(14)-Fe(1) | 69.0(5) |
| C(15)-C(14)-Fe(1) | 67.6(6) |
| C(11)-C(15)-C(14) | 112.0(11) |
| C(11)-C(15)-Fe(1) | 70.3(6) |
| C(14)-C(15)-Fe(1) | 72.0(7) |
| N(11)-C(16)-C(11) | 122.4(9) |
| C(22)-C(17)-C(18) | 122.6(7) |
| C(22)-C(17)-N(11) | 120.0(8) |
| C(18)-C(17)-N(11) | 117.4(7) |
| O(11)-C(18)-C(17) | 124.6(7) |
| O(11)-C(18)-C(19) | 119.4(8) |
| C(17)-C(18)-C(19) | 116.0(9) |
| C(20)-C(19)-C(18) | 121.4(10) |
| C(21)-C(20)-C(19) | 121.6(8) |
| C(20)-C(21)-C(22) | 120.8(9) |
| C(17)-C(22)-C(21) | 117.4(9) |
| C(36)-C(31)-C(35) | 131.9(9) |
| C(36)-C(31)-C(32) | 121.3(10) |
| C(35)-C(31)-C(32) | 106.2(9) |
| C(36)-C(31)-Fe(1) | 119.4(7) |
| C(35)-C(31)-Fe(1) | 69.5(5) |
| C(32)-C(31)-Fe(1) | 68.8(5) |
| C(33)-C(32)-C(31) | 102.8(11) |
| C(33)-C(32)-Fe(1) | 68.3(6) |
| C(31)-C(32)-Fe(1) | 68.7(5) |
| C(32)-C(33)-C(34) | 113.7(9) |
| C(32)-C(33)-Fe(1) | 70.9(6) |
| C(34)-C(33)-Fe(1) | 72.2(6) |
| C(35)-C(34)-C(33) | 103.3(10) |
| C(35)-C(34)-Fe(1) | 68.9(6) |
| C(33)-C(34)-Fe(1) | 67.0(6) |
| C(34)-C(35)-C(31) | 114.1(10) |
| C(34)-C(35)-Fe(1) | 72.5(6) |
| C(31)-C(35)-Fe(1) | 70.2(6) |
| N(21)-C(36)-C(31) | 124.6(9) |
| C(38)-C(37)-N(21) | 118.2(8) |
| C(38)-C(37)-C(42) | 116.3(8) |
| N(21)-C(37)-C(42) | 125.5(8) |
| C(39)-C(38)-C(37) | 123.4(10) |
| C(39)-C(38)-O(21) | 115.8(9) |
| C(37)-C(38)-O(21) | 120.6(8) |
| C(38)-C(39)-C(40) | 119.4(10) |
| C(39)-C(40)-C(41) | 117.7(9) |
| C(42)-C(41)-C(40) | 119.8(9) |
| C(41)-C(42)-C(37) | 123.3(9) |

# APPENDIX II

Table A.II.1. Crystal data and structure refinement for L2.$BH_3$

| | | |
|---|---|---|
| Identification code | alf2b | |
| Molecular formula | [(cp)Fe(cp-CH=NH-$C_5NH_4BH_3$)] | |
| Empirical formula | $C_{16}$ $H_{18}$ B Fe $N_3$ | |
| Formula weight | 318.99 | |
| Temperature | 293(2) K | |
| Wavelength | 0.71073 Å | |
| Crystal system | Monoclinic | |
| Space group | P2(1)/n | |
| Unit cell dimensions | a = 7.512(2) Å | alpha = 90 ° |
| | b = 10.928(2) Å | beta = 100.14(3) ° |
| | c = 18.801(4) Å | gamma = 90 ° |
| Volume | 1519.3(6) $Å^3$ | |
| Z | 4 | |
| Density (calculated) | 1.395 $Mg/m^3$ | |
| Absorption coefficient | 0.987 $mm^{-1}$ | |
| F(000) | 664 | |
| Crystal size | 0.40 x 0.30 x 0.20 mm | |
| Theta range for data collection | 2.16 to 27.97 ° | |
| Index ranges | 0<=h<=9, 0<=k<=14, -24<=l<=24 | |
| Reflections collected | 3928 | |
| Independent reflections | 3658 [R(int) = 0.0141] | |
| Refinement method | Full-matrix least-squares on $F^2$ | |
| Data / restraints / parameters | 3658 / 0 / 190 | |
| Goodness-of-fit on $F^2$ | 1.087 | |
| Final R indices [I>2sigma(I)] | R1 = 0.0318, wR2 = 0.0782 | |
| R indices (all data) | R1 = 0.0447, wR2 = 0.0850 | |
| Largest diff. peak and hole | 0.382 and -0.198 e. $Å^{-3}$ | |

# APPENDIX II

Table A.II.2. Atomic coordinates ( x $10^4$) and equivalent isotropic displacement parameters ($Å^2$ x $10^3$) for L2.$BH_3$. U(eq) is defined as one third of the trace of the orthogonalized Uij tensor.

| | x | y | z | U(eq) |
|---|---|---|---|---|
| Fe | -5379(1) | 11093(1) | 3055(1) | 33(1) |
| N(1) | -5507(2) | 9716(2) | 1076(1) | 41(1) |
| N(2) | -6681(2) | 9357(2) | 457(1) | 42(1) |
| C(1) | -5726(4) | 10239(3) | 3986(1) | 70(1) |
| C(2) | -6644(3) | 9604(2) | 3386(2) | 63(1) |
| C(3) | -7923(3) | 10414(3) | 2990(2) | 64(1) |
| C(4) | -7760(4) | 11550(3) | 3358(2) | 76(1) |
| C(5) | -6392(4) | 11422(3) | 3972(2) | 78(1) |
| C(6) | -4883(3) | 12334(2) | 2315(1) | 45(1) |
| C(7) | -3574(3) | 12442(2) | 2951(1) | 49(1) |
| C(8) | -2675(2) | 11312(2) | 3070(1) | 44(1) |
| C(9) | -3417(2) | 10495(2) | 2511(1) | 39(1) |
| C(10) | -4794(2) | 11133(2) | 2036(1) | 36(1) |
| C(11) | -5933(3) | 10676(2) | 1381(1) | 40(1) |
| N(3) | -7392(2) | 8008(2) | -496(1) | 38(1) |
| C(13) | -6957(3) | 7015(2) | -861(1) | 48(1) |
| C(14) | -5374(3) | 6394(2) | -677(1) | 53(1) |
| C(15) | -4122(3) | 6816(2) | -102(1) | 53(1) |
| C(16) | -4517(3) | 7814(2) | 279(1) | 46(1) |
| C(17) | -6195(2) | 8396(2) | 83(1) | 36(1) |
| B(1) | -9280(3) | 8683(3) | -750(1) | 56(1) |

# APPENDIX II

Table A.II.3. Bond lengths [Å] and angles [°] forL2.$BH_3$

| | | | |
|---|---|---|---|
| Fe-C(6) | 2.024(2) | C(3)-C(4) | 1.415(4) |
| Fe-C(4) | 2.032(2) | C(4)-C(5) | 1.410(4) |
| Fe-C(3) | 2.034(2) | C(6)-C(7) | 1.412(3) |
| Fe-C(5) | 2.034(2) | C(6)-C(10) | 1.419(3) |
| Fe-C(7) | 2.035(2) | C(7)-C(8) | 1.407(3) |
| Fe-C(2) | 2.036(2) | C(8)-C(9) | 1.416(3) |
| Fe-C(1) | 2.040(2) | C(9)-C(10) | 1.424(2) |
| Fe-C(10) | 2.040(2) | C(10)-C(11) | 1.459(2) |
| Fe-C(8) | 2.041(2) | N(3)-C(17) | 1.352(2) |
| Fe-C(9) | 2.044(2) | N(3)-C(13) | 1.355(3) |
| N(1)-C(11) | 1.264(2) | N(3)-B(1) | 1.596(3) |
| N(1)-N(2) | 1.387(2) | C(13)-C(14) | 1.360(3) |
| N(2)-C(17) | 1.350(2) | C(14)-C(15) | 1.382(3) |
| C(1)-C(5) | 1.384(4) | C(15)-C(16) | 1.365(3) |
| C(1)-C(2) | 1.399(4) | C(16)-C(17) | 1.401(3) |
| C(2)-C(3) | 1.418(4) | | |
| | | | |
| C(6)-Fe-C(4) | 107.81(11) | C(17)-N(2)-N(1) | 117.8(2) |
| C(6)-Fe-C(3) | 119.18(10) | C(5)-C(1)-C(2) | 108.8(3) |
| C(4)-Fe-C(3) | 40.74(12) | C(5)-C(1)-Fe | 69.9(2) |
| C(6)-Fe-C(5) | 127.28(12) | C(2)-C(1)-Fe | 69.80(14) |
| C(4)-Fe-C(5) | 40.58(12) | C(1)-C(2)-C(3) | 107.8(3) |
| C(3)-Fe-C(5) | 68.15(12) | C(1)-C(2)-Fe | 70.06(14) |
| C(6)-Fe-C(7) | 40.72(8) | C(3)-C(2)-Fe | 69.52(14) |
| C(4)-Fe-C(7) | 118.91(11) | C(2)-C(3)-C(4) | 107.4(2) |
| C(3)-Fe-C(7) | 153.28(10) | C(2)-C(3)-Fe | 69.71(13) |
| C(5)-Fe-C(7) | 107.99(11) | C(4)-C(3)-Fe | 69.59(14) |
| C(6)-Fe-C(2) | 153.83(10) | C(5)-C(4)-C(3) | 107.5(3) |
| C(4)-Fe-C(2) | 68.26(12) | C(5)-C(4)-Fe | 69.77(14) |
| C(3)-Fe-C(2) | 40.77(10) | C(3)-C(4)-Fe | 69.67(13) |
| C(5)-Fe-C(2) | 67.57(13) | C(1)-C(5)-C(4) | 108.5(3) |
| C(7)-Fe-C(2) | 164.35(9) | C(1)-C(5)-Fe | 70.35(14) |
| C(6)-Fe-C(1) | 164.39(11) | C(4)-C(5)-Fe | 69.65(14) |
| C(4)-Fe-C(1) | 67.68(13) | C(7)-C(6)-C(10) | 108.6(2) |
| C(3)-Fe-C(1) | 67.92(11) | C(7)-C(6)-Fe | 70.07(11) |
| C(5)-Fe-C(1) | 39.74(12) | C(10)-C(6)-Fe | 70.17(11) |
| C(7)-Fe-C(1) | 127.03(11) | C(8)-C(7)-C(6) | 107.7(2) |
| C(2)-Fe-C(1) | 40.14(11) | C(8)-C(7)-Fe | 70.00(12) |
| C(6)-Fe-C(10) | 40.87(8) | C(6)-C(7)-Fe | 69.21(11) |
| C(4)-Fe-C(10) | 127.12(11) | C(7)-C(8)-C(9) | 108.6(2) |
| C(3)-Fe-C(10) | 107.85(10) | C(7)-C(8)-Fe | 69.61(11) |
| C(5)-Fe-C(10) | 165.05(11) | C(9)-C(8)-Fe | 69.83(10) |
| C(7)-Fe-C(10) | 68.69(8) | C(8)-C(9)-C(10) | 107.7(2) |
| C(2)-Fe-C(10) | 119.52(10) | C(8)-C(9)-Fe | 69.59(11) |
| C(1)-Fe-C(10) | 153.69(11) | C(10)-C(9)-Fe | 69.46(10) |
| C(6)-Fe-C(8) | 68.14(9) | C(6)-C(10)-C(9) | 107.3(2) |
| C(4)-Fe-C(8) | 152.95(12) | C(6)-C(10)-C(11) | 124.7(2) |
| C(3)-Fe-C(8) | 165.05(10) | C(9)-C(10)-C(11) | 128.0(2) |
| C(5)-Fe-C(8) | 119.20(11) | C(6)-C(10)-Fe | 68.96(11) |
| C(7)-Fe-C(8) | 40.39(9) | C(9)-C(10)-Fe | 69.74(10) |
| C(2)-Fe-C(8) | 127.32(10) | C(11)-C(10)-Fe | 126.49(13) |
| C(1)-Fe-C(8) | 108.62(10) | N(1)-C(11)-C(10) | 120.7(2) |
| C(10)-Fe-C(8) | 68.39(8) | C(17)-N(3)-C(13) | 118.3(2) |
| C(6)-Fe-C(9) | 68.51(8) | C(17)-N(3)-B(1) | 121.8(2) |
| C(4)-Fe-C(9) | 165.10(11) | C(13)-N(3)-B(1) | 120.0(2) |
| C(3)-Fe-C(9) | 127.29(10) | N(3)-C(13)-C(14) | 123.2(2) |
| C(5)-Fe-C(9) | 152.98(11) | C(13)-C(14)-C(15) | 118.5(2) |
| C(7)-Fe-C(9) | 68.41(9) | C(16)-C(15)-C(14) | 119.7(2) |
| C(2)-Fe-C(9) | 108.27(10) | C(15)-C(16)-C(17) | 119.5(2) |
| C(1)-Fe-C(9) | 119.71(10) | N(2)-C(17)-N(3) | 117.4(2) |
| C(10)-Fe-C(9) | 40.80(7) | N(2)-C(17)-C(16) | 122.0(2) |
| C(8)-Fe-C(9) | 40.57(8) | N(3)-C(17)-C(16) | 120.6(2) |
| C(11)-N(1)-N(2) | 116.2(2) | | |

# APPENDIX III

The following is a record of complex reactions that were tried, but failed to give characterisable products.

## A.III (a) COMPLEXES OF L5

The 1,3-diamino-2-hydroxypropane ferrocenyl derivative, L5. is a product formed by an intra-cyclisation reaction. It was expected to coordinate by either one of two methods:

1) The annular ring would undergo tautomerism to form the imine bond, which would then undergo cleavage, similar to that observed in disulphide bond cleavage. If this were to occur, then the resultant deprotonated ligand would be a tridentate anion, which would have a vacant coordination site occupied by a counter ion (assuming tetrahedral geometry).

2) The annular ligand would be stable and deprotonation of the hydroxy group would result in a normal monodentate anion ligand.(See Fig 2.30 in Chapter 2).

The ligand L5 was reacted with $CuCl_2$ in a slightly basic solution of ethanol, but the result was the formation of an unidentifiable compound with no compatiblity obtained between the observed and theoretical elemental analysis. No other complexation reactions were tried.

## A.III(b) COMPLEXES OF L3

The unstable nature of this ligand in the presence of any moisture, and the high solubility, indicated that the complex would be very difficult to recover from the solvent without any decomposition of the ligand occurring. Only one complex reaction was attempted, involving $CuCl_2$ dissolved in ethanol with triethylorthoformate. A black compound formed, but characteristion of this compound was not possible.

### A.III (c) COMPLEXES OF L4

Complexes of this ligand have been reported with Cu(II) in a 2:1 complex [54]. But no attempts to coordinate any metals in this work were tried.

### A.III (d) COMPLEXES OF L11

L11 was a potential tetradentate di-anionic ligand, which would chelate to a metal even if the imine nitrogen atoms where not involved in bonding. However, examination of a model of the ligand coupled with evidence from the single-crystal X-ray structure, showed that the strain imposed within the ligand 'arms' by a coordinating metal would make complexation difficult. Also the size of the cavity in which the metal has to fit is very small. A reaction of L11 with copper acetate in thf failed to produce a characterisable product, possibily due to the factors discussed above.

### A.III (e) COMPLEXES OF L22

The evidence from the mono parent ligand L2 suggested that this could possibly be an effective ligand with which to complex first row transition metals. A thf solution of $CuCl_2$ was reacted with a thf solution of L2, to produce an uncharacterisable black powder. It is suggested that this could be the result of the geometry of the substituted arms on the ferrocene moiety conforming to a cis configuration as has occurred in the reaction of pyridlyhydrazone with 1,1'-diacetylferrocene [56]. The authors of this reference stated that the instability was not due to the hydrolysis of the ligand resulting in the free 1,1'-diacetylferrocene, but the formation of an iron (III) product which was not a ferrocinium type complex. It was tentatively suggested by the authors from Mossbauer data, that the iron (III) species, were μ-oxo iron (III) bridged complexes, and that the hydrazones did not show promise as organometallic ligands. In light of this infomation no more complex reactions were attempted on this system.

### A.III (f) TEMPLATE REACTION

A complex involving the reaction of ethylenediamine with $CuCl_2$ in a 2:1 molecular ratio (to act as a template for a futher reaction) was synthesised in a soution of thf. To this

complex was added 1,1'-ferrocene dicarboxaldehyde refluxed for 3 hours in a nitrogen atomosphere. The resultant product was filtered, but the black powder was uncharacterisable. No more reactions using this method of synthesis were attempted.

## LIQUID SIMS SPECTROSCOPIC ISOTOPE ABUNDANCE CALCULATIONS FOR THE COMPLEXES OF L1 AND L2

Isotope abundance observation values that appear in Table 4.3 for $[Zn(L1)Cl]_2$.xDBU.yDBUClH.zthf are shown below along with their calculated isotope abundance's.

Observed spectrum for $[Zn(L1)Cl]_2(DBU)(DBUH)^+$.

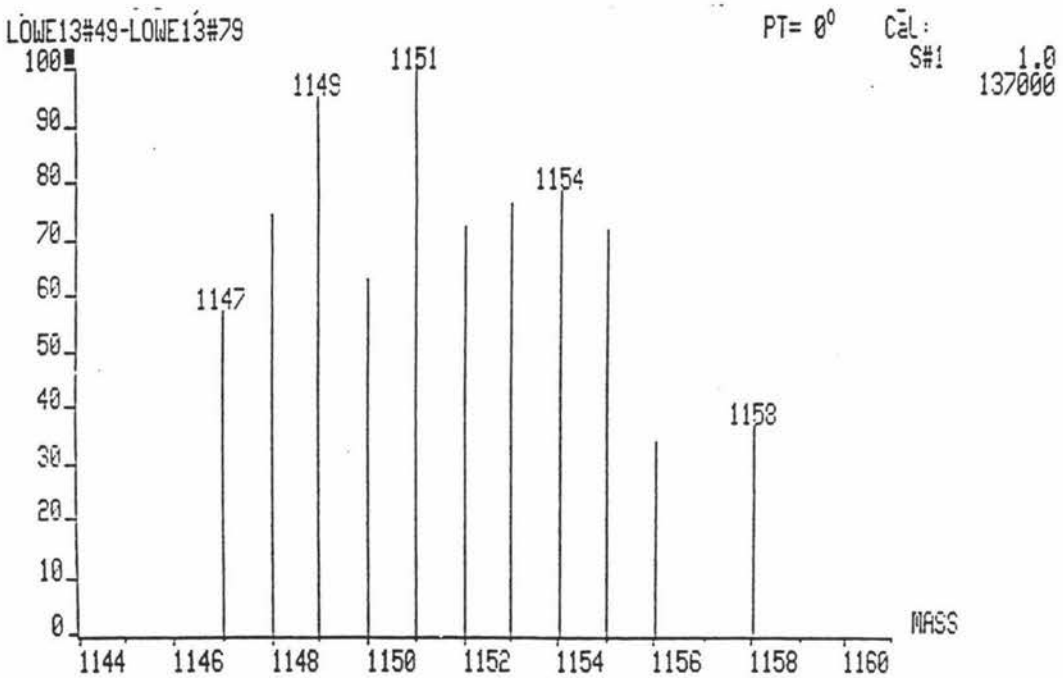


Calculated spectrum.

ISO — Isotope Cluster Abundance Calculations — 23-MAY-95

Formula: (NOM,ACC,SPE) Mode: [NOM,ACC,SPE] NOM

| Element | #Atoms | #Isotopes | Element | #Atoms | #Isotopes | Element | #Atoms | #Isotopes |
|---|---|---|---|---|---|---|---|---|
| C | 52 | 2 | FE | 2 | 4 | | | |
| H | 62 | 1 | ZN | 2 | 5 | | | |
| O | 2 | 1 | | | | | | |
| N | 6 | 1 | | | | | | |
| CL | 3 | 2 | | | | | | |

Spectrum: (SPE)

| Mass | ZInt | Mass | ZInt | Mass | ZInt | Mass | ZInt | Mass | ZInt |
|---|---|---|---|---|---|---|---|---|---|
| 1143 | 0.1183 | 1146 | 2.4433 | 1149 | 79.8837 | 1152 | 64.1106 | 1155 | 48.0368 |
| 1144 | 0.0691 | 1147 | 38.5176 | 1150 | 52.9279 | 1153 | 82.9644 | 1156 | 26.5270 |
| 1145 | 4.0115 | 1148 | 24.4689 | 1151 | 100.0000 | 1154 | 50.0358 | 1157 | 19.4356 |

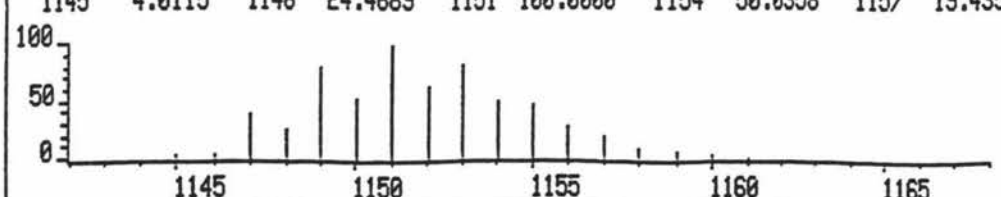


'Q=return to edit mode 'X=exit 'H=hardcopy ?=Help

Observed spectrum for $[Zn(L1)Cl]_2thf^+$.

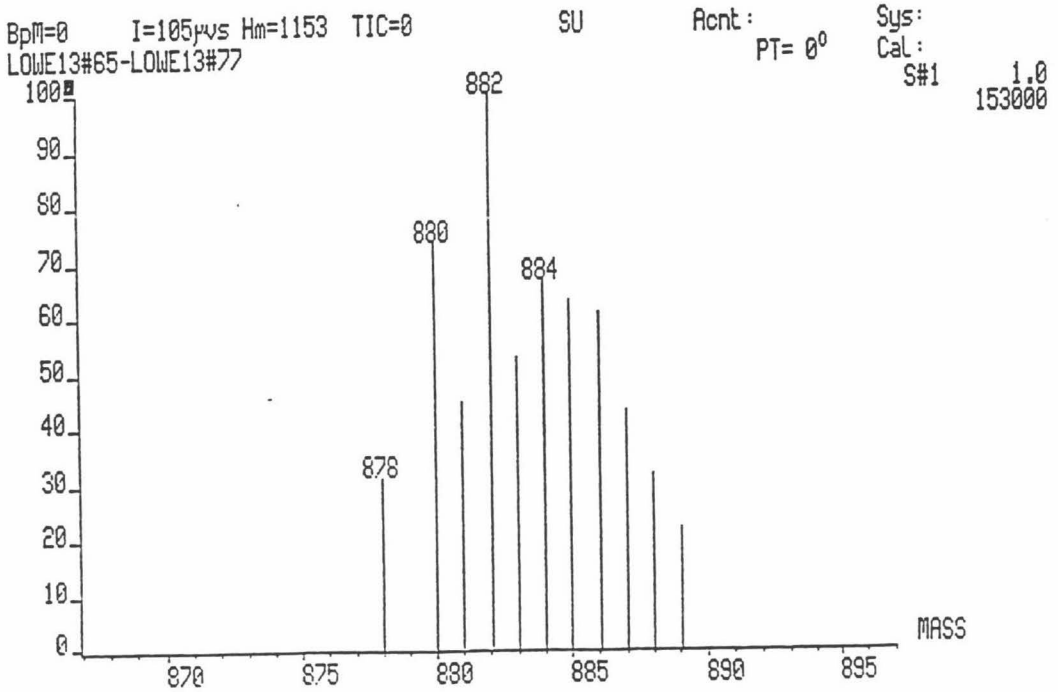


Calculated spectrum.

ISO Isotope Cluster Abundance Calculations 23-MAY-95

Formula: (NOM,ACC,SPE) Mode: [NOM,ACC,SPE] NOM

| Element | #Atoms | #Isotopes | Element | #Atoms | #Isotopes | Element | #Atoms | #Isotopes |
|---|---|---|---|---|---|---|---|---|
| C | 38 | 2 | FE | 2 | 4 | | | |
| H | 36 | 1 | ZN | 2 | 5 | | | |
| O | 3 | 1 | | | | | | |
| N | 2 | 1 | | | | | | |
| CL | 2 | 2 | | | | | | |

Spectrum: (SPE)

| Mass | %Int | Mass | %Int | Mass | %Int | Mass | %Int | Mass | %Int |
|---|---|---|---|---|---|---|---|---|---|
| 889 | 4.3206 | 892 | 0.1820 | 895 | 0.0014 | | | | |
| 890 | 1.9992 | 893 | 0.0427 | 896 | 0.0002 | | | | |
| 891 | 0.6398 | 894 | 0.0084 | | | | | | |

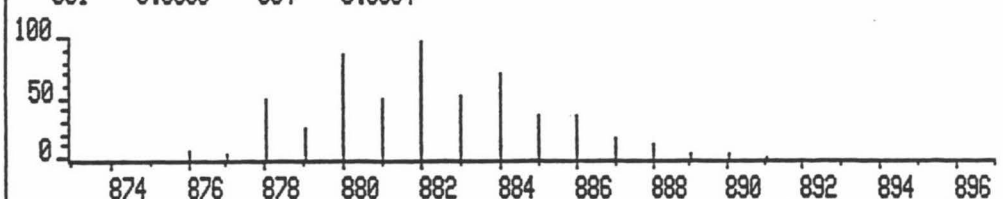


?=help RETURN=next ESC=previous 'G=compute 'X=exit 'H=hardcopy 'L('LX)=List(&exit)

Observed spectrum for $[Zn(L1)Cl]_2^+$.

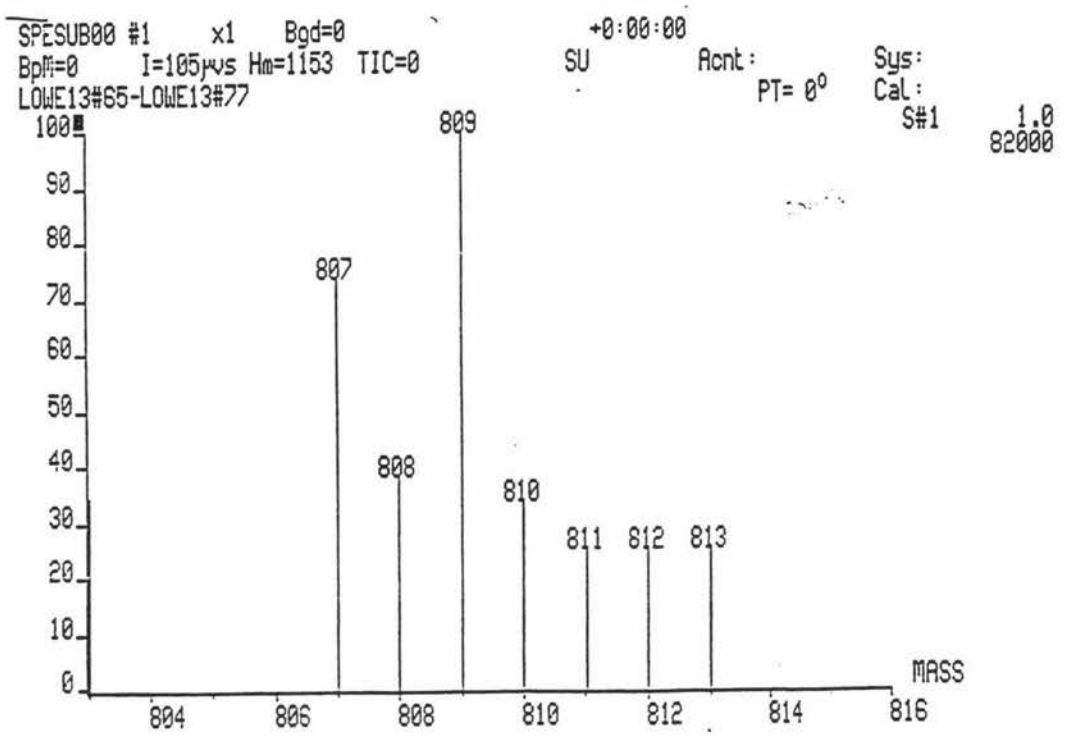


Calculated spectrum.

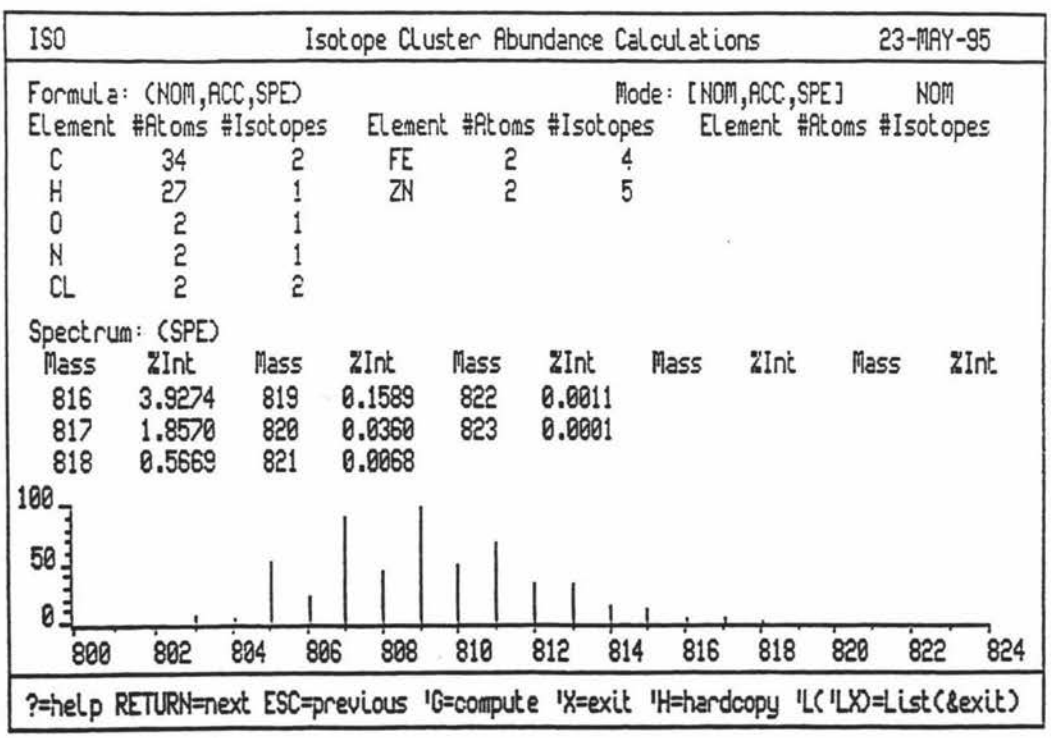

Oserved spectrum for $[Zn(L1)Cl_2(DBU)]^+$.

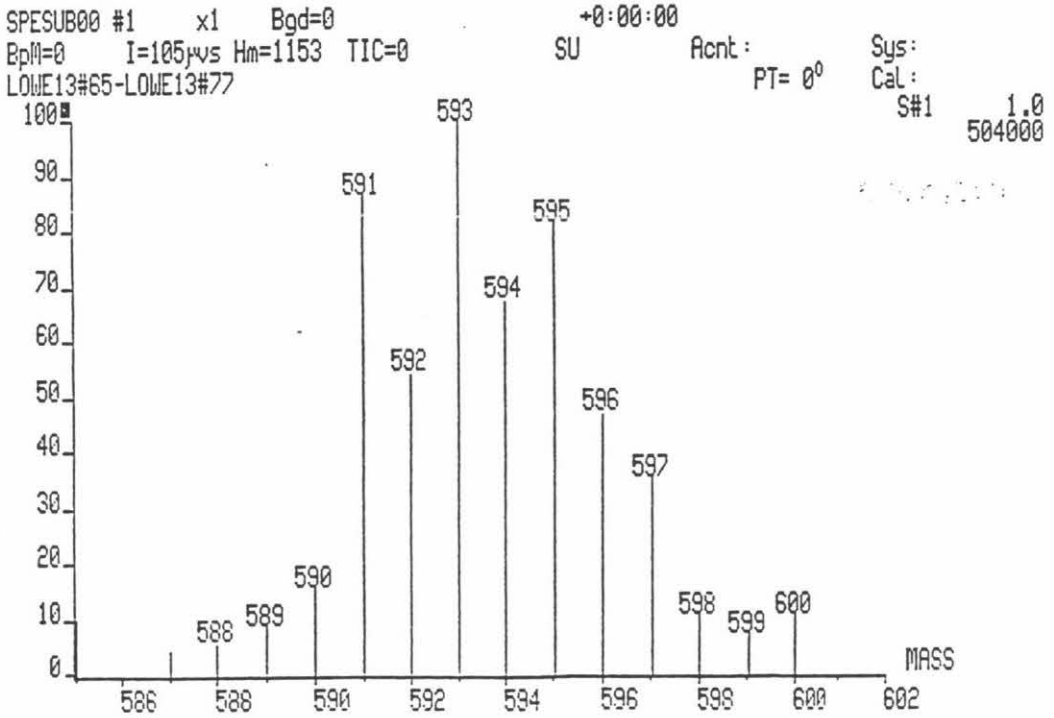


Calculated spectrum.

ISO — Isotope Cluster Abundance Calculations — 23-MAY-95

Formula: (NOM,ACC,SPE) Mode: [NOM,ACC,SPE] NOM

| Element | #Atoms | #Isotopes | Element | #Atoms | #Isotopes | Element | #Atoms | #Isotopes |
|---|---|---|---|---|---|---|---|---|
| C | 26 | 2 | FE | 1 | 4 | | | |
| H | 31 | 1 | ZN | 1 | 5 | | | |
| O | 1 | 1 | | | | | | |
| N | 3 | 1 | | | | | | |
| CL | 2 | 2 | | | | | | |

Spectrum: (SPE)

| Mass | %Int | Mass | %Int | Mass | %Int | Mass | %Int | Mass | %Int |
|---|---|---|---|---|---|---|---|---|---|
| 589 | 4.7779 | 592 | 25.9758 | 595 | 73.1869 | 598 | 8.8970 | 601 | 0.2932 |
| 590 | 1.3944 | 593 | 100.0000 | 596 | 25.8564 | 599 | 5.0863 | 602 | 0.0510 |
| 591 | 81.5515 | 594 | 37.2441 | 597 | 29.0283 | 600 | 1.3054 | 603 | 0.0065 |

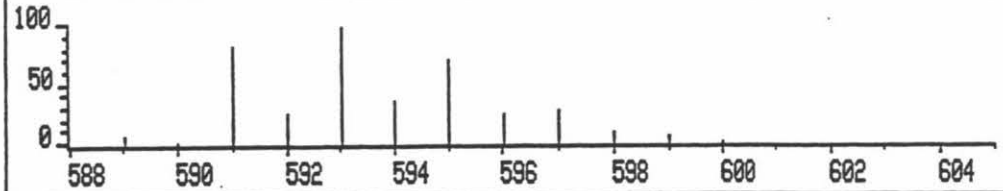


!Q=return to edit mode !X=exit !H=hardcopy ?=Help

Observed spectrum for $[Zn(L1)Cl]^+$.

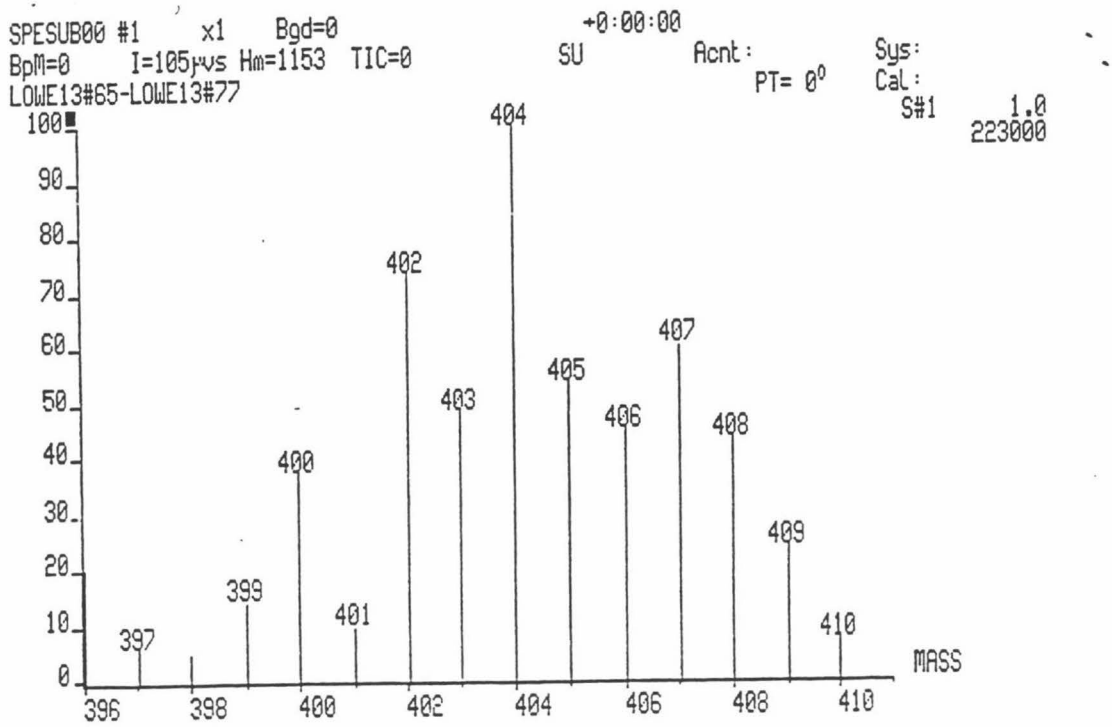


Calculated spectrum.

ISO Isotope Cluster Abundance Calculations 23-MAY-95

Formula: (NOM,ACC,SPE) Mode: [NOM,ACC,SPE] NOM

| Element | #Atoms | #Isotopes | Element | #Atoms | #Isotopes | Element | #Atoms | #Isotopes |
|---|---|---|---|---|---|---|---|---|
| C | 17 | 2 | FE | 1 | 4 | | | |
| H | 15 | 1 | ZN | 1 | 5 | | | |
| O | 1 | 1 | | | | | | |
| N | 1 | 1 | | | | | | |
| CL | 1 | 2 | | | | | | |

Spectrum: (SPE)

| Mass | %Int | Mass | %Int | Mass | %Int | Mass | %Int | Mass | %Int |
|---|---|---|---|---|---|---|---|---|---|
| 402 | 5.9791 | 405 | 21.8404 | 408 | 58.6545 | 411 | 2.9383 | 414 | 0.0107 |
| 403 | 1.1409 | 406 | 90.4571 | 409 | 14.6605 | 412 | 0.7034 | 415 | 0.0008 |
| 404 | 100.0000 | 407 | 27.1420 | 410 | 14.8103 | 413 | 0.1059 | | |

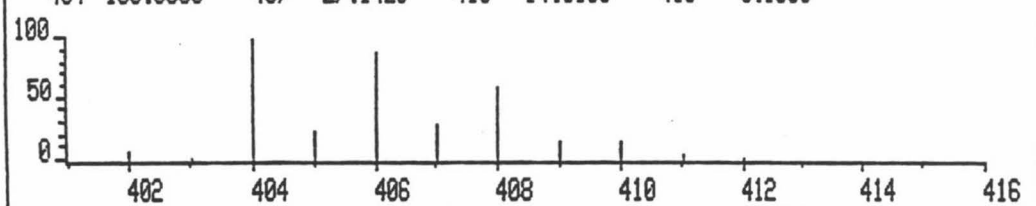


?=help RETURN=next ESC=previous 'G=compute 'X=exit 'H=hardcopy 'L('LX)=List(&exit)

The following isotope abundance calculations and observed spectra are from Table 4.4 and are the results from ions formed from the complexes base on the L2 ligand.

Observed spectrum for $[Cu(L2)_2Cl]^+$.

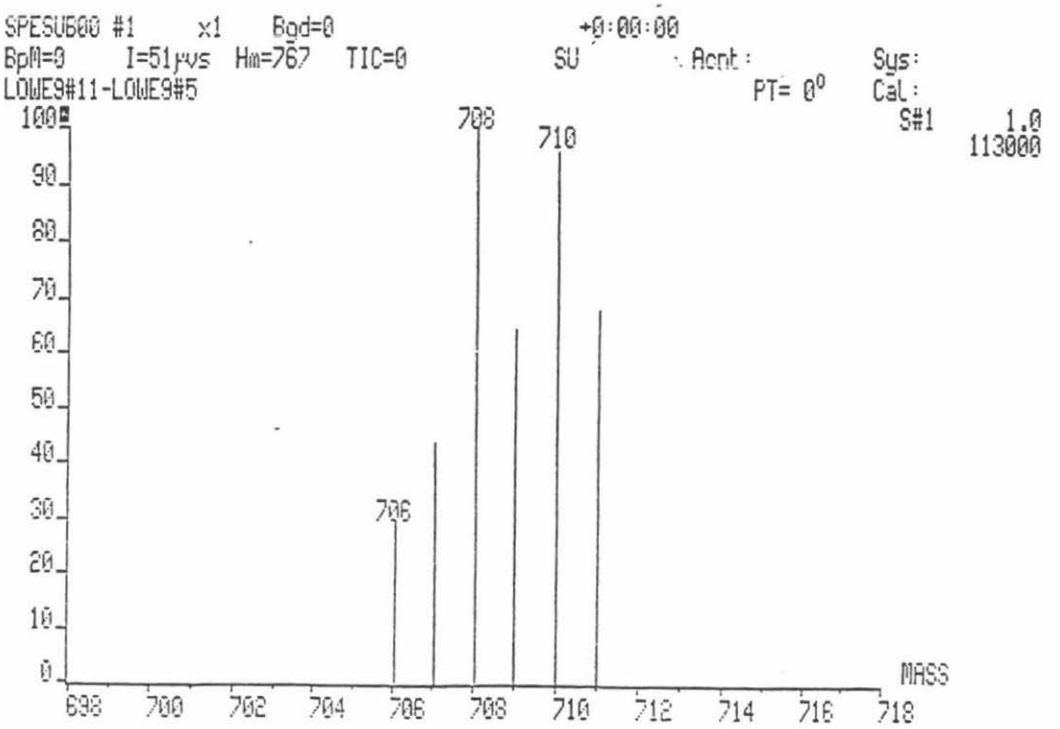


Calculated spectrum.

ISO Isotope Cluster Abundance Calculations 14-SEP-95

Formula: (NOM,ACC,SPE) Mode: [NOM,ACC,SPE] NOM

| Element | #Atoms | #Isotopes | Element | #Atoms | #Isotopes | Element | #Atoms | #Isotopes |
|---|---|---|---|---|---|---|---|---|
| C | 32 | 2 | CL | 1 | 2 | | | |
| H | 30 | 1 | | | | | | |
| N | 6 | 1 | | | | | | |
| FE | 2 | 4 | | | | | | |
| CU | 1 | 2 | | | | | | |

Spectrum: (SPE)

| Mass | %Int | Mass | %Int | Mass | %Int | Mass | %Int | Mass | %Int |
|---|---|---|---|---|---|---|---|---|---|
| 704 | 0.3612 | 707 | 4.4797 | 710 | 79.2499 | 713 | 6.1382 | 716 | 0.0183 |
| 705 | 0.1298 | 708 | 100.0000 | 711 | 30.0001 | 714 | 1.2106 | 717 | 0.0016 |
| 706 | 11.7243 | 709 | 40.2633 | 712 | 19.1053 | 715 | 0.1702 | 718 | 0.0001 |

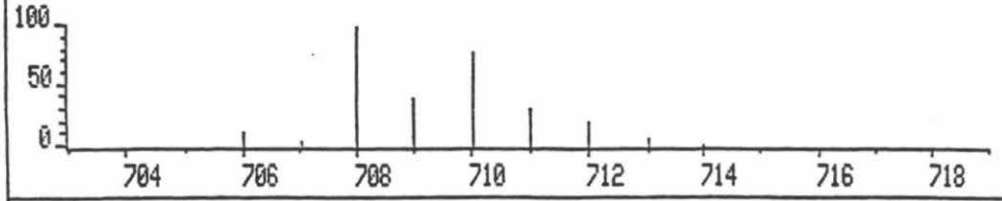


!Q=return to edit mode !X=exit !H=hardcopy ?=Help

Observed spectrum for $[Cu(L2)_2]^+$

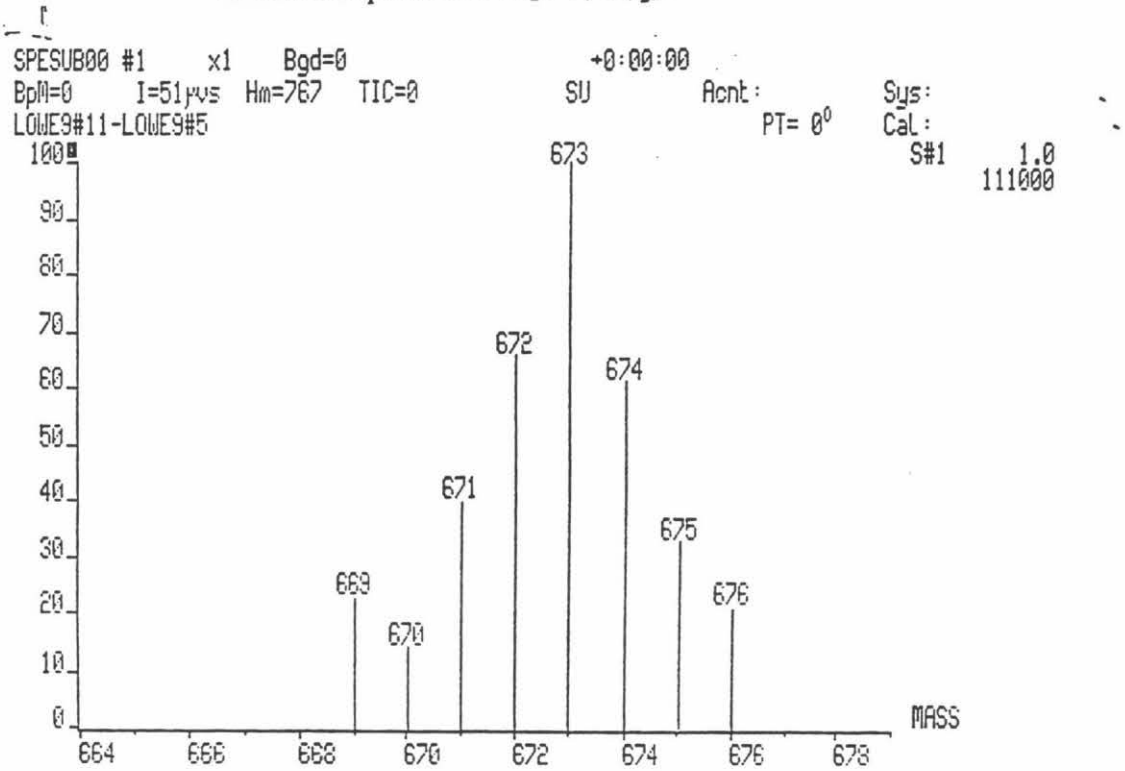


Calculated spectrum.

ISO Isotope Cluster Abundance Calculations 14-SEP-95

Formula: (NOM,ACC,SPE) Mode: [NOM,ACC,SPE] NOM

| Element | #Atoms | #Isotopes | Element | #Atoms | #Isotopes | Element | #Atoms | #Isotopes |
|---|---|---|---|---|---|---|---|---|
| C | 32 | 2 | | | | | | |
| H | 30 | 1 | | | | | | |
| N | 6 | 1 | | | | | | |
| FE | 2 | 4 | | | | | | |
| CU | 1 | 2 | | | | | | |

Spectrum: (SPE)

| Mass | %Int | Mass | %Int | Mass | %Int | Mass | %Int | Mass | %Int |
|---|---|---|---|---|---|---|---|---|---|
| 669 | 0.3752 | 672 | 4.6093 | 675 | 50.3269 | 678 | 0.5369 | 681 | 0.0003 |
| 670 | 0.1348 | 673 | 100.0000 | 676 | 18.2561 | 679 | 0.0586 | | |
| 671 | 12.0563 | 674 | 40.3416 | 677 | 3.7481 | 680 | 0.0051 | | |

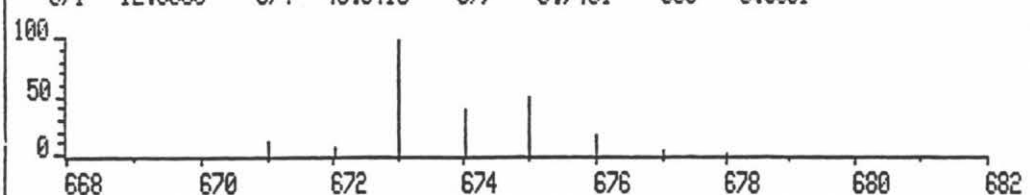


?=help RETURN=next ESC=previous 'G=compute 'X=exit 'H=hardcopy 'L('LX)=List(&exit)

Observed spectrum for $[Cu(L2)Cl_2].^+$

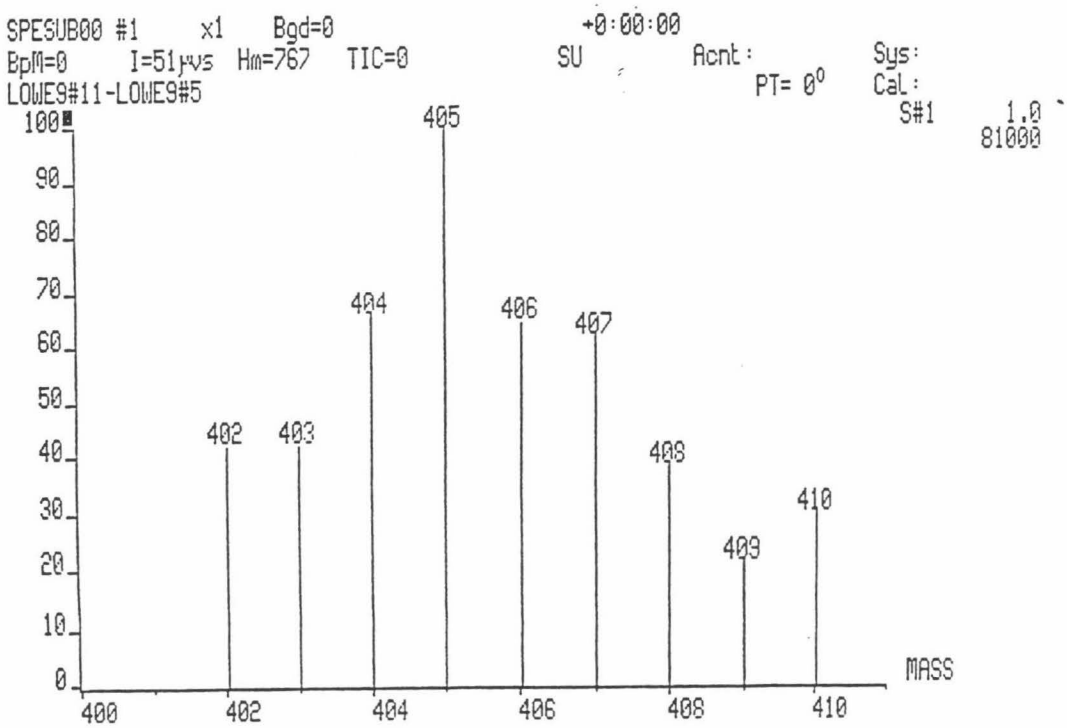


Calculated spectrum.

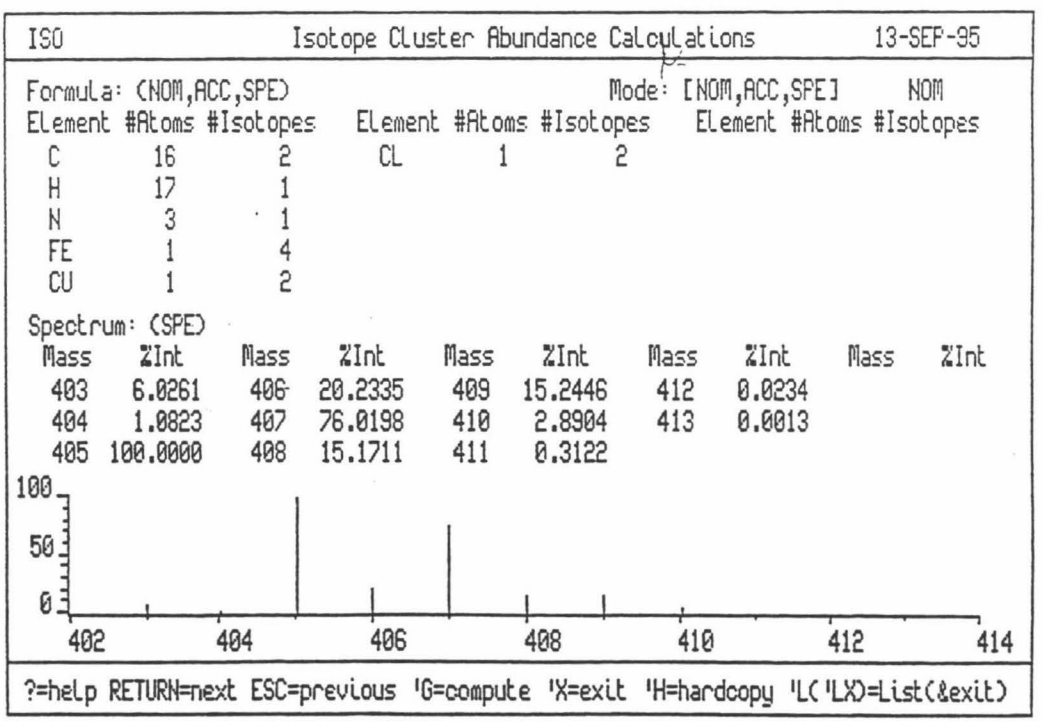

Observed spectrum for $[Co(L2)_2Cl]^+$.

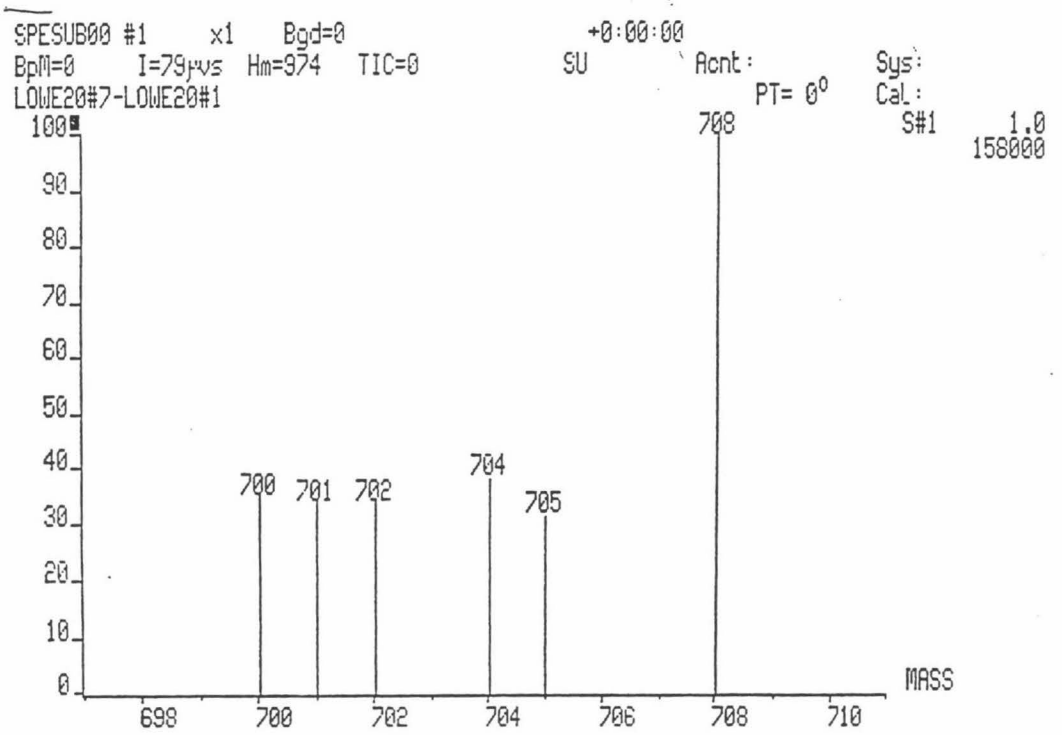


Calculated spectrum.

ISO Isotope Cluster Abundance Calculations 14-SEP-95

Formula: (NOM,ACC,SPE) Mode: [NOM,ACC,SPE] NOM

| Element | #Atoms | #Isotopes | Element | #Atoms | #Isotopes | Element | #Atoms | #Isotopes |
|---|---|---|---|---|---|---|---|---|
| C | 32 | 2 | CL | 1 | 2 | | | |
| H | 32 | 1 | | | | | | |
| N | 6 | 1 | | | | | | |
| FE | 2 | 4 | | | | | | |
| CO | 1 | 1 | | | | | | |

Spectrum: (SPE)

| Mass | %Int | Mass | %Int | Mass | %Int | Mass | %Int | Mass | %Int |
|---|---|---|---|---|---|---|---|---|---|
| 702 | 0.3809 | 705 | 4.6621 | 708 | 38.9849 | 711 | 0.3943 | 714 | 0.0002 |
| 703 | 0.1368 | 706 | 100.0000 | 709 | 13.6354 | 712 | 0.0429 | | |
| 704 | 12.1916 | 707 | 40.3732 | 710 | 2.7673 | 713 | 0.0037 | | |

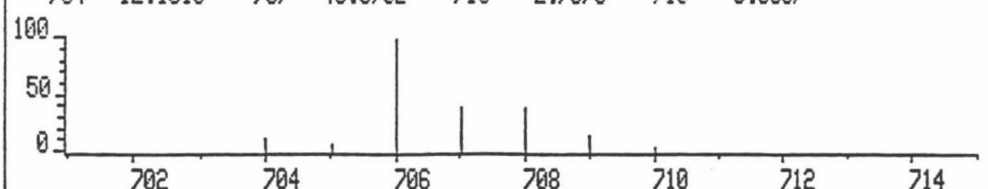


?=help RETURN=next ESC=previous 'G=compute 'X=exit 'H=hardcopy 'LC 'LX)=List(&exit)

Observed spectrum for $[Co(L2)_2]^+$.

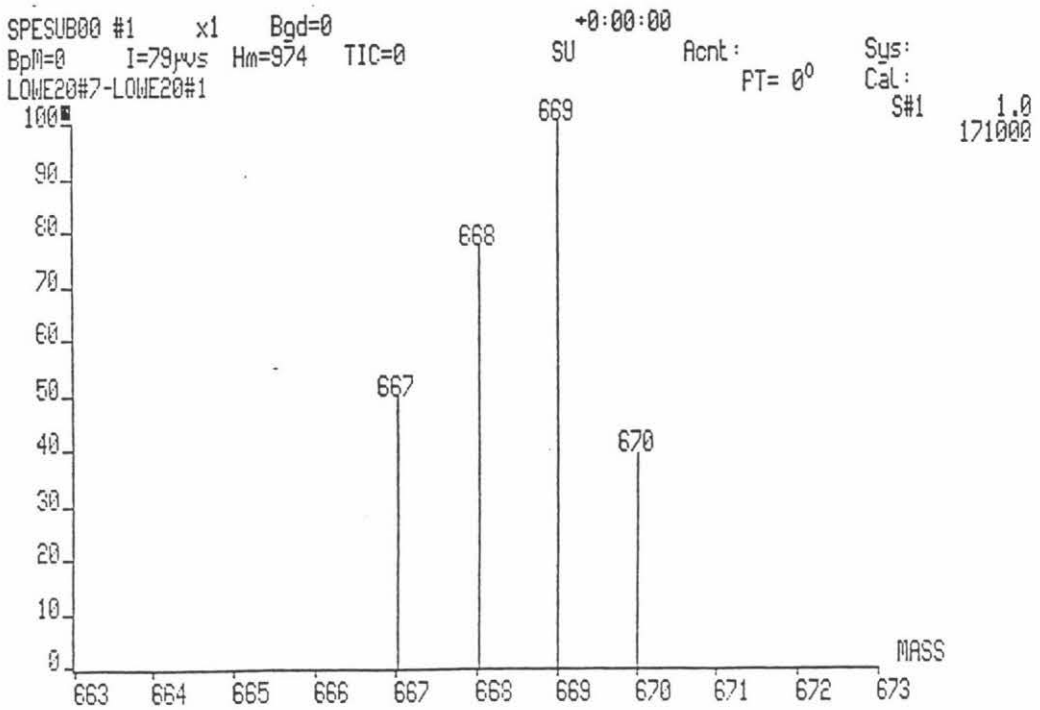


Calculated spectrum.

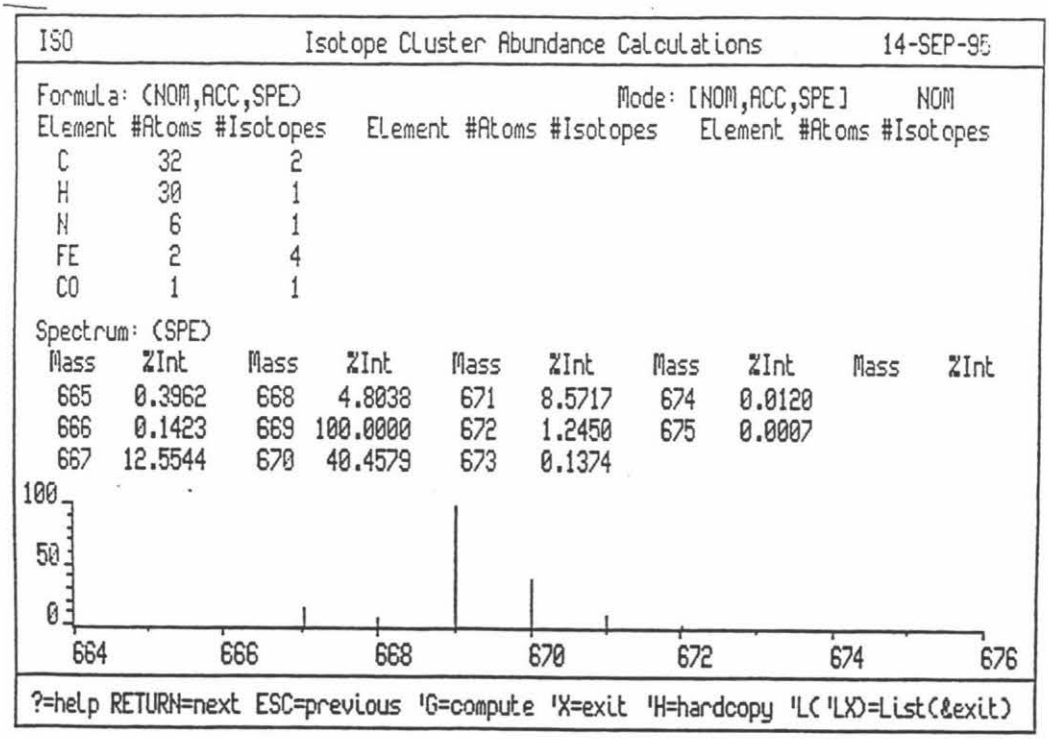

Observed spectrum for $[Co(L2)Cl]^+$

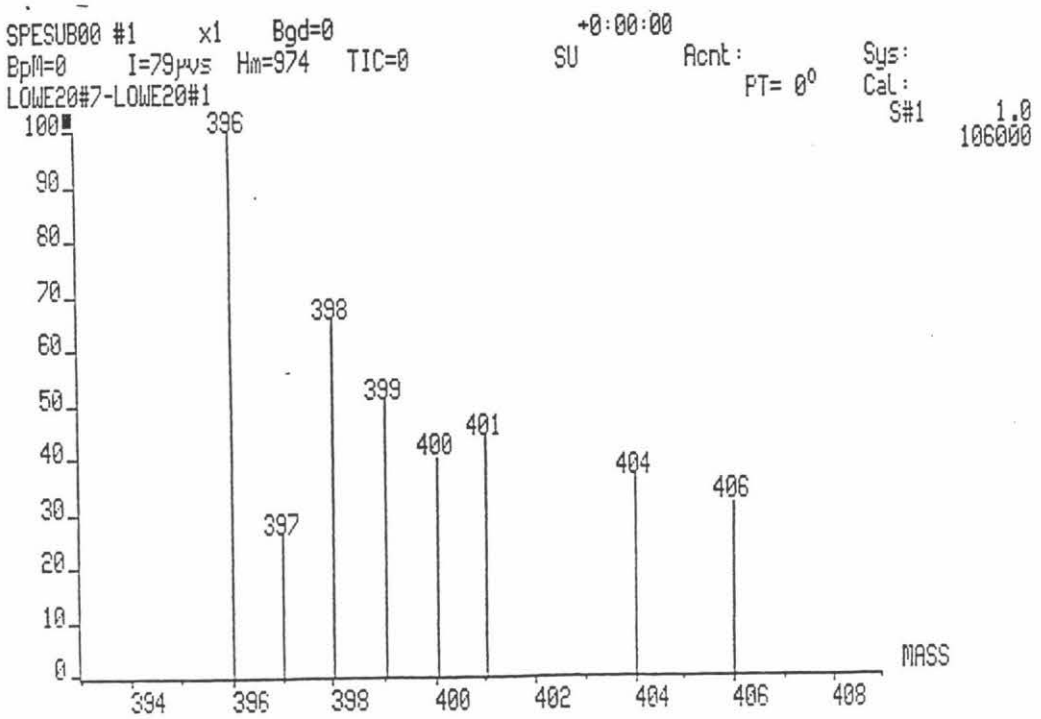


Calculated spectrum.

ISO Isotope Cluster Abundance Calculations 14-SEP-95

Formula: (NOM,ACC,SPE) Mode: [NOM,ACC,SPE] NOM

| Element | #Atoms | #Isotopes | Element | #Atoms | #Isotopes | Element | #Atoms | #Isotopes |
|---|---|---|---|---|---|---|---|---|
| C | 16 | 2 | CL | 1 | 2 | | | |
| H | 15 | 1 | | | | | | |
| N | 3 | 1 | | | | | | |
| FE | 1 | 4 | | | | | | |
| CO | 1 | 1 | | | | | | |

Spectrum: (SPE)

| Mass | %Int | Mass | %Int | Mass | %Int | Mass | %Int | Mass | %Int |
|---|---|---|---|---|---|---|---|---|---|
| 397 | 6.1925 | 400 | 20.2963 | 403 | 0.7132 | 406 | 0.0001 | | |
| 398 | 1.1121 | 401 | 33.5466 | 404 | 0.0536 | | | | |
| 399 | 100.0000 | 402 | 6.5434 | 405 | 0.0029 | | | | |

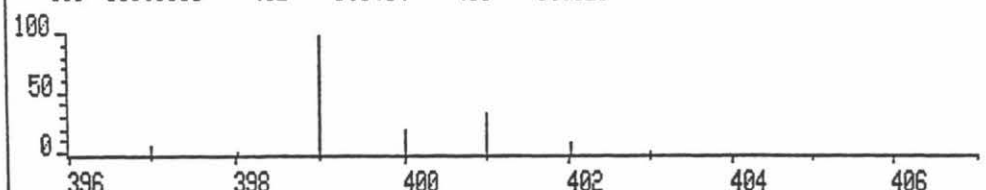


?=help RETURN=next ESC=previous 'G=compute 'X=exit 'H=hardcopy 'L('LX)=List(&exit)

Observed spectrum for $[Co(L2)]^+$

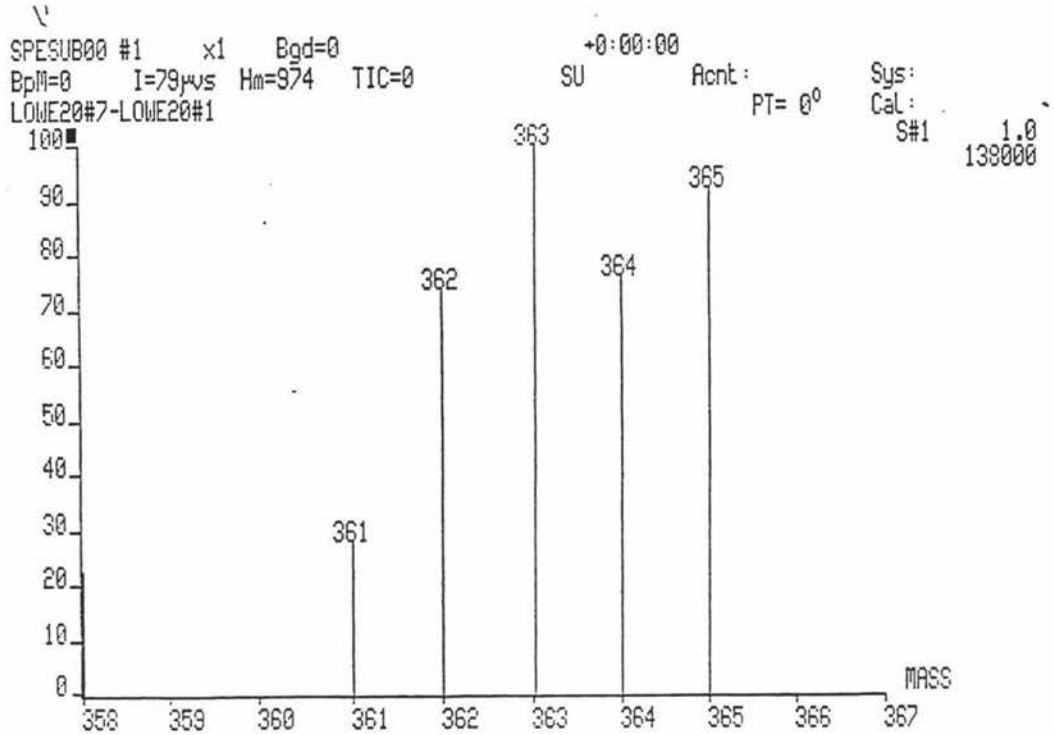


Calculated spectrum.

ISO Isotope Cluster Abundance Calculations 14-SEP-95

Formula: (NOM,ACC,SPE) Mode: [NOM,ACC,SPE] NOM

| Element | #Atoms | #Isotopes | Element | #Atoms | #Isotopes | Element | #Atoms | #Isotopes |
|---|---|---|---|---|---|---|---|---|
| C | 16 | 2 | | | | | | |
| H | 14 | 1 | | | | | | |
| N | 3 | 1 | | | | | | |
| FE | 1 | 4 | | | | | | |
| CO | 1 | 1 | | | | | | |

Spectrum: (SPE)

| Mass | %Int | Mass | %Int | Mass | %Int | Mass | %Int | Mass | %Int |
|---|---|---|---|---|---|---|---|---|---|
| 361 | 6.3176 | 364 | 20.3435 | 367 | 0.0093 | | | | |
| 362 | 1.1346 | 365 | 2.2460 | 368 | 0.0003 | | | | |
| 363 | 100.0000 | 366 | 0.1701 | | | | | | |

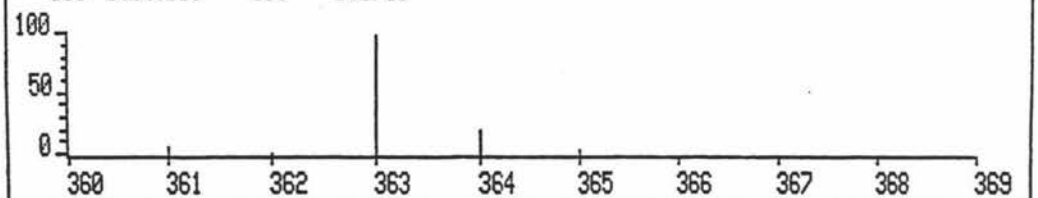


?=help RETURN=next ESC=previous 'G=compute 'X=exit 'H=hardcopy 'L('LX)=List(&exit)

Observed spectrum for $[Ni(L2)_2Br]^+$.

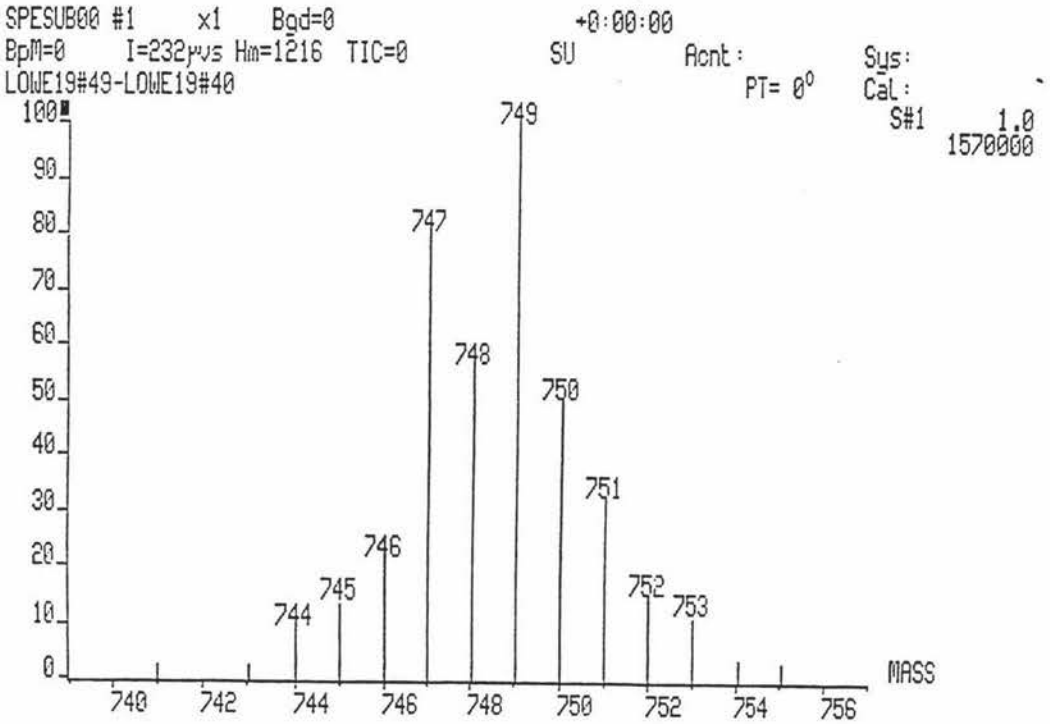


Calculated spectrum.

ISO Isotope Cluster Abundance Calculations 14-SEP-95

Formula: (NOM,ACC,SPE) Mode: [NOM,ACC,SPE] NOM

| Element | #Atoms | #Isotopes | Element | #Atoms | #Isotopes | Element | #Atoms | #Isotopes |
|---|---|---|---|---|---|---|---|---|
| C | 32 | 2 | BR | 1 | 2 | | | |
| H | 30 | 1 | | | | | | |
| N | 6 | 1 | | | | | | |
| FE | 2 | 4 | | | | | | |
| NI | 1 | 5 | | | | | | |

Spectrum: (SPE)

| Mass | %Int | Mass | %Int | Mass | %Int | Mass | %Int | Mass | %Int |
|---|---|---|---|---|---|---|---|---|---|
| 758 | 0.0113 | | | | | | | | |
| 759 | 0.0012 | | | | | | | | |
| 760 | 0.0001 | | | | | | | | |

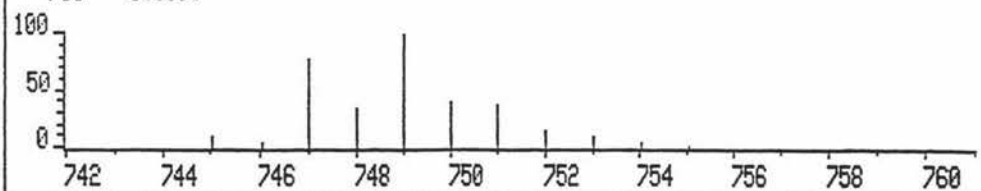


?=help RETURN=next ESC=previous 'G=compute 'X=exit 'H=hardcopy 'L('LX)=List(&exit)

Observed spectrum for $[Ni(L2)_2Br]^+$

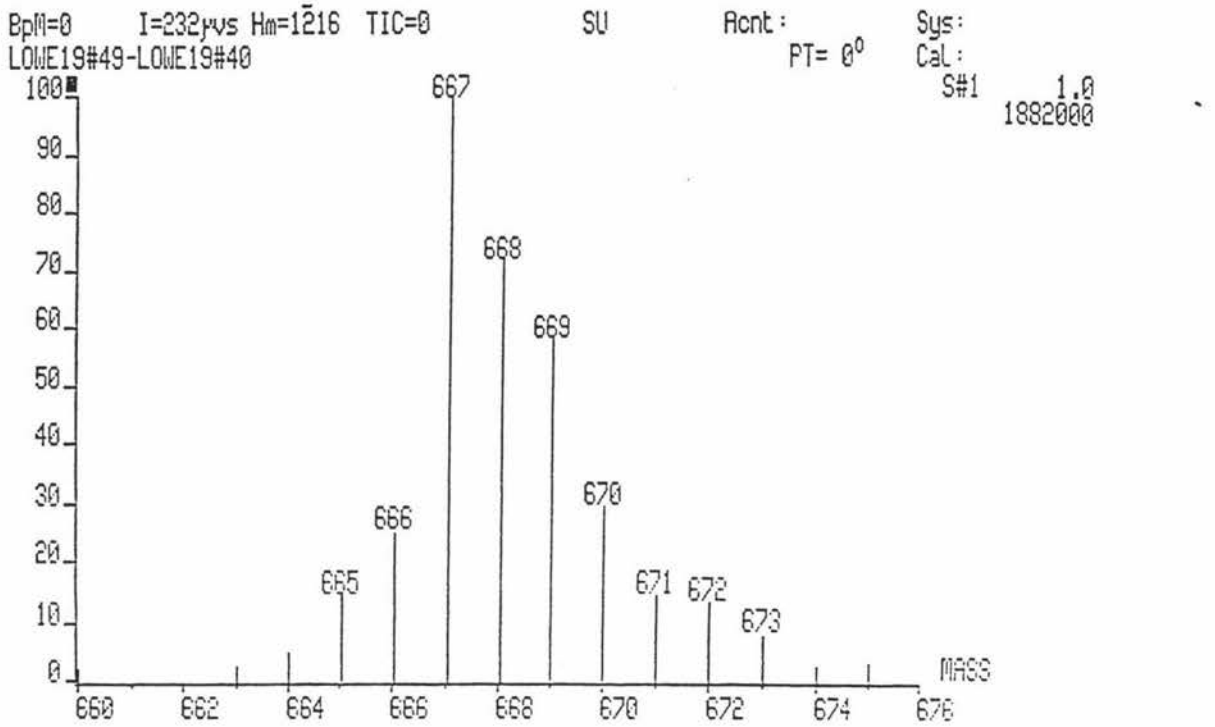


Calculated spectrum.

ISO Isotope Cluster Abundance Calculations 14-SEP-95

Formula: (NOM,ACC,SPE) Mode: [NOM,ACC,SPE] NOM

| Element | #Atoms | #Isotopes | Element | #Atoms | #Isotopes | Element | #Atoms | #Isotopes |
|---|---|---|---|---|---|---|---|---|
| C | 32 | 2 | | | | | | |
| H | 29 | 1 | | | | | | |
| N | 6 | 1 | | | | | | |
| FE | 2 | 4 | | | | | | |
| NI | 1 | 5 | | | | | | |

Spectrum: (SPE)

| Mass | %Int | Mass | %Int | Mass | %Int | Mass | %Int | Mass | %Int |
|---|---|---|---|---|---|---|---|---|---|
| 663 | 0.3779 | 666 | 4.6409 | 669 | 45.3596 | 672 | 2.6916 | 675 | 0.1163 |
| 664 | 0.1357 | 667 | 100.0000 | 670 | 17.7652 | 673 | 1.7720 | 676 | 0.0164 |
| 665 | 12.1213 | 668 | 40.5539 | 671 | 9.0724 | 674 | 0.5835 | 677 | 0.0018 |

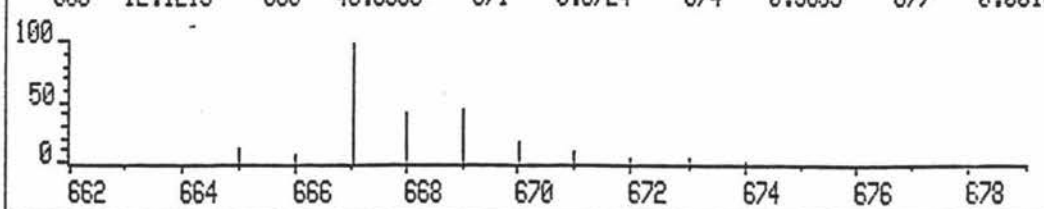


'Q=return to edit mode 'X=exit 'H=hardcopy ?=Help

Observed spectrum for [Ni(L2)Br]$^+$

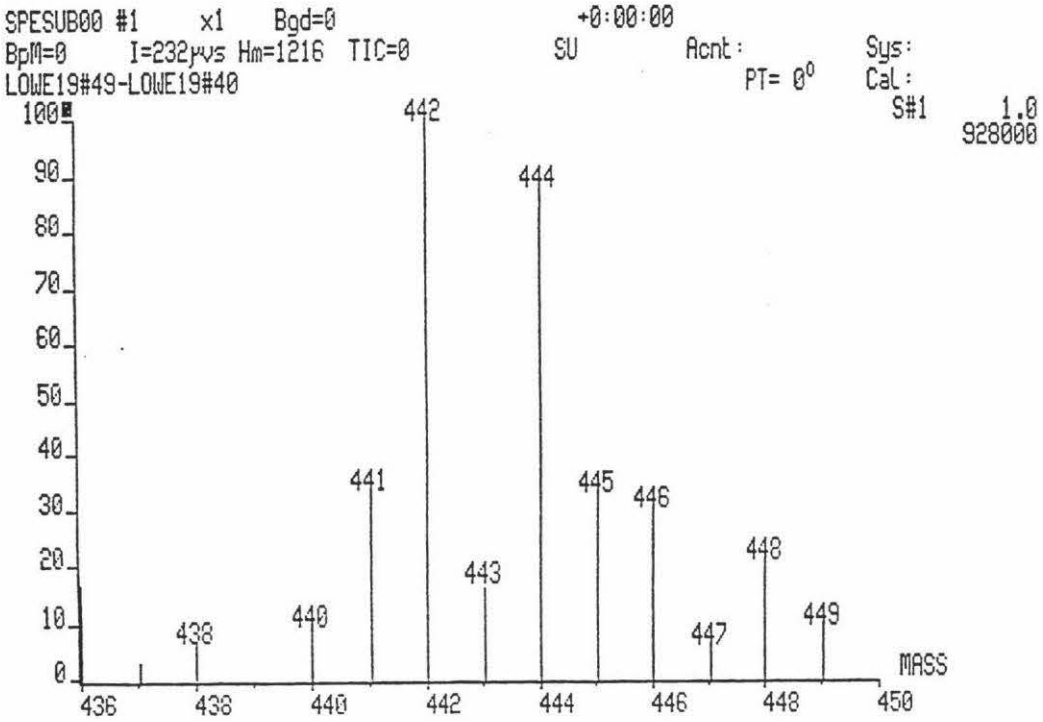


Calculated spectrum.

ISO Isotope Cluster Abundance Calculations 14-SEP-95

Formula: (NOM,ACC,SPE) Mode: [NOM,ACC,SPE] NOM

| Element | #Atoms | #Isotopes | Element | #Atoms | #Isotopes | Element | #Atoms | #Isotopes |
|---|---|---|---|---|---|---|---|---|
| C | 16 | 2 | BR | 1 | 2 | | | |
| H | 15 | 1 | | | | | | |
| N | 3 | 1 | | | | | | |
| FE | 1 | 4 | | | | | | |
| NI | 1 | 5 | | | | | | |

Spectrum: (SPE)

| Mass | %Int | Mass | %Int | Mass | %Int | Mass | %Int | Mass | %Int |
|---|---|---|---|---|---|---|---|---|---|
| 440 | 4.4979 | 443 | 15.6531 | 446 | 32.9384 | 449 | 1.0220 | 452 | 0.0212 |
| 441 | 0.8078 | 444 | 100.0000 | 447 | 7.5375 | 450 | 1.0311 | 453 | 0.0016 |
| 442 | 77.2925 | 445 | 21.3420 | 448 | 5.5724 | 451 | 0.1958 | 454 | 0.0001 |

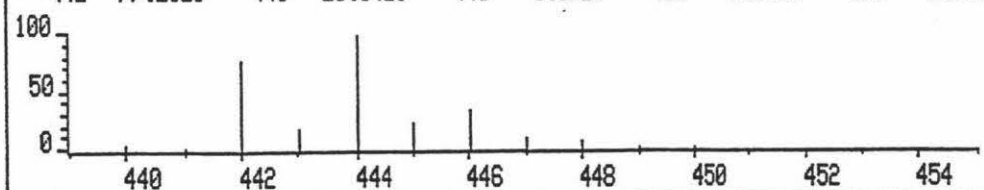


'Q=return to edit mode 'X=exit 'H=hardcopy ?=Help

Observed spectrum for $[Ni(L2)]^{+}$

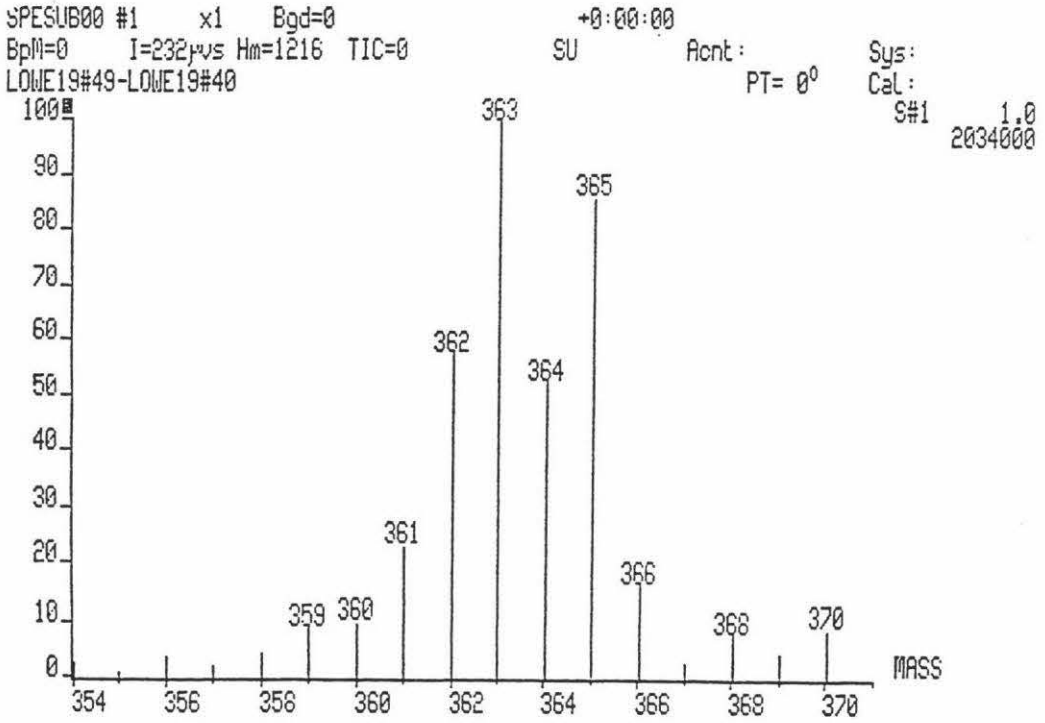


Calculated spectrum.

ISO Isotope Cluster Abundance Calculations 14-SEP-95

Formula: (NOM,ACC,SPE) Mode: [NOM,ACC,SPE] NOM

| Element | #Atoms | #Isotopes | Element | #Atoms | #Isotopes | Element | #Atoms | #Isotopes |
|---|---|---|---|---|---|---|---|---|
| C | 16 | 2 | | | | | | |
| H | 15 | 1 | | | | | | |
| N | 3 | 1 | | | | | | |
| FE | 1 | 4 | | | | | | |
| NI | 1 | 5 | | | | | | |

Spectrum: (SPE)

| Mass | %Int | Mass | %Int | Mass | %Int | Mass | %Int | Mass | %Int |
|---|---|---|---|---|---|---|---|---|---|
| 361 | 6.1686 | 364 | 20.3894 | 367 | 6.3930 | 370 | 0.2738 | 373 | 0.0001 |
| 362 | 1.1078 | 365 | 39.8647 | 368 | 1.1594 | 371 | 0.0297 | | |
| 363 | 100.0000 | 366 | 9.4345 | 369 | 1.4231 | 372 | 0.0022 | | |

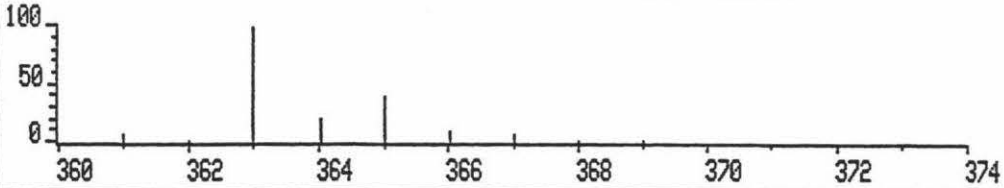


?=help RETURN=next ESC=previous 'G=compute 'X=exit 'H=hardcopy 'L('LX)=List(&exit)

Observed spectrum for $[L2]^+$.

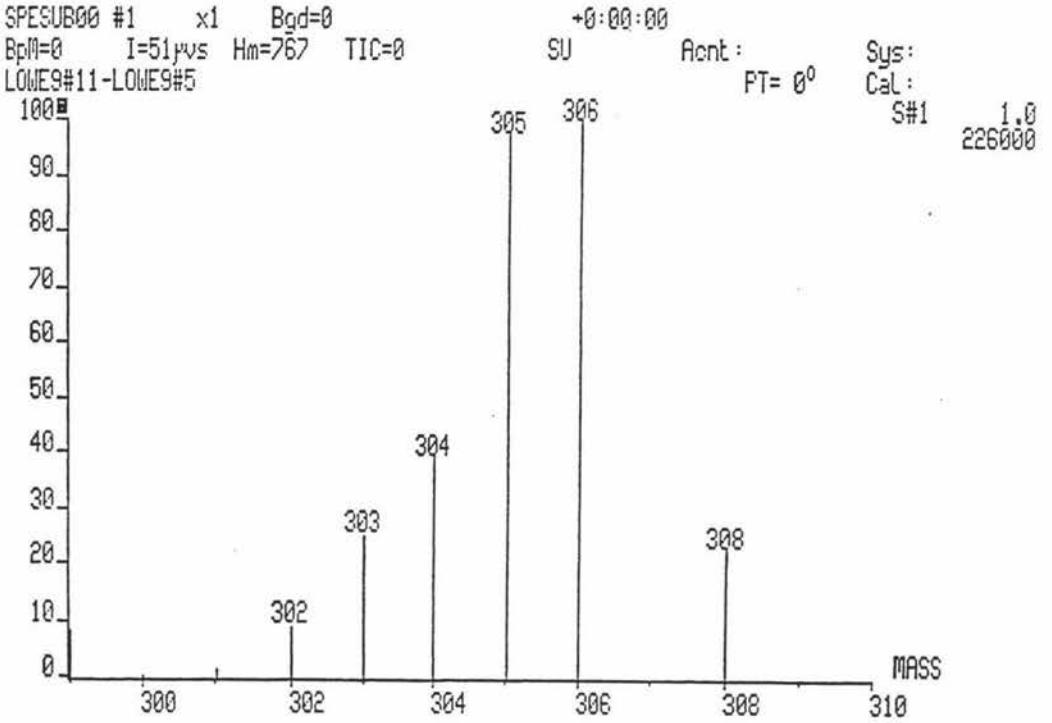


Calculated spectrum.

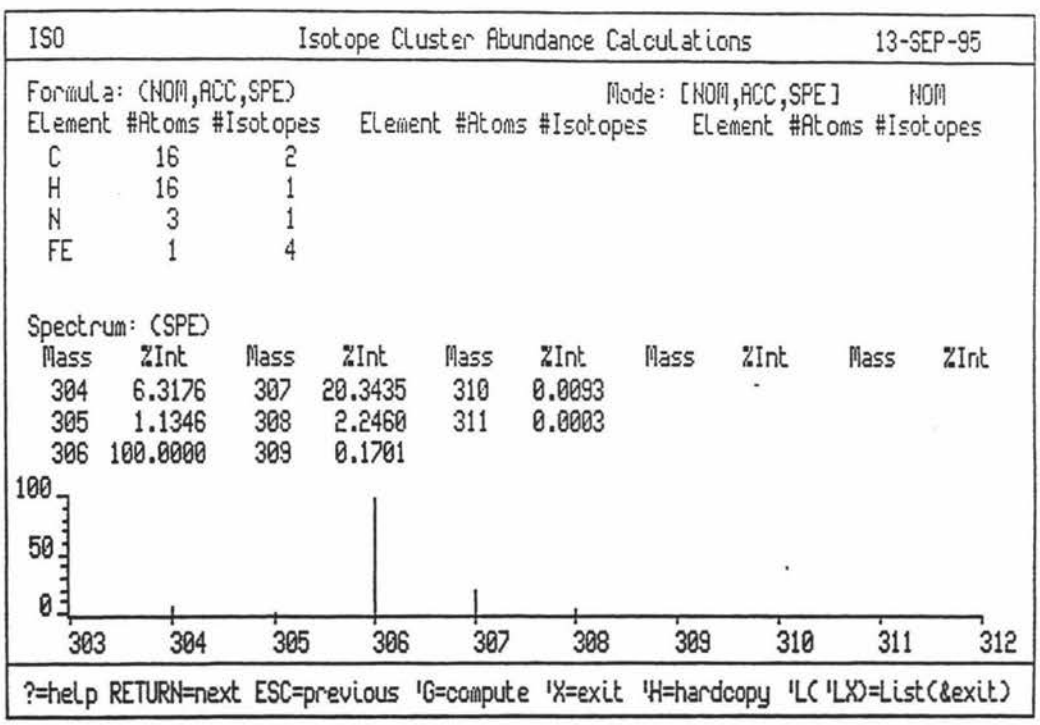

# APPENDIX IV

## A.IV (a) GENERAL EXPERIMENTAL TECHNIQUE

Most compounds synthesised in this thesis were air-stable. All synthetic reactions were performed under an atmosphere of purified nitrogen or argon gas.

## A.IV (b) PURIFICATION OF SOLVENTS

The solvents, such as dichloromethane and acetonitrile, were distilled from $CaH_2$. Methanol and ethanol were distilled from their respective magnesium alkoxides. Tetrahydrofuran was pre-dried over KOH pellets, and then distilled from sodium benzophenone under an atmosphere of purified nitrogen gas. Benzene and toluene were pre-dried with sodium wire and then distilled from sodium benzophenone under an atmosphere of purified nitrogen gas. These solvents were stored over type 4A molecular sieves (excluding tetrahydrofuran). The deuterated NMR solvent $CDCl_3$ and $d_6$-dmso were used as supplied commercially (Aldrich Chemical Co.)

## A.IV (c) REAGENTS

Organic compounds were laboratory grade chemicals and used as supplied.

The following chemicals were supplied by the respective manufactures.

| | |
|---|---|
| Strem Chemicals | Ferrocene carboxaldehyde |
| Aldrich | thf:$BH_3$ solution<br>Nickel (II) Bromide |
| G.F.S Chemicals | Tetraethylammonium perchlorate |
| B.D.H | Thiosemicarbazide<br>Palladium on Charcoal<br>Cobaltous Chloride |
| Merck | 2-Aminophenol |
| Fluka A.G. | Orthoameisensaure-trimethylester |
| Riedel-de Haen | Zinc Chloride<br>Sodium Borohydride |

| | |
|---|---|
| 1,1'-ferrocene dicarboxaldehyde | prepared from the following reference: U.T. Mueller-Westerhoff, Z. Yang, G. Ingram, *Journal of Organometallic Chemistry*, **463**, 163-167, (1993) |

## A.IV (d) INSTRUMENTATION

Nuclear Magnetic Resonance Spectroscopy was performed at 6.34 Tesla on a JEOL GX270W Spectrometer operating in the Fourier transform mode at 270 MHz for $^1H$ nuclei. Chemical shift data ($\Delta$) were expressed in parts per million (ppm) to high-frequency shift from tetramethylsilane as an internal reference for $^1H$ nuclei.

Infra-red Spectra were recorded on a BIO-RAD FTS-40 Spectrophotometer as a thin film of a nujol-mull between NaCl disks.

Mass Spectra were recorded by using a Varian VG70-250S double focussing magnetic sector Mass Spectrometer using the method of liquid secondary ion mass spectrometer (LSIMS) at AgResearch Ltd., Palmerstom North. The samples were dissolved in a suitable solvent (usually $CH_2Cl_2$) and *m*-nitrobenzylalcohol was used as a matrix.

Elemental analysis were carried out using standard technique at the Microanalytical Laboratory of the University of Otago, Dunedin.

Measurement of melting points employed a Reichert hot stage melting point apparatus and are uncorrected.

Cyclic voltammetry experimentation was conducted using a BAS B/W electochemical workstation, with a 3mm glassy carbon working electrode, Ag/AgCl reference electrode and a platinium auxiliary electrode.

The Mossbauer spectra were recorded using a dilution of glucose, to achieve a 5mg concentration of iron in the Ci (Co) beam, of which approximately 2% was $^{57}Fe$.